Universidade do Porto
FEUP Faculdade de Engenharia

"Contributions for MicroGrids Dynamic Modelling and Operation"

Fernanda de Oliveira Resende

Thesis submitted to Engineering Faculty of Porto University to obtain the PhD in Electrical and Computer Engineering (Engenharia Electrotécnica e de Computadores)

Porto – Portugal

2007

Thesis realized under the supervision of:

Professor Doctor João Abel Peças Lopes

(Associated Professor with Aggregation of Engineering Faculty of Porto University)

To my daughter, Raquel and to my husband, Filipe

Á minha filha, Raquel e ao meu marido, Filipe

Acknowledgements

This thesis is the result of some years of research, where I had opportunity to work closely with many people. I would like to take this opportunity to express my gratitude to all who helped me making this thesis a reality. I would like to specially recognise some of them here.

I would like to express my deeply gratitude to my research supervisor, Professor Peças Lopes, for the trust he puts in me at the beginning of the PhD long walk. I am also grateful for his encouragement, precious advises and discussions that contributed to the elaboration of this thesis.

I am grateful with INESC-Porto for the availability and support given during this work. I am happy to participate in the European research projects MicroGrids and More-MicroGrids. In this context, I am also very grateful with my supervisor and to INESC-Porto.

I would like to express my gratitude to my colleagues and friends in Power Systems Unit of INESC-Porto, especially to Carlos Moreira for the useful cooperation, insights and valuable discussions during these years of research, to Rogério Almeida for valuable discussions and to Nuno Gil for technical support in *Eurostag*. I am also greatful with Paula and Mauro for their friendship.

I would like to thank to Professor Vladimiro Miranda for his encouragement to use Information Theoretic Learning criteria and for the availability of Evolutionary Particle Swarm Optimization. I am also greatful with Professor Nuno Fidalgo for his clarifications concerning Artificial Neural Networks.

I would like to thank to the Program PRODEP (Programa de Desenvolvimento Educativo para Portugal/Programme of Educative Development for Portugal) for the financial support granted (under the measure PRODEP III - 5.3/N/199.023/03), that allowed the teaching activities dispense during the last years, being crucial to the completion of this work.

I am also grateful with the Department of Electrical Engineering of Superior School of Technology and Management of Polytechnic Institute of Bragança.

Last, but not least, I am grateful to my family for always being there. A special thank to Filipe for the constant support and for his patience, mainly during the last year, to my daughter Raquel and to my children Miguel, Tomás, Marta, Vasco, Simão, Catarina, João Pedro and Miguel “pequenino”, with the promise that I will try to spend more time with them.

Abstract

The need of reducing greenhouse gas emissions in the electrical energy supply field, recent technological developments in the microgeneration domain and electricity business restructuring are the main factors responsible for the growing interest in microgeneration. Large scale integration of small, modular generation units - the microsources - with power ratings less than a few tens of kilowatts to Low Voltage (LV) networks is leading with a new concept, the MicroGrid (MG).

A MG comprises a LV network, its loads, several microsources connected to it through inverter interfaces and a hierarchical control and management system. Microgeneration technologies include mainly renewable energy systems, such as small wind generators and photovoltaics, microturbines, fuel cells, and storage devices such as flywheels or batteries. The MG advanced control and management system allows the MG operation as a flexible active cell either interconnected to the Medium Voltage (MV) distribution network or isolated from it.

Large deployment of MG will lead with the Multi-MicroGrid (MMG) concept. In order to lead with the future challenges of operation and development of these electrical networks exploiting adequately the benefits provided by MG, namely whenever the upstream system has been lost, new computational tools based on mathematical models are required. However, in dynamic behaviour studies, the whole MMG system cannot be represented in a detailed manner, because the huge system dimension implies a computational burden that can render the study of MMG dynamic behaviour unfeasible. Therefore, reduced order models for MG need to be derived.

This research work aimed to derive dynamic equivalents for MG in order to reduce the complexity of the whole MMG to a computational feasible size and, at the same time, speed up numerical simulations with limited technical resources. As the MG own features did not recommend classical dynamic equivalency techniques commonly used to derive dynamic equivalents for conventional power systems, the MG dynamic equivalents are built upon the nonlinear MG detailed models using system identification techniques for a model defined on the basis of physical considerations and also exploiting Artificial Neural Networks.

The MG dynamic equivalents thus obtained are able to represent the MG dynamic behaviour with respect to the MV network following MMG islanding and during load following transients when the MMG is operated autonomously. The performance of the developed MG dynamic equivalents was assessed for different MMG, different types of disturbances as well as different operating conditions.

Resumo

A necessidade de reduzir as emissões de gases com efeito de estufa aliada à reestruturação dos mercados de energia eléctrica, bem como os recentes desenvolvimentos tecnológicos no domínio da microgeração constituem os principais factores responsáveis pelo crescente interesse neste domínio. A interligação dessas pequenas fontes de geração modulares, com potências nominais não excedendo algumas dezenas de quilowatt, nas redes de distribuição de Baixa Tensão (BT) dá lugar à formação de um novo tipo de sistema de energia – a Micro Rede (MR).

Uma MR é constituída por uma rede de BT à qual, para além das cargas, estão ligadas unidades de microgeração através de interfaces baseadas em electrónica de potência e por uma estrutura de controlo hierárquico suportada por um sistema de comunicações, sendo a gestão de operações feita de uma forma centralizada. As tecnologias de microgeração incluem, principalmente, fontes renováveis, tais como pequenos geradores eólicos e painéis solares fotovoltaicos, microturbinas, pilhas de combustível e unidades de armazenamento de energia, tais como volantes de inércia (*flywheels*) e baterias. As MR devidamente controladas podem ser ligadas à rede de distribuição de Média Tensão (MT) ou operadas de forma autónoma, quando isoladas da rede a montante.

A integração de MR em larga escala irá dar lugar à formação de Multi-Micro Redes (MMR). De modo a lidar com os desafios futuros associados ao desenvolvimento e exploração destas redes eléctricas, tirando partido dos benefícios associados às MR, nomeadamente quando a MMR é operada de forma autónoma, são necessárias ferramentas computacionais baseadas em modelos matemáticos adequados. No entanto, em regime dinâmico, a representação da MMR de forma detalhada conduz a sistemas com um elevado número de equações diferenciais não lineares, cuja resolução poderá comprometer a realização de estudos de comportamento dinâmico, pelo que é necessário dispor de modelos de ordem reduzida para as MR.

Este trabalho de investigação teve como objectivo o desenvolvimento de equivalentes dinâmicos para MR de modo a reduzir a complexidade do modelo da MMG e, em simultâneo, reduzir os elevados tempos de simulação. Dado que as características especificas das MR não aconselham a aplicação das técnicas convencionais, foram utilizadas técnicas de identificação de sistemas para desenvolver equivalentes dinâmicos para MR e adoptandas representações matemáticas baseadas em considerações físicas e em Redes Neuronais Artificiais. Os equivalentes dinâmicos obtidos permitem simular correctamente o comportamento dinâmico de MR relativamente à rede de distribuição de MT considerando a passagem da MMR a rede isolada e variações súbitas de carga, quando a MMR é operada de forma autónoma. O desempenho dos equivalentes dinâmicos para MR foi avaliado considerando MMR distintas e diferentes tipos de perturbações.

Résumé

Le besoin de réduire les émissions de gaz en effet de serre alliée à la réorganisation des marchés d'énergie électrique, ainsi que les récents développements technologiques dans le domaine de la micro génération constituent les principaux facteurs responsables du progressif intérêt dans ce domaine. L'interconnexion de ces petites sources de génération modulaires, avec des puissances nominaux en ne dépassant pas quelques dizaines de kilowatt, dans les réseaux de distribution de Basse Tension (BT) fait place à la formation d'un nouveau type de système d'énergie - le Micro Réseau (MR).

Un MR est constituée par un réseau de BT à laquelle les unités de micro génération sont liées à travers des interfaces basées sur l'électronique de puissance ayant en plus une structure de contrôle hiérarchique supportée par un système de communications, en présentant une gestion d'opérations locale faite d'une forme centralisée. Les technologies de micro génération incluent principalement des sources renouvelables, tels comme de petits générateurs éoliens et panneaux solaires photovoltaïques, micro turbines, piles de combustible et unités de stockage d'énergie, tels comme volants d'inertie (*flywheels*) et batteries.

L'intégration sur large échelle de MR conduira à la formation de Multi Micro Réseaux (MMR). Afin de traiter les défis futurs associés au développement et à l'exploration de ces réseaux électriques en obtenant des bénéfices que MR peut fournir, notamment quand MMR est opéré de forme indépendante, il nous faut des outils informatiques ajustés, en utilisant des modèles mathématiques appropriés. Cependant, dans le régime dynamique, on ne doit pas adopter des modèles détaillés pour MMR, puisque la résolution de systèmes avec un élevé nombre d'équations différentielles non linéaires qui décrivent le comportement des unités de micro génération exige un grand effort de calcul qui pourra rendre impraticable l'analyse de MMR dans un régime dynamique. Donc, il faut disposer de modèles d'ordre réduit pour les MR.

Ce travail de recherche a eu pour but le développement d'équivalents dynamiques pour MR afin de réduire la complexité du modèle de MMG et, simultanément, de réduire les temps de simulation. Vu les caractéristiques spécifiques de MR, l'application des techniques conventionnels, n'est pas recommandée au cas de MR. En effect les correspondants équivalents dynamiques ont été construits à partir du modèle détaillé de MR en utilisant des techniques d'identification de systèmes pour un modèle defini sur la base des considérations physiques et aussi en exploitant des Réseaux de Neurones Artificiels. Les équivalents dynamiques ainsi obtenus permettent de simuler correctement le comportement dynamique de MR à l'égard du réseau de distribution de MT dans le passage de MMR au réseau isolé et dans les situations transitoires provoquées par les variations subites de charge quand MMR est opérée de forme indépendante. La performance des équivalents dynamiques développés a été évaluée pour de différents MMR et pour différents types de perturbations et de conditions d'operation.

Table of Contents

List of Tables

List of Figures

List of Abbreviations

RES – Renewable Energy Systems

DG – Distributed Generation

CHP – Combined Heat and Power

DER – Distributed Energy Resources

RTD – Research, Technology and Development

IRED – Integration of Renewable Energy Sources and Distributed Generation into the European Electricity Grid

PF5 – 5th. Framework Programme

FP6 – 6th. Framework Programme

FP7 – 7th. Framework Programme

MG – MicroGrid

MMG – Multi-MicroGrid

MV – Medium Voltage

HV – High Voltage

LV – Low Voltage

PV – Photovoltaic

MS – Microsource

MC – Microsource Controller

LC – Load Controller

MGCC – MicroGrid Central Controller

DMS – Distribution Management System

DSM – Demand Side Management

CAMC – Central Autonomous Management Controller

DSO – Distribution System Operator

RTU – Remote Terminal Units

DC – Direct Current

AC – Alternate Current

SOFC – Solid Oxide Fuel Cell

MCFC – Molten Carbonate Fuel Cell

PMSM – Permanent Magnet Synchronous Machine

PI – Proportional-Integral

STC – Standard Test Conditions

NTC – Nominal Test Conditions

MPPT – Maximum Power Point Tracker

VSI – Voltage Source Inverter

PWM – Pulse Width Modulation

SMO – Single Master Operation

MMO – Multi Master Operation

RMS – Root Mean Square

SVD – Singular Value Decomposition

emf – electromotive force

REI – Radial Equivalent Independent

AVR – Automatic Voltage Regulator

ANN – Artificial Neural Network

AR – Autoregressive

MA – Moving Average

PRBS – Pseudo Random Binary Signals

MSE – Mean Square Error

AIC – Akaike's Information Criterion

BIC – Bayesian Information Criterion

FPE – Final Prediction error Criterion

NFIR – Nonlinear Finite Impulse Response

ARX – Autoregressive with eXogenous input

NARX – Nonlinear Autoregressive with eXogenous input

NARMAX – Nonlinear Autoregressive Moving Average with eXogenous input

NOE – Nonlinear Orthonormal Basis Functions

NBJ – Nonlinear Box-Jenkins

MLP – Multilayer Perceptron

RBF – Radial Basis Functions

TDNN – Time Delay Neural Network

PEM – Prediction Error Methods

ITL – Information Theoretical Learning

ML – Maximum Likelihood

PDF – Probability Density Function

IP – Information Potential

MEE – Minimum Error Entropy

EA – Evolutionary Algorithms

SA – Simulated Annealing

TS – Tabu Search

BB – Branch and Bound

ES – Evolutionary Strategies

GA – Genetic Algorithms

GP – Genetic Programming

PSO – Particle Swarm Optimization

σSA-ES – Self-Adaptive Evolution Strategies

EPSO – Particle Swarm Optimization

FIS – Fuzzy Inference System

GAST – Gas Turbine

MISO – Multiple Input Single Output

Chapter 1
Introduction

1.1 Preliminary considerations

Energy supply in Europe has been dominated by the large scale centralized combustion of fossil fuels (coal, oil and gas), nuclear and hydro power, with energy delivered over long distances to consumers. Concerning the Europe sustainable development, this traditional economy of scale presents some drawbacks. On the one hand, a significant amount of Europe's generation capacity, both coal and nuclear fuelled, is reaching the end of its useful life and the network infrastructure is also old, requiring investments in a short-term on the transmission and distribution systems. On the other hand, the continuous increasing demand for energy, in particular for electricity, has stressed a number of shortcomings:

- High level of dependency of imported fuels leading to potential price rises and potential supply disruptions;
- Large environmental impact on greenhouse gases and other pollutants;
- Increased transmission losses;
- Necessity for continuous upgrading of transmission and distribution systems.

Whilst energy remains a major component of economic growth, such deficiencies have a direct impact on the world economical development, stability concerning the security of energy supply, environmental protection and well-being of world's citizens. These issues provided the main drivers for energy research within the framework of EU sustainable development.

Wind generators, photovoltaic panels, fuel cells and microturbines – just to mention a few – are new forms of electricity generation under development. They define the so called RES and involve the exploitation of distributed sources through the concept of DG. Today, wind power and CHP are entering into a competitive level with traditional forms of energy generation. Tomorrow it is expected that one speaks also about microgeneration (microturbines, micro-CHP, photovoltaic systems and fuel cells).

RES and DG for heating, cooling and electricity have the potential to become the foundation of a future more sustainable energy supply system. Their large scale deployment

will transform the energy landscape from a system dominated by the centralized combustion of fossil fuels to a new one in which new technologies, environmentally friendly, contribute to a substantial development. On the other hand, DG can offer additional value to the grid system operators by providing [1]:

- Deferral of investments to transmission and distribution systems;
- Reduction of losses in the distribution system;
- Provision of network support services or ancillary services.

From an investment view point, it is generally easier to find sites for RES and DG than for large central power plants and, in addition, such units can be installed in a short time, near to the end consumer. The widespread integration of RES and DG together with energy efficiency, covering supply and demand, have provided support to achieve the major EU policy objectives [2, 3]:

- Sustainable development, combating climate changes and reducing air pollutants. The shift from the large scale combustion of fossil fuels to a more decentralized energy supply based on RES has contributed for meeting the Kyoto commitments, regarding the emission of greenhouse gases, particularly CO_2: 8% reduction of emissions from 1990 levels by 2008-2010 and 20% by 2020 compared to 1990;
- Security and diversity of energy supply. Reducing the external energy dependence is crucial for the development of a dynamic and sustainable economy for Europe;
- Increasing the penetration of RES, doubling their share in energy supply quota from 6% to 12% of gross energy consumption and raising their part in electricity production from 14% in 2001 to 22% is an objective to be attained by 2010;
- Energy market liberalization, increasing opportunities for smaller scale generators.

However, the integration of both RES and DG into the overall power systems operation requires that energy generation in both transmission and distribution systems can no longer be considered as a passive appendage. Reliability, safety and quality of power are the main issues linked to the large-scale deployment of DER so that their effect on the European transmission and distribution networks cannot be neglected. Rather, it must be addressed with a comprehensive system approach [3].

Therefore, DG current issues are how to increase the penetration level of DER in order to gain the highest benefits, ensuring, at the same time, future power supply reliability and quality. In addition, major technological and regulatory changes will be needed to

accommodate the new open and unified electricity service market approach during the next decades in Europe. For this purpose a substantial and continued RTD effort is required.

The research projects successfully developed under the Target Action "*Integration of Renewable Energies and Distributed Generation in European Electricity Networks*" in EU FP5 are considered as the start point for the development of the first generation of new architectures for electricity grids. The EU cluster IRED involved seven projects dealing with the integration of RES and DG. The MicroGrids project, *MicroGrids: Large scale integration of MicroGeneration to Low Voltage Grids*, Contract ENK5-CT-2002-00610 [4], is one of them and was the first attempt at EU level to deal in-depth with MicroGrids.

Activities in this area are continuing in FP6 with very promising large integrated projects, in which more and more utilities and other stakeholders in the electricity sector, usually competitors in the international market, are showing their readiness to share know-how and efforts [3] . More-MicroGrids Project, *More-MicroGrids: Advanced grid architectures for the integration of DER within local distribution networks, including MicroGrids*, Contract No. 019864 (SES6) [5], is one of them, aiming the increase of DER integration in electrical networks through the exploitation of the MicroGrid concept.

The Commission proposal for the FP7, within the theme energy, confirms power networks and distributed generation as a priority for future research activities. The research area referred to as "*Smart Energy Networks*" is the natural evolution of both past and current RTD activities on integration of DER. Thus, the objective of this area is to increase the efficiency and reliability of the European electricity and gas systems and networks e.g. by transforming the current electricity grids into an interactive (customers/operators) service network, and to remove the technical barriers to the large scale deployment and effective integration of DER [3].

Following the increasing penetration of DG in MV networks, dissemination of small size dispersed microgeneration systems connected to LV distribution systems is expected to become one of the means to face the continuous demand growth. The need of reducing greenhouse gas emissions, recent technological developments related with the improvement of microgeneration efficiency and the possibility of exploiting RES are important factors that will contribute, in a short term, to an effective integration of microgeneration in LV grids. Such large deployment of microgeneration is leading to the adoption of the MicroGrid concept, which was investigated within the framework of the MicroGrids EU R&D project.

A MicroGrid (MG) comprises a LV network, its loads, several small and modular generation units in the range of a few tens of kilowatts or even less connected to it through inverter interfaces and an embedded hierarchical control and management system [6]. Thus, the MG concept is defined as a LV distribution system with DG sources - the microsources - operated as a single coordinated entity, being a new paradigm for the development of electric power systems. Microgeneration technologies include RES, such as wind and PV generators, DG, like microturbines and fuel cells, and also storage devices such as flywheels or batteries.

A key economic potential of the application of distributed energy sources at customer premises lies in the opportunity to use locally the waste heat from conversion of primary fuel to electricity. There have recently been significant progresses in developing small, kW-scale, CHP applications, known as micro-CHP. These systems, based currently on Stirling Engines, will later use fuel cells and are expected to play a very significant role in the MG of Northern EU countries. On the other hand, PV systems are anticipated to become increasingly popular in Southern EU countries. The application of micro-CHP and PVs potentially increases the overall efficiency of utilizing primary energy sources and consequently provides substantial environmental gains regarding carbon emissions.

In addition, MG offer considerable advantages to network operation due to their much more sophisticated control capabilities. MicroGrids can be mostly operated interconnected to the MV distribution network, but they can also be operated isolated from the main grid, in case of faults in the upstream network [6, 7]. Preliminary experiments on a real MG islanded operation were performed in a prototype system installed in the Laboratories of the National Technical University of Athens [8]. From the customer point of view, MG can provide both thermal power and electricity to feed the needs of local consumers, and in addition enhance local reliability, reduce emissions, improve power quality by supporting voltage and reducing voltage dips. MG can also provide network support in times of stress by relieving branch congestions. Reducing of LV consumer's interruption time can be performed by allowing MG islanded operation until MV network is available and by exploiting the MG generation and control capabilities to provide fast black-start at the LV level, after a general system black-out [9, 10].

1.2 Motivations and objectives of this thesis

It is expected that, in a near future, several MG can be connected on several adjacent MV feeders coexisting with MV loads and distributed generation units. The MG operation flexibility will then be extended to the MV level through suitable control schemes, leading with the Multi-MicroGrid concept, which is being developed within the framework of the More-MicroGrids project.

Large deployment of MG will have a considerable impact on the future operation and development of electricity networks. Therefore, new tools and simulation approaches are required to address this subject and to quantify the benefits of MG. From the possibility to have hundreds of these active cells connected to the MV network, a large number of active sources together with their inverter interfaces should be considered and therefore a very high dimensional system will arise. So, the use of detailed models for MG components implies a computational burden which will render the study of MMG dynamic behaviour unfeasible, justifying thus the need of appropriate dynamic equivalents for MG in order to speed up numerical simulations.

Thus, the main objective of this thesis is to derive dynamic equivalents for MG, able to represent its dynamic behaviour with respect to the MV network when the MMG is operated autonomously. The MG dynamic equivalents are then established from the MG nonlinear detailed model and will replace MG in dynamic simulation tools, reproducing their relevant dynamics in time domain simulations.

Conventional dynamic equivalence techniques are mainly based on either modal analysis or coherency based methods. The first techniques use a linearized version of the entire power system state space model and have been used to study dynamics related to small perturbations around an operating point. In contrast, coherency based methods allows to represent dynamic nonlinearities and have been widely used to build dynamic equivalents for conventional large power systems. However, as these methods are based on the coherency concept and its key step is coherency recognition between generators, their application to MG do not make sense, since MS are connected to the LV grid through inverter interfaces and, in addition some of them, like fuel cells and PV systems are not characterized by rotor angles or angular speeds.

With technical advancements mainly in communications and computer technologies, alternative methodologies do develop dynamic equivalents are emerging. These methodologies are based on system identification theory and then they use measurements of important

signals/variables to find parameters for a suitable system representation. Also ANN have been used to derive power system dynamic equivalents not only for conventional power systems, but also for distribution networks containing a significant capacity of distributed generation, without the need of a detailed knowledge of the power subsystem to be reduced. This fact can be viewed as an advantage to build dynamic equivalents for MG.

Thus, the structure of this thesis follows the organization presented in the following section.

1.3 Thesis organization

The research work presented in this thesis is structured over 7 chapters as follows.

Firstly, in **chapter 1**, an introduction is presented.

In **chapter 2**, both MicroGrid and Multi-MicroGrid concepts are presented. Mathematical models able to represent the dynamic behaviour of microgeneration systems connected to the LV network are also described. This involves the description of their inverter interfaces as well as of the integrated control inside the MG, focusing particularly the case when the MMG is operated autonomously following a disconnection from the upstream main network.

In **chapter 3**, the state-of-the art of dynamic equivalent techniques used to derive dynamic equivalents for conventional power systems is presented. In order to pursue the development of MG dynamic equivalents, a detailed analysis of these main techniques, such modal analysis and coherency based methods is presented and their applicability to MG is also assessed. Tacking into account the particular features that characterize these new power systems, both modal analysis and coherency based methods are not recommended for developing MG dynamic equivalents purposes.

In **chapter 4**, system identification theory is exploited in order to derive suitable dynamic equivalents for MG. The theoretical concepts behind the main techniques of nonlinear dynamic systems identification as well as the state of the art of these main techniques are presented and discussed, taking into account the physical knowledge that can be extracted from chapters 2 and 3 as well as the purpose of the MG dynamic equivalents to be derived.

From this discussion two promising methodologies arose concerning the MG mathematical representation. They are black-box modelling approaches based on ANN and physical modelling approaches. However, their applicability to MG deserves a more in-depth investigation for two main reasons:

- The classical stages to derive dynamic equivalents for conventional power systems have to be replaced by appropriate system identification procedures;
- An acceptable trade-off between development effort and validity domain should be achieved.

Therefore a common system identification procedure is also presented and afterwards identification techniques suitable to cope with both black-box and physical modelling approaches are also addressed in **chapter 4**.

In **chapter 5**, the development of the two promising solution approaches identified in chapter 4 is carried out. A dedicated dynamic simulation platform was developed for generating high quality data sets and for validation purposes, playing the role of the numerical set-up. Thus, two main simulation packages were included:

- The MMG detailed model, which includes the dynamic models of microgeneration systems described in chapter 2 linked together with the LV network algebraic equations in order to build the MG detailed model, which, in turn, is connected to the MV network. This module is used to generate high quality data sets;
- The MMG equivalent model, in which the MG detailed model is replaced by the derived MG dynamic equivalents in order to further evaluate their performances.

In chapter 6, the two methodologies developed in chapter 5 are applied to MG and the performances of the dynamic equivalents thus obtained are evaluated. For this purpose two study cases are considered and the time domain responses provided from both MMG detailed and equivalent models following disturbances are compared.

The main conclusions and future developments are presented in **chapter 7**.

Finally, the mathematical model of round rotor synchronous machines as well as the parameters corresponding to the dynamic models of microgeneration systems of the test systems used in this thesis are presented in **appendix A**.

Chapter 2
Models for Microgeneration and MicroGrids

2.1 Introduction

The Multi-Microgrid concept, which is being developed within the framework of the EU R&D More-MicroGrids Project [5], involves a structure formed at the MV level, comprising LV MicroGrids and distributed generation units connected at several adjacent MV feeders together with MV loads. Technical operation of such a system requires the development of a hierarchical control structure [5] able to manage the distribution grid either in normal interconnected mode or emergency mode. This emergency mode involves namely islanding operation of MV distribution grid, which requires a careful dynamic behaviour assessment. Adequate dynamic models for these microgeneration devices are therefore required.

This chapter aims at the description of mathematical models able to represent the dynamic behaviour of microgeneration devices connected to the LV network, as well as the dynamic behaviour of the MG with respect to the upstream MV network over time ranges of a few tens of milliseconds up to a few seconds, which involves also the description of integrated control of the microgeneration units inside the MG. These models were identified through a bibliographic research from the available literature and developed within the framework of the EU R&D MicroGrids Project. Concerning those models, two main issues must be stressed:

- The inverter interfaces are modelled based on their control functions only, so that switching transients, harmonics and inverter losses are neglected. This is considered a general procedure as described in [11-15], since fast transient phenomena are not relevant for the purpose of dynamic behaviour;
- Only three-phase balanced operation is considered, despite the fact that it is not a common situation in LV networks.

The microgeneration devices can be of different types and technologies, namely: fuel cells, micro wind turbines, solar PV panels, microturbines, micro CHP with Stirling engines, Diesel generators, etc. In this thesis only the first 5 generation devices are addressed.

Due to the lack of more realistic models reported in the literature, this research deals therefore with three-phase models of microgeneration systems, which describe the MG dynamic behaviour only under balanced conditions. These models involve also models of inverter interfaces. The development of models able to simulate the dynamic behaviour of single-phase microgeneration systems and MG operating under unbalanced conditions as well as the corresponding MG dynamic equivalents constitute, right now, a subject for future research.

The mathematical models adopted to represent the dynamic behaviour of each MG generation system were adapted in order to be linked together with the algebraic equations describing the LV network forming thus the whole model of a MG as a multi-machine power system model [16, 17] in chapter 5. Particular attention is given to represent the MG dynamic behaviour when the MMG is operated autonomously following a disconnection from the upstream main network.

Section 2.2 describes both MG and MMG concepts. Section 2.3 is devoted to dynamic models of microsources as well as the corresponding interface inverters. In section 2.4, control strategies for MG operation are discussed and finally, in section 2.5, the summary and the main conclusions are presented.

2.2 The MicroGrid and Multi-MicroGrid concepts

As already mentioned previously, the MG concept is a logical evolution of simple distribution networks with high penetration of DG. MicroGrids comprise LV distribution systems, in which small and modular generation units, in the range of a few tens of kW or even less, are connected together with loads and storage devices. Furthermore, a MG is an extremely flexible cell of the electrical power system if properly controlled and managed. Advanced control strategies allow two different operation modes [6, 7, 9, 10, 18, 19]:

- Normal interconnected mode, when the MG is connected to the MV network, being either supplied from it or injecting some amount of power into it;

- Emergency mode, when the disconnection from the MV network occurs following a fault in the upstream system.

Therefore, MG offer considerable advantages to network operation either from the utility or from the customer view points. Thus, distributed generation located close to loads will reduce flows in both transmission and distribution systems with, at least, two important effects: loss reduction and deferral of investments related to future grid reinforcements and expansion, since branch congestion can be controlled. On the other hand, MG can provide both thermal and electricity needs to consumers and, at the same time, enhance local reliability and improve power quality by supporting voltage and reducing voltage dips. In addition, MG potentially lower costs of energy supply [4].

The increase of penetration of microgeneration in electrical networks through the exploitation and extension of the MG concept leads with the MMG concept, which is being developed within the framework of the EU More-MicroGrids Project [5], as already mentioned previously.

In order to highlight both MG and MMG concepts, their control and management architectures are presented in the following two subsections.

2.2.1 The MicroGrid control and management architecture

The MG concept involves an operational architecture, developed within the EU R&D MicroGrids project [4, 20], which is presented in figure 2.1.

This MG example includes:

- Several feeders supplying electrical loads;
- Microgeneration systems;
- Storage devices;
- A hierarchical-type management and control scheme supported by a communication infrastructure.

In terms of current available technologies, the microgeneration systems can include several types of devices, like fuel cells, small wind turbines, PV systems and microturbines, typically in the range of 25-100 kW powered by natural gas or bio fuels. CHP is one of the most promising applications, leading to an increase of the overall energy effectiveness of the whole system [20]. Most of the MS are not suitable for LV network direct connection, due to the type

of energy conversion system used. Therefore power electronic interfaces are required for grid interconnection, as it can be observed from figure 2.1.

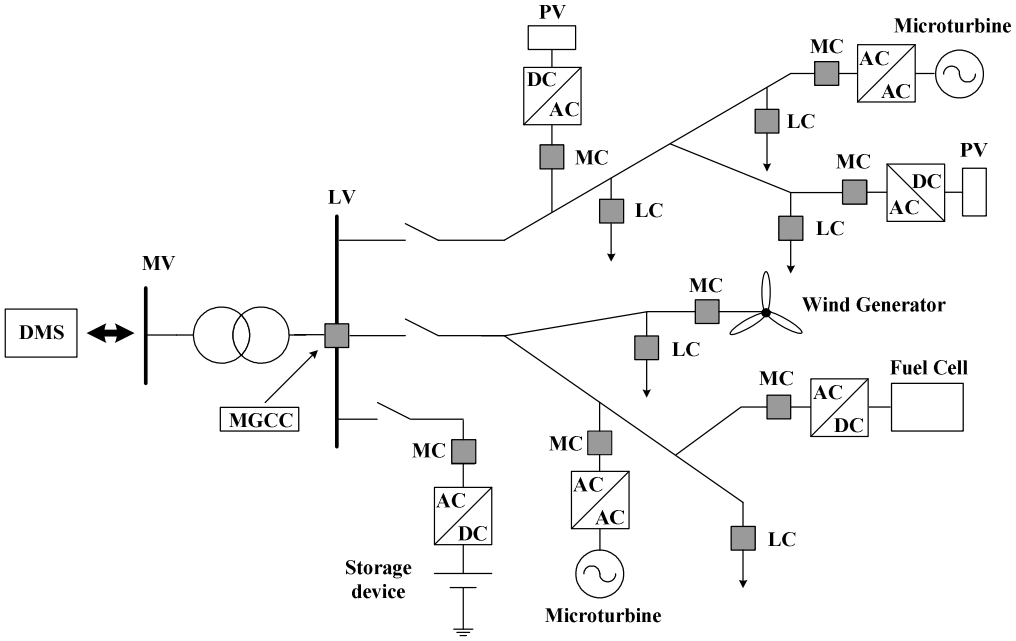

Figure 2.1. MicroGrid architecture comprising microsources, loads and control devices

A special issue related to MG operation concerns MS slow response to the control signals in order to change the output power. Therefore, when the MG is operated autonomously, the absence of synchronous machines connected to the LV networks requires that power balance during transients have to be provided by energy storage devices, either flywheels connected to the LV network through AC/DC/AC power electronic interfaces or batteries and supercapacitors connected to the dc-link of microgeneration systems, which are continuously charged by the primary energy sources.

Although MG are dominated by inverter interfaced MS that are inertia-less, they offer the possibility of a very flexible operation allowing the MG ability to behave as a coordinated entity in both interconnected and islanded operation. Storage technologies become important components with the duty of helping on MG stabilization during transient phenomena and in the moments subsequent to islanding. However, in order to achieve the full benefits from the MG operation, a hierarchical control and management systems have also been envisaged, which comprises three important control levels, as depicted in figure 2.1.

- Local Microsource Controllers and Load Controllers. The MC take advantage of the MS power electronic interface and can be enhanced with various degrees of intelligence in order to control both voltage and frequency of the MG during transient conditions based on only local information.
- MicroGrid Central Controller. The MGCC functions can range from monitoring the active and reactive power of MS to assuming full responsibility of optimizing the MG operation by sending set points to the MC and LC in order to control microgenerators and controllable loads, respectively.
- Distribution Management System, which can be used to manage the integration and operation of a MG and the upstream distribution network.

2.2.2 The Multi-MicroGrid control and management architecture

As stated before, the MMG concept being developed under the framework of Multi-MicroGrid project is related to a higher level structure, formed at the MV level, consisting of DG units and LV MicroGrids connected on several MV feeders. Microgrids, DG units and MV loads under DMS control, can be considered as active cells for control and management purposes. Technical operation of such systems requires the adoption of a control structure, where all these active cells, as well as MV/LV passive substations, should be controlled by the CAMC to be installed at the MV bus level of a HV/MV substation, under the responsibility of the DSO [5].

The tremendous increase in dimension and complexity that the management of such a distribution system presents requires the use of a flexible decentralized control and management architecture. A central management for a DMS centre would not be effective enough, due to the large amount of data to be processed and treated, and would not assure an autonomous management namely during islanding mode of operation. The CAMC is therefore playing here a key role and being responsible for the data acquisition process, for enabling the dialogue with the DMS upstream, for running specific network functionalities and for scheduling the different active cells in the downstream network [5]. Generally speaking, this new management and control architecture is represented in figure 2.2.

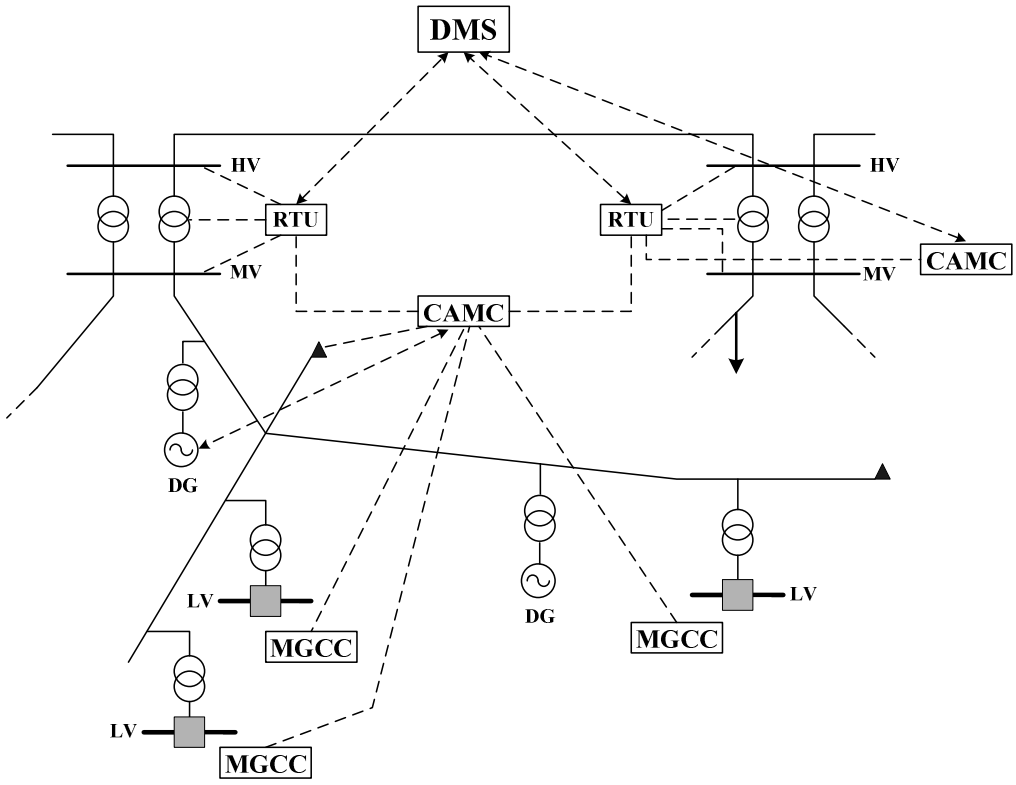

Figure 2.2. Control and management architecture of a Multi-MicroGrid

The management of the MMG will be performed through the CAMC, acting as an intermediate DMS controller, that will receive information from the upstream DMS, measurements from MV networks and RTU, existing MGCC and will have to deal with constraints and contracts to manage the MMG in both HV interconnected and emergency modes of operation. This requires namely tackling with the following aspects: state estimation, coordinated voltage support and flow control, coordinated frequency support and emergency functions. The effect of such a combined interaction and new global operation strategy is expected to enable an increase of the global penetration of microgeneration.

The analysis of the dynamic behaviour of several MG and other DG units operating all together is therefore required. However, dynamic simulations using detailed models of several MS, spitted throughout different MG, together with DG units connected in the MV network, requires a very large computational effort. In addition, this is a very time consuming procedure.

Therefore dynamic equivalents for MG need to be derived taking into account the MS connected to the MG, the storage devices installed as well as the MG control strategies to be followed when it is operated under the framework of the MMG concept.

2.3 Dynamic modelling of MicroGrids

The technical feasibility of the MG concept described previously has been demonstrated within the framework of the EU MicroGrids Project [4, 21]. For this purpose, a simulation platform able to simulate the steady state and dynamic operation of LV networks that include micro generation sources was developed [6, 7, 9, 10, 18, 19, 21-23]. This included several models able to describe the MS dynamic behaviour considering their inverter interfaces over a few tens of seconds [22, 23].

Microsources connected to the network through inverter interfaces have been commonly represented by a DC voltage source placed before the inverter [12], as depicted in figure 2.3.

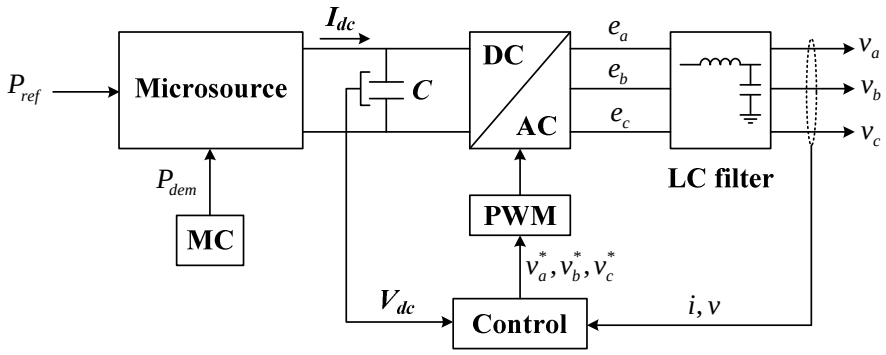

Figure 2.3. Model of an inverter interfaced microsource

The main blocks are:

- A DC voltage source connected to the DC stage of the inverter;
- An inverter interfacing the DC system to the AC network. Limiting the analysis of the fundamental frequency supplied by the inverter, it can be modelled as the generated fundamental amplitude, e, before the filter;
- A low-pass LC filter which blocks the inverter generated high frequency harmonics. At the fundamental frequency it is represented through the equivalent impedance of the filter, Z_f.

A brief overview of dynamic models suitable to describe the response of different microsources and storage devices as well as their inverter interfaces in order to evaluate the global response of the MG system namely during islanding operating conditions is presented in the following three subsections.

2.3.1 Micro-sources modelling

Several MS models able to describe their dynamic behaviour have been developed during the last years and are available from the literature. These models include the main microgeneration technologies currently available, such as microturbines, fuel cells, photovoltaic arrays and small wind generators.

There are essentially two types of microturbines, which differ basically from the shaft construction [24]. One is a high-speed single-shaft unit with both the compressor and turbine mounted on the same shaft as the electrical synchronous machine. In this case, turbine speeds mainly range from 50000 to 120000 rpm. The other type of microturbines is a split-shaft designed one that uses a power turbine rotating at 30000 rpm and a conventional generator connected through a gearbox. Although this is a proven and robust technology, the split-shaft design has not been widely used for small scale power generation. Rather, it is typically used for machine drive applications, since it does not require power electronic interfaces [25]. Therefore, in this research only single-shaft microturbines are considered.

As stated before, fuel cells are an emerging class of small scale power generation technology. Two types of fuel cells are likely to be used as power plants, namely SOFC and MCFC [26]. In order to study the dynamics of generating units based on SOFC and MCFC technologies several dynamic models have been reported in the literature [22, 24, 27-39]. Most of them are focused on SOFC system dynamic behaviour modelling with the expectation that the response of MCFC system would be similar [24, 28, 35, 36]. Therefore, in this research, the SOFC model described in [24, 35] was adopted.

Concerning small wind turbines, although it is not the most common solution, a dynamic model based on an induction generator directly connected to the network like in [7, 10] was considered.

In order to model a PV system, it was assumed that the array is always working at its maximum power level for a given temperature and irradiance as described in [23].

Then, the dynamic models for SSMT, SOFC, small wind generators and PV systems are presented in the following subsections.

2.3.1.1 Single-shaft microturbines

Single shaft microturbines are small and simple-cycle gas turbines with outputs ranging from around 25 to 500 kW [40], which have been used in small scale distributed generation systems either for electrical power generation or CHP applications. Although microturbines can burn different fuels, most of the available systems use natural gas as the primary fuel.

The basic technology used in microturbines is derived from aircraft auxiliary power systems where the need for light weight, compact, high powered generators has traditionally prevailed over both the significant development and production costs. However, R&D efforts in the last years have changed the structure of these systems. On one hand microturbines are considered one part of a general evolution in gas turbine technology, since techniques incorporated into the larger machines to improve performance can be typically found in microturbines as well. These techniques include recuperation, low NO_x technologies and the potential use of advanced materials such as ceramics for hot section parts [41]. On the other hand, power electronics, advanced control and communication systems are included in modern microturbines [42].

Concerning to the operating principle, microturbines deal with the same combustion process of gas turbines, involving a gas that is expanded at roughly the same speed whether inside a large turbine or a small one. Therefore, the tips of the microturbine blades have to move at high speed in order to capture the energy from this expanding gas. This means that, in general, the smaller the turbine the higher the revs [43]. In fact, turbine speeds mainly range from 50 000 to 120 000 rpm while large gas turbines designed for utility applications turn at fairly standard 1000, 2000 or 3000 rpm depending on the number of poles built into the generator [43].

As already mentioned before, SSMT comprise a compressor and a power turbine mounted on the same shaft. They operate by forcing air through a turbine, causing it to spin at a very high speed. This high-speed power turbine is connected to a generator, which generates electric power at high and variable frequency. Therefore this power is converted to DC and then an inverter is employed to produce 50 Hz AC power for commercial use. A block diagram of a SSMT system [24, 42] is presented in figure 2.4.

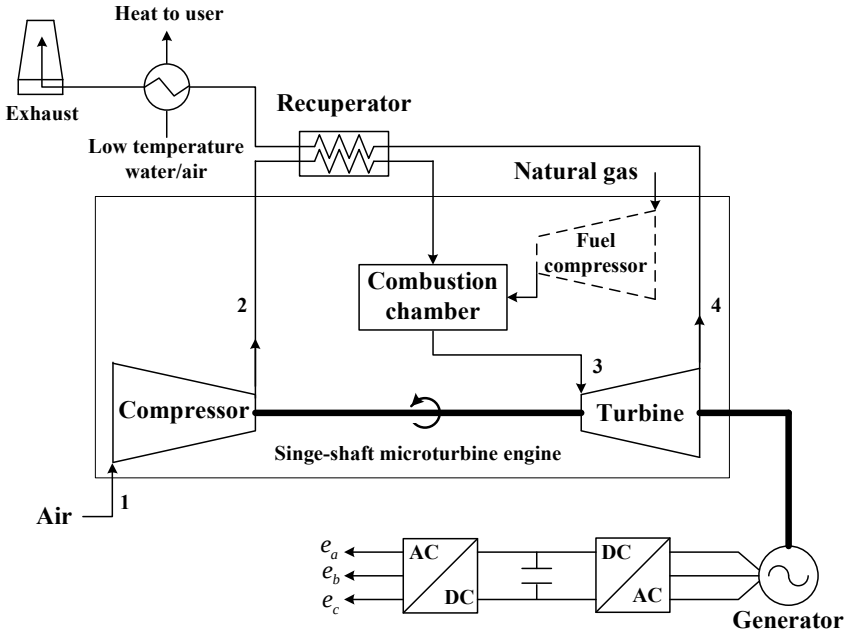

Figure 2.4: The single-shaft microturbine generation system

In the single-shaft microturbine engine a radial flow compressor compresses the inlet air that is then preheated in the recuperator using heat from the turbine exhaust. The recuperator is a heat exchanger that transfers heat from the hot turbine exhaust gas (typically around 1200ºF) to the compressed air (typically around 300ºF) going into the combustor, thereby reducing the fuel needed to heat the compressed air to turbine inlet temperature. Depending on microturbine operating parameters, recuperators can more than double machine efficiency [25]. Next, the heated air from the recuperator mixes with fuel in the combustion chamber and the hot combustion gas expands through the power turbine, which turns both the compressor and the generator. Finally the exhaust of the power turbine is used in the recuperator to preheat the air from the compressor.

As it can be observed from figure 2.4, a SSMT has a gas combustion turbine integrated with an electrical generator that produces electric power while operating at a high speed, ranging from 50000 to 120000 rpm. The rotor is either a two- or four-pole permanent magnet design and the stator is a conventional copper wound design [24]. Electric power is then produced at a very high frequency three-phase voltage ranging from 1500 to 4000 Hz. This high frequency voltage is first converted to DC voltage and then inverted back to a 50 Hz AC voltage by an inverter in order to allow grid interconnection. The power electronics interface provides the protection and interconnection functionalities. In addition it provides power factor correction

and control of the produced power. Among these advantages of the single-shaft design, the gearbox elimination should be mentioned.

In order to assess the dynamic behaviour of microturbines connected to the LV network a detailed nonlinear dynamic model should be used. However, while it is widely accepted that microturbines play an important role in small scale power generation, there is little work on modelling these devices [40, 42].

Modelling of SSMT was reported in [32], where the generic model of the grid connected microturbine converter is developed based on the assumption that there is sufficient energy storage on the DC bus to consider the microturbine as a constant DC voltage source. Other works reported in the literature [40, 44, 45] consider a one way frequency converter AC-DC-AC with a diode rectifier that interfaces the high frequency alternator and the DC bus. Based on the dynamic model of combustion gas turbines, which had been discussed in [46-48], a dynamic model for microturbines is proposed in [24] for purposes of load following performance analysis. More recently, a bidirectional frequency changer interfacing a high-speed PMSM with the grid considering the alternation operation as either motoring or generating was described in [42].

In order to describe the SSMT dynamics with respect to the LV network a microturbine model focused on the microturbine's electric-mechanical behaviour was developed based on the models presented in [24, 42]. This SSMT model is based on the following assumptions:

- The microturbine engine, while small in size, is similar to gas combustion turbines;
- The microturbine is under normal operating conditions. Start-up, shutdown and fast dynamics are not considered, since during these transients the unit is not connected to the grid;
- The recuperator is not included in the model as it is only a heat exchanger to raise engine efficiency. In addition, due to the recuperator's very slow response time, it has little influence on the time scale of dynamic simulations;
- Both the gas turbine temperature and acceleration control are omitted in the turbine model, since they are of no impact under normal conditions;
- Most microturbines do not have governors, so that a governor model is not considered.

Therefore the model of a microturbine unit consists mainly of three parts: The active power control, SSMT engine and the PMSM connected to the AC-DC bidirectional converter. A simplified block diagram is presented in figure 2.5.

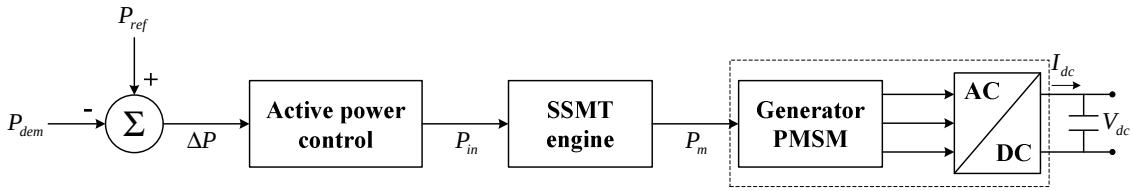

Figure 2.5: Block diagram of the single-shaft microturbine model

The details of the SSMT main parts are presented in the following subsections.

2.3.1.1.1 Active power control

The active power control of the microturbine involves only a real power Proportional-Integral (PI) control function, as depicted in figure 2.6.

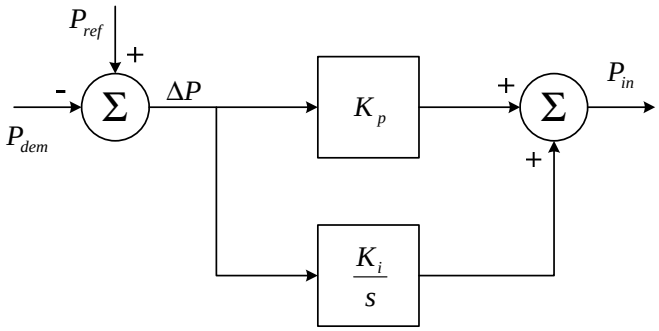

Figure 2.6: Load following control system model

where:

P_{dem} is the demand power;

P_{ref} is the reference power:

P_{in} is the power control variable to be applied to the turbine;

K_p is the proportional gain in the PI controller;

K_i is the integral gain in the PI controller.

The controlled real power, P_{in}, is then applied to the turbine [24].

2.3.1.1.2 SSMT engine

Similar to combustion gas turbine, the microturbine engine mainly involves an air compression section, a recuperator, a combustion chamber and a power turbine. The gas from

the combustion chamber forces the high-pressure compressor turbine that drives the PMSM. Therefore it is more suitable to model the microturbine engine as a simple-cycle single-shaft gas turbine [24].

The GAST turbine-governor model is one of the most commonly used dynamic models of gas turbine units, since it is simple and follows typical modelling guidelines [48]. Thus, for simplicity and wider acceptability, the microturbine engine is modelled as a GAST model without the droop [24], as depicted in figure 2.7.

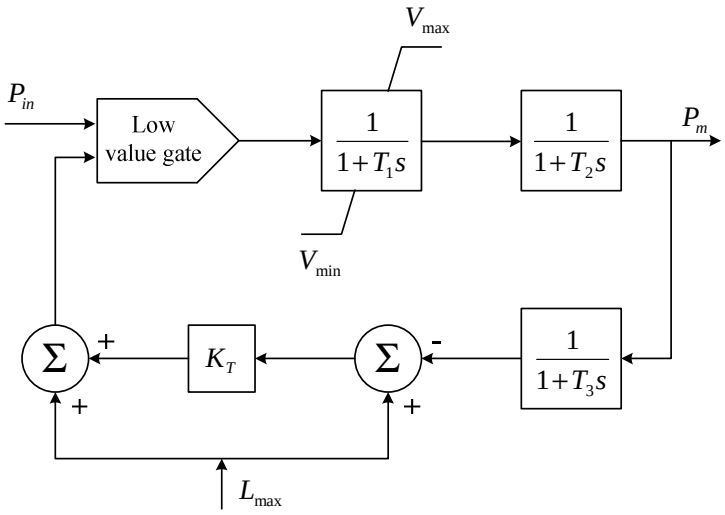

Figure 2.7: Microturbine engine model

where:

P_m is the mechanical power;

T_1 is the fuel system lag time constant 1;

T_2 is the fuel system lag time constant 2;

T_3 is the load limit time constant;

L_{max} is the load limit;

V_{max} is the maximum value position;

V_{min} is the minimum value position;

K_T is the temperature control loop gain.

2.3.1.1.3 PMSM, regulation and control

The model adopted for the electrical generator is a two poles PMSM with a nonsalient rotor. The dynamics of this machine are described by the following equations written in the *dq* reference frame [48]:

Electrical equations:

$$v_d(t) = R_s i_d(t) - p\omega_r L_q i_q(t) + L_d \frac{di_d(t)}{dt} \tag{2.1}$$

$$v_q(t) = R_s i_q(t) + p\omega_r L_d i_d(t) + L_q \frac{di_q(t)}{dt} + p\omega_r \Phi_m \tag{2.2}$$

$$T_e = \frac{3}{2} p\left[\Phi_m i_q + (L_d - L_q) i_d i_q\right] \tag{2.3}$$

Mechanical equations:

$$T_e = J\frac{d\omega_r}{dt} + F\omega_r + T_m;\ \omega_r = J\frac{d\theta_r}{dt};\ T_m = \frac{P_m}{\omega_r} \tag{2.4}$$

where:

L_d, L_q are the d and q axis inductances in H;

R_s is the resistance of the stator windings in Ω;

i_d, i_q are the d and q axis currents in A;

v_d, v_q are the d and q axis voltages in V;

ω_r is the angular velocity of the rotor in $rad/\sec$;

Φ_m is the flux induced by the permanent magnets in the stator windings in Wb;

p is the number of pole pairs;

T_e is the electromagnetic torque;

J is the combined rotor and load inertia in $kg \cdot m^2$;

F is the combined rotor and load viscous friction;

θ_r is the rotor angular position;

T_m is the shaft mechanical torque.

The grid-side converter regulates the DC bus voltage while the machine-side converter controls the PMSM speed and displacement factor. This control structure decouples effectively the two converters control scheme. Therefore issues related to the inverter are addressed in subsection 2.3.2.

Machine-side converter control

The machine-side converter in generating mode operates as a power source with controlled current [48]. This converter controls generator speed and phase between current and voltage at the output of the PMSM [49]. A block diagram of the machine-side converter controller presented in [42] is illustrated in figure 2.8.

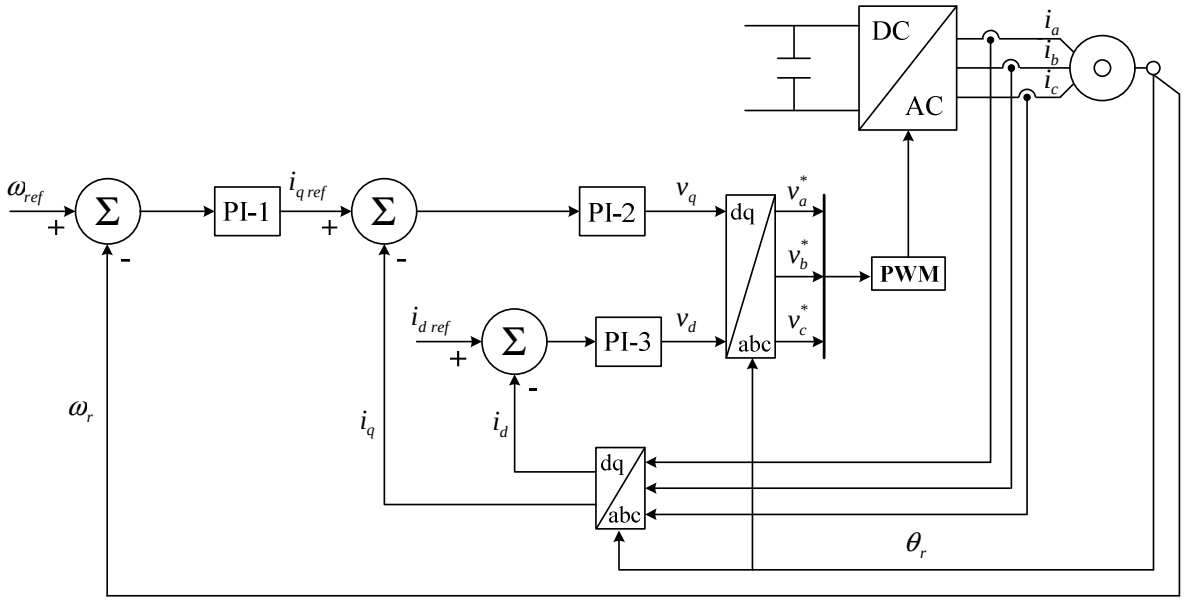

Figure 2.8: Permanent magnet synchronous machine-side converter control

The PI-1 controller that supplies a current component reference, $i_{q\,ref}$, to a second PI controller, PI-2, regulates the microturbine speed. The $i_{d\,ref}$ current component is precalculated and regulated by the PI-3 regulator to ensure a unity displacement factor. The turbine speed reference, ω_{ref}, is also precalculated so that the microturbine operates with optimal efficiency [42].

2.3.1.2 Solid Oxide Fuel cells

As already mentioned previously, fuel cells are an emerging class of small-scale power generation technology. Although the basic principle of fuel cells operation was discovered by William Grove in 1839, the commercial potential of this technology was recognized only in 1960 when fuel cells were successfully applied in the space industry [50]. In 1984, the Office of Transportation Technologies at the US Department of Energy began supporting research and development of fuel cell technology. As a result, commercialization of fuel cells for a variety of applications has been encouraged on by their reliability, efficiency and being environmentally friendly [51].

Actually there are a number of types and configurations of fuel cells, but they all use the same basic principle. A fuel cell consists basically of a cathode (positively charged electrode), an anode (negatively charged electrode) and an electrolyte (non-electrically conductive medium) [28]. A simplified diagram of a SOFC is presented in figure 2.9.

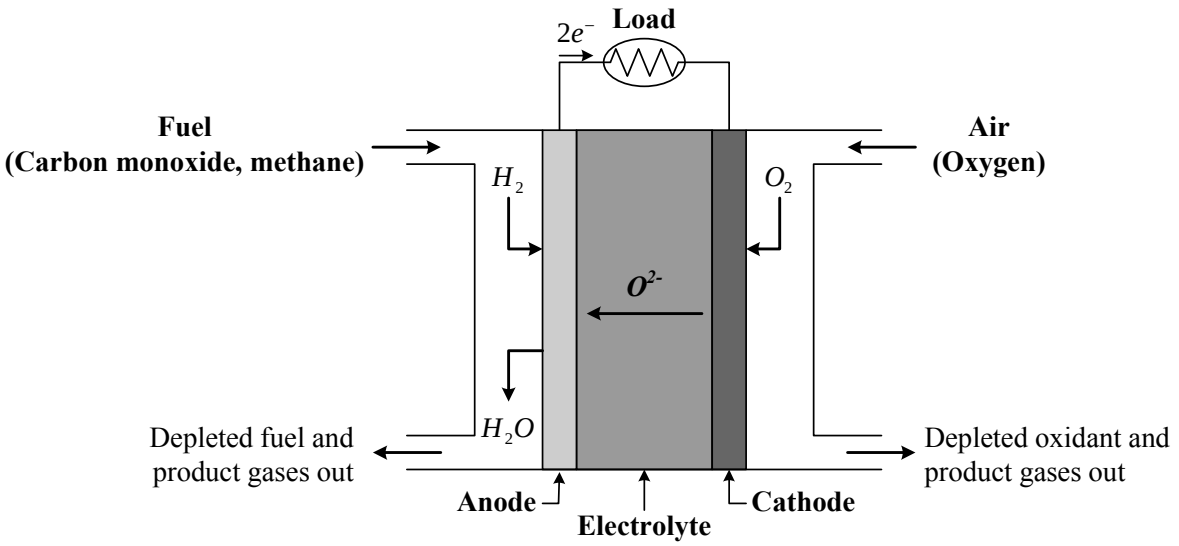

Figure 2.9: Simplified diagram of a solid oxide fuel cell

Carbon monoxide, CO, and hydrocarbons such as methane, CH_4, can be used as fuels in SOFC. However, the CO – shift reaction is chemically favoured if the fuel gas contains water [24, 35]. Thus, the CO – shift reaction is

$$CO + H_2O \rightarrow CO_2 + H_2 \tag{2.5}$$

Therefore, hydrogen obtained from the $CO-$shift reaction and oxygen from the ambient air are fed into the SOFC through its anode and cathode, respectively, where the following electrochemical reactions take place [50]:

$$H_2 + O^{2-} \rightarrow H_2O + 2e^- \text{ (anode)} \tag{2.6}$$

$$\frac{1}{2}O_2 + 2e \rightarrow O^{2-} \text{ (cathode)} \tag{2.7}$$

Then, the overall SOFC reaction is

$$H_2 + \frac{1}{2}O_2 \rightarrow H_2O \tag{2.8}$$

The SOFC electrolyte is a ceramic material, which is an excellent conductor of negatively charged ions, O^{2-}, at high temperatures $(800-1000\,^{o}C)$, allowing the transportation of mobile ions between the electrodes. Moreover, it acts as a separator between hydrogen and oxygen in order to avoid mixing and the resulting direct combustion. As the free electrons cannot move through the electrolyte, they move through the external circuit that connects both anode and cathode. This movement of electrons is then controlled to generate DC electrical energy.

2.3.1.2.1 A SOFC generating system

A generic fuel cell plant involves mainly six basic systems: The fuel cell stack, the fuel processor, the power conditioning subsystems, air management, water management and thermal management. The design of each subsystem must be integrated with the characteristics of the fuel cell stack in order to provide a complete system [51] as can be observed from figure 2.10.

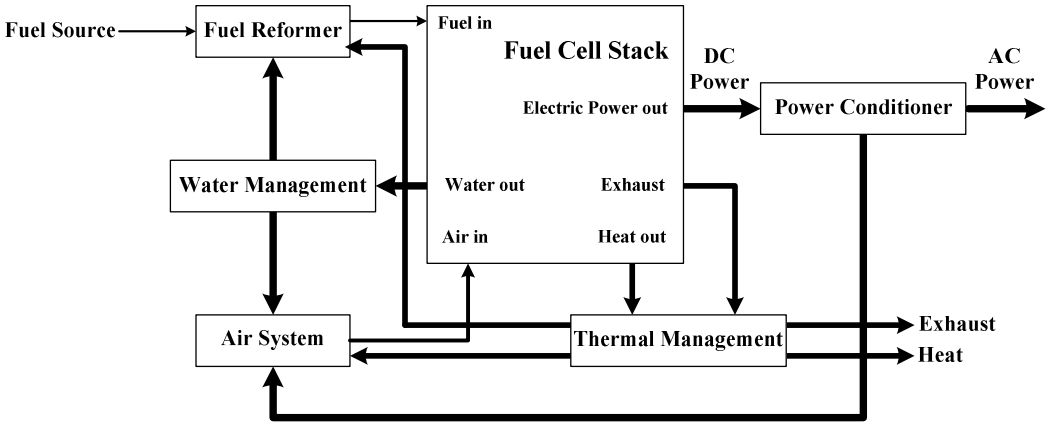

Figure 2.10: Block diagram of a fuel cell generation system

The complete mathematical model of a fuel cell generation system is very difficult to obtain because the fuel cell plant consists of many subsystems, each one interacting with the others in a complex manner, where the electrical, chemical and thermodynamic processes are strongly nonlinear in nature. Moreover, the parameters of such complex models are difficult to obtain [52]. Therefore, in a SOFC generation system, only the following three main parts have been considered for dynamic modelling purposes [22, 24].

- Fuel processor: The fuel processor converts fuel, such as natural gas, to hydrogen rich fuel stream. In the SOFC case, fuel processing from methane, CH_4, or carbon monoxide, CO, consists simply on desulfurizing and preheating the fuel stream before introducing it into the internally reforming anode compartment of the fuel stack.
- Fuel cell stack: The fuel cell stack, also called power section, performs the fuel oxidation and delivers DC power by means of many individual cells combined in stacks. The number of cells is conditioned by the particular power application.
- Power conditioner: Converts the DC to AC power according to the conditions that the network may require. It is addressed further in subsection 2.3.2.

2.3.1.2.2 The SOFC power plant

The cell DC voltage and current depend on the conditions that include fuel flow, oxidant flow, pressure, temperature and the demands of the load circuit. These parameters affect the electrochemical process that ultimately determines the generated power and terminal voltage. Changes in the load circuit or its demand for power change the operating conditions for the

SOFC. For example, an increased demand of power out of the SOFC must eventually be met with increased flow of reactants [29].

The SOFC dynamic model described in [24, 35], involves both the fuel processor and the SOFC dynamic model. In addition, it is based on the following assumptions:

- The gases are ideal;
- The channels that transport gases along the electrodes have a fixed volume, but their lengths are small, so that it is only necessary to define one single pressure value in their interior;
- The exhaust of each channel is via a single orifice. The ratio of pressures between the interior and exterior of the channel is large enough to consider that the orifice is choked;
- The temperature is stable at all times;
- The only source of losses is ohmic, as the working conditions of interest are not close to the upper and lower extremes of current;
- The Nernst equation can be applied.

Under these assumptions, the potential difference between the anode and the cathode is determined using the Nernst equation, as

$$V_{fc} = N_0 \left[E_0 + \frac{RT}{2F} \ln\left(\frac{p_{H_2} \sqrt{p_{O_2}}}{p_{H_2O}} \right) \right] - r I_{fc}^{r} \tag{2.9}$$

where:

V_{fc} is the stack output voltage in V;

N_0 is the number of fuel cells in series collected into the stack;

E_0 is the voltage associated with the reactions free energy in V;

r describes the ohmic losses of the stack in Ω;

p_{H_2}, p_{H_2O} and p_{O_2} are the partial pressures of hydrogen, water and oxygen, respectively in N/m^2;

R is the universal gas constant, $8{,}31\ J/(mol \cdot {}^{o}K)$;

T is the SOFC operating temperature in ${}^{o}K$;

F is the Faraday constant, $96487\ C/mol$;

I_{fc}^{r} is the stack current in A.

The SOFC stack dynamic model is presented in figure 2.11.

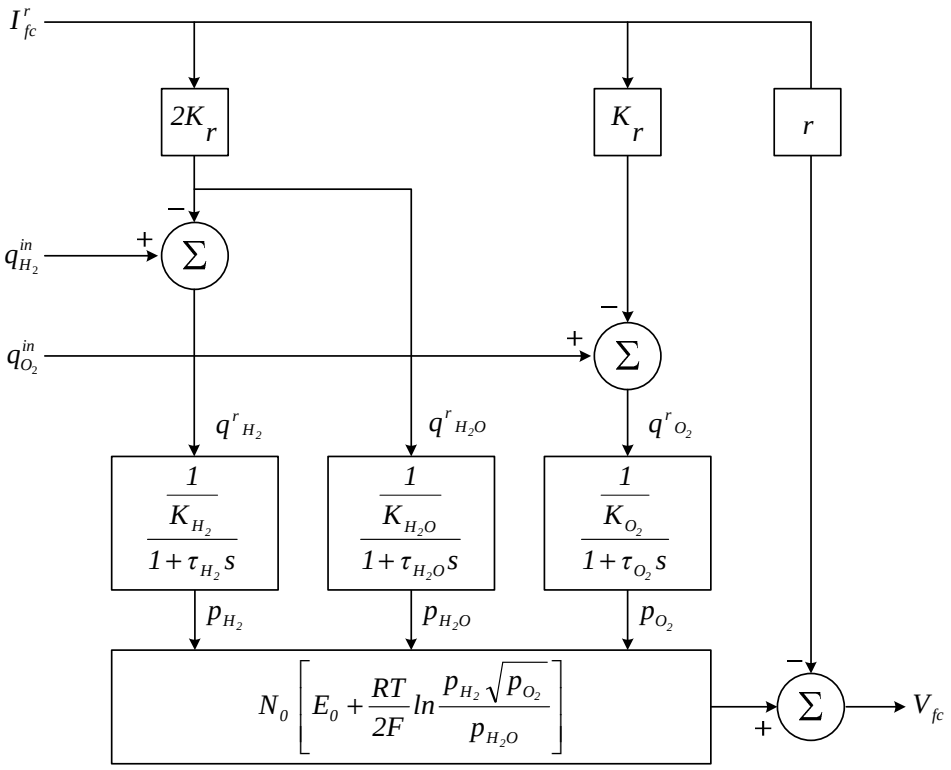

Figure 2.11: SOFC stack dynamic model

where

τ_{H_2}, τ_{H_2O} and τ_{O_2} are time delay constants, which designate the response time of hydrogen, water and oxygen flows, respectively [24] in s;

K_{H_2}, K_{H_2O} and K_{O_2}, denote the molar constants for hydrogen, water and oxygen, respectively in $kmol/(s \cdot atm)$.

$q_{H_2}^{in}$ and $q_{O_2}^{in}$ are the input flows of hydrogen and oxygen, respectively, in $kmol/s$;

$q_{H_2}^{r}$, $q_{H_2O}^{r}$ and $q_{O_2}^{r}$ are the flows that react for hydrogen, water and oxygen, respectively, in $kmol/s$.

Determination of stack current

According to [35], the hydrogen flow that reacts is given by:

$$q_{H_2}^r = \frac{N_0 I_{fc}^r}{2F} = 2K_r I_{fc}^r \tag{2.10}$$

where $K_r = N_0/(4F)$ is a constant defined for modelling purposes in $kmol/(s \cdot A)$.

From (2.8), the values of the flows that react for oxygen and water can be obtained as

$$q_{O_2}^r = \frac{q_{H_2}^r}{2} = K_r I_{fc}^r \tag{2.11}$$

$$q_{H_2O}^r = q_{H_2} = 2K_r I_{fc}^r \tag{2.12}$$

The fuel utilization concept, U_f, is defined as the ratio between the fuel flow that reacts and the fuel flow injected into the SOFC stack, as

$$U_f = \frac{q_{H_2}^r}{q_{H_2}^{in}} \tag{2.13}$$

As described in [35], the desired range of fuel utilization is from 0,8 to 0,9 in order to avoid both overused and underused fuel conditions. An overused fuel condition could lead to permanent damage of the cells due to fuel starvation while underused fuel situations result in unexpectedly high voltages [35]. Therefore, for a certain input hydrogen flow, the demand current of the fuel cell can be limited in the range:

$$\frac{0{,}8 q_{H_2}^{in}}{2K_r} \le I_{fc}^{in} \le \frac{0{,}9 q_{H_2}^{in}}{2K_r} \tag{2.14}$$

The electrical response time in SOFC is generally fast and mainly associated with a speed at which the chemical reaction is capable of restoring the charge that has been drained by the load. This dynamic response is modelled as first order transfer function with a time constant $T_e = 0{,}8\,\text{s}$ [30]. Thus, for a given demanded power, P_{dem}, the SOFC stack current can be obtained as can be observed from figure 2.12.

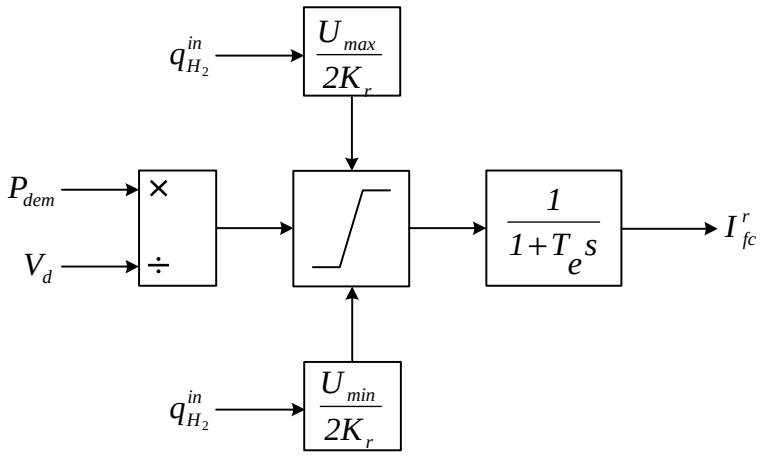

Figure 2.12: SOFC stack current

Determination of hydrogen and oxygen input flows

The input fuel flow can be controlled in order to keep U_f at its optimum value, as

$$q_{H_2}^{in} = \frac{2K_r I_{fc}^r}{U_{opt}} \tag{2.15}$$

where U_{opt} is the optimal value of the fuel utilization, which is typically $0{,}85$ [24].

Hydrogen and oxygen are fed into the stack, where the overall reaction described by (2.8) occurs. It shows that full reaction ratio between hydrogen and oxygen is 2 to 1. However, excess of oxygen should be provided in order to allow its complete reaction with hydrogen while the pressure difference between the anode and the cathode is kept below a certain threshold value. Hence, this means that $r_{H\_O} < 2$, but typically $1 < r_{H\_O} < 1.25$ [24, 53]. Therefore, the input oxygen flow in controlled by the speed control of the air compressor in order to match

$$q_{O_2}^{in} = r_{H\_O} \times q_{H_2}^{in} \tag{2.16}$$

where r_{H_O} is the ratio between hydrogen and oxygen molar flows, which should be kept around $1{,}145$ in order to maintain the SOFC pressure below $4\,kPa$ under normal operation [35].

The chemical response in the fuel processor is usually slow. It is associated with the time to change the chemical reaction parameters after a change in the flow reactants. This dynamic response function is modelled as a first order transfer function with a time constant $T_f = 5\,\mathrm{s}$ [30]. Then, the fuel processor can be modelled as depicted in figure 2.13.

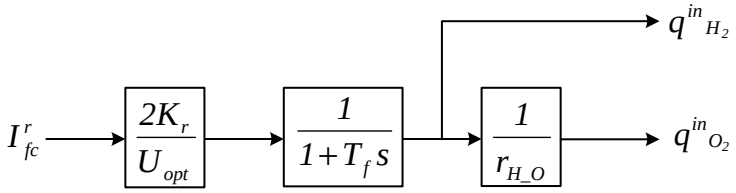

Figure 2.13: SOFC fuel processor block diagram

The active DC power produced by the fuel cell is then given by

$$P_{fc} = V_{fc} I_{fc}^{r} \tag{2.17}$$

With the inverter, the SOFC system can supply not only real power, but also reactive power.

2.3.1.3 Photovoltaic systems with MPPT

The origin of PV energy conversion technology goes back in 1839, when Becquerel first discovered the PV effect. In 1954 the Bell Telephone Laboratories produced the first practical solar cell, a single crystal silicon type cell with energy conversion efficiency up to 6%. In 1955 the Western Electric was the first company to commercialise solar cells, even the photovoltaic technology was mainly used to provide power to earth-orbiting satellites. As the technology improved and cost became more reasonable, photovoltaics were used in terrestrial applications. In the 1980s, PV became a popular power source for consumer electronic devices and for a variety of off-grid applications, including water pumping, rural residential and transportation safety systems. Today, a major international market for photovoltaics is providing power to the billions of people throughout the world who live without electrical service, for applications such as health care facilities, community centres, water delivery, purification systems and rural residences. In developed countries, grid-connected PV systems applications are now being deployed in great numbers not only for residential and commercial applications, but also for either centralized or distribution power generation [54].

2.3.1.3.1 Solar cells and PV modules

Photovoltaic or solar cells, as they are often referred to, are semiconductor devices that convert sunlight into direct current electricity. Silicon cells are the most widespread ones [54]. A typical silicon PV cell is a thin wafer consisting of an ultra-thin layer of phosphorus-doped ($N-$type) silicon on top of a thicker layer of boron-doped ($P-$type) silicon. An electric field is created near the top surface of the cell where these two materials are in contact, called the $P-N$ junction.

When sunlight hits on silicon, the photons will transmit their energy to the valence electrons of the semiconductor allowing it to break their link to atoms. As a result free electrons and gaps can be in motion inside the solid. The electric field provides momentum and direction for both free electrons and gaps, resulting in a flow of current when the cell is connected to an electrical load, as can be observed from figure 2.14 (a).

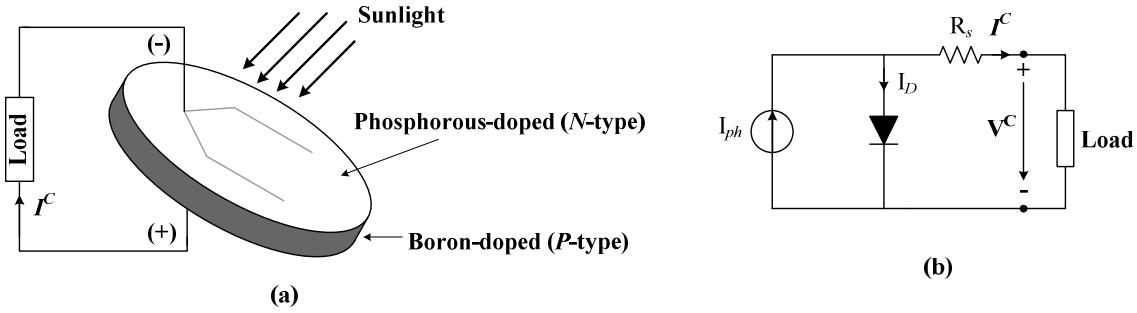

Figure 2.14: A photovoltaic cell: (a) Simplified diagram; (b) Simplified single diode model

Although there are several models of varying complexity to describe the behaviour of a PV cell [55, 56], the most widespread ones are based on the use of lumped circuits, such as single- and double-diode models [23]. The solar cell is commonly represented through a simplified single diode model as depicted in figure 2.14 (b), in which the current source and the diode represent the conversion of solar energy in electrical energy while the series resistance accounts for electrical losses [57]. Thus the solar cell output current can be determined as

$$I^C = I_{ph}\left(1 - e^{\frac{V^C - R_S I^C}{m V_t^C}}\right) \tag{2.18}$$

where m is the diode quality factor ($m=1$ for an ideal diode) and V_t^C is the cell thermal voltage.

Usually manufacturers provide both the short-circuit current, I_{SC}^C, and the open circuit voltage, V_{OC}^C, of PV cells values, which were determined either under STC or NTC.

Table 2.1: Irradiance and ambient temperature in NTC and STC

	NTC	**STC**
Irradiation	$G_{a,ref} = 800\,W/m^2$	$G_{a,0} = 1000\,W/m^2$
Ambient temperature	$T_{a,ref} = 20^oC$	$T_{C,0} = 25^oC$

Figure 2.15 represents a typical current-voltage (I-V) characteristic of a generic solar cell.

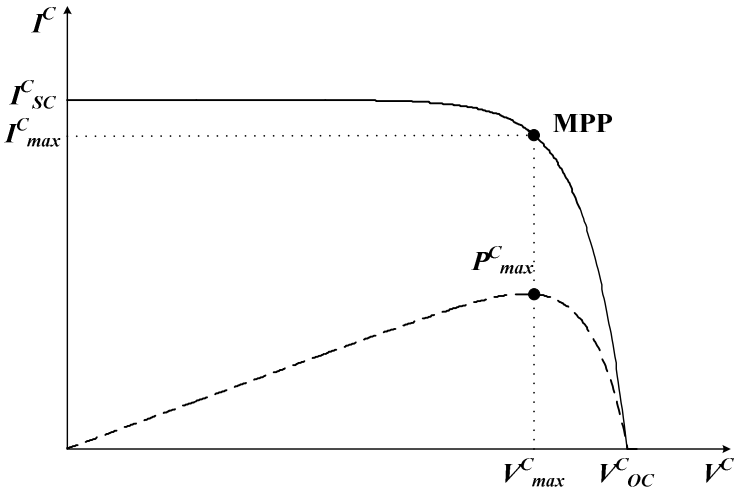

Figure 2.15: A typical I-V characteristic for a solar cell

For arbitrary operating conditions (ambient irradiation, G_a, and cell temperature, T_C), the solar cell can be characterized by the following fundamental parameters:

- Short circuit current, I_{SC}^C;
- Open circuit voltage, V_{OC}^C;
- Maximum power point, MPP;
- Maximum efficiency, $\eta = \frac{P_{\max}}{P_{in}} = \frac{P_{\max} \times V_{\max}}{A \times G_a}$, where A is the cell area;

- Fill factor, $FF = \frac{V_{\max} \times I_{\max}}{V_{OC}^{C} \times I_{SC}^{C}}$;

In practice, the operating conditions of PV systems differ from the STC. Then, under arbitrary operating conditions G_a and T_a, the working temperature of the cells is given by

$$T_C = T_a + G_a \frac{NOTC - 20}{800} \tag{2.19}$$

where $NOTC$ is the normal operating temperature of the cell.

The expression (2.18) can be rewritten as

$$I^C = I_{SC}\left(1 - e^{\frac{V^C - V_{OC}^C - R_S I^C}{m V_t^C}}\right) \tag{2.20}$$

At the cell operating temperature I_{SC}^C, V_{OC}^C and V_t^C are given as follows

$$I_{SC}^C = \frac{G_a}{G_{a,0}}\left[I_{SC,0}^C + \mu_{I_{SC}}\left(T_C - T_{C,0}\right)\right] \tag{2.21}$$

$$V_{OC}^C = V_{OC,0}^C + \mu_{V_{OC}}\left(T_C - T_{C,0}\right) \tag{2.22}$$

$$V_t^C = \frac{KT_C}{q} \tag{2.23}$$

where

$I_{SC,0}^C$ is the cell short-circuit current under STC;

$V_{OC,0}^C$ is the cell open voltage under STC;

$\mu_{I_{SC}}$ is the cell short-circuit current variation coefficient with temperature;

$\mu_{V_{OC}}$ is the cell open circuit voltage variation coefficient with temperature;

K is the Boltzmann constant;

q is the electron charge;

As the output power of a single PV cells is relatively small, they are connected electrically in series and/or parallel circuits, as depicted in figure 2.16, in order to produce a desired I-V characteristic.

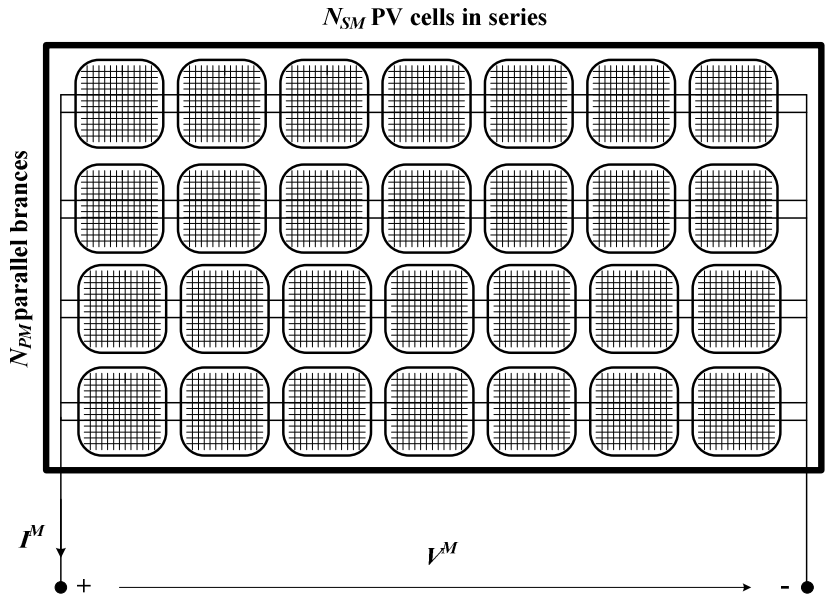

Figure 2.16: A schematic representation of photovoltaic modules

The current and voltage of the PV module can be derived as

$$I^M = N_{PM} I^C \tag{2.24}$$

$$V^M = N_{SM} V^C \tag{2.25}$$

Manufacturers supply only a limited range of modules. Therefore, when designing a PV system, these modules are usually combined into panels, which will be connected together to built up the entire PV array in order to generate the required DC power. The current and voltage of the PV array are calculated as

$$V^A = N_{SA} V^M \tag{2.26}$$

$$I^A = N_{PA} I^M \tag{2.27}$$

where N_{SA} and N_{PA} represent the modules connected in series and parallel, respectively.

2.3.1.3.2 Model of a PV array with integrated MPPT

The grid connected PV system involves two main components:

- The PV array containing $N = N_{SA} \times N_{PA}$ PV modules;

- An inverter to convert the DC power to AC three-phase voltage.

The PV array has an I-V characteristic with similar form to that presented in figure 2.15 for arbitrary operating conditions. Thus a MPPT control scheme is used to assure that the PV array generates the maximum power for all irradiance and temperature values [22]. The typical configuration of a grid connected PV system is presented in figure 2.17.

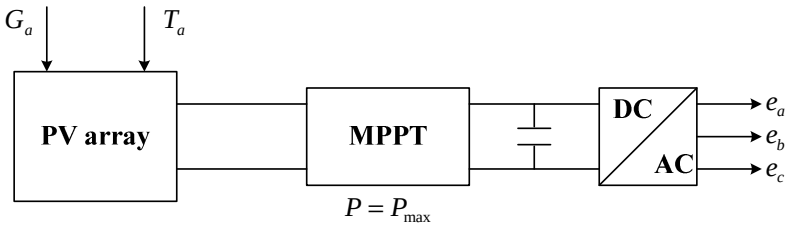

Figure 2.17: A grid-connected PV system

As the PV array with integrated MPPT control is a very simple model [22], it was adopted in this research. However, it is assumed that:

- All the cells of the PV array are identical and they work with the same irradiance and temperature;
- No losses in the PV array with MPPT system;
- The PV array is always working on its maximum power point for a given irradiance and ambient temperature conditions;
- If the irradiance and ambient temperature conditions change, the model instantaneously changes its maximum power point;
- Temperature of the solar cells depends exclusively on the irradiance and ambient temperature.

Under these assumptions the module output power can be estimated using the ambient temperature and the solar irradiance as inputs, as [22, 23]

$$P_{Max}^{M} = \frac{G_a}{G_{a,0}}\left[P_{Max,0}^{M} + \mu P_{Max}\left(T_M - T_{M,0}\right)\right] \tag{2.28}$$

where:

P_{Max}^{M} is the PV module maximum power (W);

$P_{Max,0}^{M}$ is the PV module maximum power STC (W);

$G_{a,0}$ is the irradiance at STC $\left(1000\,W/m^2\right)$;

μP_{Max} is the maximum power variation with module temperature $\left(W/^oC\right)$;

T_M is the module temperature $\left(^oC\right)$;

$T_{M,0}$ is the module temperature at NTC $\left(20^oC\right)$;

For arbitrary operating conditions $T_M = T_a$ and $T_{M,0}$ corresponds to the cell temperature at STC. Then the power output of the plant can be obtained as

$$P_{Max} = N\frac{G_a}{1000}\left[P_{Max,0}^M + \mu P_{Max}\left(T_a + G_a\frac{NOCT-20}{800} - 25\right)\right] \tag{2.29}$$

where N is the number of modules.

2.3.1.4 Wind microgeneration systems

Small wind generators comprise several subsystems that are modelled independently. These subsystems are the aerodynamic, the generator, the mechanical and the power converters in case of variable speed wind turbines [22]. Most of the micro wind generators require an electronic interface for grid connection. However, as already mentioned previously, in this research it was considered that the wind microgeneration system uses a squirrel-cage type of induction generator that is directly connected to the LV grid. Therefore the small wind generator model involves both the wind turbine and the induction generator models, as presented in the following two subsections.

2.3.1.4.1 The wind turbine

Focusing the wind turbine model on the electrical dynamic behaviour of the wind microgeneration system, the mechanical power extracted by the wind turbine from the wind kinetic energy, based on the aerodynamic coefficient curves, is given by [23]:

$$P_m = \frac{1}{2}\rho \times C_p(\lambda,\beta) \times A \times V^3 \tag{2.30}$$

where

P_m is the mechanical power in *Watt* ;

$C_p(\lambda,\beta)$ is the dimensionless performance coefficient;

λ is the tip speed ratio;

β is the pitch angle;

ρ is the air density;

$A=\pi R^2$ is the rotor area;

V is the wind speed;

The mechanical torque can be obtained as

$$T_m=\frac{P_m}{\omega_r} \tag{2.31}$$

where T_m is the mechanical torque in $N\cdot m$ and ω_r is the blade rotating speed in mechanical rad/s.

2.3.1.4.2 The induction machine

For dynamic simulation purposes, it is a common practice to represent the induction machine through a third order model [58]. Then, the per unit induction machine electrical equations with the time represented in seconds can be written as follows

$$\begin{cases} v_{ds}=-R_s i_{ds}+X' i_{qs}+e_d \\ v_{qs}=-R_s i_{qs}-X' i_{ds}+e_q \end{cases} \tag{2.32}$$

$$\begin{cases} \dfrac{de_d}{dt}=-\dfrac{1}{T_0}\left[e_d-\left(X-X'\right)\times i_{qs}\right]+s\times 2\pi f_s\times e_q \\ \dfrac{de_q}{dt}=-\dfrac{1}{T_0}\left[e_q+\left(X-X'\right)\times i_{ds}\right]-s\times 2\pi f_s\times e_d \end{cases} \tag{2.33}$$

where:

v_{sd} and v_{qs} are the per unit rotor voltages;

e_d and e_q are the per unit voltage components behind the transient reactance X';

i_{ds} and i_{qs} are the per unit current components;

X is the per unit open circuit reactance;

T_0 is the transient open-circuit time constant of the induction machine in seconds;

f_s is the system frequency in Hz;

s is the slip;

R_s is the per unit stator resistance.

The transient open-circuit time constant is given as

$$T_0 = \frac{L_r + L_m}{2\pi f_{base} \times R_r} \tag{2.34}$$

where R_r is the per unit rotor resistance. The transient reactance, X', as well as the open circuit reactance, X, in per unit are defined as

$$X' = X_s + \frac{X_r \times X_m}{X_r + X_m} \tag{2.35}$$

$$X = X_s + X_m \tag{2.36}$$

where X_s and X_r represent the per unit leakage reactances for the stator and rotor windings, respectively, and X_m is the per unit magnetising reactance.

Concerning the slip, it can be derived as follows

$$s = 1 - \frac{\omega_r}{\omega_s} \tag{2.37}$$

where ω_s is the per unit stator angular frequency.

In order to complete the induction machine model, it is necessary to combine the differential equations describing the electrical voltage and current components of the machine with the rotor swing equation, as

$$\frac{d\omega_r}{dt} = \frac{1}{J}\left(T_m - T_e - D\omega_r\right) \tag{2.38}$$

where J is the moment machine inertia, D is the damping and T_e is the per unit electromechanical torque, which is given as

$$T_e = e_d i_{ds} + e_q i_{qs} \tag{2.39}$$

2.3.2 Storage devices

As mentioned previously, when a MG is operated in islanded mode, the power balance during transients must be provided by energy storage devices: MG main storage installed in the LV bus of the MV/LV transformer and frequently batteries connected to the DC bus of several MS [6, 9, 10, 18]. Flywheels are very promising units to be used as the MG main storage device. Unlike batteries, flywheel's life is almost independent of the depth of discharge and can operate equally well on either frequently shallow discharges or on very deep discharges [59].

Considering the time period under analysis, storage devices, such as flywheels and batteries, are modelled as constant DC voltage sources using power electronic interfaces to be coupled with the electrical network (AC/DC/AC converters for flywheels and DC/AC inverters for batteries). These devices act as controllable AC voltage sources, with very fast output characteristics, to face sudden system changes such as in load-following situations [6, 9].

In spite of acting as voltage sources, these devices have physical limitations and thus a finite capacity for storing energy. The active power is injected into the MG using a proportional to frequency deviation control approach with a specified droop characteristic; the energy delivered to grid is evaluated as the time integral of the active power injected by the storage device for the simulation time considered [6].

2.3.3 Inverter modelling

In a MG environment, the inverter interface model can be derived according to two possible control strategies [11]:

- PQ inverter control: the inverter is used to supply a given active and reactive power according to a given set-point;
- Voltage Source Inverter control logic: the inverter is controlled to "feed" the load with pre-defined values for voltage and frequency. Depending on the load, the VSI real and

reactive power output is defined.

The control functions used to model both PQ inverter control and VSI control for purposes of MG dynamic behaviour analysis are described in the following two subsections.

2.3.3.1 PQ inverter control

The PQ inverter injects the power available at its input into the grid. The reactive power injected corresponds to a pre-specified value, defined locally using a local control loop or centrally from the MGCC. Thus, this control scheme was implemented as a current-controlled voltage source [6], as can be observed from figure 2.18.

Current components in phase, i_{act}, and in quadrature, i_{react}, are computed based on a method presented in [60] for power calculation in single-phase inverters. Power variations in the MS induce a DC link voltage error, which is corrected via the PI-1 regulator by adjusting the magnitude of the active current output delivered to the grid. The reactive power output is controlled via the PI-2 regulator by adjusting the magnitude of the inverter reactive current output.

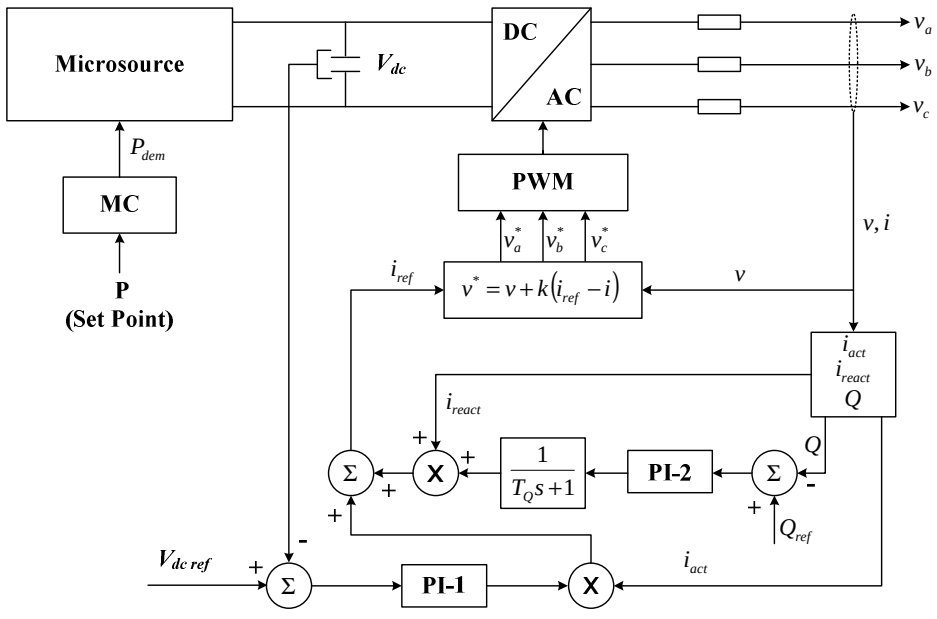

Figure 2.18. PQ inverter control system

This inverter can be operated with a unit power factor or receive a set-point (locally or from the MGCC) for the output reactive power.

2.3.3.2 Voltage source inverter control

The voltage source inverter control scheme emulates the behaviour of a synchronous machine, controlling both voltage and frequency of the AC system [8, 15, 61]. The VSI acts as a voltage source with the magnitude and frequency of the output voltage controlled through droops as follows [6, 9]:

$$\omega = \omega_0 - k_P \times P \tag{2.40}$$

$$V = V_0 - k_Q \times Q \tag{2.41}$$

where P and Q are the inverter active and reactive power outputs, k_P and k_Q are the droop slopes (positive quantities), ω_0 and V_0 are the idle values of the angular frequency and voltage, which correspond to the inverter angular frequency and terminal voltage at no load conditions, respectively.

When a VSI is interconnected with a stiff AC system, characterized by an angular frequency ω_{grid} and terminal voltage V_{grid}, both voltage and frequency references are externally imposed [8]. In this case, the desired output powers P_1 and Q_1 can be obtained in the VSI output by adjusting the idle values of the angular frequency and voltage as follows:

$$\omega_{01} = \omega_{grid} + k_P \times P_1 \tag{2.42}$$

$$V_{01} = V_{grid} + k_Q \times Q_1 \tag{2.43}$$

Figure 2.19 illustrates this procedure for the idle frequency case [10].

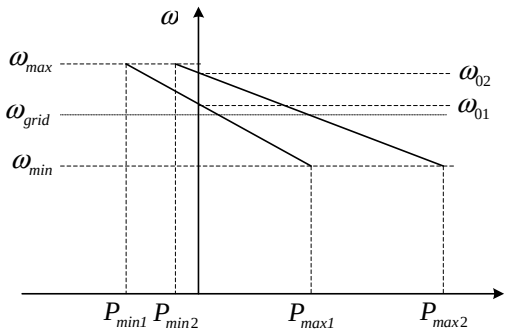

Figure 2.19. Frequency versus active power droops

If a cluster of VSI operates in stand alone AC system, frequency variations leads automatically to power sharing, such that for a system with n VSI, the following equality stands:

$$\Delta P = \sum_{i=1}^{n} \Delta P_i \tag{2.44}$$

where ΔP_i is the power variation in the $i-th$ VSI. The frequency variation can be computed as [6]:

$$\Delta\omega = \omega_{0i} - k_{Pi} \times P_i - \left[\omega_{0i} - k_{Pi} \times \left(P_i + \Delta P_i\right)\right] = k_{Pi} \times \Delta P_i \tag{2.45}$$

Similar considerations can be made for the voltage/reactive power VSI control mode based on droops [6, 15, 61]. However, as voltage has local characteristics, network cable impedances do not allow a precise sharing of reactive power among VSI [62].

Figure 2.20 represents a three phase balanced model of a VSI implementing the described droop concepts [10]. The VSI output voltage and current are measured to compute active and reactive power levels. This measuring stage introduces a delay that corresponds to a decoupling, performed through the Decoupling transfer functions presented in figure 2.20.

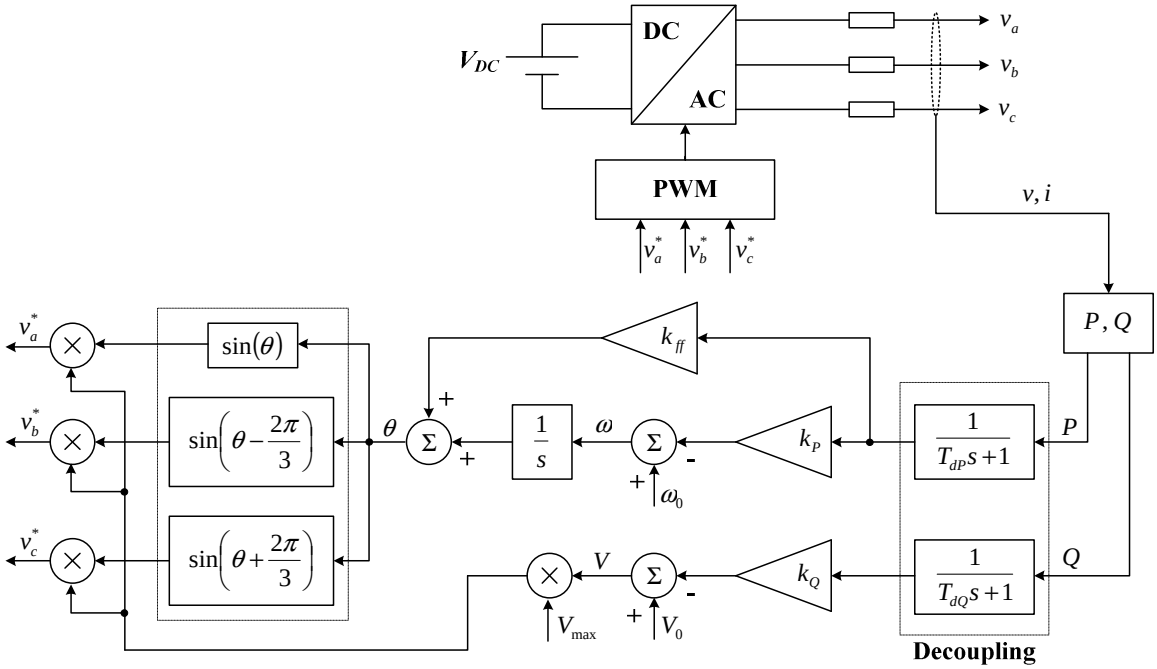

Figure 2.20. VSI three-phase control model

The active power determines the frequency of the output voltage by the active/frequency droop, k_P. Similarly, the reactive power determines the magnitude of the output voltage by the reactive power droop, k_Q. A phase feed-forward control was included for stability purposes [62], corresponding to the K_{ff} in figure 2.20. The output voltages are the reference signals that control the VSI switching sequence using a PWM modulation technique.

2.3.4 LV network and load modelling

As stated before, the simulation of MG dynamic behaviour was performed considering only three-phase balanced operation. Thus, the LV grid is modelled as a balanced network through the corresponding nodal admittance matrix. LV loads are represented as constant impedances. The LV network and load modelling are addressed later, in chapter 6, where a more detailed description is presented.

2.4 Control strategies for MicroGrid operation

If a cluster of MS is operated within a MG and the main power supply (the MV network) is available, all the inverters can be operated in PQ mode, because there are voltage and frequency references. In this case, a sudden disconnection of the main power supply would lead to the loss of the MG, since there would be no possibility for load/generation balancing, and therefore for frequency and voltage control. However, if a VSI is used to provide a reference for frequency it is thus possible to operate the MG in islanded mode and a smooth moving to islanded operation can be performed without changing the control mode of any inverter [6, 8].

As already mentioned previously, the VSI can react to network disturbances based only on information available at its terminals. This working principle provides a primary voltage and frequency regulation in the islanded MG. After identifying the key solution for MG islanded operation, two main control strategies are possible, as identified from the research developed within the MicroGrids project [6, 7, 10, 18, 19, 21]:

- Single Master Operation;
- Multi Master Operation.

In both cases, a convenient secondary load-frequency and voltage-reactive power control during islanded operation must be considered to be installed in controllable MS.

2.4.1 Single master operation

In this case, a VSI – acting as master – can be used as voltage reference when the main power supply is lost; all the other inverters can then be operated in PQ mode (slaves). Droop settings of the VSI can be modified by the MGCC based on information about the state of charge of the storage device, according to the operating conditions and in order to avoid large frequency excursions and minimize load curtailment [6]. This SMO control scheme is presented in figure 2.21.

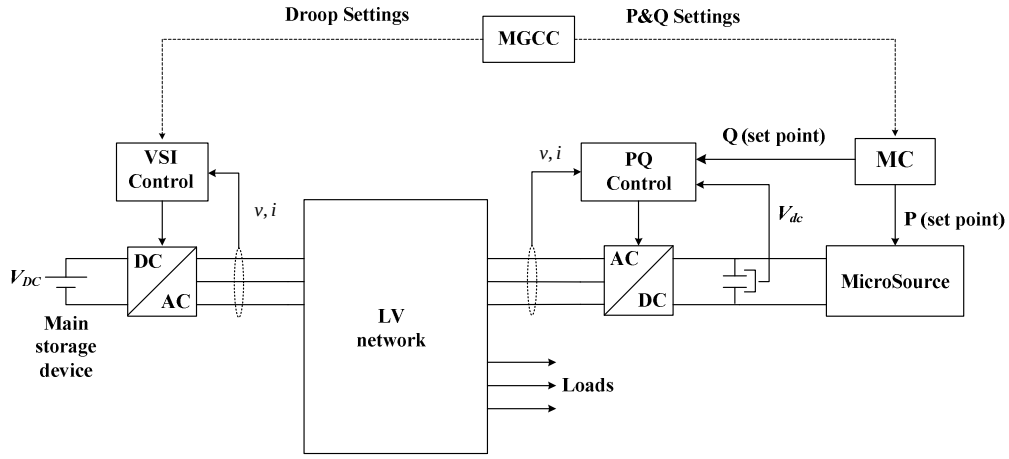

Figure 2.21. Control scheme for single master operation

The SMO control strategy should be used when the MG is operated in interconnected mode. Thus, if a fault occurs on the upstream network, a smooth moving of the MG operation from interconnected to islanded mode can be assured. Therefore, the MG is able for participating in primary frequency control of the MMG being operated autonomously.

2.4.2 Multi master operation

In a multi master approach, several inverters are operating as VSI with pre-defined frequency/active power and voltage/reactive power characteristics [6], as illustrated in figure 2.22. Eventually, other PQ-controlled inverters may also coexist.

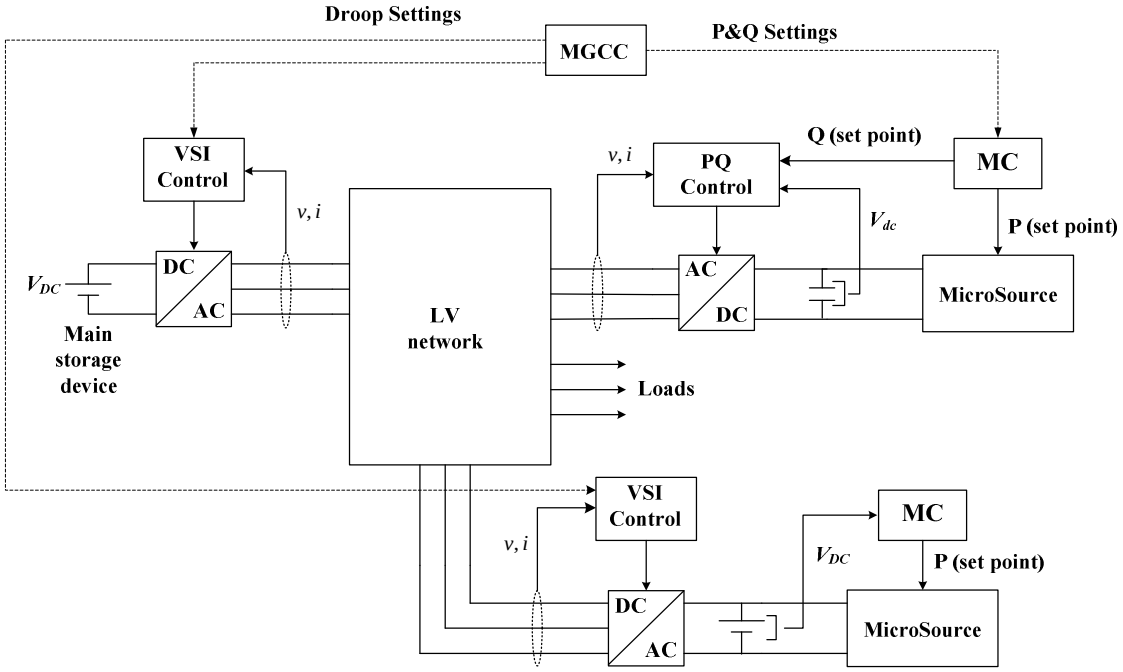

Figure 2.22. Control scheme for multi master operation

This control strategy can be used in MG islanding, when several MS have storage capabilities connected to the inverter DC link and is most relevant in the case of the definition of black start procedures at the LV microgrid, assuming that this MG is separated from the rest of the network [9, 10].

2.4.3 Secondary load frequency control

Whenever the MG is operated in islanded mode, a steady state deviation from the nominal frequency will be observed following transients. As a result of the droop control implemented in the VSI, the main storage unit will support all power deviations by injecting or absorbing some amount of active power proportionally to the MG frequency deviation [6, 17].

Although acting as a voltage source, storage devices have a finite capacity for storing energy due to physical limitations. Therefore, the system frequency should be restored to the nominal value, ω_0, in order to the VSI active power returns to zero. For this purpose, two main secondary control strategies can be followed: local secondary control using a PI controller at each controllable MS or centralized secondary control mastered by the MGCC. In both cases,

target values for active power outputs of the primary energy sources are defined based on the frequency deviation error [6], as depicted in figure 2.23.

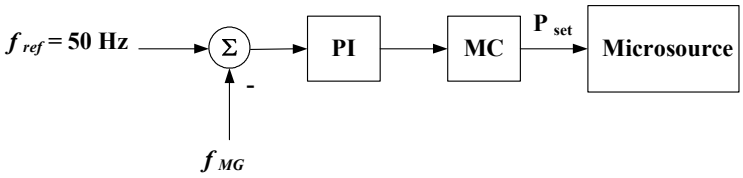

Figure 2.23. Local secondary load frequency control for controllable microsources

For SMO, the target value is directly an active power set-point to the MC of a controllable MS as can be seen from figure 2.21. The MG operated under a SMO control strategy, provides also secondary load frequency control for MMG being operated autonomously.

For MMO, the target value can be both an active power set-point for a controllable MS connected to a PQ inverter or a new value for the idle frequency of a VSI.

Reactive power set-points can be sent to MC by the MGCC based on information about the MG load profile in order to optimize the voltage/reactive power control.

2.5 Summary and main conclusions

In this chapter both MicroGrid and Multi-MicroGrid concepts were presented as well as their corresponding advanced hierarchical control architectures. Suitable models to study the microgeneration systems and their inverter control schemes were also presented and discussed.

Afterwards, control strategies for MG operation were also described. The SMO control strategy can be commonly used when the MG is operated in interconnected mode, thereby assuring a smooth MG moving to islanded operation if a fault occurs in the upstream MV network. Then, when the MMG is operated in islanded mode, the MG will participate in primary frequency control through the VSI control of the MG main storage device, and, in addition, will provide secondary load frequency control by means of the controllable microsources. This physical knowledge is exploited in chapter 4 as prior knowledge to derive dynamic equivalents for MG using system identification techniques.

Chapter 3
Dynamic Equivalencing Techniques

3.1 Introduction

With the enhanced stability requirements to operate power systems in a reliable manner, system dynamic behaviour needs to be carefully studied online and offline, which includes system stability, dynamic security assessment, coordinating system control in a global manner, etc [63]. Concerning offline studies, transient stability analysis plays an important role in planning and operation. Such studies are performed almost exclusively by means of time domain simulations using numerical integration to solve the nonlinear differential equations that describe the power systems dynamics. With the growth in size and complexity of such systems, the cost to perform dynamic behaviour studies has increased significantly [64].

Although the computer technology advancements and the application of efficient numerical methods, detailed power system analysis may thus be too large and too complex, requiring a very high computational effort as well as excessive computation times, particularly when a large number of scenarios have to be studied [65]. Therefore reducing the problem to a solvable size and, at the same time, improving the solution speed without significantly loss of accuracy has been considered an important goal to overcome the difficulties related to dynamic behaviour analysis. As the main analysis are usually focused on a specific part of the power system, it has been a common practice to replace those subsystems that are not of primary interest by suitable dynamic equivalents.

Owing to the dimension of large interconnected power systems it is neither practical nor necessary to perform dynamic studies using detailed models of their components. At high voltage levels it is necessary to obtain manageable models suitable for simulations and analysis, allowing to interpret the results and translate them into operating guidelines or planning recommendations. In addition, the complete structure of the neighbourhood networks as well as the parameters of their components are not known in detail. On the other hand, as the main analysis are focused on a specified portion of the interconnected systems, the subsystems

that are not of primary interest do not need too many details and therefore can be accurately approximated through suitable dynamic equivalents.

In general, when performing dynamic studies, the whole power system is divided into two parts, called the study or internal subsystem and the external subsystem. The study subsystem model is retained in detail since the response of this part of the system is of direct interest and all disturbances and configuration changes are assumed to occur here. The remainder subsystem is the part of the system to be simplified and subsequently to be replaced by the reduced order model. Then dynamic equivalencing concerns to the process of reducing the complexity of the entire power system network to a computationally feasible size while maintaining a reasonable level of accuracy regarding the approximation of the external subsystem relevant dynamics with respect to the study subsystem. Obviously, the dynamics to retain will depend on both the application and the use of the dynamic equivalent.

A dynamic equivalent is thus a reduced order model of the external subsystem that allows to reduce the storage and the computational burden that arises from dynamic simulation. In turn, the entire power system reduced order model is commonly referred in the literature as the equivalent model. It should also be noted that in any equivalencing procedure it is always important that the equivalent model preserves the important features of the original system when it is represented through its detailed model [66].

In what concerns to develop suitable dynamic equivalents for MG, the methodology to be followed should preserve these aims described previously. However, the main theoretical concepts behind the procedures commonly used to build dynamic equivalents for conventional power systems should be assessed, in order to determine its applicability to MG or even to exploit their main features for these purpose. These main questions are discussed in this chapter.

Therefore, the background of power system dynamic equivalents is presented in section 3.2 and the classical techniques that have been used to build dynamic equivalents for conventional power systems are described in section 3.3. Afterwards, in section 3.4, the main requirements arising from the widespread of DG into distribution networks are pointed out and the corresponding solutions concerning dynamic equivalents that represent the relevant dynamics of distribution systems integrating a large capacity of DG with respect to the high voltage level are addressed. In section 3.5, the applicability of the existing methodologies to build dynamic equivalents for MG is discussed. Finally, the main conclusions are presented in section 3.6.

3.2 Background of dynamic equivalents for large power systems

Dynamic equivalents for large power systems were initially defined based on empirical methods, such as replacement of all the generators within the external subsystem by one equivalent generator [67] or determination of equivalent generators, one of each boundary bus, from an empirical distribution of the active powers and inertias of the external subsystem generators [68]. Both methods are based on the ideas proposed by Ward [69].

The methods reported later in the literature to derive dynamic equivalents are based mainly on modal analysis [70-72] or on the so-called coherency property, which means that coherent generators tend to swing together during transient periods [73-75]. There are also works with the aim of unifying the theoretical basis of calculations of dynamic equivalents based on both coherency and modal analysis [76].

Although the development of dynamic equivalencing techniques has a long history, few analysis tools have been available, mainly because the rigorous requirements to handle the complexity of modern interconnected power systems [77]. As a result, industry experience in the area of dynamic equivalencing is limited [63, 66, 78-80] and often reductions are done using heuristic methods [77].

Early work in power systems dynamic equivalents includes the development of modal equivalencing techniques [72, 81-83]. Methods based on modal analysis suggest that those modes of the system that are not easily affected by the disturbances can be eliminated. Since it is difficult to find these modes and additional modifications have to be made in the original dynamic simulation programs in order to make use of the state matrix form of the equivalent model, methods based on modal analysis have not been widely applied [84].

Alternative approaches are based on the coherency concept. Following a disturbance occurring in the study subsystem, coherency between generators belonging to the external subsystem should be recognized in order to subsequently form groups of coherent generators. Each one of these groups will be further replaced by one equivalent machine. The concept of coherency was previously used by Chang and Adibi [73]. A coherency based approach was developed further by Podmore [75] in the late of 1970s and integrated in Dynamic Equivalencing software package – DYNEQ - developed under the American Electric Power Research Institute - EPRI [77].

Taking into account that coherency is an observed phenomenon and coherency properties between generators depend on both the disturbance nature and location, some previous attempts to recognize coherency between generators were heuristically based [85]. Lee and Schweppe suggested in [86] a pattern recognition approach based on criteria involving generator inertia, admittance and machine acceleration to identify coherent generators [87]. Because of the lack of accuracy and consistency in the heuristic methods, the approach proposed by Podmore [75] involves numerically solving the simplified and linearized power system equations and then processing the swing curves through a clustering algorithm in order to determine coherent groups of generators. Although this approach had experimented some applications, several weaknesses have been pointed out, since for a large power system, time domain simulations require a considerable computational effort and generally the coherent groups were disturbance dependent. Therefore confidence was limited [66].

In order to overcome these limitations, several research effort resulted in the slow coherency or two-times-scale method proposed in [88] in the early 1980s. It was further improved in [89] and has been a commonly adopted method for coherency identification [44, 65]. This is based on singular perturbations theory and combines the insights of both modal and coherency analysis to find groups of coherent machines [90-92]. In 1993s, Ontario Hydro developed a new EPRI dynamic equivalencing program, the DYNRED [48, 77], which included the techniques from the DYNEQ program and the slow coherency method [93].

DYNRED found many successful applications in large power systems. An evaluation of the performance of its dynamic equivalencing techniques in given in [66, 77] and provides a discussion of several factors that affect the quality of dynamic equivalents; coherency identification is the key step in the reduction procedure. In fact, this subject has been investigated extensively in the past and, as a result, many techniques have been reported in the literature [44, 64, 65, 76, 86, 87, 91-112]. Most of them used the linearized power system model to obtain some coherency identification criteria without solving the swing equations. After define and compute the coherency measure a suitable clustering algorithm is then applied to derive groups of coherent generators [64, 87, 113].

Coherency measures, such as the RMS [76, 112] and those based on the electromechanical distance measure [106, 114] have been proposed to identify groups of coherent generators. Several other methods are also reported in the literature, based on the rate of change of kinetic energy of the faulted system [109] and evaluation of the Lyapunov function [105]. This late

method was improved in [98], where coherency of generators is determined through some proposed coherency identification criteria based on critical energy required for system separation. Other authors [111] proposed the computation of the system singular point or the unstable equilibrium point to recognize coherent generators. This method was significantly improved in [99] through a combination of faulted system dynamics, unstable equilibrium points and electrical coupling measure between generators. The faulted generator angles are estimated through a Taylor series expansion [97]. More recently, several authors proposed other coherency identification methods based on neural networks [87, 103], fuzzy sets [110], epsilon decomposition [94] and on selective modal analysis [107], such as a synchronic modal equivalencing technique presented in [108].

Taking into account that many coherency methods do not consider the effect of voltage variation on the coherency of generators due to the weak coupling between real power and voltage, new enhancement techniques for coherency identification are reported in [44]. The accuracy of dynamic reduction techniques was further improved through incorporation of both voltage and rotor dynamics [65]. In an attempt to avoid the burden to find modes as the size of the power system becomes large, methods that allow to identify coherent groups of generators directly from the system state matrix were presented in [101, 115].

Once coherent groups of generators in a power system are identified, generators in the same group are aggregated and reduced to a single equivalent generator. DYNRED contains several weighted-average and least squares frequency domain algorithms to compute the parameters of the aggregated generator as well as its control models [116]. The simulation program Network Torsion Machine Control - NETOMAC [117] integrates an optimization/identification mode [118] for solving several optimization tasks and parameter estimation problems. With a modified Gauss-Newton algorithm readily integrated, network reduction can be executed under the dynamic conditions either in time or frequency domain in coping with the nonlinear nature of the system involved. In addition a newly developed dynamic coherency approach determines coherent generators on nonlinear basis in the time domain using cross correlation techniques, taking dynamic characteristics of the system involved into consideration [63].

More recently ANN based models were proposed in [119, 120] to directly derive dynamic equivalents from measurements at points connecting both the study and external subsystems. In these works a neural network is used to extract states of the reduced order equivalent and

another neural network is used to predict the new states values of the external system. Similar methodologies successfully applied to derive dynamic equivalents for large power systems are also presented in [121, 122]. In these works the external system is represented through an input-output formulation and only one neural network is used to predict its dynamic behaviour.

Although the research in dynamic equivalencing area dates back to 1960s, few mature industrial analysis tools have been available, mainly because of the rigorous requirements to handle the complexity of modern interconnected power systems [77]. In fact three decades of research effort resulted in two industrial software packages, DYRED and NETOMAC.

From the background of the existing techniques to derive dynamic equivalents for large power systems, one can say that with the exception of some earlier heuristic methods, many of the proposed techniques can basically be related to the following categories: Modal analysis, coherency based approaches and techniques that allow to derive dynamic equivalents from measurements also called system identification in [120, 121, 123, 124]. A general overview of these techniques is presented in the following subsections.

3.3 Conventional dynamic equivalencing techniques

Conventional dynamic equivalencing techniques involve those methodologies that have been widely used to build dynamic equivalents for conventional power systems. Although coherency based approaches have been very popular, most often coherency recognition is performed using modal analysis, as described in the following subsections.

3.3.1 Modal analysis

Modal analysis approaches are traditionally based on a linearized description of the external subsystem dynamic model,

$$\begin{cases} \dfrac{d}{dt}x(t) = Ax(t) + Bu(t) \\ y(t) = Cx(t) + Du(t) \end{cases} \tag{3.1}$$

which is obtained through the Taylor expansion of the classical state space model around a steady state operating point. After linearization dominant modes are identified and the model reduction is achieved by neglecting the non-dominant modes.

Therefore, modal analysis techniques attempt to reduce the size of the complex nonlinear representation of the external subsystem by building a reduced order linear state space equivalent model, while the detailed representation of the study subsystem is retained, as schematically represented in figure 3.1.

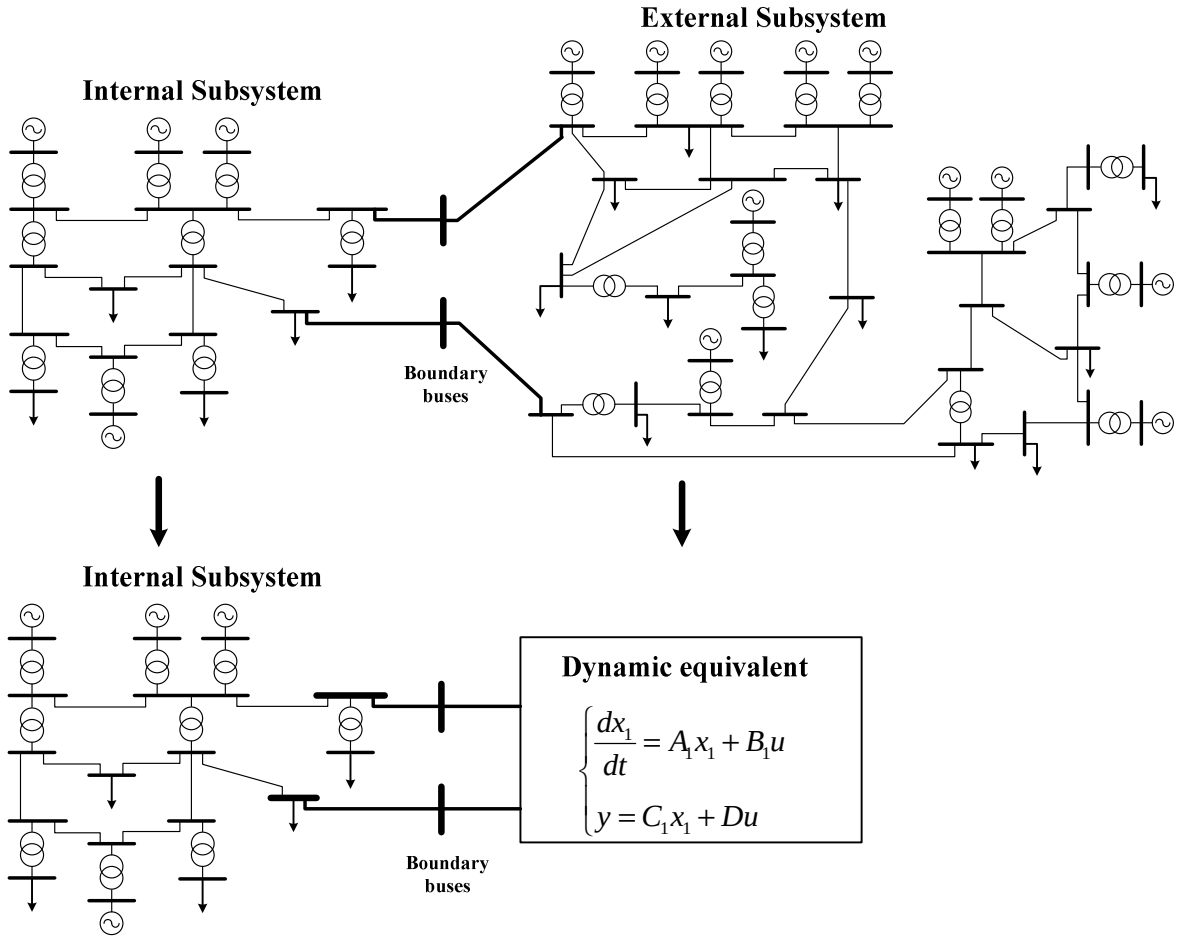

Figure 3.1: Dynamic equivalencing based on modal analysis approaches

The dynamic equivalent is then a reduced order linear state space model, often called a modal equivalent [125] or simply a reduced order model [126].

Modal approaches can be interpreted as performing a given transformation on the system matrices yielding

$$\begin{bmatrix} [A] & [B] \\ [C] & [D] \end{bmatrix} = \begin{bmatrix} \begin{bmatrix} A_1 & 0 \\ 0 & A_2 \end{bmatrix} & \begin{bmatrix} B_1 \\ B_2 \end{bmatrix} \\ \begin{bmatrix} C_1 & C_2 \end{bmatrix} & [D] \end{bmatrix} \tag{3.2}$$

where A_1 and A_2 contain the r dominant and respectively the $(n-r)$ non-dominant modes of A, defining then the reduced model on the basis of this partitioned representation, as represented in figure 3.1.

As modal analysis methods are typically based on the linearization of the external subsystem, the obtained dynamic equivalents are not directly integrated into most standard simulation programs, as already mentioned previously. Thus they require data converting from/to a simulation program for receiving the established operating point and for verifying the results. Although the inputs and outputs of the linearized model vary from one approach to the other, a typical methodology is based on the Norton model, in which boundary bus voltages are used as inputs to the linear model and the outputs are injected currents [127].

Depending on the external system properties that have to be retained in the reduced order model, different model reduction methodologies can be applied. Hence, there are techniques based on directly identifying and preserving certain modes of interest – Modal truncation [71, 72, 128, 129] – or based on the SVD, such as balanced realizations [130], focusing on the observability and controllability properties of the system, and optimal Hankel-norm approximation [131], which tries to achieve a compromise between a small worst case error and a small energy error [132]. Singular perturbations theory [133, 134], exploits the different time scales of power systems. Another family of modal analysis approaches is the moment matching methods in which the property of interest is the leading coefficients of a power series expansion of the transfer function of the reduced system around an user defined point that have to match those of the original system transfer function [126].

Modal analysis methods have been applied to derive dynamic equivalents for wind parks under transient situations. These reduced order models are able to retain the wind park relevant dynamics with respect to the utility grid, taking into account the effect of wind speed fluctuations, which constitute small perturbations around a steady state operating point [132]. Singular perturbations theory presented better performance [135].

More recently, in [136], the balanced realizations technique was used to build dynamic equivalents for a small distribution network containing different DG units suitable to describe

its dynamic behaviour with impact to the high voltage level. As the electrical distance from the fault to distribution network is significant, it is considered that all dynamic elements connected to the distribution network can be represented with sufficient accuracy by linear models.

A brief overview of the most commonly used linear based approaches is given in the following subsections.

3.3.1.1 Modal truncation

Modal truncation is one of the first reduction schemes that has been applied to electric power systems [72]. This technique is based on pole location of the linear system and the reduced order model is then obtained by neglecting the fast decay poles and/or those associated with high frequencies.

For this purpose, the matrix A of the state space model should be described through the Jordan diagonal form, so that the state variables are transformed into modal variables corresponding at each Jordan block one pole location. The state space matrices are further transformed in order to take the form given by (3.2) and the reduced order model can thus be obtained by eliminating the non-dominant modes associated with the fast poles. However, either poles with very high absolute values, associated with high frequencies or poles with high real parts, in turn, related with fast decay responses, are formally defined as fast poles and therefore a suitable definition is required.

The selection of the modes to be eliminated is a twofold problem. On the one hand, a suitable definition for rapid pole requires previous knowledge about the external subsystem features, which indicate what are the dominant modes. On the other hand, the suitable order determination stage lacks from an effective criterion. Since the model order is the key issue in a successful modal equivalent development, modal truncation is a very dependent application procedure. Moreover, although modal truncation is though to be well suited to steady state applications because the fast dynamic phenomena are neglected, a good performance in what concerns the transient behaviour is not expected.

3.3.1.2 Balanced realizations

As already mentioned previously, balanced realizations are based on the input-output properties of the external system. The linear state space model is transformed through a special coordinate transformation into a balanced state space realization, which preserves several important properties of the original representation, such as the Hankel singular values, the Hankel-norm, both controllability and observability properties and also the balanced relationship between both the input to state behaviour and the state to output behaviour, while provides a rank ordering of the Hankel singular values [80]. The reduced order model is thus obtained by truncation of the states that are weakly controllable and observable, corresponding to small singular values, whereas the states associated with the large singular values, which are strongly influenced by inputs and simultaneously strongly connected to the outputs, are retained.

Given a system described by the linear state space model (3.1), its controllability and observability Gramians, Q and P, respectively, are defined as the single solutions of the following Lyapunov equations [135]

$$\begin{cases} AQ + QA^T + BB^T = 0 \\ A^T P + PA + C^T C = 0 \end{cases} \tag{3.2}$$

The square roots of the eigenvalues of the product of the two Gramians, QP, are called the Hankel singular values decomposition of (3.1) and are commonly denoted by σ. The largest singular value characterizes the Hankel norm [137].

According to Moore [130], balancing the linear state space model (3.1) means to find a linear coordinate transformation, such that, for the transformed state space model, both the observability and controllability Gramians, $\overline{P}$ and $\overline{Q}$, respectively, are identical

$$\overline{P} = \overline{Q} = \Sigma \tag{3.3}$$

where

$$\Sigma = diag(\sigma_1, \sigma_2, \ldots, \sigma_n); \sigma_1 \geq \sigma_2 \geq \ldots > 0 \tag{3.4}$$

Based on the Hankel singular values, the balanced model can be divided into two subsystems like (3.2); one associated with the large singular values and the other associated with the small singular values. Therefore, the states corresponding to small singular values are eliminated and the reduced order model is thus described through the subsystem associated with the dominant or large singular values. However, like in modal truncation, the point of demarcation between large and small singular values is most often doubtful.

Although producing good approximation of transient response, the main drawback of balanced reduction methods is the high reduction errors at low frequencies, so that these methods are not well suited for steady state applications.

3.3.1.3 Optimal Hankel-norm

As already mentioned in the previous subsection the Hankel-norm is defined as the largest Hankel singular value of the system (3.1), σ_1.

If the system described by (3.1) is denoted by $G(n)$, the reduced order method based on the Hankel norm attempts to find a discrete system $G(k)$, with $k < n$, which minimizes the Hankel norm of $[G(n)-G(k)]$, minimizing thus the error for the worst case [131].

Since both optimal Hankel-norm and balanced realizations share the same limitations, it is expected that the reduced order model thus obtained does not describe the steady state behaviour. Generally SVD based methods are hardly applicable to systems of very large dimensions, since singular values of the unreduced system have to be computed and such a computation might be cumbersome for systems of large order [135].

3.3.1.4 Singular perturbations theory

The applicability of the previous modal analysis techniques is restricted, in the sense that both the Hankel norm and balanced realizations are not suitable for steady state applications while a good performance of the application of modal truncation in what concerns the transient behaviour is not expected, as referred in previous subsections. Moreover, due to the lack of an efficient modal dominance analysis procedure, modal analysis methods become very dependent of the specific system. Singular perturbations theory seems to be more general,

namely in what concerns the prediction of both steady-state and transient behaviour of the systems [132].

The interaction of fast and slow dynamic phenomena in a detailed model of power systems results in stiff numerical problems, which require expensive integration routines. In this sense, a singular perturbation approach alleviates both dimensionality and stiffness difficulties. First the model order is lowered by neglecting the fast phenomena and further the approximation is improved by reintroducing their effect as "boundary layer" corrections calculated in separate time scales [133].

The underlying assumption is that during the fast transients the slow variables remain constant and that by the time their changes become noticeable fast transients have already reached their quasi steady states. Based on this quasi steady state assumption and experience, the state variables are divided into n slow states x and m fast states z, so that the full scale model can be written as [134]

$$\frac{dx}{dt} = f(x, z, t), \; x(t_0) = x^0 \tag{3.5}$$

$$\frac{dz}{dt} = G(x, z, t), \; z(t_0) = z^0 \tag{3.6}$$

Then, only the states z are used for short term studies by neglecting the variations described by (3.5) and considering the states x as constant parameters. In long term studies only the states x are used and the differential equations for z are reduced to algebraic or transcendental equations by formally setting $\frac{dz}{dt} = 0$. The quasi steady state model is thus

$$\frac{dx_s}{dt} = f(x_s, z_s, t), \quad x(t_0) = x^0 \tag{3.7}$$

$$0 = G(x_s, z_s, t) \tag{3.8}$$

An inconsistency of this classical quasi steady state approach is the requirement that z_s equals a constant, as implied by $\frac{dz_s}{dt} = 0$, is violated by (3.8) which defines z_s as a time varying quantity. Furthermore, the initial condition for z had to be dropped in (3.8), since

there is no freedom to satisfy it. If a quasi steady state model fails to provide a good approximation of the actual solution $x(t)$ and $z(t)$, there is no provision for improving the approximation [134]. The singular perturbations approach provides a tool to overcome this lack of provision that characterizes other reduction order techniques [132, 134].

Assuming that t is properly scaled for the slow phenomena, a new time variable, τ, is introduced and scaled for the fast phenomena. The ratio of these time scales is a small positive parameter, ε, which allows the definition of the new time variable τ as:

$$\tau = \frac{t - t'}{\varepsilon} \tag{3.9}$$

The wider the separation of the time scales, the smaller ε will be. On the other hand, the smaller ε is, the larger τ will be for a given $(t - t')$ interval. When τ is sufficiently large, the fast phenomena have adequate time to reach their steady states, which, however, does not contradict the assumption that $(t - t')$ is sufficiently short to consider the slow variables as constants. Thus, the limit of $\varepsilon \to 0$ is equivalent to the quasi steady state assumption, but without its inconsistencies [134].

If it is known that the dynamics of the states z are $\frac{1}{\varepsilon}$ times faster than x, then $\frac{dz}{dt}$ is about $\frac{1}{\varepsilon}$ times larger than $\frac{dx}{dt}$ and G can be rescaled as

$$g = \varepsilon G \tag{3.10}$$

such that f and g are of the same order of magnitude. The model (3.5) and (3.6) then becomes

$$\frac{dx}{dt} = f(x, z, t),\ x(t_0) = x^0 \tag{3.11}$$

$$\varepsilon \frac{dz}{dt} = g(x, z, t), z(t_0) = z^0 \tag{3.12}$$

The above qualitative reasoning is based on some empirical estimates of $\frac{dx}{dt}$ and $\frac{dz}{dt}$. When this information is not available, then physical parameters are examined to determine which states are slow and which are fast. Not every choice of state variables will be separable in this sense. Where separable, a model (3.11), (3.12) will be obtained by expressing the small time constants and the inverses of the high gain coefficients as multiples of a single small parameter ε.

In the limit $\varepsilon \to 0$, the model (3.11) and (3.12) defines the quasi steady states $x_s(t)$ and $z_s(t)$, in the t time scale, as

$$\frac{dx_s}{dt} = f(x_s, z_s, t),\ x_s(t_0) = x^0 \tag{3.13}$$

$$0 = g(x_s, z_s, t) \tag{3.14}$$

To obtain the fast parts of x and z, (3.13) and (3.14) can be written in the fast time scale τ.

$$\frac{dx}{d\tau} = \varepsilon f(x, z, t' + \varepsilon\tau) \tag{3.15}$$

$$\frac{dz}{dt} = g(x, z, t' + \varepsilon\tau) \tag{3.16}$$

When $\varepsilon \to 0$ x is constant in the fast time scale and the only fast variations are the deviations of z from its quasi steady state z_s, $z_f = z - z_s$. If $\varepsilon = 0$ in (3.16), the fast subsystem can be written as

$$\frac{dz_f}{dt} = g(x^0, z_s^0 + z_f(\tau), t_0),\ z_f(0) = z^0 - z_s^0 \tag{3.17}$$

With (3.13) and (3.14) describing the slow states and (3.17) associate with fast states, the approximations for x and z are then given by

$$x(t) \cong x_s(t) \tag{3.18}$$

$$z(t) \cong z_s(t) + z_f\left(\frac{t-t_0}{\varepsilon}\right) \tag{3.19}$$

The application of singular perturbations theory allows to eliminate the inconsistencies of the classical quasi steady state approaches to model reduction due to the presence of the scaling parameter ε.

While the full order models (3.11), (3.12), (3.15) and (3.16) are exact, the separated lower order models (3.13), (3.14) and (3.17) are in error, because they assume $\varepsilon = 0$, instead of $\varepsilon > 0$. This parameter change is called singular perturbation, since it results in an inherent perturbation in model order. The approximations (3.18) and (3.19) can now be improved by constructing asymptotic expansions in ε [134].

Concerning to the parameter ε, the problem now is to find a criterion to determine the separation between slow and fast states. In fact, there is no general parameter definition. Rather, the identification of the parameter ε depends on several issues, such as experience acquired previously with the detailed system modelling, physical intuition that indicts the possibilities of choices or also preliminary analysis that will provide the selection bases. In order to reduce the model order it is supposed that $\varepsilon = 0$. However, it should be taken into account that this parameter is neglected only for a time because the fast transients owing the parameter ε are subsequently introduced through an adjustment of the frontier conditions [132]. Due to this fact singular perturbations seem to be more general when compared with modal truncation and balanced realizations, namely in what concerns the prediction of both steady state and transient behaviours, as already mentioned previously.

3.3.2 Coherency-based methods

Linear methods cannot properly capture complex dynamics of power system, especially during major disturbances, such as critical faults. Thus, dynamic equivalents established to provide the desired performance at a small signal condition might not guarantee acceptable performance in events of major disturbances. Therefore, nonlinear approaches, also called coherency-based methods, have been proposed and widely used to reduce the computational effort associated with the study and analysis of power system dynamics.

Methods belonging to this category depend on the coherency concept to recognize coherent properties between generators, as already mentioned previously. Coherent generators are grouped in order to be further replaced by one equivalent machine, which it is expected to represent its dynamics of interest [75, 116, 126]. With this approach the obtained dynamic equivalents are based on nonlinear models similar to the replaced machines but with new parameters resulting from its aggregation and hence they are compatible with other components of the network. This fact can be viewed as an advantage, since it allows an easy attachment of the dynamic equivalent to the internal subsystem detailed model and, as a result, a direct integration of the standard dynamic simulation tools as depicted in figure 3.2.

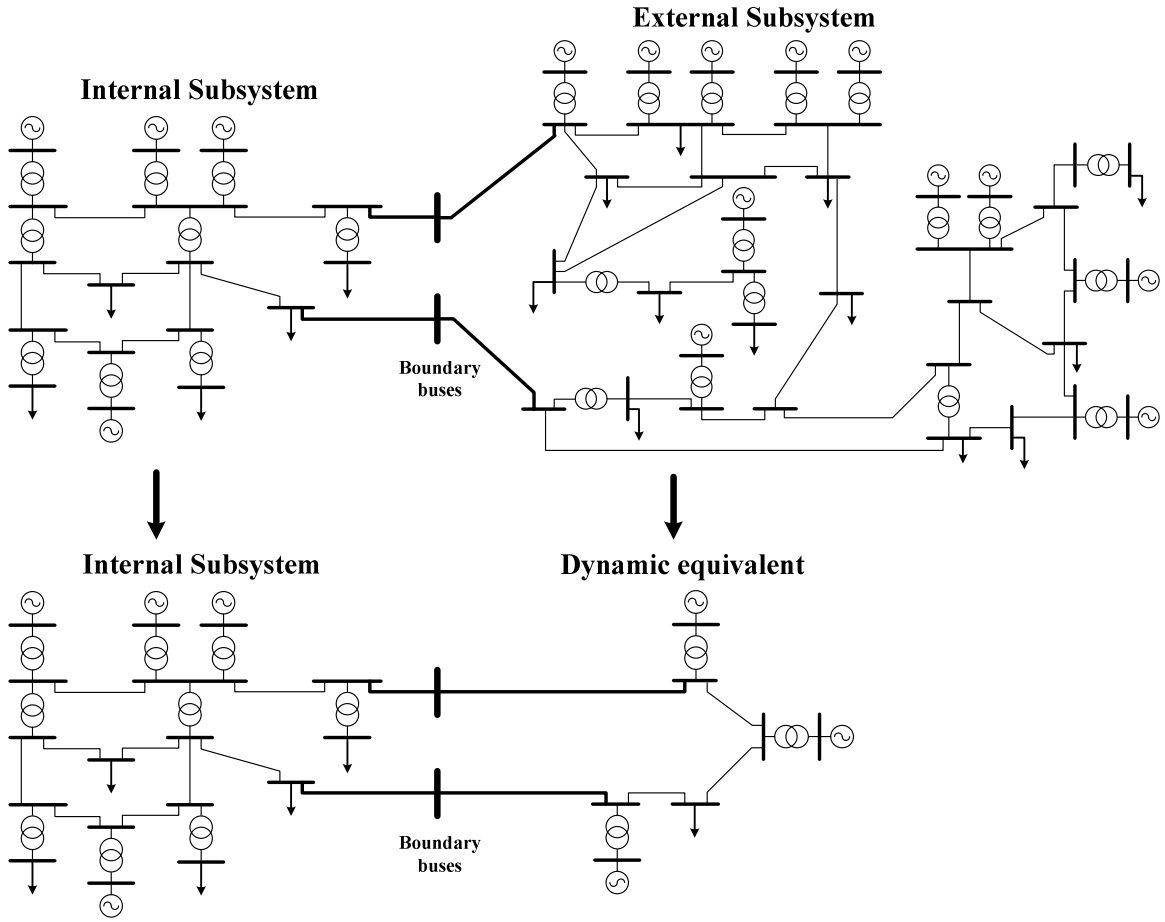

Figure 3.2: Dynamic equivalencing using coherency-based approaches

The computations of coherency based methods can be divided into three separate and independent stages [66]:

1. Determination of coherent groups of generators;

2. Aggregation of coherent generators within each coherent group onto one equivalent bus;
3. Elimination of the remaining buses by network reduction.

Based on a suitable coherency measure, generators coherent with others are recognized and included in the same group according to a pre-defined criterion. Groups of coherent generators are aggregated into one equivalent machine and, at last, the network is reduced.

As already mentioned previously, in section 3.2, coherency recognition procedure is typically based on a linearized model of the entire power system. Then, in the following subsection, this model is presented and afterwards in subsections 3.2.3.2, 3.2.3.3 and 3.2.3.4, common procedures to carry out each one of the coherency based methods main stages is briefly addressed.

3.3.2.1 The mathematical model

Concerning with coherency recognition and grouping of coherent generators purposes, a simplified and linearized model is used to describe the dynamic behaviour of a power system under transient conditions [85]. This model has the following features:

- The classical generator model is used to represent the synchronous machines;
- The power system model is linearized;
- The decoupling between active power phase angle and reactive power voltage magnitude is assumed.

The linear model is usually justified considering that coherency properties between coherent generators are approximately independent of the disturbance magnitude as well as of the amount of detail in the generating unit's models. Therefore linearized equations of the network and the classical model of synchronous machines have been used to reduce computational efforts without significant loss of accuracy regarding coherency recognition and subsequent grouping of coherent generators [64].

The classical synchronous generator model, widely used for a simplified analysis of power system dynamics, assumes that neither the $d-$axis armature current I_d nor the internal emf E_f, representing the excitation voltage change very much during the transient state. In this

model the generator is represented by the swing equation and a constant emf E' behind the transient reactance $X_d^{'}$ [138], as follows.

$$\frac{d}{dt}\delta = \omega_i \tag{3.20}$$

$$M_i \frac{d}{dt}\omega_i = P_{mi} - P_{gi} - D_i\omega_i \tag{3.21}$$

The linearized swing equations for the $i-th$ synchronous generator can be written as

$$\frac{d}{dt}\Delta\delta_i = \omega_0\Delta\omega_i \tag{3.22}$$

$$M_i \frac{d}{dt}\Delta\omega_i = \Delta P_{mi} - \Delta P_{gi} - D_i\Delta\omega_i \tag{3.23}$$

where:

deviations Δ are counted from the specified pre fault steady state operating point;

M represents the inertia constant in $p.u.$;

ω represents the angular speed in $p.u.$;

ω_0 represents the synchronous speed in rad/s;

δ is the rotor angle in rad;

D denotes the damping coefficient in $p.u.$;

P_m is the mechanical input power in $p.u.$;

P_g represents the electrical output power in $p.u.$.

The linearized decoupled load flow equations are used to represent the network [64]. The changes in active electrical power vectors ΔP_g and ΔP_l at the generator internal buses and at both generator terminal and load buses, respectively, can be expressed in the matrix form as

$$\begin{bmatrix}\Delta P_g \\ \Delta P_l\end{bmatrix} = \begin{bmatrix}H_{gg} & H_{gl} \\ H_{lg} & H_{ll}\end{bmatrix} \times \begin{bmatrix}\Delta\delta \\ \Delta\theta\end{bmatrix} \tag{3.24}$$

where H_{gg}, H_{gl}, H_{lg} and H_{ll} are sensitivity sub matrices obtained from the partial derivatives of active powers P_g and P_l with respect to the generator internal bus voltage angles, δ, and to generator and load bus voltage angles, θ.

Underlying assumptions in (3.24) are that the changes in active powers with respect to voltage magnitudes are neglected and the partial derivatives or sensitivity coefficients are calculated using the voltages and angles at the pre-fault steady state operating point.

3.3.2.2 Determination of coherent groups of generators

For a given disturbance, a group of generators is defined as coherent if every generators within the group oscillate with the same angular speed and terminal bus voltages in a constant complex ratio [64].

According to [138], two terminal generator buses i and j are said to be coherent for a disturbance occurring at time t_0 if

$$\frac{\underline{V}_i(t)}{\underline{V}_j(t)} = \frac{V_i(t)}{V_j(t)} e^{j[\theta_i(t)-\theta_j(t)]} = \frac{V_i(t_0)}{V_j(t_0)} e^{j[\theta_i(t_0)-\theta_j(t_0)]} = \underline{v}_i \text{ for all } t \geq t_0 \tag{3.25}$$

If the voltage magnitude can be assumed to be constant, the coherency condition (3.25) simplifies to

$$\theta_i(t) - \theta_j(t) = \theta_i(t_0) - \theta_j(t_0) = c \tag{3.26}$$

for any constant c.

As with the classical model of generators each generator emf behind its own transient reactance is assumed to be constant, two internal generator nodes i and j are coherent if the transient rotor angles satisfy the coherency condition (3.26) [138], that is

$$\delta_i(t) - \delta_j(t) = \delta_i(t_0) - \delta_j(t_0) = c \text{ for all } t \geq t_0 \tag{3.27}$$

for some constant c. This condition is equivalent to

$$\Delta\delta_i(t) = \Delta\delta_j(t) \text{ for all } t \geq t_0 \tag{3.28}$$

where $\Delta\delta_i(t) = \delta_i(t) - \delta_i(t_0)$ and $\Delta\delta_j(t) = \delta_j(t) - \delta_j(t_0)$.

Thus, two generators are coherent for a given disturbance if the response curves of their rotor angles have identical wave shape and a group of generators is said to be coherent if all the generators within the group are pair wise coherent within a given tolerance.

For a small time increase the rotor angle of generators i and j could be approximated as

$$\delta_i(t+\Delta t) = \delta_i(t) + \omega_i(t)\Delta t \text{ and } \delta_j(t+\Delta t) = \delta_j(t) + \omega_j(t)\Delta t \tag{3.29}$$

where $\omega_i(t)$ and $\omega_j(t)$ denote, respectively, the rotor speeds of generators i and j at the instant t. Thus

$$\delta_{ij}(t+\Delta t) - \delta_{ij}(t) = (\omega_i(t) - \omega_j(t))\Delta t \tag{3.30}$$

where $\delta_{ij}(t+\Delta t) = \delta_i(t+\Delta t) - \delta_j(t+\Delta t)$ and $\delta_{ij}(t) = \delta_i(t) - \delta_j(t)$. Then, for a fixed time interval, two generators are defined as coherent if

$$\omega_i(t) = \omega_j(t) \tag{3.31}$$

From the previous coherency conditions, (3.26), (3.27) and (3.31), the following coherency measures arise for two generators i and j:

$$\delta_i(t) - \delta_j(t) = const \pm \varepsilon \text{ for } t \geq t_0 \tag{3.32}$$

$$\left|\Delta\delta_i(t) - \Delta\delta_j(t)\right| \leq \varepsilon \text{ for } t \geq t_0 \tag{3.33}$$

$$\left|\omega_i(t) - \omega_j(t)\right| \leq \sigma \text{ for } t \geq t_0 \tag{3.34}$$

where ε and σ denote tolerance parameters. Therefore both rotor angles and speeds can be used to recognize coherency between pairs of generators.

However, coherency based methods will only give valid results if following a disturbance inside the internal subsystem the generators within each coherent group are effectively coherent. Therefore, the main problem is how to assess the coherency between generators.

In section 3.2 it is highlighted that two major approaches have been used to recognize coherency between generators: The first one is to apply a disturbance directly and observe the swing curves of the generators. The second one is to assess generators coherency without the need for time domain simulation, that is, to evaluate coherency properties independently of the disturbance [92]. Analytical methods, such as weak links coupling [115] and slow coherency [88, 89, 92, 139, 140] have been used for this purpose and were also included in the DYNRED software package [118].

Linear time simulation is the classical method to check coherency between generators [75]. It involves mainly the numerical integration of the linearized power system dynamic equations presented in subsection 3.2.3.1 and then processing either the rotor angles or speeds trajectories by a clustering algorithm in order to form groups of coherent generators. Based on the fact that the high computational effort involved in this method may offset the advantages of the dynamic equivalencing strategy, simple and direct determination of coherent generators without explicitly solving the system dynamic equations have been reported in the literature. Most of them are based on the parameters of the transfer network matrix that links the boundary buses with the generator nodes of the external subsystem [138]. Therefore the following formulation should be considered.

As already mentioned previously both study and external subsystems are linked through the tie lines which connect the boundary buses to the external subsystem as depicted in figure 3.3.

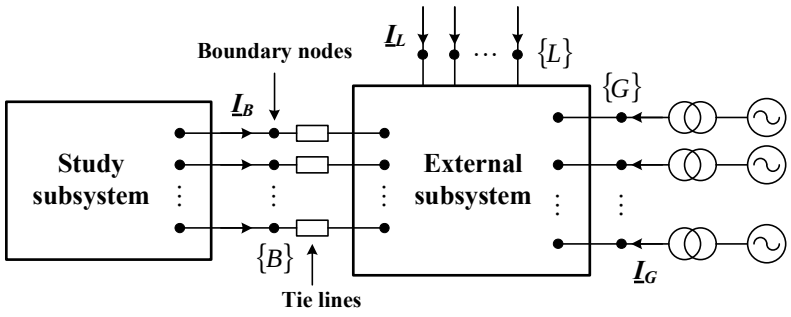

Figure 3.3: Schematic representation of the external subsystem

In what concerns to the external subsystem, the currents $\underline{I}_B$ flowing through the tie lines become the injected currents of the boundary nodes. As all the generators are represented by the classic model and considering that all the load nodes have been eliminated, the incremental decoupled active power flow equations (3.24) can be written as

$$\begin{bmatrix} \Delta P_G \\ \Delta P_B \end{bmatrix} = \begin{bmatrix} H_{GG} & H_{GB} \\ H_{BG} & H_{BB} \end{bmatrix} \times \begin{bmatrix} \Delta\delta \\ \Delta\theta \end{bmatrix} \tag{3.35}$$

where ΔP_G, ΔP_B, $\Delta\delta$ and $\Delta\theta$ represent increments of the active power and angles at both the internal generator and boundary buses, respectively.

All the generators in the external subsystem are represented by the linearized swing equations (3.22) and (3.23) and the following assumptions are considered [44]:

- During the period of interest, the mechanical power is constant, $\Delta P_m = 0$;
- Damping terms does not affect natural frequencies and can thus be neglected.

Under these assumptions, equation (3.23) simplifies to

$$M_i \frac{d^2}{dt^2}\Delta\delta_i = -\Delta P_i \tag{3.36}$$

Any disturbance inside the study subsystem influences the generators in the external subsystem through the tie lines and boundary buses. From the external subsystem point of view, the disturbance is caused by a change in the voltage angle of boundary bus k from the initial value θ_k^0 to a new value $\theta_k = \theta_k^0 + \Delta\theta_k$. According to [138], as the voltages at generation nodes are kept constant the network equations (3.35) simplifies to $\Delta P_G = H_{GB}\Delta\theta$ and thus, the change in angle θ_k provokes a change in the power generation at bus i equal to

$$\Delta P_i(\Delta\theta_k) \approx -h_{ik}\Delta\theta_k \tag{3.37}$$

where $h_{ik} = V_i V_k B_{ik} \cos(\delta_i^0 - \theta_k^0)$ is the synchronizing power between a given generator $i \in \{G\}$ belonging to the external subsystem and a given boundary bus $k \in \{B\}$. V_i and V_k are the magnitude of voltages at buses i and k, respectively, B_{ik} is the line susceptance and both δ_i^0 and θ_k^0 denote the initial values of the voltage angles at buses i and k, respectively. Therefore, equation (3.36) can be written as

$$M_i \frac{d^2}{dt^2}\Delta\delta_i = h_{ik}\Delta\theta_k \Leftrightarrow \frac{d^2}{dt^2}\Delta\delta_i = \frac{h_{ik}}{M_i}\Delta\theta_k \tag{3.38}$$

Thus the considered disturbance yields the rotor acceleration of generator i

$$\varepsilon_i = \frac{\Delta P_i(\Delta\theta_k)}{M_i} = \frac{h_{ik}}{M_i}\Delta\theta_k \tag{3.39}$$

A similar expression for acceleration can be written for another generator in the external subsystem

$$\varepsilon_j = \frac{\Delta P_j(\Delta\theta_k)}{M_j} = \frac{h_{jk}}{M_j}\Delta\theta_k \tag{3.40}$$

Generators i and j are coherent if their rotor accelerations ε_i and ε_j caused by the disturbance are the same, that is when

$$\frac{h_{ik}}{M_i} = \frac{h_{jk}}{M_j} \text{ for } i, j \in \{G\},\ k \in \{B\} \tag{3.41}$$

Equation (3.41) constitutes the coherency condition during the post fault state and means that the synchronizing power divided by the inertia constants must be identical.

Taking into account that coherent generators have high coupling coefficients among them, in the weak links method the coherency is determined by analyzing the coupling coefficients of generators in the system state matrix A [115].

On the slow coherency methods the coherency recognitions among generators is based on the modes of the system. The power systems network is partitioned into groups containing coherent generators based on the two time scale method [88]. The fundamental idea is based on the concept that a slow oscillation is caused by two groups of strongly coherent generators interconnected through weak ties. Thus, the coherency between two generators can be easily checked by means of the eigenvector associated with the mode of oscillation [118]. Using the state space matrix A, the slow eigenbasis matrix is calculated and the r most linearly independent rows of this matrix will become the corresponding reference generators. A grouping algorithm is then applied to group non reference generators to the reference generators [92]. This method was applied not only for generators [140] but also for generators and weak tie lines [92].

Slow coherency methods describe an algorithm for fault independent area grouping, by selecting only the lowest electromechanical modes of the linearized model [139]. The tolerance based slow coherency method is similar to the previous two time scale method, but includes additional constrains to ensure that widely separated generators are not aggregated [89]. Both methods require the computation of selected eigenvalues and eigenvectors of the full system and therefore, the modified Arnoldi eigenvalue solver [141] was added to allow the application of these methods to large power systems.

3.3.2.3 Aggregation of generating units

In this stage each group of coherent generators resulting from the application of any of the methods described in the previous subsection are aggregated in order to be replaced by one equivalent generating unit to be connected in parallel to the equivalent bus [138], as depicted in figure 3.4.

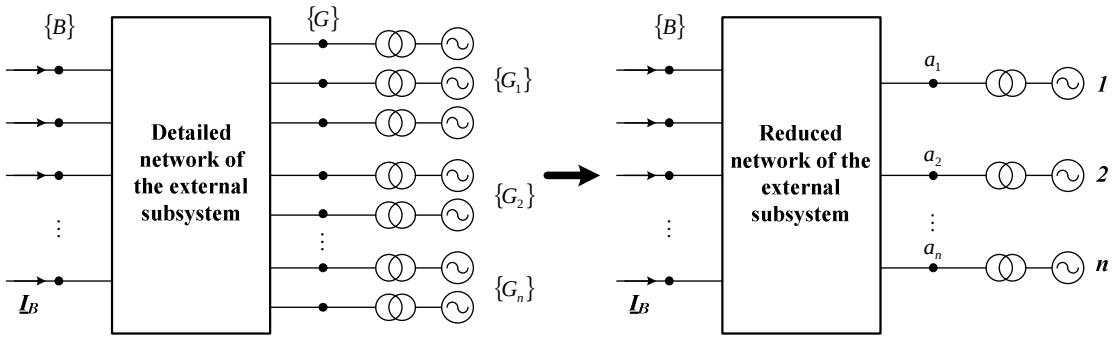

Figure 3.4: Grouping coherent generators and reduced model of the external subsystem

As the original model of the power system contains a large number of both load and generation nodes already divided into coherent groups, $\{G\}=\{G_1\}+\{G_2\}+\cdots+\{G_n\}$, after aggregation of coherent generators, the next step is to use Zhukov's method to aggregate the nodes in these groups. The load nodes are either completely eliminated or aggregated into a few equivalent nodes using Dimo's method [138]. These two later steps are addressed in subsection 3.3.2.4. This subsection is devoted to a brief review of generating units aggregation procedure.

While coherency identification have been covered quite extensively in the literature, generator aggregation is treated superficially in most of the works by considering either classical models or omitting the associated control devices [142]. However, other methods have been developed considering not only the detailed model of the synchronous generators, but also their control devices. Generally the methods developed in the past few decades for dynamic aggregation of the generating units can be classified into two forms: the classical aggregation and the detailed aggregation [143].

In classical aggregation each group of coherent generators is replaced by an equivalent generation unit represented by the classic model of synchronous generators. Under coherency conditions, a disturbance taking place in the study subsystem will not provoke any relative motions between coherent machines since they will remain in synchronism. To an observer outside the coherent area, the motions of these machines are seen as if they were originated from one single machine. From the mechanical view point, the rotors of coherent generators can be treated as if they rotated on one common rigid shaft [138], as depicted in figure 3.5.

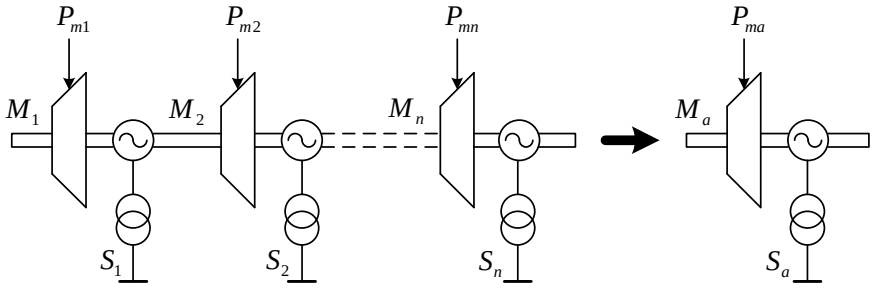

Figure 3.5: Aggregation of coherent generators

A group of such generators can be replaced by one equivalent generator with mechanical power input P_{ma} and electric power output P_{ea} given by

$$P_{ma} = \sum_{i=1}^{n} P_{mi} \; ; \; P_e = \sum_{i=1}^{n} P_{ei} \tag{3.42}$$

where P_{mi} and P_{ei} are the mechanical power input and electrical power output, respectively, of the $i-$th generator.

As the angular frequencies of coherent generators are identical and thus assumed to be ω, the swing equation of the equivalent generator can then be described as

$$\left(\sum_{i=1}^{n} M_i\right)\frac{d\omega}{dt} = \sum_{i=1}^{n} P_{mi} - \sum_{i=1}^{n} P_{ei} - \left(\sum_{i=1}^{n} D_i\right)\omega \Leftrightarrow M_a \frac{d\omega}{dt} = P_a - P_e - D_a\omega \tag{3.43}$$

where M_i and D_i denote the inertia coefficient and damping of the $i-$th generator and both M_a and D_a the coefficient inertia and damping of the equivalent generator.

The transient reactance of the equivalent generator can be obtained by paralleling the transient reactances of all the coherent generators [84]:

$$X_d^{'} = \frac{1}{\sum_{i=1}^{n} \frac{1}{X_{di}^{'}}} \tag{3.44}$$

Concerning to detailed aggregation, if some or all generators in a coherent group have similar control systems, they can be aggregated to a detail generator model with an equivalent exciter, stabilizer and governor [142, 143]. The parameters of the equivalent machine can be found by matching either the frequency or time domain response of the equivalent unit to the characteristics of the aggregated units. As already mentioned previously, DYNRED program contains several weighted average and least squares frequency domain algorithms to compute the parameters of the equivalent generators and its control models. This software package was used in [116] to perform the aggregation of an excitation system using a trajectory sensitivity method to tune the equivalent parameters, but the algorithms for parameter aggregation purposes have not been extensively tested [142, 144]. NETOMAC software package use iterative procedures to determine the equivalent parameters of generator and control systems in frequency domain [63]. Other methods based on nonlinear optimization algorithms have been reported in the literature to estimate parameters of the equivalent generator detailed model in time domain using measured data [145]. In [142, 144] an improved method using structure preservation in time domain is presented. In this method, the equivalent parameters are determined by structure preservation of the coefficient matrices in time domain representation in order to preserve the physical structure of the generating unit model and its control as well [143]. Technical literature extensively reports the use of ANN to estimate unknown parameters of a dynamic equivalent [146]. Proper input features of study system are extracted and transient stability indices are used to predict the inertia constant, reactances and other parameters of the equivalent machine.

3.3.2.4 Network reduction

Once equivalent generators are recognized and grouped into coherent groups, the network reduction is performed. As already mentioned previously, this reduction is typically achieved in two steps:

- The equivalent generators are inserted into the system and the generators in the associated coherent groups are removed. The network is modified to maintain the balanced steady state power flow conditions;
- The load nodes are eliminated and/or aggregated.

These two steps are described in the following.

3.3.2.4.1 Aggregation of generating buses

After generators aggregation, their terminal buses are lumped together to form an equivalent bus, as it can be shown in figure 3.4. This operation is performed by means of the Zhukov's method [90, 138], as already mentioned previously. Given a group of coherent generators, $\{G_i\}$, the boundary buses of the external subsystem have to be retained while the set of coherent nodes have to be aggregated, as represented in figure 3.6. These two sets of buses are then denoted by retained, $\{R\}$, and aggregated, $\{A\}$, respectively.

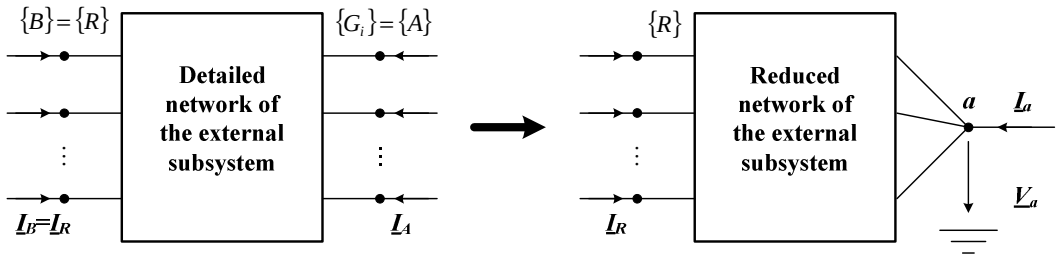

Figure 3.6: Aggregation of generating buses using Zhukov's method

Aggregation of generating nodes must satisfy the following two conditions [138]:

1. It does not change the currents and voltages $\underline{I}_R$ and $\underline{V}_R$ at the retained buses;
2. The active and reactive power injections at the equivalent node must be equal to the sum of injections at the aggregated nodes, $\underline{S}_a = \sum_{i \in \{A\}} \underline{S}_i$.

The transformation of the network can be described by

$$\begin{bmatrix} \underline{I}_R \\ \underline{I}_A \end{bmatrix} = \begin{bmatrix} \underline{Y}_{RR} & \underline{Y}_{RA} \\ \underline{Y}_{AR} & \underline{Y}_{AA} \end{bmatrix} \times \begin{bmatrix} \underline{V}_R \\ \underline{V}_A \end{bmatrix} \Rightarrow \begin{bmatrix} \underline{I}_R \\ \underline{I}_a \end{bmatrix} = \begin{bmatrix} \underline{Y}_{RR} & \underline{Y}_{Ra} \\ \underline{Y}_{aR} & \underline{Y}_{aa} \end{bmatrix} \times \begin{bmatrix} \underline{V}_R \\ \underline{V}_a \end{bmatrix} \tag{3.45}$$

where the subscripts refer to the appropriate set.

The first condition is satisfied when

$$\underline{Y}_{RR}\underline{V}_R + \underline{Y}_{RA}\underline{V}_A = \underline{Y}_{RR}\underline{V}_R + \underline{Y}_{Ra}\underline{V}_a \;\Leftrightarrow\; \underline{Y}_{RA}\underline{V}_A = \underline{Y}_{Ra}\underline{V}_a \tag{3.46}$$

As this condition is to be satisfied for any vector $\underline{V}_A$, it must hold that

$$\underline{Y}_{Ra} = \underline{Y}_{RA}\underline{\vartheta} \tag{3.47}$$

where $\underline{\vartheta} = \dfrac{\underline{V}_A}{\underline{V}_a}$ is the vector of voltage transformation ratios between the aggregated and the equivalent nodes.

Each terminal bus is connected through an ideal transformer with complex turns ratio to the equivalent bus as it can be shown in figure 3.7. The secondaries of transformers are then connected together to create the equivalent node a and the nodal matrix equation for the reduced network can then be derived [138].

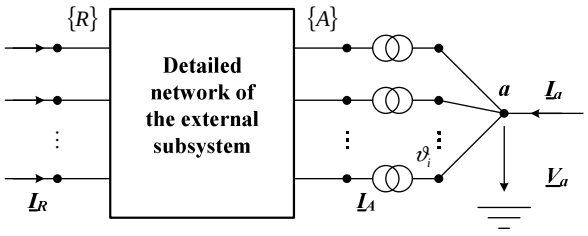

Figure 3.7: Electrical interpretation of Zhukov's aggregation

The second condition is satisfied when the injection at the equivalent bus equals the sum of all the aggregates injections,

$$\underline{V}_a\underline{I}_a^* = \underline{V}_A^T\underline{I}_A^* \tag{3.48}$$

Substituting into equation (3.48) $\underline{I}_A$ and $\underline{I}_a$ calculated from equation (3.45), yields

$$\underline{V}_a\underline{Y}_{aR}^*\underline{V}_R^* + \underline{V}_a\underline{Y}_{aa}^*\underline{V}_a^* = \underline{V}_A^T\underline{Y}_{AR}^*\underline{V}_R^* + \underline{V}_A^T\underline{Y}_{AA}^*\underline{V}_A^* \tag{3.49}$$

As this equation must be satisfied for any vector $\underline{V}_A$ the following two conditions must hold

$$\underline{Y}_{aR} = \underline{\vartheta}^{*T} \underline{Y}_{AR} \tag{3.50}$$

$$\underline{Y}_{aa} = \underline{\vartheta}^{*T} \underline{Y}_{AA} \underline{\vartheta} \tag{3.51}$$

Equations (3.47), (3.50) and (3.51) describe the admittances of the equivalent network. The admittances of the equivalent branches linking the equivalent node with the retained nodes depend on the vector transformation ratios, $\underline{\vartheta}$, and on the voltage angle at the equivalent node. It is commonly assumed to be the weighted average of voltage angles at the aggregated nodes

$$\theta_a = \frac{\sum_{i \in \{A\}} \underline{S}_i \theta_i}{\sum_{i \in \{A\}} \underline{S}_i} \text{ or } \delta_a = \frac{\sum_{i \in \{A\}} M_i \delta_i}{\sum_{i \in \{A\}} M_i} \tag{3.52}$$

where $\underline{S}_i$ is the apparent power injection at the aggregated node i and M_i is the inertia coefficient of the unit installed at the $i-th$ aggregated node.

3.3.2.4.2 Aggregation and/or elimination of load nodes

For some power systems analysis problems it may be more convenient not to eliminate the load nodes altogether, but to replace a few of them by equivalent load nodes after to carry out some load aggregation procedure. The equivalent nodes can then be used to change the power demand of the external subsystem if a change in tie line flows is required.

According to [147], load aggregation can be performed into two ways:

1. Analytically, by lumping similar loads and then using pre-determined values of each parameter of the load;
2. Selecting a load model and then performing parameter estimation using an appropriate identification technique.

As already mentioned previously, aggregation of load nodes can be performed using Dimo's method [138]. This method is illustrated in figure 3.8 and consists of replacing a group of nodes $\{A\}$ by an equivalent node a. As before $\{R\}$ is the set of retained buses.

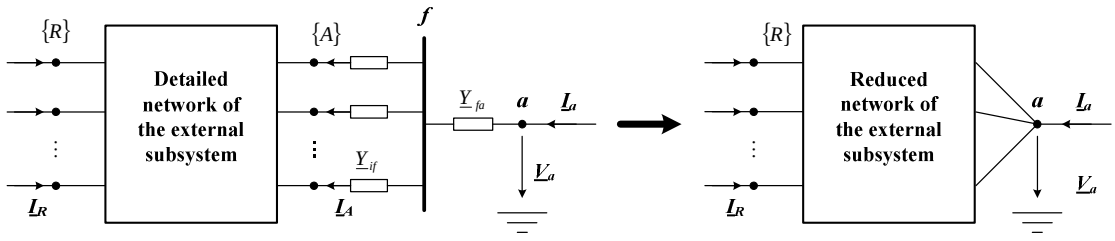

Figure 3.8: Load bus aggregation using Dimos's method

In the first step of transformation, some fictitious branches are added to the aggregated nodes, $\{A\}$. Each branch admittance is chosen in such a way as to make the terminal voltage of all the added branches equal. Usually these admittances are made to correspond to the nodal injections at a given voltage in the aggregated nodes

$$\underline{Y}_{fi} = \frac{\underline{S}_i^*}{V_i^2} \text{ for } i \in \{A\} \tag{3.53}$$

and then the voltage at the fictitious node f is zero. As it is inconvenient to have an equivalent node operating at zero voltage, an extra fictitious branch with negative admittance is usually added to node f. A typical choice of the negative admittance is

$$\underline{Y}_{fa} = -\frac{\underline{S}_a^*}{V_a^2}, \text{ where } \underline{S}_a = \sum_{i \in \{A\}} \underline{S}_i \tag{3.54}$$

This makes the voltage $\underline{V}_a$ at the equivalent node equal to the weighted average of the voltages at the aggregated nodes:

$$\underline{V}_a = \frac{\sum_{i \in \{A\}} \underline{S}_i}{\sum_{i \in \{A\}} \left(\frac{\underline{S}_i}{\underline{V}_i} \right)^*} \tag{3.55}$$

The auxiliary node f is eliminated together with the nodes belonging to the set $\{A\}$, giving an equivalent network, referred to as the REI circuit [64, 138], connecting the equivalent node a with the retained nodes $\{R\}$.

If the operating conditions are different from the ones for which the reduction was performed, then the obtained equivalent will only imitate the external network accurately if the admittances of the fictitious branches (3.53) can be assumed to remain constant. For load nodes this is equivalent to assuming that the loads can be modelled as constant admittances [138].

Dimo's method produces a large number of fictitious branches due to the elimination of node f and nodes $\{A\}$. As aggregation introduces a branch with negative admittance, the branches in the final network model may have negative admittances. Moreover, large nodal injections in the aggregated nodes produce large resistance values in the equivalent branches. Negative branch admittances combined with large resistances may cause problems for some load flow programs [138].

Node elimination relies on modelling loads by constant admittances and eliminating them by using a Ward equivalencing technique, as illustrated in figure 3.9.

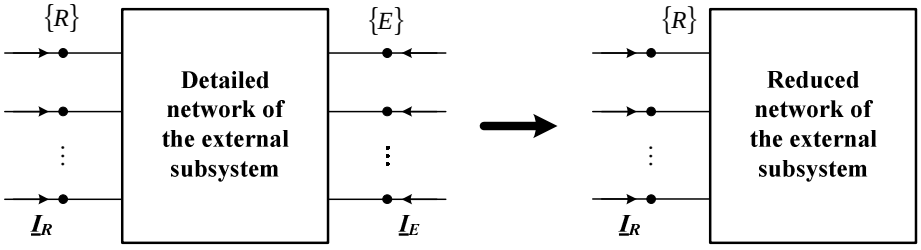

Figure 3.9: Elimination of nodes

When nodes are eliminated from the network model, $\{E\}$, they must be removed in such a way that the currents and nodal voltages at the retained nodes, $\{R\}$, are unchanged.

Before any nodes are eliminated the network is described by the following nodal equation

$$\begin{bmatrix} \underline{I}_R \\ \underline{I}_E \end{bmatrix} = \begin{bmatrix} \underline{Y}_{RR} & \underline{Y}_{RE} \\ \underline{Y}_{ER} & \underline{Y}_{EE} \end{bmatrix} \times \begin{bmatrix} \underline{V}_R \\ \underline{V}_E \end{bmatrix} \tag{3.56}$$

where the subscripts refer to the eliminated $\{E\}$ and retained $\{R\}$ sets of nodes. The eliminated voltages and currents can be swapped using simple matrix algebra to give

$$\begin{bmatrix} \underline{I}_R \\ \underline{V}_E \end{bmatrix} = \begin{bmatrix} \underline{Y}_R & \underline{K}_I \\ \underline{K}_V & \underline{Y}_{EE}^{-1} \end{bmatrix} \times \begin{bmatrix} \underline{V}_R \\ \underline{I}_E \end{bmatrix} \tag{3.57}$$

where

$$\underline{Y}_R = \underline{Y}_{RR} - \underline{Y}_{RE}\underline{Y}_{EE}^{-1}\underline{Y}_{ER},\ \underline{K}_L = \underline{Y}_{RE}\underline{Y}_{EE}^{-1},\ \underline{K}_V = -\underline{Y}_{EE}^{-1}\underline{Y}_{ER} \tag{3.58}$$

The square matrix in equation (3.57) is the partial inversion of the admittance matrix. The nodal currents in the set $\{R\}$ are

$$\underline{I}_R = \underline{Y}_R\underline{V}_R + \Delta\underline{I}_R \tag{3.59}$$

where $\Delta\underline{I}_R = \underline{K}_L\underline{I}_E$ is the vector consisting of the equivalent currents replacing the eliminated nodes.

Equation (3.59) describes the relationship between the currents and voltages of the retained nodes in the reduced network. As any electrical network is uniquely described by its admittance matrix, $\underline{Y}_R$ corresponds to a reduced equivalent network that consists of the retained nodes and equivalent branches linking them. This network is often referred to as the transfer network and the matrix describing it as the transfer admittance matrix. Matrix $\underline{K}_L$ passes the nodal currents from the eliminated nodes to the retained nodes and is referred to as the distribution matrix. Each equivalent current is a combination of the eliminated currents.

Another form of equation (3.59) can be obtained by replacing the nodal power injection at each eliminated node by a constant shunt admittance $\underline{Y}_{Ei} = \dfrac{\underline{S}_i^*}{V_i^2}$ added, with an appropriate sign, to the diagonal elements of the sub matrix $\underline{Y}_{EE}$. The nodal injections at the eliminated nodes then become zero, $\underline{I}_E = 0$, and the reduced model does not contain any equivalent currents $(\Delta\underline{I}_R = 0)$. This is quite convenient but has a drawback. The equivalent shunt branches have large conductance values, corresponding to the real power injections, which become part of the equivalent branches in the reduced model. Therefore, the branches of the equivalent network may have a poor X/R ratio causing convergence problems for some load flow computer programs.

Node elimination and aggregation can be done by separating the external subsystem from the study subsystem and by making the injected currents at the boundary nodes equal to the tie line currents [138].

3.4 Dynamic equivalents derived from measurements

Taking into account that analysis of transients is of greater importance for successful planning, operation and control of large interconnected power systems, industry trends and new technologies have changed the methods used by power systems engineers for this purpose over the last decades.

In recent years, the desire to increase efficiency with concomitant reduction in both energy costs and losses as well as both the ongoing deregulation of the power utility industry and the interest in connecting generation to distributed networks will change the main issues in modelling and control of power systems for several reasons [148]:

- The increase of both complexity and number of components with relevant dynamic behaviour will increase the complexity of models;
- Technical advances in sensing, communication and computational capabilities allow to exploit alternative techniques.

In response to the need to accurately analyse the dynamics of such power systems, the development of adequate dynamic equivalents for parts of the power system that are not in the primary focus of the study are required. Benefiting of the communications and computer technology to maintain a stable system operation, such models will have to be derived and validated from locally available prior information and measurements. In fact the availability of measurements opened a new research route in the field of power systems dynamic equivalents [119-124, 148].

Techniques based on measurements have been exploited to build dynamic equivalents for conventional power systems and for distribution networks with large penetration of DG. The different reasons that motivate their application to these two application fields are outlined in the following two subsections.

3.4.1 Dynamic equivalents for conventional power systems

The application of measurements based techniques to build dynamic equivalents for conventional power systems has been based on two main motivations. First, while most of the power systems components can be modelled by considering the physical laws that govern them, aggregating power system loads in order to obtain manageable models suitable for

dynamic analysis and simulations at high voltage levels, is quite a complicated exercise due to the absence of precise information. Therefore, one of the most reliable ways to obtain an accurate model is to apply an identification technique [147, 149, 150].

Taking into account that conventional dynamic equivalencing techniques require a considerable amount of knowledge about the external subsystem, as it can be concluded from section 3.3, the second motivation relies on the fact that in some cases the available knowledge may be not enough to develop accurate and reliable equivalents [119]. This is true especially in detailed aggregation with the development of equivalent regulators, such as suitable AVR and governors for the equivalent generator [44, 151]. When there is the need to improve the dynamic equivalent, the tuning task may prove difficult, since there is little indications about which parameters should be adjusted [152, 153] and there is still no common approach to analyse the identifiability of nonlinear models [30]. The industrial experience is also that dynamic equivalents derived from one class of events is typically not very successful for other classes [66, 77].

In order to overcome these difficulties, an alternative to conventional dynamic equivalencing techniques is to directly derive dynamic equivalents from measurements at points connecting the study subsystem with the remainder that will be reduced. Similar procedures have already been adopted for aggregation of loads, as mentioned previously. These methods aim to estimate a set of parameters belonging to a model that is assumed to represent the external subsystem, based on measurements of important signals. This kind of techniques has the advantage that detailed information of the external subsystem is not required. However, the key issues are the parameterization of the target model and the quality of the available signals.

A linearized generator model was selected for this purpose and expected natural system fluctuations were used for parameter estimation in [154]. More recent works reported in the literature proposed the use of ANN to build dynamic equivalents for large power systems, providing a new way to answer a question presented in previous equivalencing procedures: Are equivalent synchronous generators a good target model under all operating conditions [120]? Following the steps of [154], and with the benefits of almost three more decades of technological advances, such as the huge development in communications, signal processing and computing tools, these recent works demonstrated both the feasibility and usefulness of the methodologies based on ANN to build dynamic equivalents for large power systems. With

these methods the dynamic equivalent is derived from measurements at points connecting the study subsystem with the external subsystem, which will be reduced using ANN based strategies.

Once identified, such equivalent of external subsystem can be used in transient simulations and in other analysis and control design procedures, because ANNs are used as function approximators in a structure that assures the overall model compatibility with standard models of power systems components and therefore with transient stability formulations [119]. Since an ANN based dynamic equivalent is distinct from classic procedures, these works demonstrated also that it can work in conjunction with classic equivalents to reduce the effects of uncertainties, improving thus the accuracy [120].

In these works a neural network is used to extract states of the reduced order equivalent and another neural network is used to predict the new values of states of the external subsystem. In more recent works [121, 122], the external subsystem is represented in an input-output formulation and only one neural network is used to predict dynamic behaviour. The basis concept underlies the replacement of the nonlinear dynamic external area, considering all power system components, i.e., generators with controllers, by an ANN, which is connected to the study subsystem through tie lines and boundary buses. Using the ANN-based approaches the classical steps of dynamic equivalencing are omitted [122]. Simulation results proved the robustness of these approaches.

3.4.2 Dynamic equivalents for distribution networks with DG

Nowadays the number of dispersed generators is growing rapidly [136]. In the near future, it is expected that a considerable number DG units with significant capacity will be connected to the existing distribution systems [123, 124]. Approximating the dynamics of these networks using passive lumped loads, as it was done before, lacks the accuracy to simulate the dynamic behaviour of these systems with respect to the high voltage areas on large interconnected networks [124]. Therefore, replacing distribution systems that comprises a large number of active components with suitable dynamic equivalents is essential for power system dynamic analysis [155]. This arises not only due to the computational time saving but also from the difficulties of modelling a large number of active sources within the distributed area.

The classical methods to build dynamic equivalents have been developed for transmission systems with relatively small number of large synchronous generators concentrated into a few areas. In contrast, DG units are numerous and not limited only to synchronous generators. Many of them are based on induction machines, use power electronics and have quite different control systems which can be hardly aggregated [136]. Moreover, term coherency widely adopted by classical reduction methods becomes not so meaningful since induction generators do not have synchronizing torques and power electronic interfaces can almost completely separate, in a dynamic sense, the generator from the network.

Therefore, some works reported in the literature proposed strictly mathematical techniques originated from system theory to develop dynamic equivalents for distribution networks considering mainly the impact of such active units on the dynamics of the high voltage networks and, at the same time, reduce the simulation times.

As already mentioned previously, in [136] a balanced realizations method with truncation performed through singular perturbations theory was suggested and successfully applied to a small distribution network. However, taking into account that some restrictions may arise when applying this method to high dimensional systems [156] and based on the fact that linear models provide a limited accuracy to represent nonlinear dynamic distribution systems integrating a large number of different DG units with effective dynamic impact when major disturbances occur in the study subsystem, other authors developed a new equivalencing procedure that uses measurements provided by nonlinear time simulations. Then, a generic nonlinear dynamic equivalent model based on recurrent ANN is presented and used to replace such a distribution system in [123, 124].

The development of such dynamic equivalent did not obligate to specify a particular model configuration in advance. Rather, the target model is defined through both the structure and parameter description of the ANN. Concerning the lack of detailed information and the difficulty of modelling a large number of different active sources, this can be considered as an advantage. However, the authors recognize the need for measurements only at boundary buses between study and external subsystems as the main advantage of this dynamic equivalent. In addition, the accuracy of the developed model is not significantly affected by changing the operating point and hence it is not restricted to certain initial power flow conditions. Once well trained and tested, the ANN based dynamic equivalent can be used in simulation, analysis and control design procedures [123, 124].

3.5 Some remarks of dynamic equivalencing techniques concerning suitable dynamic equivalents for MG

Although research of power systems dynamic equivalents dates back to the late of 1960's [83, 157], the work in this field still continuing today. This is not only due to advancements in power system dynamic simulation software, but also due to fast changes in power systems composition and operation. In fact, large-scale widespread of DG connected to the distribution networks leads to a gradual transition from the current vertically-operated power system, which is supported mainly by several big centralized generators, into a future horizontally-operated power system, having also a large number of small to medium size generators and therefore it will be not possible to neglect the dynamics introduced by generators connected on the distribution network with respect to the high voltage levels as referred in section 3.4. At the same time, detailed modelling of the whole power system is not practical due to computational and time constraints. Therefore, finding dynamic equivalents for distribution networks with DG will become more and more important [123, 124, 136].

On the other hand, large deployment of microgeneration in LV networks under the framework of the MicroGrid concept described in chapter 2 will extend the philosophy of horizontally-operated power systems to the LV level. Local equilibrium of load and generation in combination with the MG hierarchical control architecture, inverter controls and storage devices allows to operate the MG autonomously like a physical island. In turn, large deployment of MG, connected on several adjacent MV feeders, coexisting with MV loads and DG units, will extend the MG operation flexibility to the MV level through suitable control schemes, leading with the MMG concept also presented in chapter 2. MMG will operate with cooperation with the whole power system resulting in a manageable network, which can also be operated autonomously.

In order to operate a MMG reliably, namely when it is operated in islanded mode, transient stability analysis should be performed at the MV level. Taking into account the possibility of having many MG connected to the MV network, an high dimensional system will arise and therefore the use of detailed models that are able to accurately simulate the MG dynamic behaviour with impact to the MV level will become not practical due to the considerable computational effort required to solve the resulting system of nonlinear differential equations, as already mentioned previously. Thus, in order to study the relevant dynamics of several MG

with respect to the MV networks, it is necessary to speed up numerical simulations with limited technical resources and therefore the development of dynamic equivalents for MG is required [16, 17].

For this purpose, the MG should be envisaged as a controllable and active cell similar to a controllable active source connected to the MV network, whose dynamics have an effective impact with respect to the MV network. Therefore, the dynamic equivalent to be developed will replace the MG detailed model, which is assumed to be the external subsystem, by a reduced order model according to the following guidelines:

- The MG dynamic equivalent must be an accurate representation of the detailed model concerning the transient analysis to be performed;
- The cost of building the dynamic equivalent must be much smaller than the cost of performing the transient analysis using the MG detailed model;
- The obtained dynamic equivalent has to be integrated into dynamic simulation tools.

When compared to a conventional power system, MG have no centralized synchronous machines. Rather, although their lower dimensions, MG can comprise many microsources with quite different technologies connected at several buses of the LV network through inverter interfaces. In addition different MG can have quite different compositions and to obtain detailed information about all of their components will be a difficult task. Therefore, in the following subsections the dynamic equivalencing techniques presented in this chapter are assessed regarding their applicability to build dynamic equivalents for MG, taking into account their main features.

3.5.1 Modal analysis

The power systems model order reduction using linear based approaches represents a simple task in spite of the long computing time required when dealing with large interconnected power systems. However, the linear based approaches have the following drawbacks:

- It is difficult to define the modes, which could be safely eliminated without affecting the results. The reduced order model will not be adequate to study some modes if their dynamics are cancelled during the reduction process;

- The results are accurate only around the operating point at which the reduction has been developed and will not adequately represent the system when the operating point moves away from the base case;
- Some restrictions arise when applying this method to strongly nonlinear problems;

Furthermore, the weaknesses pointed out in subsection 3.4.2, concerning distribution networks with high penetration of DG, will extend for developing MG dynamic equivalents purposes. In addition considering the MG dynamics with respect to the MV network as small perturbations around a steady state operating point and representing all the MG components by linear models will lack the accuracy for the resulting MG dynamic equivalent.

3.5.2 Coherency based methods

Coherency based methods allow to build nonlinear dynamic equivalents for conventional power systems. As described in subsection 3.3.2, these methods are based on the coherency concept and all methods for coherency recognition analyse the electromechanical behaviour of the synchronous generators, which is described by rotor angles or speeds based on the linearized model of the entire power system. These variables are not suitable for MS since they are connected to the LV networks through power electronic interfaces. Furthermore the dynamic behaviour of several MS, such as fuel cells and PV is not characterized by rotor angles or angular speeds. Therefore, coherency based methods do not make sense for MG. On the other hand, since the MG is a very resistive network, decoupling between active and reactive powers is not practical and therefore the linearized model cannot be applied.

3.5.3 ANN based dynamic equivalents

As the main features outlined in the previous two subsections do not recommend the applicability of both modal analysis and coherency based methods to develop suitable dynamic equivalents for MG, methods based on power system measurements are assessed for this purpose.

In contrast with conventional dynamic equivalencing techniques, ANN based dynamic equivalents have been characterized as approaches of general applicability. In fact, they have

been successfully applied to derive dynamic equivalents to replace some parts of conventional large power systems as well as distribution networks comprising a large number of DG units.

The main features of ANN based methods recognized as advantages in these previous two applications seem to have no practical applicability restrictions to MG. Rather, the main characteristics of measurement based dynamic equivalents motivate the exploitation of methods based on system identification theory to develop suitable dynamic equivalents for MG.

3.6 Summary and main conclusions

This chapter presented the state-of-the-art of dynamic equivalents in the power system field. The conventional approaches, such as modal analysis and coherency based methods that have been used to develop dynamic equivalents for large power systems were described as well as the main theoretical concepts and practical issues behind them.

With the technological and organizational advancements of conventional power systems new requirements of classical dynamic equivalencing approaches arose. In response alternative approaches, which are derived from system measurements have emerged. These approaches were also presented in this chapter.

In order to build dynamic equivalents suitable to represent the MG dynamics with respect to the MV network when the MMG is operated in islanded mode, the applicability of these main approaches to MG was discussed, taking into account the nature of different MS and the MG own specificities. From this discussion two main conclusions arise:

- Conventional dynamic equivalencing techniques are not practical for MG.
- Due to its general applicability, ANN based dynamic equivalents seems to be a promising approach.

Therefore, as a general conclusion, methodologies based on system identification theory should be exploited in order to develop suitable MG dynamic equivalents. Thus, the main nonlinear dynamic system identification techniques are addressed in chapter 4.

Chapter 4
Development of Dynamic Equivalents for MicroGrids exploiting System Identification Theory

4.1 Introduction

System identification is the theory and art of building models of dynamic systems based on observed inputs and outputs related with some pattern of behaviour [158, 159]. As a scientific discipline it dates back to the first attempts to model time series using *autoregressive* and *moving average* techniques. Nowadays typical applications pass over simulation, prediction, fault detection and control systems design. Even though a substantial part of the development of system identification techniques can be linked to the control community, these techniques are basically built on statistical approaches, in particular on linear and nonlinear regression methodologies [160]. Thus, in general, if the burden associated with building a model using physical laws is considered overwhelming, system identification techniques are naturally of particular interest.

Due to the large domain of application, system identification is a diverse field that can be presented in many different ways having different terminologies based on the historic development of models within different disciplines. Thus some expressions stem from time series modelling in economics [161] and [159, 162] established them as the now widely accepted standard in linear system identification. Since nonlinear system identification techniques emerge as natural extensions from the linear ones [161], the terminology used in [159, 162] was adopted in this thesis.

System identification based on linear models is today well established in research and in practice. In contrast, algorithms and available theoretical support are more scattered in the nonlinear field. A first reason for this is that it is more difficult to find models with a wide application, although the general framework can be formulated [163]. However, motivated by the fact that, in practice, all systems exhibit some kind of nonlinear behaviour, a significant effort has been made on the development of different approaches to perform nonlinear systems

identification, even in control applications. One of the key players in this endeavour are the ANN [164]. In fact, with the introduction of ANN, fuzzy models and powerful optimization techniques a much wider class of nonlinear systems has been handled [161].

Neural networks constitute a very large research field with application in many areas, including power systems, particularly in the dynamic equivalencing field as described in chapter 3, since in a general sense they can learn nonlinear mappings from experience. When this experience is interpreted as knowledge about how certain inputs affect a system, it is obvious that neural networks must have something in common with the techniques applied in system identification. Additionally neural networks based tools allow the use of the same approach for a broad variety of systems, although almost each nonlinear system is unique.

A system is a broad concept that plays an important role in system identification, since the modelling approaches are solved in a system oriented framework. Therefore, before starting any system identification procedure, a solid system definition should be given. Section 4.2 provides the system definition concerning MicroGrids for finding MG dynamic equivalent purposes with identification techniques. In order to cope with this problem the fundamentals of nonlinear dynamic system identification are described in section 4.3 through the description of common system identification procedures. Model quality issues are also addressed in this section.

As to build a nonlinear model is, in general, a very complex task, a general guideline is to make use of the available prior knowledge to derive a MG dynamic equivalent following its intended use with an acceptable trade-off between development effort and performance. Thus, in section 4.4, promising approaches to build dynamic equivalents for MG with identification techniques are formulated. Based on the available physical knowledge effectively used during the system identification procedure applied to this problem, two possible solution approaches are envisaged, which rely on using either a black box model structure based on MLP neural networks or a physical model structure.

- The first one tries to exploit the full response of the MG when excited after a disturbance;
- The second one tries to understand the physical behaviour of the different components of the MG.

The most adequate procedures adopted to derive MG dynamic equivalents either in terms of models and parameter of these models are also presented and discussed in this section.

Although there is a vast literature on parameter estimation and system identification in general, section 4.4 is restricted to the theory that can be exploited to build suitable dynamic equivalents for MG.

The summary and main conclusions are given in section 4.5.

4.2 The MicroGrid system definition

Like in a conventional power system, for purposes of analysis and to get a better sight to put up a reduced equivalent system, the detailed model of the whole MMG network is divided into two parts: The internal area that has to be retained for detailed analysis and the external area that has to be replaced by the equivalent model, as depicted in figure 4.1.

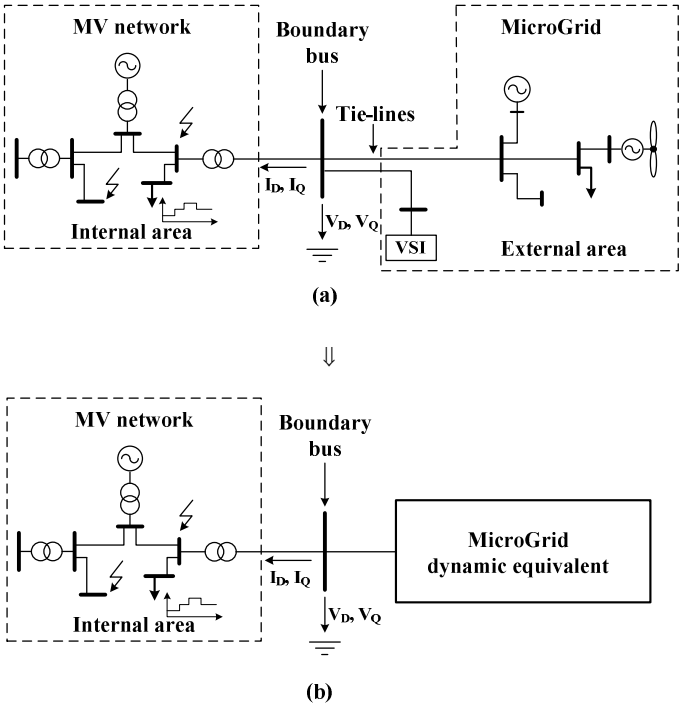

Figure 4.1: MMG system: (a) before reduction; (b) after reduction

As it can be observed from figure 4.1, the external area involves the MG detailed model while the internal area comprises the remaining MMG detailed model, corresponding to both the external and the study subsystems, respectively. In this sense, the dynamic system to be identified consists of a set of differential and algebraic equations corresponding to the dynamic models of the several microgeneration systems presented in chapter 2, describing the state evolution over time of the physical system – the MicroGrid.

Therefore the system identification procedure consists on finding just another mathematical representation of the physical MG built upon the corresponding MG detailed model. The evolution over time computed using the MG detailed model is called a process under system identification termination [161].

Since data is the main source of information, among other issues, the system definition involves to specify which signals are considered as inputs and which ones are considered as outputs in order to define where the measurements take place, that is, the system boundary. Afterwards suitable input signals have to be designed in order to collect informative enough data sets.

In contrast with linear systems, PRBS are inappropriate for nonlinear systems and, probably due to the highly application specific nature of the problem, few tools exist and little research is devoted to this subject [161]. Aspects such as the purpose of the model, characteristics of different input signals, equal data distribution and dynamic properties should be taken into account in order to choose persistently exciting inputs. From this list of general guidelines, it follows that a high engineering expertise is required in order to design adequate input signals.

Thus, in order to collect an informative enough data set, the MG detailed model has to be excited through efficiently generated disturbances scenarios into the internal area and the MG dynamics following these disturbance scenarios should be captured by means of the electrical variables, measured at the system boundary. Another issue to be taken into account concerns the electrical network reduction. As described in subsection 3.3.2.4 of chapter 3, node elimination and aggregation can be done by making the MG dynamic equivalent injected currents at the boundary bus equal to the currents in tie-lines.

Therefore, boundary bus voltage expressed through its both $D-$ and $Q-$axis components and MMG system frequency are considered as inputs while the $D-$ and $Q-$axis components of the tie-line currents are considered as system outputs, as illustrated in figure 4.1. Thus, the dynamic equivalent will react to boundary bus voltage and system frequency changes resulting from the internal area disturbances scenarios, by varying the injected current into the retained subsystem.

In order to derive dynamic equivalents for MG using system identification techniques based on this system definition, the fundamentals of nonlinear dynamic systems identification are addressed in the following section.

4.3 Fundamentals of nonlinear dynamic systems identification

Although that almost all practical systems are in principle nonlinear, most of the available system identification literature has focused on dealing with models and controllers described by linear differential or difference equations, i.e., identification of linear systems. There are many reasons for this. Some of them derive from the fact that models have been used in many cases oriented towards control applications. Identification for control deals mainly with the question of how identify a model that serves as basis for control design and thus the goal is not a very accurate model but good control performance. In addition, it is much simpler to design controllers for a system described by a linear model [164]. Furthermore, linear system identification is less complicated to perform from a computation perspective and the analysis is less complicated from a statistical view point.

Nowadays nonlinear dynamic systems identification is considered as a field of very active research; many new methods have been developed and old methods will be improved. Nevertheless, the linear underlying principles are valuable. In this sense local linear model approaches constitute a very promising approach to nonlinear systems identification. A practical case was *NNSYSID* software package, which is described in [165], as an extension of the *System Identification Toolbox* [166] developed for *MATLAB*®. However, building a nonlinear model is a much complex task than a linear one and some stages are not well established. Prior knowledge and intended purpose of the model are the general guidelines, as already mentioned previously.

4.3.1 How to build mathematical models

Models, in general, are derived from the knowledge of system properties, namely those that are considered relevant for the intended purpose of the model. This prior knowledge can result from two possible sources:

- Mechanistic descriptions of the system;
- Observations or measured data.

Then mathematical models can be obtained either theoretically based on physical relationships – physical modelling – or empirically based on experimental data from the system [158], as it can be observed from figure 4.2.

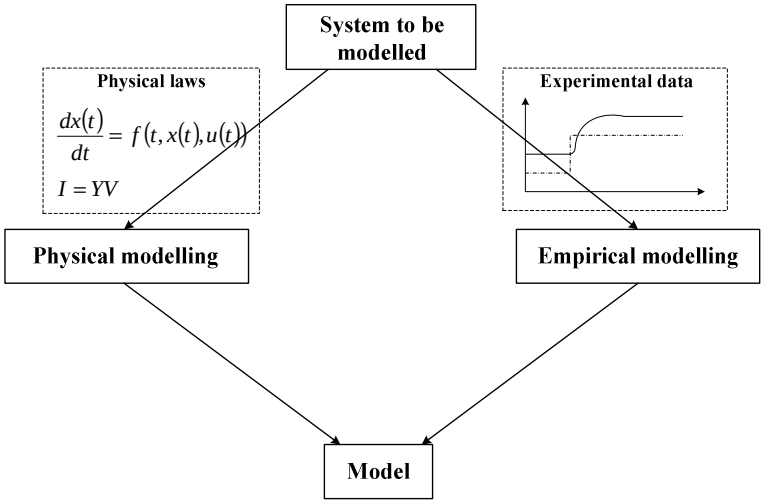

Figure 4.2: The two basic principles for mathematical model building

Many combinations of physical and empirical modelling have been pursued and, depending on the level of prior insight about the system effectively used, three different modelling approaches can be distinguished [164]. If the model is derived from measured data, assuming only a reduced knowledge about the physics of the system, the modelling approach is called black-box modelling; in contrast, white-box modelling is used for a pure physical modelling of the system. When a certain level of insight about the system exists and is used together with measured data to derive an empirical model, the gray-box modelling classification can be used.

System identification is concerned with the development and analysis of methods for performing grey and black box modelling [158, 159, 162, 164, 167-169]. Differently from white-box modelling, that is intimately related to the specific knowledge domain, system identification covers a number of methodological issues that arise whenever data are processed to obtain a quantitative model, as it can be seen in the following subsection.

4.3.2 A common system identification procedure

According to [159, 162], the techniques to build and complement models from system measurements involve fundamentally three basic entities:

- A data set;
- A set of candidate models;
- An identification criterion.

The beginning of all model building is the observed data. Then a data set is recorded during a specifically designed identification experiment. With a given observed data set, the system identification procedure main tasks are to decide on a set of candidate models and to estimate the model parameters in the sense of an identification criterion. However, an important question is whether the model is good enough for its intended purpose. Testing if a model is appropriate is known as model validation.

The above considerations have lead to a general conceptual approach including the following basic steps.

4.3.2.1 Identification experiment

Although the available software packages do not assist the user in designing the experiment, the data set is the basis for any successful identification procedure, since system behaviour that is not represented within the data set cannot be described by the model, unless prior knowledge is explicitly incorporated.

Since a typical data acquisition mode deals with input and output observations, the basic idea is to vary the system inputs and observe the corresponding impact on the outputs, as depicted in figure 4.3.

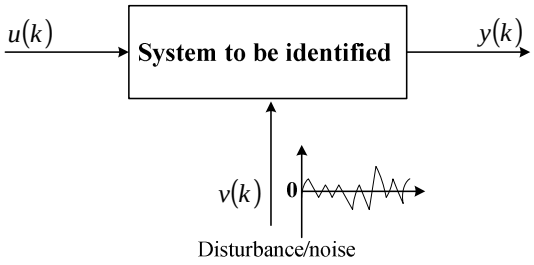

Figure 4.3: Scheme of the system to be identified

When it has been decided upon where and what to measure, the next question is when to measure. Since both system inputs and outputs are observed at sample instants $t_k = kT, k = 1,2,...N$, then a sampling time, T, has to be chosen. Finally a required number of measurements, N, to be collected should be defined. It can also be assumed that there are always signals beyond control, namely measurement noise and possibly uncontrollable inputs, denoted by $v(k)$ in figure 4.3, which will affect the system output. For ease of notation, T is

assumed to be one time unit and k is used to enumerate the sampling instants. Thus, the data set of corresponding system inputs and outputs is given by:

$$Z^N = \{[u(1), y(1)] \quad [u(2), y(2)] \quad \cdots \quad [u(N), y(N)]\} \tag{4.1}$$

However, the system experiment involves more issues than simply data collection. As the purpose of an identification experiment is to collect a set of data that describes how the system behaves over its entire range of operation, the design of appropriate excitation signals is an important task, since, independently of the modelling approach to be followed, the quality of the observed data will determine an upper bound on the accuracy that can be achieved by the model. Nevertheless, due to the fact that nonlinear models are significantly more complex, this task is even more decisive for nonlinear than for linear models since the data must contain considerably more information.

4.3.2.2 Model structure selection

In formal terms, after collecting a data set one is looking for a relationship between past observations, u^{k-1}, y^{k-1}, and future outputs, $y(k)$, as

$$y(k) = g(u^{k-1}, y^{k-1}) + v(k) \tag{4.2}$$

where the additive term $v(k)$ accounts for the fact that the next output $y(k)$ will not be an exact function of the past data.

In order to construct a model from data it should be assumed that $g(\cdot)$ belongs to a family of functions that is parameterized in terms of a finite number of parameters, commonly denoted by θ. This family of candidate model functions will be called a model structure and is defined in [159] as a differentiable mapping from the parameter domain, $D_{\mathcal{M}}$, to the space of the parameterized model outputs,

$$\mathcal{M} : \theta \to \hat{y}(k \mid \theta) = g(u^{k-1}, y^{k-1}; \theta) \in \mathcal{M}^* \tag{4.3}$$

where

$$\theta = [\theta_1 \quad \theta_2 \quad \ldots \quad \theta_{n\theta}] : \theta \in D_{\mathcal{M}} \subset R^{n\theta} \tag{4.4}$$

is the parameter vector with $n\theta$ parameters used to parameterize the mapping. Model structures have been commonly denoted by $\mathcal{M}$ while a particular model corresponding to a parameter vector θ is denoted by $\mathcal{M}(\theta)$. The set of candidate models is thus defined as

$$\mathcal{M}^* = \{\mathcal{M}(\theta) \mid \theta \in D_{\mathcal{M}}\} \tag{4.5}$$

Formally speaking, the expression (4.3) is too general and it should be useful to write $g(\cdot)$ as a concatenation of two mappings; one that takes the increasing number of past observations and maps them into a vector $\varphi(k,\theta)$ of fixed dimensions and another that takes this vector to the space of the model outputs [169]. Thus

$$g(u^{k-1}, y^{k-1}; \theta) = g[\varphi(k,\theta); \theta] \tag{4.6}$$

where

$$\varphi(k,\theta) = \varphi(u^{k-1}, y^{k-1}; \theta) \tag{4.7}$$

is the regression vector with its components referred to as the regressors. Therefore the model structure in (4.3) is decomposed into two partial problems for nonlinear dynamic systems:

- How to choose the regression vector $\varphi(k,\theta)$ from past inputs and outputs;
- How to choose the nonlinear mapping $g(\varphi,\theta)$ from the regressor to the output space.

The choice of an appropriate model structure is considered in the literature the most important and, at the same time, the most difficult decision the user has to make, because the lack of theoretical support [161]. Therefore, it is particularly important that the model structure will be linked to the intended use of the model, which means that prior knowledge, engineering intuition and insight about the system dynamics have to be combined with the formal properties of models in order to select a suitable mathematical representation for the system to be identified.

Sometimes a model set is obtained after a careful physically modelling approach; the model parameters represent unknown values of system parameters that, in principle, have physical interpretation. In other cases, standard nonlinear models without reference to physical background may be employed. Such a model set, whose parameters are basically viewed as vehicles for adjusting the fit to the data, is called a set of ready-made or black box models.

Model sets with adjustable parameters with physical interpretation may accordingly be called tailor-made or gray-box models [158, 159, 161, 162, 164, 169].

4.3.2.3 The identification method

The search for a good model is then carried out in terms of the parameters θ. The problem now is to decide upon how to use the information contained in the data set, Z^N, to select a proper value, $\hat{\theta}_N$, of the parameter vector and hence a proper member $\mathcal{M}\left(\hat{\theta}_N\right)$ of the set of models $\mathcal{M}^*$. Thus, given a set of candidate models, $y(k)=g(\varphi(k),\theta)+v(k)$, and a set of measured regressor-output pairs,

$$Z_e^N=\{[\varphi(k),y(k)]:k=1,...,N\} \tag{4.8}$$

the purpose of the identification method is to determine a mapping from Z_e^N to the set of candidate models $D_{\mathcal{M}}$,

$$Z_e^N \rightarrow \hat{\theta}_N \in D_{\mathcal{M}} \tag{4.9}$$

in order to obtain a model that provides predictions close to the system outputs in the sense of the identification criterion. The search for the optimal point, in an $n\theta$-dimensional parameter space, spanned by the parameter vector θ, is carried out through a suitable parameter estimation technique and the set of regressor-output pairs Z_e^N is referred to as the estimation data set, since the model parameter estimation will rely on it.

The identification method is equivalent to reconstructing the hyper surface $g(\varphi(k),\theta)$ from the pairs $[\varphi(k),y(k)]$. According to this view point, there are clear connections with function approximation, learning theory [170], neural networks [171, 172] and statistics [173] whenever the measurement errors are given in a probabilistic manner. Then this process is known, in statistical literature, as estimation and, for historical reasons, in the neural network community, it is usually called training or learning. Therefore the estimation data set is also known as training data set. This basic search concept is illustrated in figure 4.4 from a modelling view point.

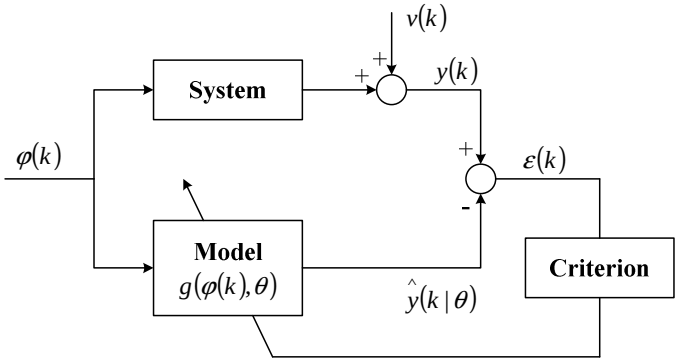

Figure 4.4: The search for the optimal point under a modelling perspective

Both system and model are fed with the same inputs, $\varphi(k)$, and the corresponding outputs, $y(k)$ and $\hat{y}(k|\theta)$, respectively, are compared yielding an error signal,

$$\varepsilon(k,\theta) = y(k) - \hat{y}(k|\theta) \tag{4.10}$$

which can be computed for $k = 1,...,N$ and used in some sense for adapting the model.

The parametric model has to be augmented with a suitable identification criterion that measures how well the model fits the system outputs and with an algorithm that will adapt the model parameters so that a minimum identification criterion can be achieved. Thus, the goal of the parameter optimization technique is to find the best approximation $\hat{y}(k|\theta)$ of the measured output $y(k)$, which may be spoilt with noise, by adapting the parameter vector θ. This procedure can be computationally intensive, but it is generally one of the easiest stages in the identification procedure.

4.3.2.4 Model validation

After settled the previous three stages a model has been estimated; the one, in the chosen set of models, that best describes the training data according to the identification criterion. Now, the obtained model must be evaluated in order to investigate whether or not it is valid for its intended purpose. Therefore two main aspects should be taken into account:

- The model agrees sufficiently well with the observed data;
- The model is good enough for its intended purpose.

Generally the method to lead with these questions is to confront the model $\mathcal{M}\left(\hat{\theta}_N\right)$ with as much information about the system as it is practical. This includes a prior knowledge, measurement data and experience of using the model. In a general identification application the most natural entity with which to confront the model is the data. Then model validation techniques tend to focus on the first aspect. However, since there is always a certain purpose with the modelling, what matters in practice is the second aspect and the ultimate validation step is then to test whether the problem that motivated the modelling exercise can be solved using the obtained model [158, 159, 161, 164].

For most applications this level of ambition is somewhat high. So, instead of investigate the particular properties of the models, it is a common procedure to apply standard tests in order to develop confidence in them. According to [158, 159], for a model structure physically parameterized, a natural and important validation is to confront the estimated values and their estimated variances with what is reasonable from prior knowledge. It is also good practice to evaluate the sensitivity of the input-output behaviour with respect to these parameters in order to check their identifiability. Concerning to black box models, the interest is focused on their input-output properties. While for linear models these properties are normally displayed as Bode diagrams, for nonlinear models they will be inspected by simulation and, in this sense, model validation is closely related to the concept of model quality [161, 164], which is addressed in subsection 4.3.3.

4.3.2.5 The system identification loop

As briefly described in the preceding subsections, in a common system identification procedure the user has to take a number of decisions: An experiment has to be designed, a model structure must be chosen, an identification criterion must be selected as well as the optimization technique and a procedure for validating the obtained model has to be devised. Each one of these choices will have an influence on both quality and amount of work of the resulting model. Thus, they may also to be revised a number of times during the identification procedure.

In the model validation block it is checked whether all preceding steps have been carried out successfully or not in the sense of the validation criterion, which of course is highly problem dependent and also closely related to the intended use of the model. As depicted in

figure 4.5, the paths going from this block back to the previous stages indicate that the procedure is executed in an iterative manner [159].

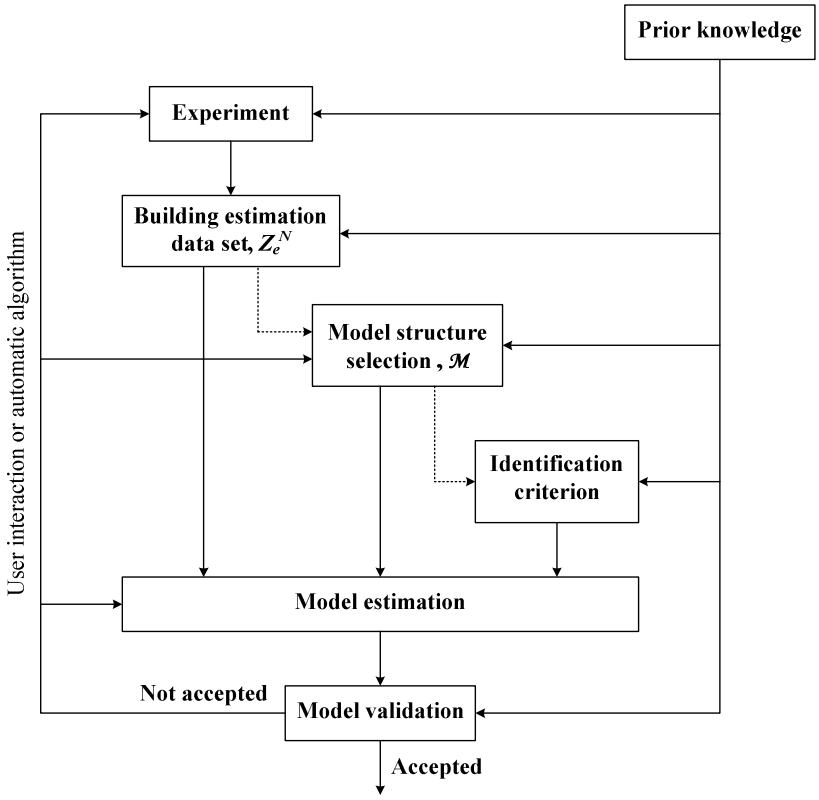

Figure 4.5: The basic system identification loop

It is quite likely that the model first obtained will not pass the model validation tests and then it is necessary to go back in the procedure and revise the various steps taking into account the reasons by which the model may be deficient. It should be necessary to determine a different model into the selected set of models, to try out another model structure or, in the worst case, even redo the experiment:

- Path leading back to model estimation, when the numerical procedure failed to find the best model according to the identification criterion.
- Path leading back to the model structure selection, when the model structure was not appropriate since it did not contain a good enough mathematical description of the system.
- Path leading back to experiment, when it seems impossible to determine a suitable model because the data set was not informative enough to provide guidance in selecting good models.

The major part of an identification application consists of addressing these problems, in particular the model structure selection, in an iterative manner guided by prior knowledge and the outcomes of previous attempts. Interactive software obviously is an important tool for handling the iterative character of this problem.

4.3.3 Model quality

Based on the assumption that there is a set of mathematical equations representing exactly the true structure of the system, S, the identification task would be to determine the true values of the parameters from the estimation data set, which should be informative enough to distinguish between different model structures as well as properties of the model structure itself. Therefore, the equivalence of the estimated model to the true system is established through the convergence of the parameter estimate to the true parameters, θ_0. Then the convergence domain is defined as

$$D_T(S,\mathcal{M}) = \{\theta_0\} \tag{4.11}$$

This set is empty if $S \notin \mathcal{M}$. Thus one important aspect to be taken into account in model structure selection is to chose $\mathcal{M}$ so that (4.11) holds for a given description S. However, in practice, nonlinear complex systems can never be completely known so that it is not possible to know a priori if the parameter estimation will be well achieved. Thus, the identification problem becomes to find a member from a given model structure, which approximates reasonably well the system in the sense of the identification criterion. In a probabilistic framework the expectation of the square error may be used as a loss function [161] and then as a measure of model quality since it allows some important analytical results [174]. Suppose that the actual data can be described by

$$y(k) = g_0(\varphi(k)) + v(k) \tag{4.12}$$

where g_0 is some unknown true model and $v(k)$ is white noise with variance λ, the average generalization error is given by

$$\overline{V}(\theta) = \frac{1}{2} E\left\{\left\| y(k) - g(\varphi(k),\theta)\right\|^2\right\} = \frac{1}{2}\lambda + \frac{1}{2} E\left\{\left\| g_0(\varphi(k)) - g(\varphi(k),\theta)\right\|^2\right\} \tag{4.13}$$

Unfortunately it is not possible to evaluate (4.13) in practice, but under suitable conditions [159], that is,

$$\bar{V}(\theta) = \lim_{N\to\infty} V_N\left(\theta, Z_e^N\right) \tag{4.14}$$

and thus, $\hat{\theta}_N \to \theta_*$ for $N \to \infty$, when θ_* is the minimizer of (4.13). In particular, if the true system described by (4.12) was contained in the model structure, $S \in \mathcal{M}$, the estimate would also be consistent: $\theta_* = \theta_0$. Then, within a given model structure parameterized by θ of dimension $n\theta$, the best model can be defined according to the following quality measure [169].

$$\theta_*(n\theta) = \arg\min_{\theta\in D_{\mathcal{M}}} \bar{V}(\theta) \tag{4.15}$$

It should be noted that $\theta_*(n\theta)$ will depend on the number of parameters and on the properties of φ. To measure the quality of a given model, $\hat{\theta}_N$, one should use

$$E\bar{V}\left(\hat{\theta}_N\right) = V_*(n\theta) \tag{4.16}$$

Here the expectation is with respect to the model $\hat{\theta}_N$. The measure (4.16) thus describes the model's expected fit to the true system, when applied to a new data set with the same distribution of the regressors φ. For a given regressor properties and a given model structure family, it depends only on the number of model parameters, $n\theta$.

4.3.3.1 Bias and variance

Assuming that the estimate $\hat{\theta}_N$ is obtained by minimization of MSE criterion and also the model $\theta_*(n\theta)$ is quite good in the sense that the model residuals are white noise, the model criterion $V_*(n\theta)$ as defined in (4.16) can be expressed as

$$V_*(n\theta) = E\overline{V}\left(\hat{\theta}_N\right) = \lambda + E\left\| g_0(\varphi(k)) - g\left(\varphi(k), \hat{\theta}_N\right)\right\|^2 =$$
$$\approx \underbrace{\lambda}_{noise} + \underbrace{E\left\| g_0(\varphi) - g(\varphi, \theta_*(n\theta))\right\|^2}_{bias} + \underbrace{E\left\| g(\varphi, \theta_*(n\theta)) - g\left(\varphi, \hat{\theta}_N\right)\right\|^2}_{variance} \quad (4.17)$$

As indicated, $V_*(n\theta)$ can be approximately decomposed into two parts: one due to the bias, the other due to the variance of the estimation. They are further examined in the following.

As $N \to \infty$, $\hat{\theta}_N \to \theta_*(n\theta)$, the variance error should be negligible and thus $V_*(n\theta)$ will only involve the bias part. The estimate will thus converge to the best possible approximation of the true system for a given model structure and model size. Thus, the bias error describes the systematic deviation between the process and the model that, in principle, exist due to an insufficient model structure; i.e., $S \notin \mathcal{M}$.

Since the test data set has a different noise realization, the estimated parameter vector, $\hat{\theta}_N$ will have a certain covariance matrix that describes its deviation from $\theta_*(n\theta)$. Concerning to the variations in θ with respect to the prediction performance, it can be shown [159] that for large estimation data sets the variance error increases approximately linearly with the number of model parameters.

$$E\left\| g\left(\varphi(k), \hat{\theta}_N\right) - g(\varphi(k), \theta_*(n\theta))\right\|^2 \approx \lambda \frac{n\theta}{N} \quad (4.18)$$

Combining (4.17) and (4.18) gives,

$$V_*(n\theta) = E\overline{V}\left(\hat{\theta}_N\right) = \lambda + \lambda\frac{n\theta}{N} + E\left\| g_0(\varphi) - g(\varphi, \theta_*(n\theta))\right\|^2 = \overline{V}(\theta_*(n\theta)) + \lambda\frac{n\theta}{N} \quad (4.19)$$

A useful interpretation of (4.19) is that it displays the expected model performance on the validation data set. It is important to recognize that the expected value of the model performance when it is applied to the estimation data set, with MSE criterion, is quite different,

$$EV_N\left(\hat{\theta}_N\right) \approx \overline{V}(\theta_*(n\theta)) - \lambda\frac{n\theta}{N} \quad (4.20)$$

In fact the variance error is only detected on fresh data that is when the model performance is evaluated on a validation data set, not used during training. Otherwise the variance error will decrease as $n\theta$ increases.

4.3.3.2 Model structure flexibility

The concept of model flexibility will be related to the number of parameters that the model possesses in the sense that a model becomes more flexible (more complex) if additional parameters are included and it becomes less flexible (simpler) if some parameters are removed, independently of the nonlinear mapping to be used.

Under the context of model flexibility, from (4.17) it becomes clear that the bias error is large for less flexible models and decreases as the number of basis functions grows, approaching to zero for a large number of model parameters. On the other hand, for a finitely sized estimation data set, the variance error works on the opposite direction and reaches its maximum when the training data contains only as many data samples as there are parameters in the model [161]. In such a case, the degree of freedom allow to fit the model perfectly on the training data set, as in (4.20), which means that the parameters precisely represent the noise contained in the estimation data set and therefore it is expected that this model performs worse in a test data set, which contains a different noise realization, as (4.19) demonstrates.

In fact bias and variance are in conflict in the sense that it is impossible to minimize both errors simultaneously. This is the well known bias/variance dilemma, which can be discussed under different disguises and particularly under a neural network framework in [175, 176]. Therefore the concept of optimal model flexibility represents the best overall solution for a specific model class. Directly from this fact follows the parsimony principle which states that from all models that can describe the process accurately, the simplest one is the best [159].

4.3.3.3 Evaluating the test error and alternatives

A validation or test data set, Z_v^T, is commonly used for evaluating the model quality. In fact, as already mentioned previously, the variance error is detected only if a data set with different stochastic effects due to noise is used. Otherwise it could not be detected since the

error in the estimation data set consists mainly on the bias part for a large training data set when compared to the number of model parameters.

This means that the error on the data set decreases with the model flexibility, while the error on test data set decreases only until the point of optimal flexibility, beyond which it starts to increase. If this effect is ignored, one typically ends up with overly complex models, which perform well on the estimation data set but poorly on the validation data set, since the model not only models the features of the system, but also the noise in the training data set. This effect is called overfitting. Likewise, the expression underfitting is used when the bias error is dominating, which means that the model have no flexibility enough to describe the system features.

The quantity $V_T\left(\hat{\theta}_N, Z_v^T\right)$ is interpreted as an estimate of the average generalization error. If $\overline{V}\left(\hat{\theta}_N\right) \cong V_T\left(\hat{\theta}_N, Z_v^T\right)$ is close to $V_N\left(\hat{\theta}_N, Z_e^N\right)$ it is likely that $\hat{\theta}_N$ is close to θ_* and that the obtained model is reasonably good.

When the amount of available data is small other approaches must be pursued for model quality evaluation, like the use of information criteria or alternatively statistical tests and correlation based methods [159, 161, 164]. Typical choices of information criteria are AIC, BIC and FPE [167, 177]. However, in this research work, the amount of data is not limited and therefore those methods are not considered.

4.4 Finding MG dynamic equivalents with identification techniques

In order to build dynamic equivalents for MG exploiting system identification theory, a similar procedure than that one described in subsection 4.3 should be followed. Then, in this section, the problem of MG dynamic equivalents development is formulated under a system identification framework and the solution approaches are envisaged, taking into account the prior knowledge that has been derived from chapters 2 and 3 as well as the intended purpose of the model to be identified. Thus, subsection 4.4.1 is devoted to the identification problem formulation and subsequently promising solution approaches are considered based on suitable model structures selection. These approaches are described in subsection 4.4.2. Afterwards appropriate identification methods have to be selected. Then, identification criteria are

addressed in subsection 4.4.3 while parameter estimation methods are presented in subsection 4.4.4, taking into account the model structures selected in subsection 4.4.2.

Finally, MG reduced order model validation issues are described in subsection 4.4.5.

4.4.1 Problem formulation

As previously described in chapter 2, to develop a power system dynamic simulation, the equations used to model the different elements are collected together to form a set of differential equations,

$$\dot{x} = f(x,u) \tag{4.21}$$

and a set of algebraic equations

$$0 = g(x,u) \tag{4.22}$$

where x is the state vector of the whole power system and u represents the inputs. The differential equations describe the power systems dynamics and are mainly related with the several generating units whilst the algebraic equations describe the network, the static loads and the generator algebraic equations.

Since *MatLab*® *Simulink*® was used as the dynamic simulation tool these two sets of equations, (4.21) and (4.22), were implemented graphically in terms of a block diagram model, in which the differential equations were represented as integral equations in order to separate their static nonlinear transformations and integrations as depicted in figure 4.6, where each block within a block diagram defines an elementary dynamic system in itself and the relationships between each one are given by the use of signals connecting the blocks.

Determining the system behaviour over time thus entails repeatedly solving the model at intervals, called time steps, from the start to the end of time span. *Simulink*® refers to this process as simulating the power system that the model represents. In this sense, simulations can be considered as an inexpensive and safe way to experiment with power systems and with effective computer power numerical experiments have been carried out.

However, due to the excessive computing time required when running dynamic simulations in time domain together with practical limitations on the size of computer memory, power systems analysis programs do not usually model the complete system in detail. As already

mentioned previously, in chapter 3, only the internal subsystem is modelled in detail and the external subsystem is represented by a dynamic equivalent also called a reduced model. The model order reduction of the external system can be done by separating the external subsystem from the internal one and by making the injected currents at the boundary nodes equal to the tie-line currents, as already mentioned previously in section 4.2.

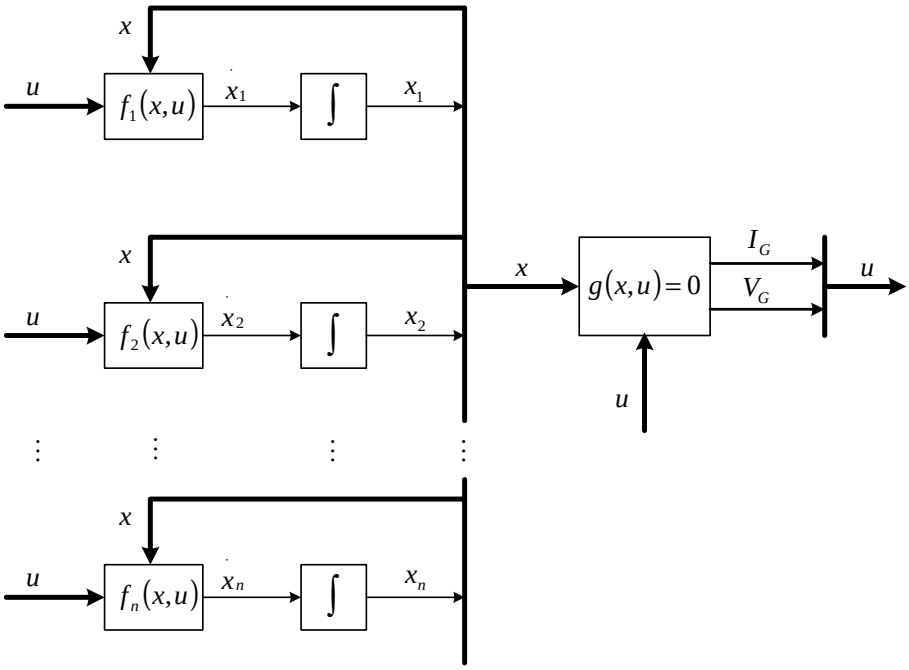

Figure 4.6: Power system block diagram for dynamic simulation

In this sense, the reduction of the external system using a conceptual system identification procedure should be envisaged as a problem of identifying an external subsystem equivalent model, guided by the available prior knowledge and the goal that motivated the identification procedure as described in the following subsections.

4.4.1.1 Physical insights

As discussed in subsection 2.4.1 of chapter 2, the MG is operated under a SMO control strategy when it is connected to the upstream MV network, even upon MMG islanding. Thus, the available physical knowledge allows to distinguish between two different time scales concerning the dynamic responses among the several microgeneration systems into the MG:

- The main storage device with a VSI control inverter scheme displays fast dynamic responses;
- The controllable MS with a PQ inverter control display slow dynamic responses.

Additionally, those microgeneration systems connected to the LV grid through inverters with PQ control schemes are the main responsible for the large simulation times.

Based on those previous assumptions, a suitable dynamic equivalent for MG comprises the detailed model of the main storage device VSI control and an aggregated model corresponding to the remainder MG detailed model, henceforth called the equivalent model of the MG slow dynamics, as depicted in figure 4.7.

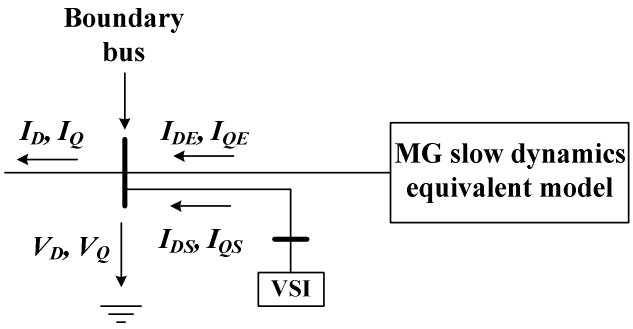

Figure 4.7: MG dynamic equivalent model

Therefore, in this case, the aim of the system identification procedure is to identify the equivalent model of the MG slow dynamic behaviour.

4.4.1.2 Purpose of the model

Under system identification framework a model can be used in two configurations, either to perform prediction or simulation [161]. Prediction means that on the basis of previous process inputs and process outputs the model predicts one step into the future, requiring that the process output is measured during operation. In contrast, simulation means that on the basis of previous process inputs only, the model simulates future outputs. Thus, simulation does not require process output measurements during operation.

As the MG dynamic equivalent is required to describe the MG dynamic behaviour without coupling to the MG system, the process output cannot be measured during operation and therefore the equivalent model of the MG slow dynamics should be identified to be used in simulation configuration. For this purpose suitable solution approaches should be carried out.

4.4.2 Solution approaches

A possible solution approach based on the collected data set starts with the model structure selection task, which involves to decide between many sets of models, which in principle are adequate to describe the process in mind, as already mentioned in section 4.3.

In order to select a suitable model structure to MG slow dynamics equivalent model, two assumptions are taken into account:

- The composition of the MG is known and the physical laws that describe the MG slow dynamics under study are understood and effectively used;
- The MG composition is not known or the available prior knowledge is not used to sort out the physical relationships.

Therefore, concerning to the model structure selection, the first decision is mainly based on the available physical knowledge about the system to be modelled effectively used. In this sense, both physical and black-box models can be used leading with gray and black-box modelling approaches.

Figure 4.8 gives a general overview of the possible solution approaches to be followed.

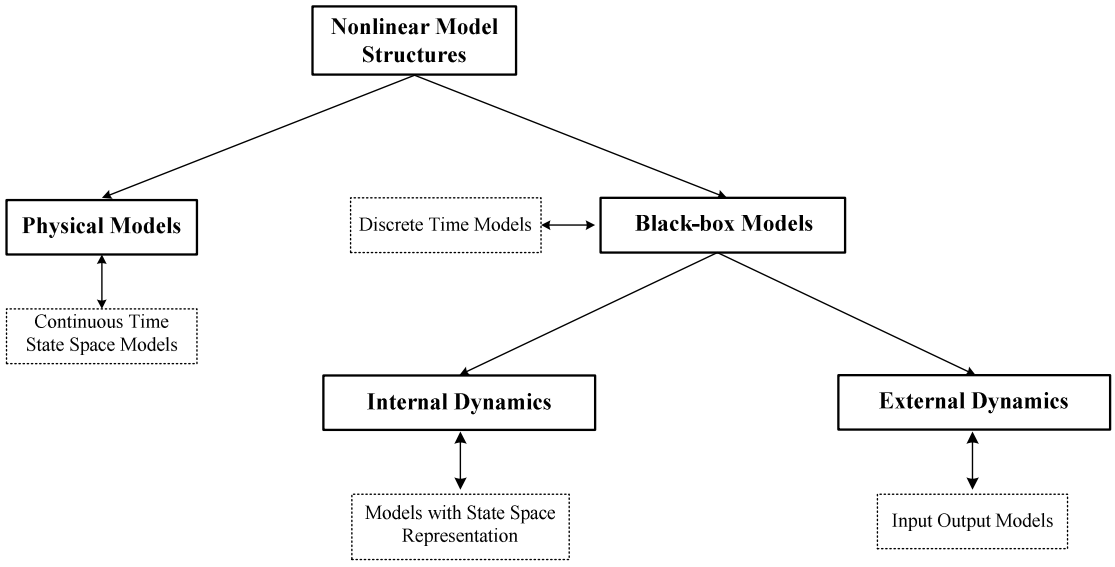

Figure 4.8: Model structures for MG slow dynamics equivalent model

4.4.2.1 Physical modelling

When it is assumed that the physics of the system are understood and it is possible to represent them using a set of ordinary differential or difference equations with unknown

parameters a physical model structure should be chosen. Since most laws of physics are expressed in continuous time, it is easier to construct models with physical insight in continuous time than in discrete time and usually a physical model structure is a continuous time state space model of a given order as

$$\begin{cases} \dfrac{dx(t)}{dt} = f\left(x(t), u(t); \theta\right) \\ \hat{y}(t \mid \theta) = h(x(t), u(t); \theta) \end{cases} \tag{4.23}$$

where θ is the parameter vector, $x(t)$ represents the states and the regression vector corresponds to the actual inputs, $u(t)$. Such a predictor is presented in a simulation configuration, since $\hat{y}(t \mid \theta)$ is constructed by simulating a noise free model using the actual system inputs. If it is assumed that measurement noise is affecting the model output, this noise should be described as white noise. When more sophisticated noise modelling is required the Kalman filter should be used to compute $\hat{y}(t \mid \theta)$ [159], [178].

From (4.23), it is possible to observe that the model structure is the point of contact between physical modelling and empirical modelling approaches, since after to obtain a model structure based on physical grounds, the values of the model parameters gathered into the parameter vector, θ, are missing and should be determined from measured data. Therefore a physical model has one important advantage which arises from the fact that the known physical relationships are built in and no parameters have to be wasted in order to estimate what is already known. Thus, the model is parsimonious with its parameters which often have a direct physical interpretation. This later fact has the added advantage that it helps to decide if the estimates are reasonable [178].

4.4.2.2 Black box modelling

When it is assumed that the available prior knowledge does not allow to design a physically parameterized model structure, it is then possible to use standard models, which by experience are known to be able to handle a wide range of different system dynamics. For a modelling view point these models thus serve as ready made models since for a given model order it should be possible to find something that fits to data. A black box model is thus a flexible

mathematical structure that is capable of describing many different systems and its parameters might not have any physical interpretation. Therefore, some advantages should be acknowledged in black box modelling over physical modelling, namely it does not need to know both the model structure and order to get started quickly, many model structures can be estimated and compared in order to choose the best one and the universality.

However, considering that there are no particular insight into the system's properties, $g(\cdot)$ would be parameterized in a flexible way covering all kinds of reasonable system behaviour, giving obviously a big family of nonlinear black-box models. Therefore, as already mentioned in subsection 4.3.2.2, the model structure selection task for modelling purposes involves, in general, two main additional decisions:

- To choose a set of regressors;
- To specify how to combine them into a one-step-ahead prediction.

In particular, for deriving MG dynamic equivalents purposes, the possibilities of these two choices are briefly addressed in the following two subsections.

4.4.2.2.1 NFIR vector of regressors

As natural extensions of linear dynamic model structures, two nonlinear dynamic model classes can be distinguished: Input-output models and models with state space representation, which are the nonlinear counterparts of both linear models with polynomial and state space representation, respectively [159-161, 163-165, 169, 172]. Therefore two fundamentally different black-box modelling approaches are distinguished in [161] between internal and external dynamics as it can be observed from figure 4.8 presented in subsection 4.4.2.

In the case when the system internal states can be measured, internal dynamics are of easy applicability and have been preferred over the input-output model structures. However, if the states have to be considered as unknown quantities they must be estimated as well. The high complexity generally involved in the simultaneous estimation of model states and parameters is the reason for the dominance of the much simpler nonlinear input-output models and, thus, the external dynamics approaches [161]. As the MG states can not be measured, nonlinear state space models cannot be applied directly and therefore internal dynamics approaches are not considered for deriving MG dynamic equivalents purposes.

In the external dynamics approaches the estimation of polynomials through either linear or pseudo-linear regressions [159, 162] extends to the problem of approximating the nonlinear function $g(\cdot)$, allowing to separate the dynamic model between the regression vector and the nonlinear mapping [161, 164, 169], as it can be observed from figure 4.9.

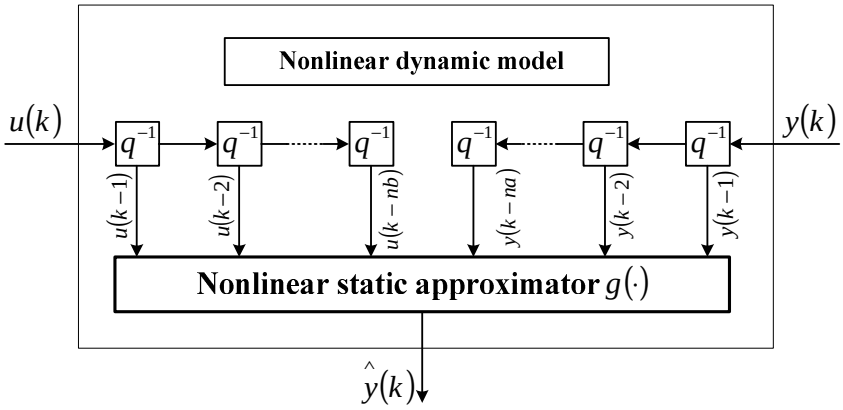

Figure 4.9: External dynamics approach

The nonlinear mapping $g(\cdot)$ in figure 4.9 corresponds to a general nonlinear static approximator and the model dynamics are represented through an external dynamic filter bank. Typically, the filters are realized as simple time delays, q^{-1}, and are thus referred to as tapped delay lines while the regressors are commonly chosen in the same way as for the linear models: past measurements, past model outputs and possibly past prediction errors.

Thus, if the regression vector is selected as for ARX models, the model structure is called NARX as the acronym for Nonlinear ARX. Likewise NARMAX, NOE and NFIR model structures are introduced as follows [161, 169]:

$$\textbf{NARX: } \hat{y}(k\mid\theta)=g\left[u(k-1)\ \ \cdots\ \ u(k-nb)\ \ y(k-1)\ \ \cdots\ \ y(k-na)\right]^T \tag{4.24}$$

$$\textbf{NARMAX: } \begin{aligned}\hat{y}(k\mid\theta)=g\big[&u(k-1)\ \ \cdots\ \ u(k-nb)\ \ y(k-1)\ \ \cdots\ \ y(k-nb)\\ &\varepsilon(k-1)\ \ \cdots\ \ \varepsilon(k-nc)\big]^T\end{aligned} \tag{4.25}$$

$$\textbf{NOE: } \hat{y}(k\mid\theta)=g\left[u(k-1)\ \ \cdots\ \ u(k-na)\ \ \hat{y}(k-1)\ \ \cdots\ \ \hat{y}(k-nf)\right]^T \tag{4.26}$$

$$\textbf{NFIR: } \hat{y}(k\mid\theta)=g\left[u(k-1)\ \ \cdots\ \ u(k-na)\right]^T \tag{4.27}$$

It should also be noted that more complex noise model structures like NARMAX and NBJ are uncommon in nonlinear dynamic system identification [161].

NARX and NARMAX model structures can be used for prediction, since they require past system outputs as regressors while NOE and NFIR model structures can be used to perform simulation, as depicted in figure 4.10. Thus, for developing MG dynamic equivalent purposes, the model parameterization decision becomes between NOE and NFIR model structures.

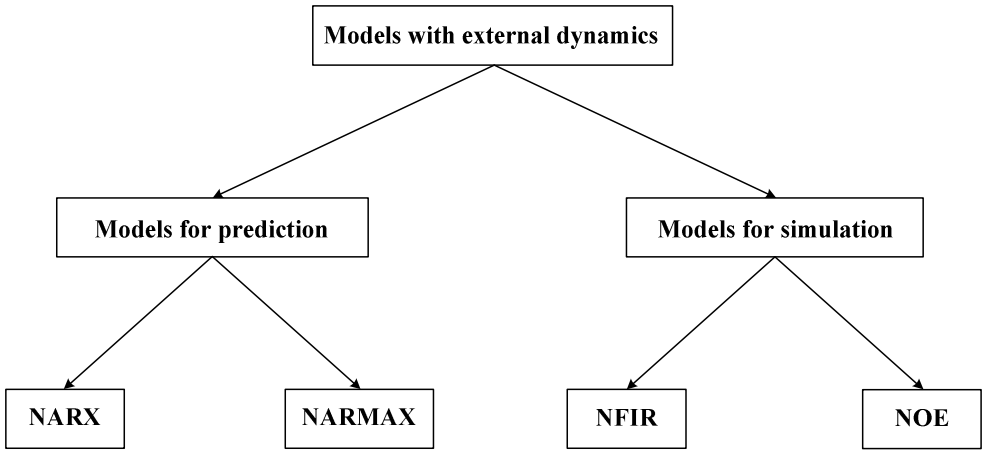

Figure 4.10: Nonlinear dynamic input-output model classes and common model structures

The basic difference between NOE and NFIR model structures is that the first one involves output feedback, since the regression vector given by (4.26) comprises past model outputs. Although NOE model structures have been more widespread, a drawback of output feedback is that, in general, stability cannot be proven for this kind of models and the user is usually left with extensive simulations in order to check under what conditions the obtained model is stable. In addition, NOE models can discover an error accumulation that might lead to inferior accuracy or even model instability. These problems have been commonly circumvented by models without output feedback such as NFIR models. However, the price to be paid for the missing feedback is that the number of model inputs – the dynamic order – has to be chosen very large to describe the process dynamics properly and therefore a high dimensional input space arises for the nonlinear function $g(\cdot)$. This drawback is already known for linear models but has more severe consequences in the nonlinear case, which restrict the application of NFIR models only with approximators that can deal well with high dimensional input spaces [161].

From this previous discussion and concerning to development of MG dynamic equivalents, it is expected that those NOE unsuitable features will be more worsened in applications of

power systems dynamic simulations due to their own recurrence characteristics, as it can be observed from figure 4.6, in subsection 4.4.1. Therefore NFIR model structures will be applied for MG modelling purposes in order to avoid or, at least, minimize error accumulation problems and subsequently numerical instability over dynamic simulation. Concerning to the static approximator of figure 4.9, in principle, any model architecture can be chosen as nonlinear mapping $g(\cdot)$. However, when combined with NFIR model structures in a multivariate system, the approximator should be able to cope with high dimensional input spaces and therefore all model architectures that fully underlie the curse of dimensionality are not well suited to derive dynamic equivalents for MG.

The term curse of dimensionality was introduced by Bellman [179] and basically expresses the intuitively clear fact that some general problems become harder to solve as the dimensionality of the input space increases, since the model complexity scales up exponentially with the input space dimensionality. Typical models that suffer from the curse of dimensionality are conventional look-up tables and fuzzy models, the so called lattice-based approaches [161].

Polynomials are the classical nonlinear approximators. However, their application is restricted to low dimensional input spaces [161]. Their severe shortcomings pointed out in [161] motivated the search for model architectures with better properties concerning external dynamics approaches, resulting in ANN.

There are several neural network architectures, which can be distinguished solely by their specific type of hidden layer neurons. Among them, the MLP and the RBF are the two most common neural network architectures used for nonlinear dynamic modelling purposes [164, 172, 180]. Some of the earliest examples are the works of [181] and [182] and the most comprehensive programme of work to date is [183] for the MLP architecture and [182] for the RBF network. From numerous practical applications published over the past years there seems to be substantial evidence that MLP indeed possess a notable ability to lead with complex systems. Lately, there have also been some theoretical results that attempt to explain the reasons for this success [168, 184]. The curse of dimensionality can be overcame best by projection based mechanisms as applied in MLP neural networks [161].

Therefore, MLP neural networks are used together with NFIR model structures to provide external dynamics approaches being the whole model usually called a TDNN [171, 185]. As

this whole model is used to derive dynamic equivalents for MG, the resulting model will be referred as the TDNN based MG dynamic equivalent.

4.4.2.2.2 MLP neural networks as the nonlinear static approximator

The nonlinear mapping, $g(\varphi,\theta)$, can be written as a basis function formulation [159, 161, 169], as

$$g(\varphi,\theta)=\sum_{i=0}^{M}\alpha_i\Phi_i(\varphi,\beta_i,\gamma_i) \tag{4.28}$$

The model output is thus obtained as a weighted sum of the M basis functions $\Phi_i(\cdot)$, which play a similar role in (4.28) to that of a functional space basis [169]. Typically β_i is related to the scale or to some directional property of $\Phi_i(\cdot)$, and γ_i represents some position or translation parameter.

For MLP neural networks, the multivariate basis functions (4.28) are constructed by elementary functions. Then, firstly a construction method is used to map the input vector $\varphi=[\varphi_1 \quad \dots \quad \varphi_d]^T$ to a scalar x_i with the help of the parameters, β_i and γ_i. Afterwards the activation function, $f(x_i)$, nonlinearly transforms the scalar x_i to the output y_i, as depicted in figure 4.11.

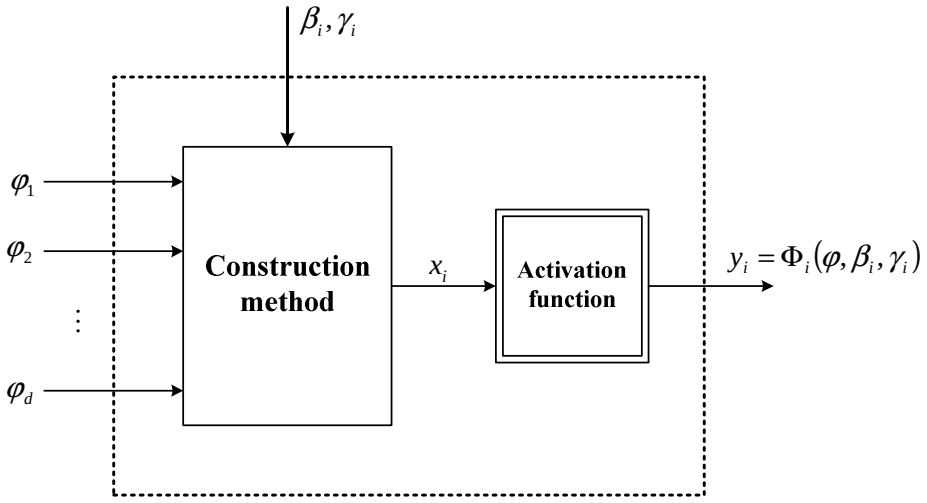

Figure 4.11: Multivariable basis function realization

According to [159, 161, 169], there are three most important mechanisms for constructing multivariable basis functions: Ridge construction, radial construction and tensor product.

MLP neural networks comprise a set of hidden layer neurons resulting from the ridge construction method. Thus, the activation function operates on a scalar x_i, which is obtained by projecting the regression vector on the parameter vector $\beta_i \in R^d$ and adjusting the projection result through the inclusion of an offset parameter $\gamma_i \in R$, as $x_i = \beta_i^T \varphi + \gamma_i$, giving

$$\Phi_i(\varphi) = f\left(\beta_i^T \varphi + \gamma_i\right) \tag{4.29}$$

An MLP hidden neuron, the perceptron, as it is also called, is a processing element whose operation realizes the basis function (4.29). Thus, the perceptron output, y_i, is given by

$$y_i = f\left(\sum_{j=1}^{d} w_{ij}\varphi_j + w_{i0}\right) \tag{4.30}$$

where $\beta_i = \begin{bmatrix} w_{i1} & \dots & w_{id} \end{bmatrix}^T$ represents the input weights and $\gamma_i = w_{i0}$ is the bias or threshold, as depicted in figure 4.12.

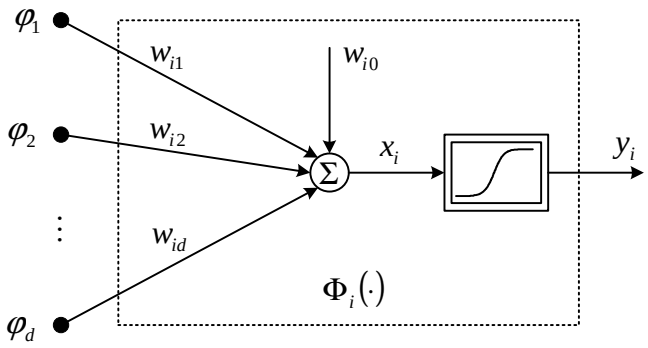

Figure 4.12: Schematic diagram of the i -th processing element of an MLP

The activation function can take any form, but common choices are functions of saturation type such as the logistic and hyperbolic tangent functions, (4.31) and (4.32), respectively, which are illustrated in figure 4.13.

$$f(x_i) = \text{logistic}(x_i) = \frac{1}{1+e^{-x_i}} \tag{4.31}$$

$$f(x_i)=\tanh(x_i)=\frac{e^{x_i}-e^{-x_i}}{e^{x_i}+e^{-x_i}} \tag{4.32}$$

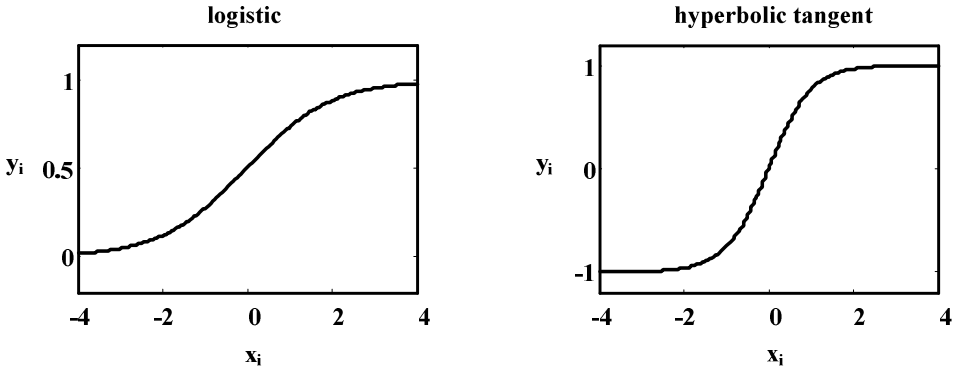

Figure 4.13: Typical activation functions for the perceptron

The logistic function has historically been a very popular choice [186] but since it is related to the hyperbolic tangent by a simple transformation

$$\tanh(x_i)=2\text{logistic}(2x_i)-1 \tag{4.33}$$

it makes no difference which of these two is used [164].

Then, a one hidden layer MLP can be written as

$$g(\varphi,\theta)=\sum_{i=0}^{M} w_i \Phi_i\left(\sum_{j=0}^{d} w_{ij}\varphi_j\right) \text{ with } \Phi_0(\cdot)=1 \text{ and } \varphi_0=1 \tag{4.34}$$

where w_i and w_{ij} denote the output layer and the hidden layer weights, respectively. The total number of parameters of an MLP with one hidden layer and one output layer is then

$$M(d+1)+M+1 \tag{4.35}$$

where M is the number of hidden layer neurons and d is the number of inputs.

The approximator inputs cannot all be directly influenced independently. Rather, only $u(k)$ is chosen by the user and all other delayed inputs follows as consequence of both the required system dynamic order and sampling time. Following directly from the fact that the sampling time has to be chosen small enough to capture the variations in the system output, the input space becomes higher for higher order systems but the data distribution characteristics stay

basically the same since the previous inputs are highly correlated and, as a result, wide regions in the input space are empty.

Since MLP hidden neurons are able to find the main directions of a process nonlinearities [161], MLP neural networks are able to exploit this property in order to weaken the curse of dimensionality, so that the number of parameters increases only linearly with the input space dimensionality. Furthermore, the MLP network performs function approximation with a set of adaptive bases that are determined from the training data set. This means that the projection manifold is data dependent, since the hidden layer weights change the bases by orienting the manifold while the output layer weights find the best projection within the manifold. Training will find the set of these weights.

Therefore MLP are relatively insensitive in what concerns to too higher dynamic orders because they can cope well with redundant inputs by driving the corresponding hidden layer weights toward zero. Nevertheless, the uneven data distribution that typically arises with the external dynamics approach [161] can easily be handled by MLP networks because the estimation of the hidden layer weights transforms the input axes in a suitable coordinate system anyway. Therefore this model architecture constitutes a promising solution to be combined with the NFIR regression vector for MG modelling purposes under the black-box modelling context.

In practice MLP with one hidden layer are most common and sometimes two hidden layers are used. Its basis functions representation is more involved since the outputs of the first hidden layer neuron are the inputs of the second hidden layer neurons, as depicted in figure 4.14. Thus, it is clear that more hidden layers make the network harder to train and the parameters become more strongly nonlinear. Due to the structure, this type of network is often referred to as a feedforward.

With M_1 and M_2 as the number of neurons in the first and second hidden layers, respectively, the basis function formulation becomes

$$g(\varphi,\theta)=\sum_{l=0}^{M2} w_l \Phi_l^{(2)}\left(\sum_{i=0}^{M1} w_{il}^{(2)} \Phi_1^{(1)}\left(\sum_{j=0}^{d} w_{ji}^{(1)} \varphi_j\right)\right), \text{ with } \Phi_0^{(1)}(\cdot)=0,\ \Phi_0^{(2)}(\cdot)=0 \text{ and } \varphi_0=1 \quad (4.36)$$

where the output layer weights are denoted as w_l and both the first and the second hidden layer weights are represented by $w_{ji}^{(1)}$ and $w_{il}^{(2)}$, respectively.

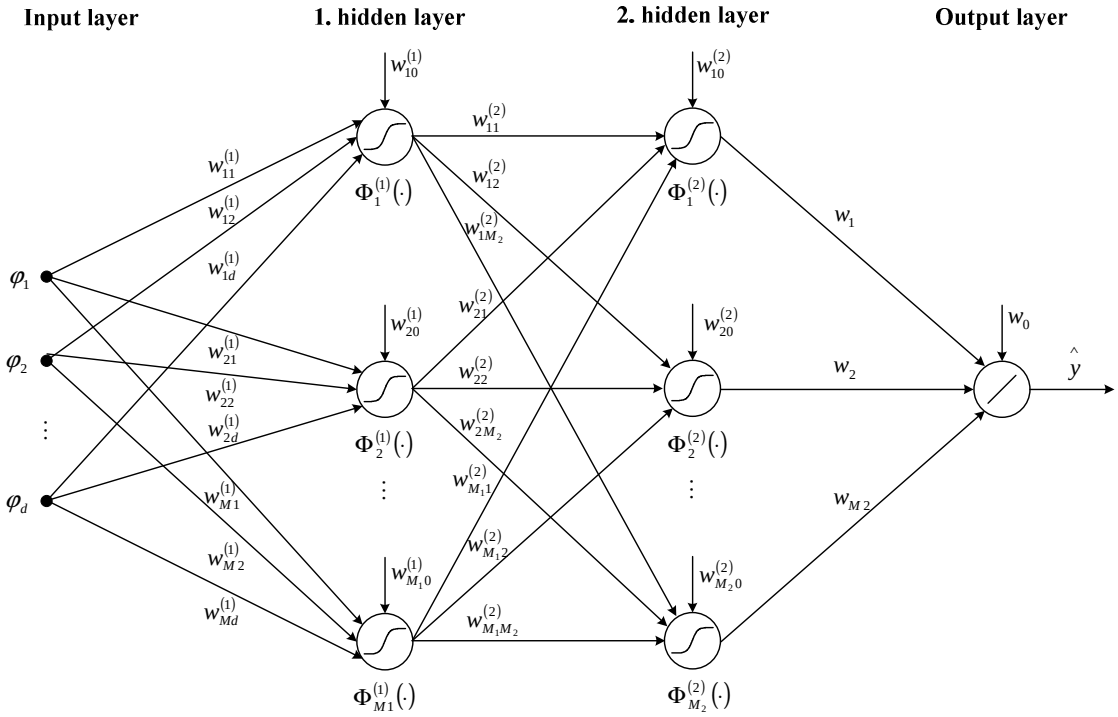

Figure 4.14: A multilayer perceptron network with two hidden layers

An MLP network consists of two types of parameters: The output layer weights that determine both the amplitude and operation point of the basis function and the hidden layer weights, which determine the directions, slopes and positions of the basis functions. The parameter vector θ contains all the adjustable parameters of the MLP neural network, i.e., all the weights and biases, since in (4.36) the biases are interpreted as weights acting on an input clamped to the unity. The values of these parameters are further estimated through a suitable identification method.

An MLP neural network is a universal approximator [187]. This means that an MLP can approximate any smooth function to an arbitrary degree of accuracy as the number of hidden neurons increases or alternatively using more than one hidden layer. The question which of these two possibilities performs better cannot be answered in general; rather it is very problem dependent [161, 164].

4.4.3 Finding suitable identification criteria

As already mentioned previously, an identification method involves both an identification criterion and a parameter estimation technique in an attempt to find the optimal point within

the search space spanned by the parameter vector. Thus, for a certain model, $\mathcal{M}(\theta_*)$, a guiding principle for parameter estimation is [163]:

- Based on $Z_e^k = \{[\varphi(k), y(k)]\}$, compute the prediction error

$$\varepsilon(k, \theta_*) = y(k) - \hat{y}(k \mid \theta_*) \tag{4.37}$$

- At time $k = N$, select $\hat{\theta}_N$, so that the prediction errors $\varepsilon\left(k, \hat{\theta}_N\right)$, $k = 1, 2, \ldots, N$ becomes as small as possible in the sense of the identification criterion.

An identification criterion corresponds to the mathematical description of what has to be optimized. For nonlinear dynamic systems the several ways to fit models from data are based on the prediction error sequence (4.37) that can be seen as a vector in R^N. The well known PEM form a scalar valued criterion function that measures the size of ε according to some norm.

Based on the traditional understanding of PEM, most of the system identification research is focused on using second order statistics as minimization criteria whether the system under consideration is linear or nonlinear. Even for nonlinear dynamic systems the assumption of a normal error distribution has been considered very reasonable and often approximately valid in practice [161, 164]. Under these assumptions further supported by the central limit theorem, which states that as the number of random variables increases its PDF approaches a Gaussian distribution, MSE would be able to extract all possible information from a signal whose statistics are solely defined by its mean and variance. Therefore, criteria that not only consider the second order statistics, but also take into account higher order characteristics of the error sequence are much desired. In a statistical learning sense a more appropriate approach would be to constrain directly the information content of error signals rather than simply their second order moments [188-190].

Entropy, as a measure of the average information contained in a signal, was first defined and proved to be useful by Shannon in communication systems domain [191]. Many other definitions followed the Shannon's entropy. Among them Kullback-Leibler information distance [159] and Kolmogorov's entropy [192] were very useful in system identification and statistics. However, a shortcoming of these entropy definitions is the lack of computationally simple and efficient estimators for random processes that can not be well described under the

Gaussian assumptions, particularly in high dimensional input spaces. Therefore, in order to overcome these drawbacks ITL approaches have been exploited in order to derive a computationally tractable definition of entropy [188-190]. Thus, both PEM and ITL criteria are presented in the following two subsections.

4.4.3.1 Prediction error methods

The size of the error sequence in (4.37) could be measured using any norm in R^N. Thus a common procedure is to use a criterion function like

$$V_N\left(\theta, Z_e^N\right) = \frac{1}{N}\sum_{k=1}^{N} \ell\left(\varepsilon(k,\theta)\right) \tag{4.38}$$

as a measure of how well the model $\mathcal{M}(\theta)$ performs.

This function is for a given Z_e^N a well defined scalar valued function of the model parameters, where $\ell(\cdot)$ represents some norm quadratic or no quadratic. The estimate $\hat{\theta}_N$ is then defined by the minimization of (4.38) as

$$\hat{\theta}_N = \hat{\theta}_N\left(Z_e^N\right) = \arg\min_{\theta \in D_{\mathcal{M}}} V_N\left(\theta, Z_e^N\right) \tag{4.39}$$

Thus $\hat{\theta}_N$ corresponds to the minimizing argument or a set of minimizing arguments, if the minimum is not unique and the mapping (4.9) is then defined implicitly by (4.39). Since the objective is to find the minimum of (4.38), $V_N\left(\theta, Z_e^N\right)$ is also called the loss or cost function [161, 164, 172, 180]. The main well known and much used procedures are based on the previous procedure to estimate θ. The family of approaches that uses (4.38) as the identification criterion is called the prediction error methods [159], since the objective is to minimize a sum over some norm of the prediction errors. Particular methods are obtained as special cases of (4.38), depending on the choice of $\ell(\cdot)$, the choice of the model structures and the choice of the method by which the minimization is carried out.

If the norm in (4.38) is defined as

$$\ell(\varepsilon(\theta,k)) = -\log f_e(\varepsilon,k;\theta) \tag{4.40}$$

the ML method is obtained as a special case of (4.39). When the prediction errors are assumed to be Gaussian with zero mean and variance λ,

$$\ell(\varepsilon(k,\theta)) = -\log f_e(\varepsilon,k;\theta) = const + \frac{1}{2}\log\lambda + \frac{1}{2}\frac{\varepsilon^2}{\lambda} \tag{4.41}$$

If λ is known, then (4.41) is equivalent to the most commonly used quadratic norm

$$\ell(\varepsilon) = \frac{1}{2}\varepsilon^2 \tag{4.42}$$

and (4.39) is specified in terms of a MSE type of criterion,

$$\hat{\theta}_N = \arg\min_{\theta\in D_M} \frac{1}{2N}\sum_{k=1}^{N}\varepsilon^2(k,\theta) \tag{4.43}$$

The reasons for the popularity of MSE are mainly concerned to its analytical tractability from both computational and analysis view points. The MSE criterion has been considered as a good choice for supervised parameter estimation methods [158] including neural networks training [180]. Sometimes other norms than the square are considered to conform to a particular noise distribution or, in the multi output case, to take into account different noise levels on different outputs [161].

4.4.3.2 Information theoretical learning criteria

Along with the property that the convolution of two Gaussian functions is also a Gaussian, ITL criteria are based on the combination of Renyi's quadratic entropy definition with Parzen windows in order to estimate the PDF of the error sequence in a manageable procedure [190]. For a random variable ε with PDF $f_e(\cdot)$, Renyi's entropy [192] with parameter α is defined as

$$H_{R\alpha} = \frac{1}{1-\alpha}\log\int_{-\infty}^{+\infty} f_e^{\alpha}(\varepsilon)d\varepsilon \tag{4.44}$$

Renyi's entropy shares the same extreme points of Shannon's definition for all values of α, i.e., its minimum value occurs when $f_e(\cdot)$ is a Dirac-δ function while the maximum occurs when the PDF is uniform [190]. In fact, Renyi's entropy represents a family of functions $H_{R\alpha}$ depending on a parameter α. When $\alpha = 2$, the Renyi's quadratic entropy is given as

$$H_{R2} = -\log \int_{-\infty}^{+\infty} f_e^2(\varepsilon) d\varepsilon \tag{4.45}$$

The PDF of a random variable ε for which the samples are given $\{\varepsilon_1, \varepsilon_2, \ldots, \varepsilon_N\}$ is obtained using the kernel function $\kappa_\sigma(\cdot)$, whose size is specified by the parameter σ, with the following expression

$$\hat{f}_e(\varepsilon) = \frac{1}{N} \sum_{i=1}^{N} \kappa_\sigma(\varepsilon - \varepsilon_i) \tag{4.46}$$

When α was restricted to two, Gaussian kernels, $G(\cdot)$, were specifically used [189], yielding

$$\begin{cases} \hat{H}_\varepsilon(\varepsilon) = -\log \hat{V}(\varepsilon) \\ \hat{V}(\varepsilon) = \frac{1}{N^2} \sum_{i=1}^{N} \sum_{j=1}^{N} \int_{-\infty}^{+\infty} G(\varepsilon - \varepsilon_i, \sigma^2) G(\varepsilon - \varepsilon_j, \sigma^2) d\varepsilon = \frac{1}{N^2} \sum_{i=1}^{N} \sum_{j=1}^{N} G(\varepsilon_i - \varepsilon_j, 2\sigma^2) \end{cases} \tag{4.47}$$

where σ is the standard deviation of the Gaussian kernel used in Parzen windows and $\hat{V}(\varepsilon)$, the argument of the logarithm in Renyi's entropy, is called the IP [190]. From (4.47) it can be noted that when the entropy is minimum all error samples are completely constants over the whole estimation data set. Therefore in training with entropy the algorithm will converge to a set of optimal parameters which may not yield zero mean error [188]. So, just after training ends the error mean should be deducted the model output in order to yield zero mean.

As the entropy quantitative measures signals information, minimizing the error entropy is equivalent to minimize the average information content of the error sequence. Thus a practical criterion that is appropriate to be used as a loss function for ITL is the Minimum Error Entropy (MEE), which can be written as

$$V_N\left(\theta, Z_e^N\right) = \hat{H}\left(\varepsilon(k,\theta)\right) \tag{4.48}$$

$$\hat{\theta}_N = \arg\min_{\theta \in D_M} V_N\left(\theta, Z_e^N\right) \tag{4.49}$$

When entropy in minimized all moments of the error PDF are constrained and therefore MEE extends MSE [188-190].

As can be shown in (4.47), minimizing the entropy corresponds to maximizing the IP for $\alpha > 1$. This means that in entropy manipulation it is possible to use simply the IP as cost function. In fact, the concept of IP fields generated by samples seen as information particles and the forces they exert on each other were defined and investigated for the quadratic Renyi's entropy with Gaussian Kernels in [193]. The potential associated with an information particle (sample) ε_j can be derived from the above IP expression, since the total IP energy is the sum of individual energies of the particles [190], as

$$\hat{V}\left(\varepsilon_j\right) = \frac{1}{N^2}\sum_{i=1}^{N} G\left(\varepsilon_j - \varepsilon_i, \sigma^2\right) \tag{4.50}$$

From (4.50) it is possible to compute the total information forces $F\left(\varepsilon_j\right)$ acting on ε_j by making the physical analogy with forces in potential fields as

$$F\left(\varepsilon_j\right) = \frac{\partial \hat{V}\left(\varepsilon_j\right)}{\partial \varepsilon_j} = \frac{1}{N^2}\sum_{i \neq j}^{N} G'\left(\varepsilon_j - \varepsilon_i, 2\sigma^2\right) \tag{4.51}$$

If the goal is to adapt the parameters of a nonlinear mapping $\hat{y}(k \mid \theta) = g(\varphi, \theta)$ in a function approximation framework, instead of the MSE an ITL criterion will be used based on the IP. The information forces are encountered when training an adaptive system with a parameter vector θ with the IP criterion and using a gradient based method. The parameters are adapted by injecting the information force for sample ε_j as the error. The gradient of the IP of the error with respect to the parameters consists of products of the information force acting on an error sample and the sensitivity of the model architecture at the error value [190].

$$\frac{\partial \hat{V}(\varepsilon)}{\partial \theta} = \sum_{j=1}^{N} \frac{\partial \hat{V}(\varepsilon_j)}{\partial \varepsilon_j} \frac{\partial \varepsilon_j}{\partial \theta} = \sum_{j=1}^{N} F(\varepsilon_j) \left(\frac{\partial \hat{y}_i}{\partial \theta} - \frac{\partial \hat{y}_j}{\partial \theta} \right) \tag{4.52}$$

The gradient of the model output with respect to the parameters can be calculated using efficient methods depending on the model type; for an MLP it can be computed by back-propagation.

The superiority of the entropy criterion over the MSE in chaotic time series prediction with MLP neural networks was demonstrated in [188]. In contrast with MSE that is only based on both the norm and variance of the error sequence, the ITL criteria are estimated with pairs of error samples, which means that more information about the data set is being extracted.

Although this superiority, ITL criteria will be computationally more expensive, $O(N^2)$, which becomes prohibitive for large estimation data sets or when numerical search methods are used [194]. Therefore, the MLP neural network will be trained with the classical MSE criterion and MEE will be exploited as the loss function when physical modelling approaches are used for deriving MG dynamic equivalents purposes.

4.4.4 Finding suitable parameter estimation methods

For many model structures, the loss function is a complicated function of θ and the minimization value, $\hat{\theta}_N$, must then be computed through a nonlinear optimization technique. Therefore, the choice of the optimization algorithm belongs firstly between local and global approaches, as depicted in figure 4.15.

The combination of many identification criteria with the several techniques to compute it has lead to a wide and sometimes confusing variety of identification methods. The computation of the estimates is a model structure dependent issue and therefore this topic is covered in many articles and books on system identification literature and the basic techniques are also the subject of many studies in numerical analysis [195].

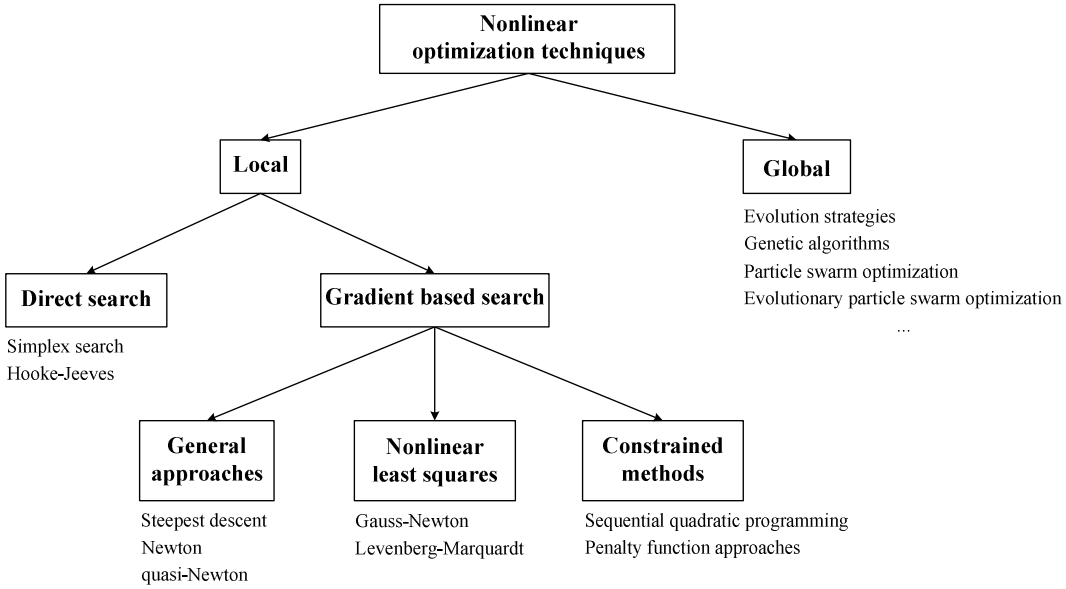

Figure 4.15: General overview about nonlinear optimization techniques

4.4.4.1 MLP training with Levenberg-Marquardt method

Concerning ANN training in batch mode, gradient based methods, such as nonlinear least squares, have been widely used to find the minimum of the criterion. As it is useful to order the computations to use the particular structure of the neural network, the training method is called the back-propagation algorithm. In order to train an MLP neural network it is generally recommended to apply the Levenberg-Marquardt method [164]. It provides a fast convergence, is robust and it is not necessary for the user to initialize any strange design parameters [195]. Since this method was derived especially for MSE type of criteria, the identification method to be used with MLP based model structures comprises the Levenberg-Marquardt optimization algorithm and the MSE as the identification criterion.

4.4.4.1.1 MLP structure optimization

Concerning MLP neural networks, from subsection 4.3.3, it is clear that, in order to improve model quality, model structure selection is much more involved than just a matter selecting a number of hidden units, since the network need not be fully connected; in fact, it is likely that it will be advantageous to leave out weights connecting certain inputs with certain hidden units or certain hidden units with certain outputs. Therefore, it will lead to a large combinatorial problem if the model has to be picked on a trial and error basis approach.

Although in practice it is impossible to investigate all possible configurations, there are several useful methods that allow to obtain a trade off between doing a fair amount of computations and obtaining an architecture that is reasonably near the optimal for the particular structure of the regression vector [161, 164].

As one has access of an unlimited amount of both training and validation data, the neural network architecture determination becomes less important and it can be possible to restrict the attention to fully connected neural networks, for which the architecture selection task is reduced to choosing both the number of hidden layers and the corresponding number of hidden units and subsequently perform explicit of implicit structure optimization [161] in order to deal with the bias/variance dilemma.

The term explicit means that the bias variance trade off is carried out by examining models with different numbers of neurons. In the context of MLP neural networks forward selection and backward elimination categories are very popular and widely applied through growing and pruning methods, respectively [196, 197]. Growing is the generic term for training techniques that increase the network complexity by adding neurons while pruning refers to decrease the network complexity by removing neurons.

In contrast to explicit, implicit structure optimization or regularization techniques influences the complexity of a model although the nominal number of parameters does not change. When regularization techniques are applied, a model is not as flexible as it might appear from considering the number of parameters alone. Thus the model behaves as though it possesses few parameters that it really has, i.e., with fewer degrees of freedom. Therefore the bias error is increased and the variance error decreased. Loosely speaking, regularization works as follows: Not all parameters of the model are optimized in order to achieve the minimal loss function. Those parameters that are still used for minimizing the loss function are called effective parameters while the others that have only an insignificant influence of the loss function are called spurious parameters [161].

The most commonly used augmentation is the so-called simple weight decay. However, a similar effect can be accomplished by stopping the training session before the minimum of the criterion has been achieved [164]. This important regularization technique is known as early stopping. It can be applied when iterative optimization methods are used. Training is not performed until the model parameters have converged to their optimal values. Rather during the iterative training algorithm the model performance on a validation data set is monitored and

training is stopped when the validation error reaches its minimum. At the minimum of the validation error the best bias variance trade off is realized. At the left hand side of this minimum the model would underfit, while to the right hand side it would overfit the data. During the iterations the number of effective model parameters increases and if the training continued until convergence, all model parameters will become effective, resulting in large variance errors.

In [169] the interesting result was shown that the effect of early stopping not only has an effect similar to regularization by weight decay, but also the two approaches are in fact closely related. However, the main reason for the early stopping popularity is its simplicity. Furthermore, it reduces the computational demand since training does not have to be completed. It is important to understand that for very flexible models, convergence of all parameters is not desired. Therefore, regularization by early stopping was adopted in order to avoid overfitting. In addition, the MSE on the validation data set was used as a primary validation criterion.

4.4.4.2 EPSO as the optimizer in physical modelling approaches

The nonlinear local optimization techniques start from an initial point in the parameter space and search in directions obtained by neighbourhood information such as first and possibly second order derivatives. As a consequence, such an approach leads to a minimum that is close to the starting point and, in general, not the global one. However, for many problems, local search is sufficient, especially if good initial parameter values are available. Then the simplest strategy for searching a good local optimum is a multi start approach, since each local run discovers a local minimum and the best one is chosen as the final result. In addition it allows to get a feeling for the quality and number of different local optima. However, if it is not possible to achieve a satisfactory solution, a global method may succeed [161].

In contrast with local approaches, nonlinear global optimization techniques, also known as stochastic search algorithms or meta-heuristics, try to find the global optimum or at least a good local optimum without many assumptions about the problems to be solved. Therefore they have been widely applied in learning and optimization problems of many areas of knowledge, including power systems. However, concerning particularly to system identification problems, the main drawbacks usually pointed out are twofold; the huge

computational demand and the slow convergence to the minimum prevents their applications to high dimensional input space problems.

Since the search for the global minimum is performed into the parameter space, the required computational effort grows exponentially with the number of parameters, which does not depend on the specific algorithm applied. Additionally, as the whole parameter space has to be examined, although with no uniform density, the convergence to any minimum is very slow even after finding a region of a loss function minimum. Loosely speaking, global methods are good at finding regions while local methods are good at finding points. Therefore in system identification it is considered a good idea to use the estimated parameters from any global method as initial values for a subsequent local optimization procedure in order to accelerate the convergence of the method to the optimum [161].

Because all the optimization techniques have their specific advantages and drawbacks, in practice, it is often effective to combine different approaches. In this sense, EA have mainly two prominent features which distinguish themselves from other global search methods like Simulated Annealing, Tabu Search and Branch and Bound. First they are based on a population of individuals and second there are communication and information exchange among individuals in a population as the result of selection, competition and recombination. Different representations, selection schemes and search operators will define different EA, such as Evolution Strategies, Genetic Algorithms and Genetic Programming, but their algorithms analysis are easy to understand and therefore make possible to exploit hybrid methods [198]. While ES and GA are mainly used for parameter estimation techniques, GP operates on a higher level by optimizing tree structures [161] and therefore is not considered here.

The classical PSO developed by Kennedy and Eberhart [199-201] was introduced in power systems area [202] and recently in nonlinear dynamic system identification [203]. Successful applications to function minimization [204], feedforward neural network design [205, 206] and a wide range of other optimization problems allow the many authors to claim superiority in speed and to recognise its searching potential. When compared with EA, PSO has some attractive characteristics and in many cases proved to be more effective [199]. However, tuning the algorithm has proven to be a hardly and problem dependent task. On the other hand, classical PSO lacks the EA learning ability, namely the σSA-ES [201], which benefit from an evolutionary process to progressively adapt the parameters that guide its own search.

Therefore, EPSO was built over the concepts of σSA-ES and PSO [207] in an attempt to combine the best of both techniques. As a result a more reliable and robust method was obtained, which may be seen as the first natural self adaptive convergent evolution of both approaches, although other attempts had been made [208, 209].

Applications of EPSO have already been reported in many power systems problems [207, 210-213], where the superiority of EPSO was confirmed giving a faster convergence and better solutions when compared with other meta-heuristics, even for no smooth objective functions. More recently EPSO was successfully applied in training a FIS model under an entropy criterion for wind power prediction [214], denoting that EPSO performs well under different criteria, and its robustness has effectively been exploited as a nonlinear global parameter estimation tool to build dynamic equivalents for MG using MSE criterion [17].

As a hybrid of ES and PSO, EPSO grants a PSO scheme with both an explicit selection procedure and self adaptation properties of its parameters. Then, EPSO can be seen under two perspectives: A special class of self adaptive EA methods or a special PSO method. However, in order to get a better insight, the authors [207] have preferred to explain the method from an evolutionary view point. Thus, at a given generation, the set of potential solutions for loss function minimization is called a set of particles. Each particle is composed by a set of object and a set of strategy parameters, corresponding to the particle position into the parameter space, $\theta_i = (\theta_{i1}, \theta_{i2}, \ldots, \theta_{in\theta})$, and to the weights that govern the movement rule, respectively, $P_i = [\theta_i, w_i]$ [207].

A general scheme of EPSO can be done as follows.

1. Choose an initial swarm of S particles, $\Theta_0 = \lfloor P_{1,0} \quad P_{2,0} \quad \ldots \quad P_{S,0} \rfloor$;

2. Iterate for $k = 1,2,...$

3. Replicate each particle r times $\Theta_{R,k} = Replication(\Theta_{k-1}), R = 1,...,r$;

4. Perform mutation of the weights of each particle $\begin{cases} \overline{\Theta}_k = Mutation(\Theta_k) \\ \overline{\Theta}_{R,k} = Mutation(\Theta_{R,k}), R = 1,...,r \end{cases}$;

5. Each mutated particle generates an offspring according to the movement rule $\begin{cases} \Theta_k^{new} = Movement(\overline{\Theta}_k) \\ \Theta_{R,k}^{new} = Movement(\overline{\Theta}_{R,k}), R = 1,...,r \end{cases}$;

6. Evaluate the fitness of each particle, $Fit(\Theta_k^{new})$, $Fit(\Theta_{R,k}^{new}), R = 1,...,r$;

7. Perform selection, $\Theta_k = Selection\left(\Theta_k^{new}, \Theta_{R,k}^{new}\right)$;

8. Test for the termination criterion and either go to step 3 or stop.

A brief description of the operators is presented as follows

4.4.4.2.1 Recombination operator or movement rule

As in PSO, the position of each particle, is updated according to the movement rule. Given a particle position, θ_i^k, into the parameter space, its new position, θ_i^{k+1}, results from

$$\theta_i^{k+1} = \theta_i^k + V_i^{k+1} \tag{4.53}$$

$$V_i^{k+1} = w_{i1}^* V_i^k + w_{i2}^* \left(b_i - \theta_i^k\right) + w_{i3}^* \left(b_g^* - \theta_i^k\right) \tag{4.54}$$

where b_i and b_g represent the best point found by the particle i upon to the generation k and the best overall point found by the whole swarm in its past life, respectively. $V_i^k = \theta_i^k - \theta_i^{k-1}$ is the velocity of particle i at generation k. w_{i1}, w_{i2} and w_{i3} are weights conditioning the inertia, memory and cooperation terms, respectively. The symbol * indicates that these parameters will undergo evolution under a mutation process. Thus, according to [207], the particle as well as its reproduction in EPSO are illustrated in figure 4.16.

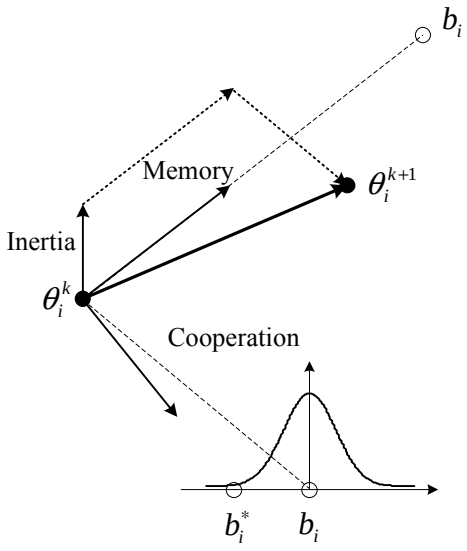

Figure 4.16: Particle reproduction in EPSO

Each particle generates an offspring at a location determined by the classical PSO movement rule. Thus the offspring receives a contribution from the global best parent and from both direct parent and its best ancestor. This means that, for practical purposes, this method includes a provision of elitism, because the particle best ancestor and the swarm global best are kept from generation to generation. On the other hand, the recombination operator is adaptive and evolve over the generations through the mutation of the particle strategy parameters.

4.4.4.2.2 Mutation of strategy parameters

As in σSA-ES, the particle object parameters are those giving the phenotypic description of a possible solution while strategy parameters are those that govern the particle evolution over iterations. According to [207], the basic mutation rule for the strategic parameters is the following

$$w_{ik}^{*} = w_{ik}\left[\log N(0,1)\right]^{\tau} \tag{4.55}$$

where $\log N(0,1)$ is a random variable with lognormal distribution derived from the Gaussian distribution $N(0,1)$ of zero mean and variance one and τ is a learning parameter, fixed externally, controlling the amplitude of the mutations, since smaller values of τ lead to high probability of having values close to the unity.

Approximations to this scheme could be obtained as

$$w_{ik}^{*} = w_{ik}\left[1+\tau N(0,1)\right] \tag{4.56}$$

provided that τ is small and the outcome is controlled so that negative weights are ruled out. This scheme is preferable to additive mutations of the type

$$w_{ik}^{*} = w_{ik} + \tau N(0,1) \tag{4.57}$$

since in this case the absolute value of the mutation is insensitive to the value w. Therefore the mutation of weights w_{ik} for $k = 1,2,3$ are performed using (4.56).

Concerning to the global best, b_g, it is randomly distributed to give

$$b_g^{*} = b_g + w_{i4}^{*} N(0,1) \tag{4.58}$$

where w_{i4} is the forth strategy parameter associated with particle i, which is also mutated according to (4.56). Thus a general particle in EPSO can be represented as in figure 4.17.

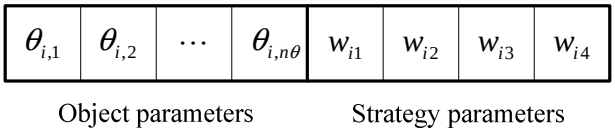

Figure 4.17: A particle representation in EPSO

The size of the neighbourhood of b_g, where it is more likely to find the global best or at least a global better than the current one, is controlled by w_{i4} allowing the search to focus on a given point, if it is convenient.

4.4.4.2.3 Selection

As it can be shown in the EPSO algorithm presented previously, at a given iteration, the operator replication generates r clones of each particle, which undergo mutation in their strategy parameters like the original particle. Then, for each particle the recombination operator generates $r+1$ offspring, corresponding to $r+1$ different locations.

The operator selection acts separately on each group of $r+1$ offspring and, based on their fitness values, only one will survive for the following generation. Under the (μ,λ) notation, usual in ES, for each particle an $(1,r+1)\sigma$SA-ES is formed and the global process can be seen as a multiple, $S(1,r+1)\sigma$SA-ES, where S is the number of particles in the swarm.

There is a solid theoretical background giving insight why ES achieve convergence and how a near optimal progress rate is obtained [215]. By application of genetic operators new individuals are generated and then selection provides a positive push towards the optimum. On the other hand, in classical PSO, each parent generates one offspring through the movement rule application and dies. It should be noted that the movement rule, only by itself, assures the progress to the optimum, which means that in average each generation will be better than the preceding one [215].

EPSO combines the action of these two mechanisms as follows: First the recombination operator, which makes use of the movement rule, induces a movement towards the optimum, producing not only better individuals but also an average better group. In a sequence, by selection, the offspring with better performance will survive assuring thus that the following

generation tends to be better than the preceding one. In addition the EPSO recombination operator is self adaptive, which avoids the need for fine tuning the strategy parameters because their evolution characteristics will learn about the best way to evolve towards the optimum [207]. All these features give robustness to EPSO models. In fact, experiences comparing EPSO with the classical PSO formulation and also with GA variants have shown that EPSO is in general more robust, as already mentioned previously.

Therefore, it is expected that the main features of EPSO combined with these ones of the MEE criterion, mentioned previously in subsection 4.4.3.1, will result in a promising identification method for physical modelling approaches purposes, concerning the development of MG dynamic equivalents.

4.4.5 Validation of MG dynamic equivalents

For validation purposes, the MG dynamic equivalents derived from the application of the two promising approaches that emerged from the previous subsection have to be integrated in the dynamic simulation platform used to generate the data set in order to replace the MG detailed model. Thus, the final validation criterion relies on the evaluation of the MG dynamic equivalent performance, concerning the reproduction of the MG dynamic behaviour using the corresponding detailed model, with respect to the upstream MV network.

Since the issues related with this ultimate validation step are very application dependent, they are addressed further in chapter 5.

4.5 Summary and main conclusions

This chapter described the fundamental theoretical concepts behind nonlinear dynamic system identification techniques. Also, a state-of-the-art regarding these main techniques has been included and a continuous exposition of the techniques that together constitute practical procedures for building dynamic equivalents for MG purposes has been given.

Firstly, a solid system definition was given. Afterwards, common system identification procedures were presented and the main features related to each stage were outlined. Since nonlinear dynamic system identification techniques are very application dependent, there are no general guidelines to be followed. As a result, the main stages to be carried out during a process modelling should be guided by both the available prior knowledge and the intended use

of the model. Then the problem of build dynamic equivalents for MG was formulated under a system identification framework.

Based on the prior knowledge about MG dynamic behaviour, described in chapter 2, effectively used for modelling purposes, two possible modelling approaches have been adopted: physical modelling and black-box modelling. The physical model structure will be selected based on the physical laws that potentially describe the MG dynamics and thus a continuous time state space model was directly adopted. In contrast, the selection of a black-box model structure involved several important decisions, such as internal or external dynamics representation, the regression vector and the nonlinear mapping. These issues have been presented and discussed, taking into account the purpose of deriving MG dynamic equivalents.

Finally, as a result, two distinct identification methodologies have been selected as promising approaches to derive MG slow dynamics equivalent models and therefore dynamic equivalents for MG:

- TDNN based models, which combine an NFIR input structure with an MLP neural network as the nonlinear mapping. The TDNN model structures are trained using the Levenberg-Marquardt method and MSE criterion . In addition, the MLP neural network structure is optimized using early stopping;
- Physical based models, in which the parameter estimation task is performed using EPSO as the global optimization tool and both MSE and MEE as the identification criteria.

Both TDNN based methods and methods based on physical modelling constitute promising nonlinear dynamic system identification approaches to derive dynamic equivalents for MG. Therefore these two solution approaches are exploited in chapter 5.

Chapter 5
MicroGrid Dynamic Equivalents based on Artificial Neural Networks and Physical Modelling Approaches

5.1 Introduction

In this chapter nonlinear dynamic equivalents for MG are developed based on the two promising approaches identified previously, in chapter 4.

These two promising approaches are:

- **Black-box modelling**. The MG dynamic equivalent is based on a TDNN model structure, which combines a NFIR configuration with an MLP neural network to represent the MG nonlinear dynamics. Internal parameters of the neural network are identified using a classic MSE criterion and a Levenberg-Marquardt algorithm;
- **Physical modelling.** The MG dynamic equivalent corresponds to a physically structure parameterized model where EPSO is used together with either the MSE or the MEE criteria to identify the parameters of the model.

The MG dynamic equivalents obtained through the application of these approaches are used to replace a MG in dynamic simulations when several disturbances at the MV level occur, like MMG islanding and load following in islanded mode. The derivation of dynamic equivalents capable of reproducing the MG dynamic behaviour during short circuits will be considered in future developments.

As stated in previous chapters, system identification procedures for the derivation of dynamic equivalents for MG start with a numerical experiment design suitable to collect appropriate data sets and ends with a MG dynamic equivalent validation task. For these purposes a dedicated dynamic simulation platform was developed under *MatLab*® *Simulink*® environment, which comprises two main packages:

- The MMG detailed model: It contains all the several microsources dynamic models and their inverter controls, as described in chapter 2, providing in this way a MG detailed model connected to the MV network. This module is used to simulate the MG relevant dynamic behaviour with respect to the MV network in order to generate high quality data sets.
- The MMG equivalent model: In this module the detailed MG model is replaced by the MG dynamic equivalents, to be developed, in order to evaluate their performances in the same environment.

This dynamic simulation platform plays the role of the experimental set-up in system identification terminology [159, 161, 169]. Thus, under the framework of developing dynamic equivalents for MG, it is called the numerical set-up, since it allows to carry out numerical experiments with MG, as well as to validate the MG dynamic equivalents to be developed.

This numerical set-up is described in section 5.2. TDNN based MG dynamic equivalents methodology is presented in section 5.3, while the physically modelling based approach is addressed in section 5.4. Section 5.6 describes the summary and main conclusions.

5.2 The numerical set-up

As stated before, the numerical set-up is a dedicated dynamic simulation platform able to design suitable numerical experiments with MG in order to collect informative enough data sets. On the other hand, the simulation platform should be able to evaluate the performance of the developed MG dynamic equivalent at the final stage of the identification procedure.

Therefore, the dynamic simulation platform involves two main simulation packages developed for these two distinct purposes: The MMG detailed model and the MMG equivalent model, as described in the following two subsections.

5.2.1 The MMG detailed model

In order to collect informative enough data sets, the dynamic behaviour of the MG, when inserted in the upstream MV network should be simulated using the detailed mathematical description of a MG. Initially it is assumed that the MMG is operated in normal interconnected mode in parallel with the upstream power system. In turn, the MG is operated in normal

interconnected mode too, under a MMG operation philosophy. Following a MMG disconnection from the upstream system, MG will be kept in operation connected with the MV network, with the synchronous machines connected to the MV grid providing voltage and frequency control. Thus, as already mentioned previously in chapter 2, the MG is operated under a SMO control strategy, either importing or exporting a certain amount of power.

Each MG is fully represented, which means that the LV network, the existing loads, their microsources and both the corresponding inverter interfaces and controls, the main storage device and both its interface and control are represented using the dynamic models described in chapter 2. At the MV level, a round rotor synchronous machine $6th$ order model [216] was implemented to represent DG units connected to the MV network. Both the automatic voltage regulator and speed governor-turbine models were also included when associated to a given synchronous generator.

The dynamic analysis of MG may span over time intervals conditioned by the slow responses of microgeneration systems, namely SOFC, which extend to several tens of seconds [6, 7, 9, 10]. A multimachine power system model was therefore derived to describe in a compact form the MMG network [216-218], employing a phasor-type representation of the electrical quantities, whereby all fast electrical transients, such as stator electric transients of both synchronous and induction machines are neglected [58, 216]. Moreover, the time constants associated with the network transients are very small and can be considered to be zero without significant loss of accuracy [219].

Dynamic models of all synchronous machines and microgeneration systems are interconnected through a balanced three-phase network of $R-L$ elements. These $R-L$ elements are used to represent transformers, MV and LV network branches, in which capacitive effects have been neglected [219]. It is also assumed that all loads are balanced symmetrical three-phase $R-L$ elements. All sources are viewed from the network as emfs behind the corresponding impedance.

Network equations are referred on the synchronous reference frame, $D-Q$. When the MMG is operated in interconnected mode, the upstream network (infinite bus) provides this reference. Otherwise, as there are synchronous machines in the MV level, the reference speed is determined as the weighted average of all rotor speeds that is the centre of inertia reference.

The integration of dynamic models of both microgeneration systems and synchronous generators with the network algebraic equations and both LV and MV loads under a multi-machine power system model is described in the following subsections.

5.2.1.1 Round rotor synchronous machine

Round rotor generators, also called high speed generators, are normally used for turbo-units driven by high-speed steam or gas turbines. To reduce centrifugal forces, they have low diameter but large axial length and are mounted horizontally. Typically they will have two or four electrical poles [138].

As already mentioned previously the dynamic behaviour of the round rotor synchronous machines is described through a $6-th$ order model, in which all quantities are expressed in per unit and referred to the $d-q$ internal machine reference frame [216], as described in appendix A. The automatic voltage regulator (IEEE type 1 model) and a governor-turbine system [218] were also included.

According to this formulation and neglecting the stator transients, the generator terminal voltage can be described in vector form as [216]

$$\begin{bmatrix} V_d \\ V_q \end{bmatrix} = \begin{bmatrix} E_{gd} \\ E_{gq} \end{bmatrix} - \begin{bmatrix} R_s & -X_q^{"} \\ X_d^{"} & R_s \end{bmatrix} \times \begin{bmatrix} I_d \\ I_q \end{bmatrix} \tag{5.1}$$

where

E_{gd}, E_{gq} are the $d-q$ components of generator internal voltage;

V_d, V_q are the $d-q$ components of generator terminal voltage;

I_d, I_q are the $d-q$ components of generator terminal current;

$X_d^{"}$, $X_q^{"}$ are the subtransient reactances of $d-q$ machine axis;

R_s is the stator resistance.

Rotor oscillations of the synchronous machines are calculated from the respective swing equations and the internal voltages of generators resulting from the numerical integration are referred to the machine $d-q$ reference frame. As the network equations are expressed in the

system reference frame, the internal voltages should be transformed from the machine to the system reference frame, using the rotor angles.

The $q-$axis of a given generator is shift with respect to the network real axis by the rotor angle δ [216], as can be shown from the phasor diagram depicted in figure 5.1.

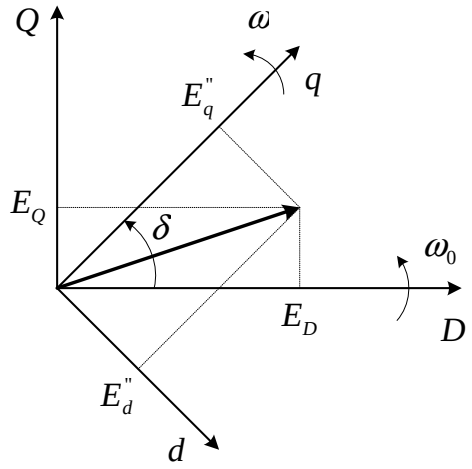

Figure 5.1: Relative position of the generator reference with respect to the network coordinates

Thus, concerning to the generator internal voltages, the relationship between the two reference frames is given by the following axis transformation [216]

$$\begin{bmatrix} E_D \\ E_Q \end{bmatrix} = T \times \begin{bmatrix} E_{gd} \\ E_{gq} \end{bmatrix} = \begin{bmatrix} \sin\delta & \cos\delta \\ -\cos\delta & \sin\delta \end{bmatrix} \times \begin{bmatrix} E_{gd} \\ E_{gq} \end{bmatrix} \tag{5.2}$$

On the other hand, terminal currents must be transformed from the system reference frame to the $d-q$ machine reference using the inverse transformation, as

$$\begin{bmatrix} I_d \\ I_q \end{bmatrix} = T^{-1} \times \begin{bmatrix} I_D \\ I_Q \end{bmatrix} = \begin{bmatrix} \sin\delta & -\cos\delta \\ \cos\delta & \sin\delta \end{bmatrix} \times \begin{bmatrix} I_D \\ I_Q \end{bmatrix} \tag{5.3}$$

The stator equations given by equation (5.1) can be rewritten in the synchronous reference frame as [216]

$$\begin{bmatrix} V_D \\ V_Q \end{bmatrix} = \begin{bmatrix} E_D \\ E_Q \end{bmatrix} - \begin{bmatrix} Z_{11} & Z_{12} \\ Z_{21} & Z_{22} \end{bmatrix} \times \begin{bmatrix} I_D \\ I_Q \end{bmatrix} \tag{5.4}$$

where

$$\begin{bmatrix} Z_{11} & Z_{12} \\ Z_{21} & Z_{22} \end{bmatrix} = \begin{bmatrix} \sin\delta & \cos\delta \\ -\cos\delta & \sin\delta \end{bmatrix} \times \begin{bmatrix} R_s & -X_q'' \\ X_d'' & R_s \end{bmatrix} \times \begin{bmatrix} \sin\delta & -\cos\delta \\ \cos\delta & \sin\delta \end{bmatrix} \tag{5.5}$$

and the per unit values of R_s, X_q'' and X_d'' are expressed in the system base.

For round rotor synchronous generators, it is a plausible assumption to consider $X_d'' = X_q''$ [220] and therefore $[Z]$ is not influenced by rotor angle δ [216]. Then the generator terminal voltage in (5.4) and (5.5) simplifies to

$$\begin{bmatrix} V_D \\ V_Q \end{bmatrix} = \begin{bmatrix} E_D \\ E_Q \end{bmatrix} - \begin{bmatrix} R_s & -X_d'' \\ X_d'' & R_s \end{bmatrix} \times \begin{bmatrix} I_D \\ I_Q \end{bmatrix} \tag{5.6}$$

The model of the round rotor synchronous machine is schematically represented in figure 5.2, where it can be observed their integration with the network equations.

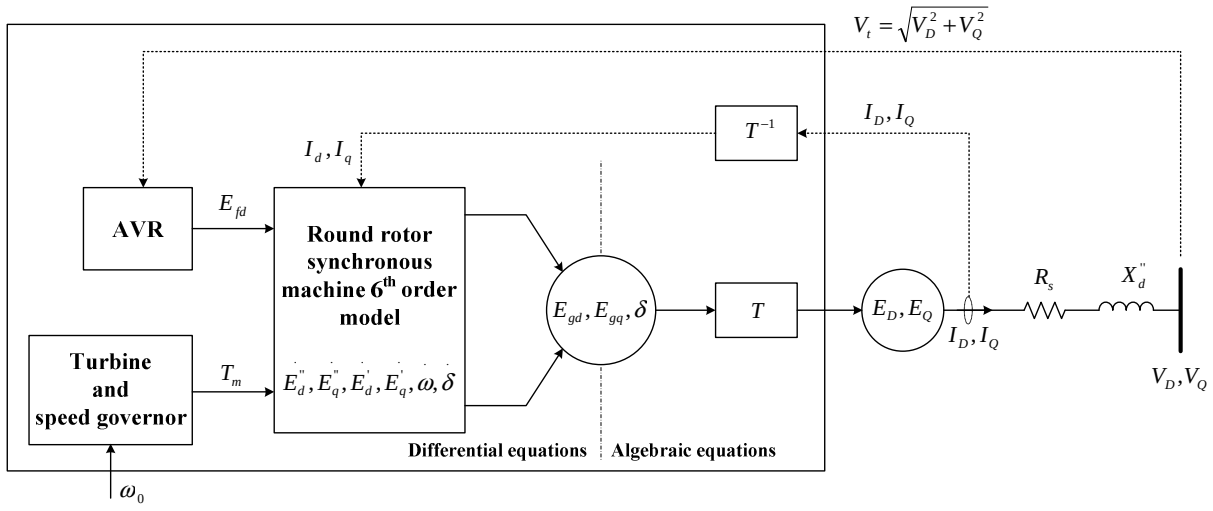

Figure 5.2: Subtransient functional model of synchronous generator

5.2.1.2 Microsources and inverter interfaces

As stated before, the MG operated under a SMO control strategy comprises the following types of microgeneration systems:

- The main storage device, which is connected to the LV network through a VSI control;

- Controllable MS, such as SSMT and SOFC, and PV systems connected to the LV network through PQ control inverters;
- Micro wind turbines, which use an induction generator directly connected to the LV network.

The mathematical description of the several microgeneration systems as well as the main storage device adopts the dynamic models described in chapter 2. Except the micro wind generator, all those models are solved in time domain, producing instantaneous values, which must be properly interfaced with the algebraic equations of the network. As the inverter interfaced microsources are presented to the LV grid as emfs behind the filter impedances, after determining the per unit values of emfs with respect to system voltage base, V_{base}, the Park's transformation [221] is used to convert the emfs from the time domain to the $D-Q$ reference frame rotating at synchronous speed, as

$$\begin{bmatrix} E_D \\ E_Q \end{bmatrix} = P \times \begin{bmatrix} e_a \\ e_b \\ e_c \end{bmatrix} \times \frac{\sqrt{3}}{\sqrt{2} \times V_{base}} \tag{5.7}$$

where

$$P = \frac{2}{3} \times \begin{bmatrix} \sin\theta & \sin\left(\theta - \frac{2\pi}{3}\right) & \sin\left(\theta + \frac{2\pi}{3}\right) \\ \cos\theta & \cos\left(\theta - \frac{2\pi}{3}\right) & \cos\left(\theta + \frac{2\pi}{3}\right) \end{bmatrix} \tag{5.8}$$

is the Park transformation and θ is the angular displacement.

In order to back transform the voltage and current from the synchronous reference frame, $D-Q$, to the time domain the Park's inverse transformation [221] is used. Thus,

$$\begin{bmatrix} e_a \\ e_b \\ e_c \end{bmatrix} = P^{-1} \times \begin{bmatrix} E_D \\ E_Q \end{bmatrix} \times \frac{\sqrt{2} \times V_{base}}{\sqrt{3}}; \begin{bmatrix} i_a \\ i_b \\ i_c \end{bmatrix} = P^{-1} \times \begin{bmatrix} I_D \\ I_Q \end{bmatrix} \times \sqrt{2} \times I_{base} \tag{5.9}$$

where I_{base} is the system current base and

$$P^{-1} = \begin{bmatrix} \sin\theta & \cos\theta \\ \sin\left(\theta - \frac{2\pi}{3}\right) & \cos\left(\theta - \frac{2\pi}{3}\right) \\ \sin\left(\theta + \frac{2\pi}{3}\right) & \cos\left(\theta + \frac{2\pi}{3}\right) \end{bmatrix} \tag{5.10}$$

The integration of the main storage device and the inverter interfaced MS with the network can be schematically represented as depicted in figures 5.3 and 5.4, respectively.

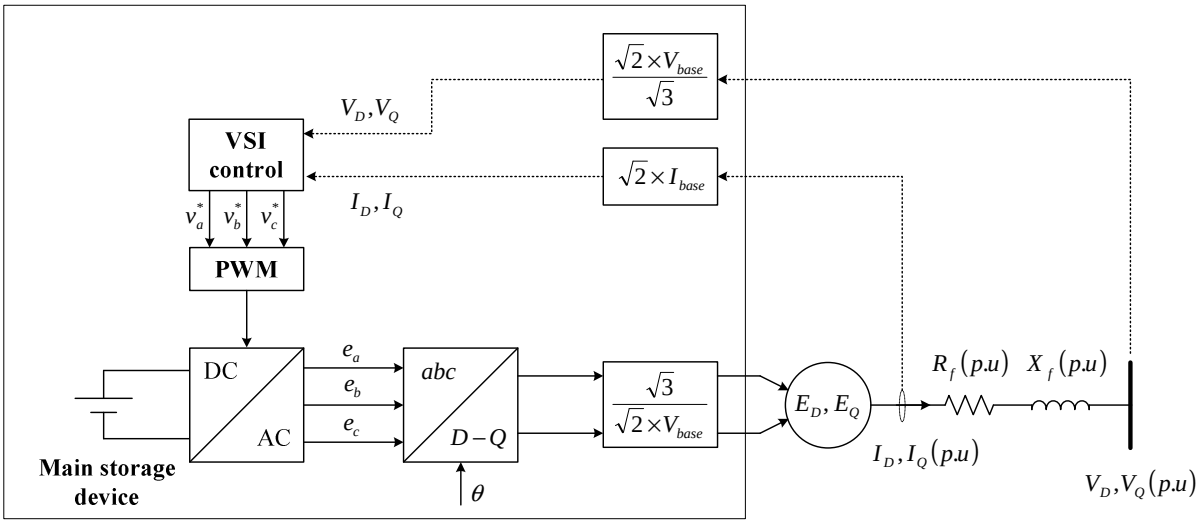

Figure 5.3: Main storage device connected to the LV network through the VSI control scheme

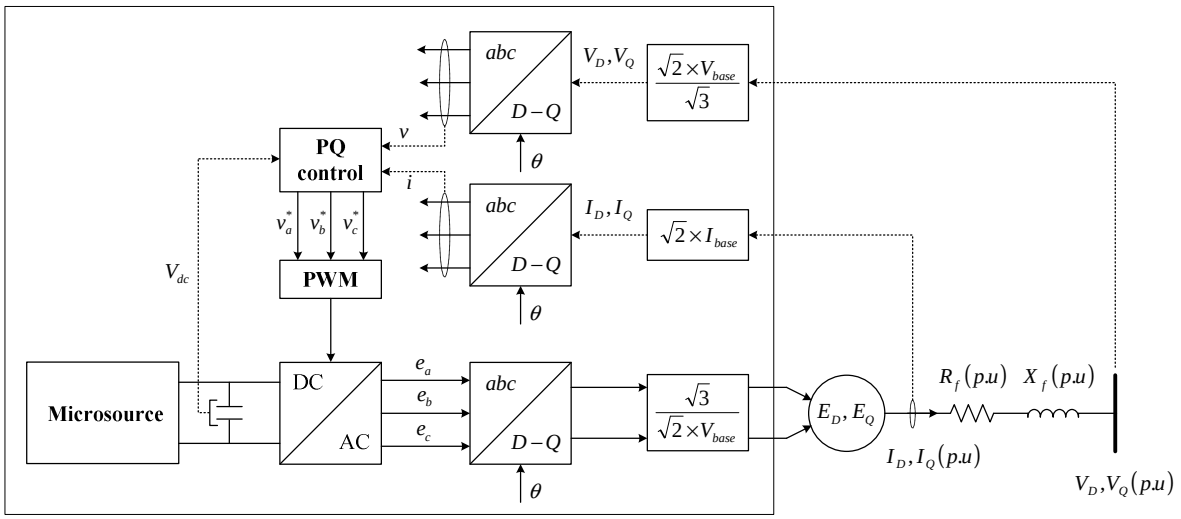

Figure 5.4: Microsources connected to the LV network through PQ inverter control

It can be observed from figures 5.3 and 5.4 that the algebraic equations that connect the inverters to the LV network can be written in the synchronous reference frame as

$$\begin{bmatrix} V_D \\ V_Q \end{bmatrix} = \begin{bmatrix} E_D \\ E_Q \end{bmatrix} - \begin{bmatrix} R_f & -X_f \\ X_f & R_f \end{bmatrix} \times \begin{bmatrix} I_D \\ I_Q \end{bmatrix} \tag{5.11}$$

where R_f and X_f are the per unit values of the filter resistance and reactance referred to the system base.

Concerning micro wind generation systems, the per unit variables of the induction generator model described in chapter 2 are represented in a system reference frame rotating at synchronous speed. Therefore the stator equations can be directly integrated in the network matrix [217, 218].

5.2.1.3 Load modelling, transformers and compensation capacitor banks

In this simulation platform loads are modelled as balanced symmetrical three-phase impedances, $\underline{Z}_L = R_L + jX_L$. When the load active and reactive power, P_L and Q_L respectively, and the bus voltage, $\underline{V}_t$, are known at steady-state then the values of resistance R_L and inductance L_L can be calculated by the relation:

$$P_L + jQ_L = \left|\underline{V}_t\right|^2 \underline{Y}_L^* \tag{5.12}$$

where $\underline{Y}_L = \underline{Z}_L^{-1}$ and $\underline{Y}_L^*$ denotes the conjugate of $\underline{Y}_L$.

The capacitor banks commonly used to compensate the reactive power that is absorbed from wind generators using induction machines are described in the dynamic simulation as injected currents into the network. After the elimination of transients, namely when there are no large deviations from the nominal frequency,

$$\underline{I}_C = j\frac{\underline{V}_t}{X_C} \tag{5.13}$$

and the reactance X_C can be introduced in the network admittance matrix.

Transformers are modelled as equivalent impedances. Thus, the variables associated with the transformers, loads and capacitor banks should be transformed to the synchronous rotating reference frame in order to be integrated in the network matrix.

5.2.1.4 The MMG network equations

Network branches are modelled by series resistance, R_{TL}, and inductance, L_{TL}, which are considered as concentrated for the total length of the line. The capacitance for small lines can be neglected. Thus, the network is modelled through the nodal admittance matrix, $[\underline{Y}]$ [216].

As the other power system components, such as capacitors banks, transformers and loads, are represented by their corresponding equivalent admittances, they are also introduced in the network admittance matrix. Thus, the whole MMG dynamic model together with the static network and loads is depicted in figure 5.5.

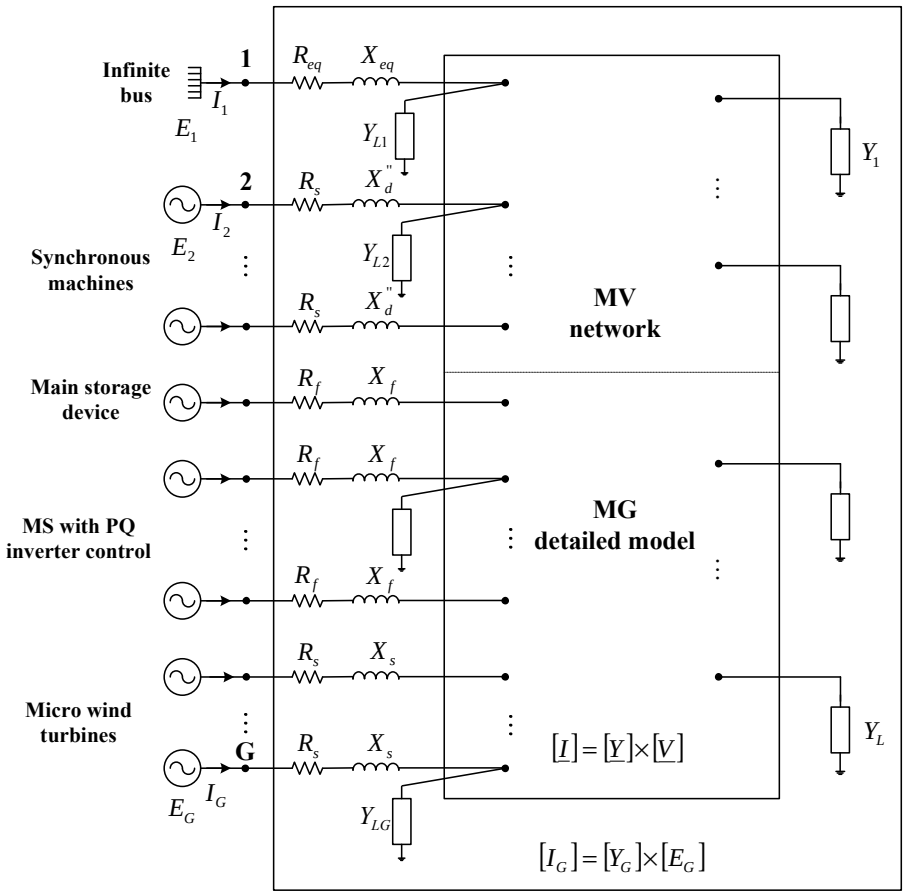

Figure 5.5: Interconnection of generation sources with the network equations

In order to build the multi-machine power system matrices necessary for the numerical simulation it is convenient to number the various bus bars following a specific order which depends on the type of components that are connected at each bus bar, as can be observed from figure 5.5. For that purpose, the infinite bus was numerated first; bus bars where synchronous generators are connected were numerated next, following this one where the main storage device is connected. Nodes with PQ control inverters, asynchronous generators and static loads, respectively, were numbered afterwards.

Under these previous assumptions, taking into account the subsections 5.2.1.1, 5.2.1.2 and 5.2.1.3, and concerning the sources internal bus bars, which have $E_G = \begin{bmatrix} E_D & E_Q \end{bmatrix}^T$ for their internal voltages, the MMG network equation of voltages and currents can be obtained as [216]:

$$\begin{bmatrix} I_{D1} \\ I_{Q1} \\ \vdots \\ I_{DG} \\ I_{QG} \\ 0 \\ 0 \\ \vdots \\ 0 \\ 0 \end{bmatrix} = \begin{bmatrix} [Y_{GG}] & [Y_{GL}] \\ [Y_{LG}] & [Y_{LL}] \end{bmatrix} \times \begin{bmatrix} E_{D1} \\ E_{Q1} \\ \vdots \\ E_{DG} \\ E_{QG} \\ V_{D1} \\ V_{Q1} \\ \vdots \\ V_{DL} \\ V_{QL} \end{bmatrix} \tag{5.14}$$

where $\{G\}$ is the set of internal generator nodes, $\{L\}$ is the set of all other nodes, including the generator terminal bus bars, which are called load nodes.

The matrix $[Y_{GG}]$ is a diagonal matrix of $\{G\}$ nodes admittances, obtained as follows

$$[Y_{GG}]=\begin{bmatrix} \begin{bmatrix} R_{eq} & -X_{eq} \\ X_{eq} & R_{eq} \end{bmatrix}^{-1} & \begin{bmatrix} 0 & 0 \\ 0 & 0 \end{bmatrix} & \cdots & \begin{bmatrix} 0 & 0 \\ 0 & 0 \end{bmatrix} \\ \begin{bmatrix} 0 & 0 \\ 0 & 0 \end{bmatrix} & \begin{bmatrix} R_s & -X_d'' \\ X_d'' & R_s \end{bmatrix}^{-1} & \cdots & \begin{bmatrix} 0 & 0 \\ 0 & 0 \end{bmatrix} \\ \vdots & \vdots & \vdots & \vdots \\ \begin{bmatrix} 0 & 0 \\ 0 & 0 \end{bmatrix} & \begin{bmatrix} 0 & 0 \\ 0 & 0 \end{bmatrix} & \cdots & \begin{bmatrix} R_s & -X_s \\ X_s & R_s \end{bmatrix}^{-1} \end{bmatrix} \tag{5.15}$$

$[Y_{GL}]$ is a rectangular matrix comprising a diagonal submatrix with elements equal to $-Y_{ii}$ of matrix $[Y_{GG}]$ and all other elements equal to zero. $[Y_{LG}]$ is the transpose of $[Y_{GL}]$. The matrix $[Y_{LL}]$ is a modified version of the total nodal admittance matrix, $[\underline{Y}]$, whose diagonal terms now include the load and generator admittances at the rows corresponding to the load nodes and generator terminal nodes respectively.

To simplify the analysis, all nodes other than the generator internal nodes are eliminated using the Khron reduction formula [138]. The admittance matrix in (5.14) is then reduced to $[Y_{RC}]$ with dimensions $2G\times 2G$, where G is the number of power systems bus bars where current is injected. The generation bus voltages and the corresponding injected currents are related by the following equation, which is written in the synchronous reference frame.

$$[I_G]=[Y_{RC}]\times[E_G] \tag{5.16}$$

where

$$[Y_{RC}]=[Y_{GG}]-[Y_{GL}]^T\times[Y_{LL}]^{-1}\times[Y_{LG}] \tag{5.17}$$

is the reduced admittance matrix.

The voltages of terminal generation buses and load buses are determined by solving the following algebraic equations:

$$\begin{bmatrix} [E_G] \\ [V_L] \end{bmatrix}=\begin{bmatrix} [Y_{GG}] & [Y_{GL}] \\ [Y_{LG}] & [Y_{LL}] \end{bmatrix}^{-1}\times\begin{bmatrix} [I_G] \\ [0] \end{bmatrix} \tag{5.18}$$

The derived equations provide a fast solution on the necessary power system algebraic equations.

5.2.2 The MMG equivalent model

The MMG equivalent model is derived by replacing the MG through its dynamic equivalent, while the MV network model is retained in detail.

As stated before, the MG dynamic equivalent comprises the dynamic model of the MG main storage device together with its VSI control interface and an aggregated model able to represent the MG slow dynamics. This equivalent model is represented as a current source directly connected to the boundary bus trying to make the injected current equal to the tie line currents in the MG detailed model.

Thus, the MMG equivalent multi-machine power system matrices are then built taking into account the following assumptions with respect to the detailed model:

- The MV network model is retained in detail;
- The MG main storage device is connected to the LV network through its VSI control interface;
- The same LV line is used to connect the MG main storage device to the boundary bus;
- All the remaining MG components as well as both generation and load buses are eliminated.

Therefore the MMG equivalent model formulated as a multimachine power system model is schematically represented in figure 5.6.

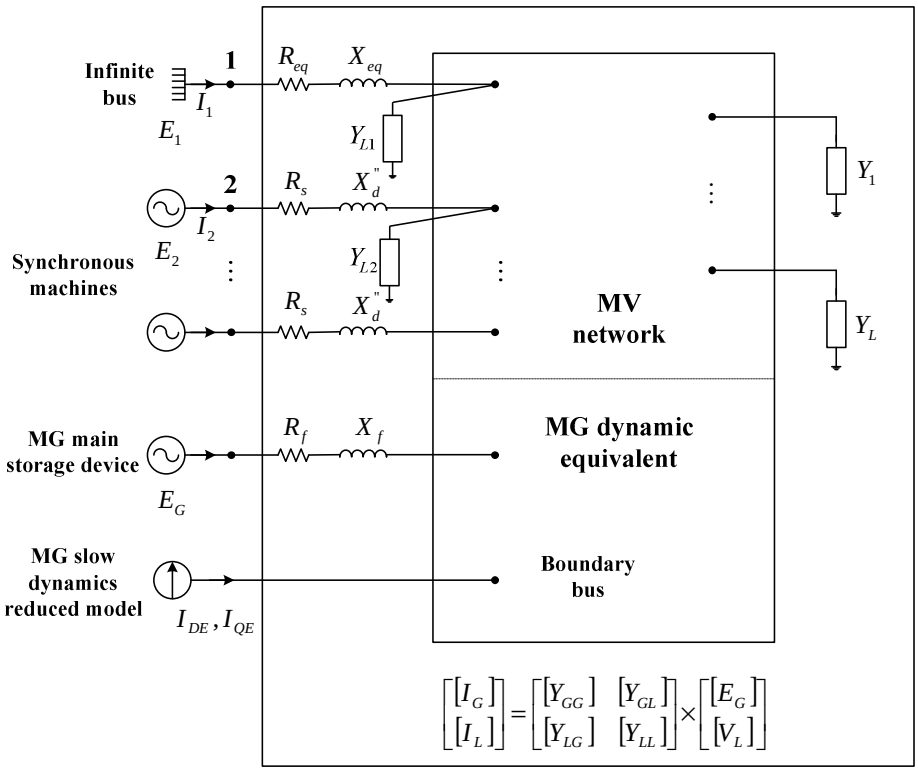

Figure 5.6: Interconnection of synchronous machine, main storage device and MS with the network equations

In this case, the algebraic equations describing the MMG equivalent model are written in the synchronous reference frame, $D-Q$, as

$$\begin{bmatrix}[I_G]\\[V_L]\end{bmatrix}=\begin{bmatrix}[Y_G] & [K_I]\\[K_V] & [Z_{LL}]\end{bmatrix}\times\begin{bmatrix}[E_G]\\[I_L]\end{bmatrix} \tag{5.19}$$

where

$$\begin{aligned}
&[Y_G]=[Y_{GG}]-[Y_{GL}]\times[Y_{LL}]^{-1}\times[Y_{LG}]\\
&[K_I]=[Y_{GL}]\times[Y_{LL}]^{-1}\\
&[K_V]=-[Y_{LL}]^{-1}\times[Y_{LG}]\\
&[Z_{LL}]=[Y_{LL}]^{-1}
\end{aligned} \tag{5.20}$$

It should be noted that all the load buses injected currents, $[I_L]$, are zero, except for the boundary bus.

5.2.3 The simulation algorithm

As described in the previous subsections dynamic models of several MS and other power system components are used to develop an integrated dynamic simulation platform able to simulate the MG dynamic behaviour based on an appropriate simulation algorithm. Although this algorithm allows the simulation of the MG dynamics inside the LV network, the attention is focused on the MG dynamic behaviour with respect to the MV network, namely when the MMG is operated in islanded conditions.

Therefore, the algorithm presented here is general and gives the possibility to analyse the relevant dynamics of MG considering arbitrary topologies with different numbers and types of microgeneration systems operating together under a SMO control strategy under different load and generation scenarios when several perturbation types take place in the MV network. The user interacts with the dynamic simulation platform by providing both the MMG input data and the simulation input parameters, as can be observed from figure 5.7.

A given MMG is described through the power system parameters. The scenarios for perturbation conditions are defined a priori for the specified steady state operating conditions. This MMG input data is written in an input m-file. Concerning to the input parameters, they are supplied directly to the S-function mask provided by *MatLab*® *Simulink*® environment and involve the matrices associated with the disturbance or the sequence of disturbances to be simulated, according to the perturbation conditions defined in the MMG input data, and the time sequence in which the disturbances occur. Based on the MMG input data and on the input parameters, the entire procedure is carried out automatically during a specified time interval using one of the available solvers.

Both the MMG detailed and equivalent models follow this simulation algorithm. However all the stages presented in figure 5.7 take into account the multimachine power system formulations presented in subsections 5.2.1 and 5.2.2, corresponding to the MMG detailed model and the MMG equivalent model, respectively.

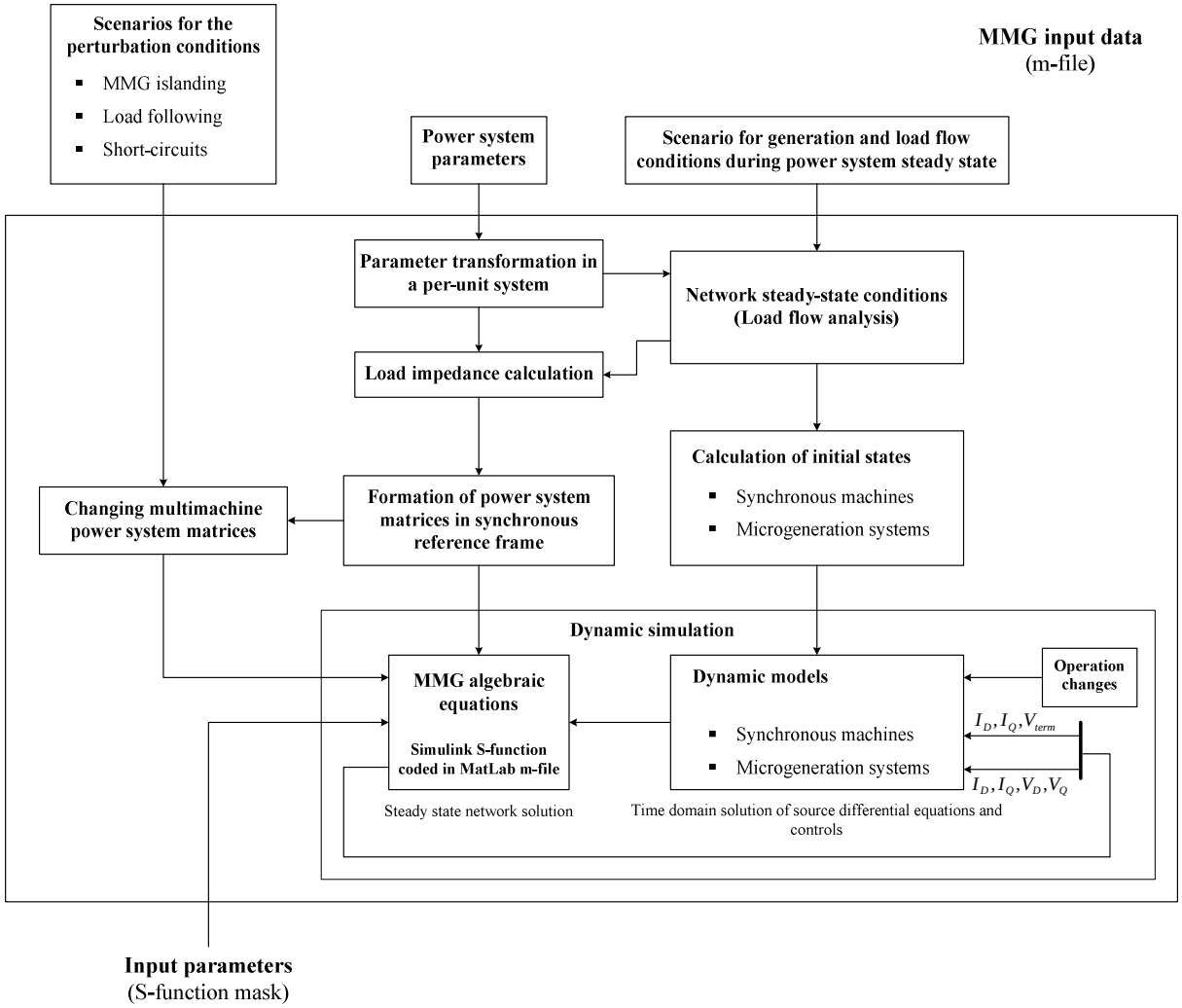

Figure 5.7: Flow-chart of the integration algorithm in *MatLab*® and *Simulink*®

The main components of this simulation tool are described in the following subsections.

5.2.3.1 Initial conditions for network quantities, synchronous generators and microgeneration systems

In order to calculate the initial values of bus bar voltages magnitudes and phase angles as well as the injected generating power under balanced steady state conditions, an initial load flow analysis is performed. The input data corresponds to a scenario describing the power system steady state generating and load conditions, taking into account the following assumptions:

- The MMG is connected to the upstream power system;
- The active power production of each DG unit connected to the MV network is known and the terminal nodes considered as PV type;
- Microgeneration systems are considered as generating units with positive active and reactive power injections. Their terminal buses are modelled as nodes type PQ;
- The classical Newton-Raphson method is applied to solve the load flow problem due to its good convergence properties and applicability to high resistive networks.

The results obtained from the load flow analysis are also used to determine the initial values of the state variables related with:

- Synchronous machines as well as their voltage regulator and speed governor;
- Microsources, such as SSMT, SOFC and small wind turbines;
- Inverter interfaces, like PQ inverter and VSI controls;
- MG slow dynamics equivalent model.

5.2.3.2 Types of disturbances

The main disturbances that occur in a MMG power system can be originated from sudden changes in the network conditions, such as MMG islanding, changes in the load of the system, short-circuits and changes in the mode of operation of the generation units.

Both MMG islanding and short-circuits are simulated as changes in the network admittance matrix of equation (5.14). Load following is an important source of perturbations especially for an autonomous power system. Since loads are modelled as constant impedances, included in the admittance matrix, a change in the static load is also modelled as a change in the multimachine power system matrices.

Concerning to changes in the mode of operation of one or more microsources, the following disturbances are considered:

- Perturbations on the microsource operating conditions;
- Connection and disconnection of microsources in the network.

These disturbances are simulated directly on the dynamic models that describe the system dynamic behaviour, as can be observed from figure 5.7.

5.3 TDNN based dynamic equivalents for MG

As described in chapter 4, TDNN based on MLP neural networks have high capability to deal with complicated nonlinear problems in a general framework, which allows their successful applications to new situations that were not used during a training phase. Therefore well trained TDNN can replace the MG slow dynamics and it is expected that it properly interacts with the retained network for a wide range of operating conditions.

With the use of TDNN for dynamic modelling purposes, no information about the system structure is required and the use of complex mathematical analysis is avoided. This represents a significant advantage especially when there is a limited understanding of the relations between system variables.

The application of TDNN for MG dynamic equivalent purposes involves four major steps, like the conceptual system identification procedure presented in chapter 4. These steps are:

- Data generation;
- Model structure selection;
- Determination of the TDNN adjustable parameters;
- Model validation.

The first three steps are performed off-line. The MG slow dynamics equivalent model thus obtained is embedded in the validation module forming a MMG equivalent network. A brief description of these main steps is presented in the following subsections.

5.3.1 Data generation

As the data set is the basis of any successful identification procedure, a numerical experiment should be designed in order to produce a set of samples that describe how the system behaves over its entire range of operation. For this purpose the MMG detailed model is used taking into account the following issues:

- The design of input signals which lead to an informative data set;
- Techniques for preparing the data for neural network modelling.

Based on the system definition presented in chapter 4 as well as in the engineering expertise, adequate input signals have been designed. Thus, after MMG islanding, several perturbations occurring in the MV network are simulated and both the input and output signals

are measured according to a suitable sample time. As already mentioned previously, boundary bus voltages expressed in the synchronous reference frame, $D-Q$, and system angular frequency are considered as inputs while the boundary bus injected current from the tie line, expressed in the $D-Q$ reference frame, are considered as outputs. Thus, the TDNN is disturbed by both boundary bus voltage and network frequency variations. It reacts to these variations by varying the injected currents into the boundary bus, operating according to the principles of a Norton model [16].

Boundary bus voltages, system frequency and injected currents are stored in a data base during the perturbation simulations in order to build suitable training patterns. Since the data set is almost the only source of information to build the TDNN based dynamic equivalent model, the number of samples should be large enough in order to form appropriate training and validation data sets.

Concerning the data preparation for neural network modelling, many different methods can be considered in order to extract the most valuable information from the measured data and to make it suitable for neural network modelling. Since signals are likely to be measured in different physical units, it is recommended to remove the mean and scale all signals to the same variance in order to avoid the tendency that the signal of largest magnitude will be too dominating. Moreover, scaling makes the training algorithm numerically robust and leads to a faster convergence and tends to give better models [164].

In order to generate a more robust TDNN, which is able to simulate the MG dynamic behaviour under different operating conditions, normalized deviations of voltage, system frequency and currents from the corresponding steady state are used as in [16, 121-124].

5.3.2 Model structure selection

Selecting a TDNN model structure basically implies to select the structure of regressors and to specify how to combine them into a one-step-ahead prediction through the MLP neural network. However, a combinatorial explosion of possible solutions arises from this procedure and therefore it is impossible to investigate all configurations. In this sense, the working procedure is to separate the two components of the problem by first selecting a particular

structure of the regression vector and subsequently to specify the number of hidden units in an attempt to determine good network architectures for this choice of regressors.

As stated before, in chapter 4, the regressor vector is based on the NFIR model structure. However, a wrong choice of the number of signals used as regressors will lead to poor results. Too small lag spaces obviously implies that essential dynamics will not be modelled, but too large ones will contain redundant information and increase significantly the input space dimensionality. Although it is desirable to decide the number of past inputs based on physical insight, when the knowledge about the system is limited the method based on the Lipschitz quotients can be considered, since it can often provide a reasonable estimate of the model order for deterministic systems. However, to compute all quotients particularly if N is large is a very time consuming task [164]. Therefore, taking into account that MLP can cope well with redundant inputs by driving the corresponding hidden layer weights toward zero, the number of past inputs selection becomes less important and the main objective is to assure the representation of the MG relevant dynamics.

In what concerns to the MLP architecture, since one has access of an unlimited amount of training data the neural network architecture determination relies on fully connected neural networks. In this case, the architecture selection is reduced to a matter of choosing a number of hidden units and the activation functions types of an MLP neural network. A regularization technique is further applied in order to deal with the bias/variance dilemma.

5.3.3 Determination of the TDNN adjustable parameters

In this stage the collected data set is applied to pick the best model among the candidates contained in the specified MLP neural network architecture. Thus the neural network is trained in order to provide the best possible one step ahead prediction in a mean square sense. Neural network toolbox of *MATLAB*® is used for this purpose [222].

The backpropagation method with Levenberg-Marquardt algorithm is used during the learning procedure. Taking into account the discussion presented previously in subsection 4.4.4.1.1 and due to its simplicity, early stopping is also used in order to avoid overfitting, realizing thus the best bias/variance trade-off. Since it is always desirable that the trained neural network model is also validated on a validation data set not used to extract training patterns, the collected data set is then split between the training and test or validation data sets.

Some care is taken into account in order to guarantee similar properties between the two data sets regarding the representation of the system entire operating range.

As several MLP neural networks with randomly initialized parameters are trained, the validation error is also used as the first criterion to reject poor models.

5.3.4 Model validation

After the training procedure, the performance of the TDNN based equivalent models with less generalization error are evaluated in the dynamic simulation platform. A MG slow dynamics equivalent model is then embedded in the validation module forming the MMG equivalent model. The model performance is evaluated by comparing its response following perturbations that occur in the retained subsystem not used during the training phase with the response obtained using the MMG detailed model.

For this purpose, in addition to the TDNN itself, this model requires two auxiliary functions to prepare the TDNN inputs and outputs to be integrated into the dynamic simulation. These two functions represent the interface between the TDNN and the retained network as depicted in figure 5.8.

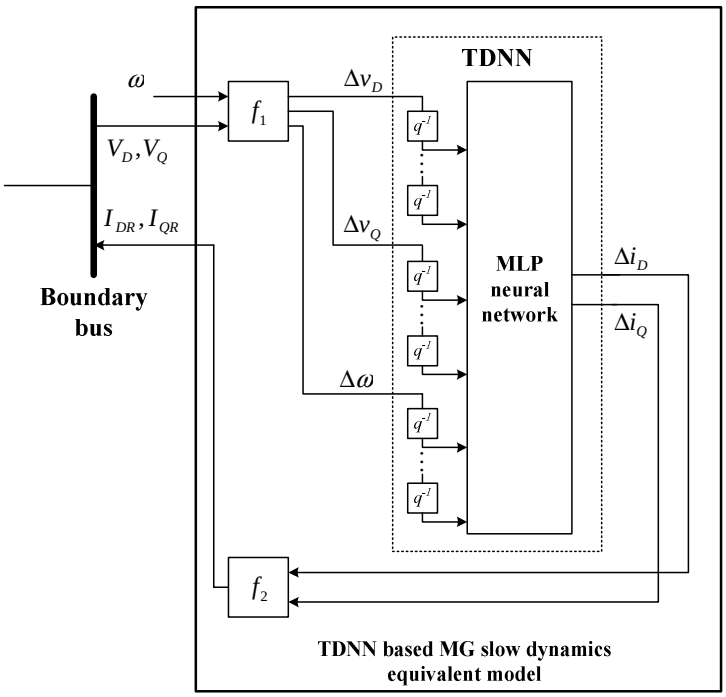

Figure 5.8: TDNN based MG slow dynamics equivalent model

At each time step, the MG slow dynamics equivalent model recognizes the operating status of the retained network through the boundary bus voltage and system frequency. The normalized voltage and system frequency deviations, Δv_D, Δv_Q and $\Delta\omega$, respectively, are computed through the function f_1. The TDNN is then used to determine the corresponding normalized current deviations, Δi_D and Δi_Q. Therefore the current to be injected into the retained network is computed using the function f_2. These normalized deviations are computed based on their initial steady state values as follows

$$\Delta v_D = \frac{V_D - V_D^{(0)}}{\Delta V_{D,\max}};\ \Delta v_Q = \frac{V_Q - V_Q^{(0)}}{\Delta V_{Q,\max}};\ \Delta\omega = \frac{\omega - \omega^{(0)}}{\Delta\omega_{\max}} \tag{5.21}$$

$$I_{DR} = \Delta i_D \times \Delta I_{D,\max} + I_{DR}^{(0)};\ I_{QR} = \Delta i_Q \times \Delta I_{Q,\max} + I_{QR}^{(0)} \tag{5.22}$$

where

Δv_D, Δv_Q, Δi_D, Δi_Q are the normalized deviations of both voltage and current $D-Q$ components;

$\Delta\omega$ is the normalized deviation of frequency;

$\Delta V_{D,\max}$, $\Delta V_{Q,\max}$, $\Delta I_{DR,\max}$, $\Delta I_{QR,\max}$ are the maximum variations considered to normalize both voltage and current $D-Q$ components;

$\Delta\omega_{\max}$ is the maximum frequency deviation considered to normalize frequency;

$V_D^{(0)}$, $V_Q^{(0)}$, $I_{DR}^{(0)}$, $I_{QR}^{(0)}$ are the initial steady state values of both voltage and current $D-Q$ components;

$\omega^{(0)}$ is the nominal value of system frequency.

The initial steady state values of boundary bus voltage and injected current of the MG slow dynamics equivalent model are determined through the initial load flow calculations. Their maximum deviations as well as frequency maximum deviation are obtained from the dynamic simulation of the largest amount of load connection and disconnection upon MMG islanding.

5.4 Dynamic equivalents for MG based on physical modelling

In contrast with TDNN based MG dynamic equivalents, the second promising approach is based on the available physical knowledge about MG dynamics and composition. Therefore, the data set requirements are less demanding.

Thus, the major issues are related to the model structure selection, the identification method and model validation, as described in the following subsections.

5.4.1 Physically parameterized model structure

As already mentioned previously, when the available knowledge allows to specify a physical model structure, the mathematical representation of the MG slow dynamics reduced model is commonly done by a continuous state space model of a given order. In this case the physical laws that approximate the MG slow dynamics under the study are similar to those that govern the active power control in a diesel group [17]. Thus, the physically parameterized model structure in represented under *MatLab*® *Simulink*® environment through the block diagram depicted in figure 5.9.

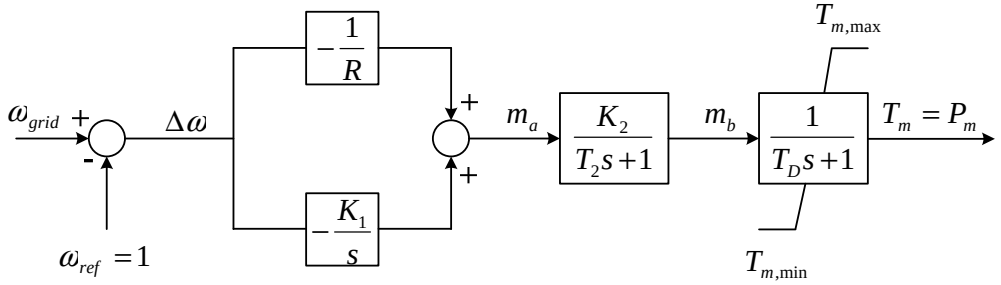

Figure 5.9: Model structure of the MG slow dynamics equivalent model

The model structure parameters whose values have to be estimated during the identification procedure are gathered into the parameter vector θ, as

$$\theta = \begin{bmatrix} R & K_1 & K_2 & T_2 & T_D \end{bmatrix} \tag{5.23}$$

Since the MG slow dynamics equivalent model should be a current source, the instantaneous power theory [223] was used in order to determine the network injected current as depicted in figure 5.10.

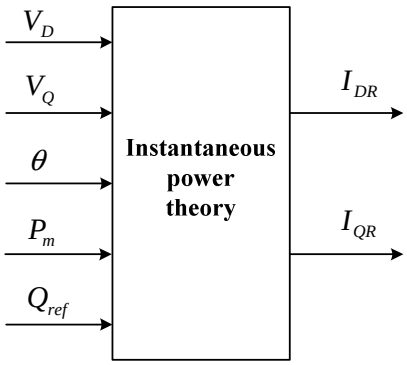

Figure 5.10: Interface between the MG slow dynamics equivalent model and LV network

The current source assumes the role of the inverter, by determining the current from both the active power delivered by the MG slow dynamics equivalent model, P_m, and a given reactive power, Q_{ref}, which corresponds either to a pre-defined value linked to a given MS power factor or a reactive power set-point sent by the MGCC, according to the reactive power control strategies described in chapter 2.

The instantaneous power theory was proposed in [223] for control of active power filters and has been used to control the PWM-VSI (*Pulse Width Modulation – Voltage Source Inverter*) or PWM-CSI (*Pulse Width Modulation – Current Source Inverter*). Voltages or current reference signals employed to turn on and turn off the switches of the inverter can be obtained from this theory [224, 225]. In this case, the instantaneous voltages and currents in three-phase circuits are adequately expressed as instantaneous space vectors in *abc* coordinates as depicted in figure 5.11.

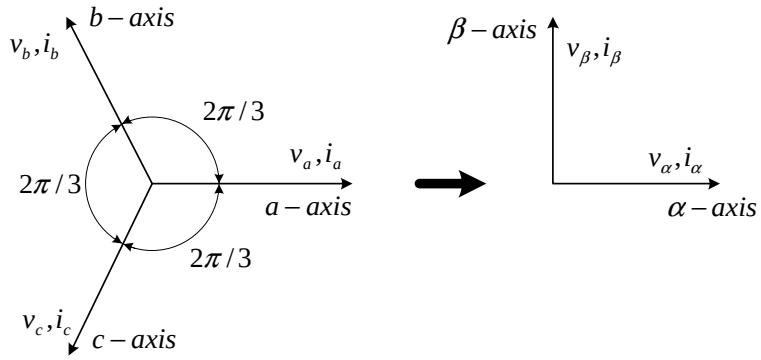

Figure 5.11: *abc* **to** $\alpha - \beta$ **coordinates transformation**

In a balanced three-phase system the *abc* space vectors are easily transformed into α and β coordinates through the Clark transformation as follows:

$$\begin{bmatrix} v_\alpha(t) \\ v_\beta(t) \end{bmatrix} = C \times \begin{bmatrix} v_a(t) \\ v_b(t) \\ v_c(t) \end{bmatrix} \tag{5.24}$$

$$\begin{bmatrix} i_\alpha(t) \\ i_\beta(t) \end{bmatrix} = C \times \begin{bmatrix} i_a(t) \\ i_b(t) \\ i_c(t) \end{bmatrix} \tag{5.25}$$

where

$v_a(t)$, $v_b(t)$ and $v_c(t)$ are the instantaneous voltages in *abc* coordinates, respectively;

$i_a(t)$, $i_b(t)$ and $i_c(t)$ are the instantaneous currents in *abc* coordinates, respectively;

$v_\alpha(t)$ and $v_\beta(t)$ are the instantaneous voltages in $\alpha - \beta$ coordinates, respectively;

$i_\alpha(t)$ and $i_\beta(t)$ are the instantaneous currents in $\alpha - \beta$ coordinates, respectively;

C is the Clark transformation given by

$$C = \sqrt{\frac{2}{3}} \times \begin{bmatrix} 1 & -\frac{1}{2} & -\frac{1}{2} \\ 0 & \frac{\sqrt{3}}{2} & -\frac{\sqrt{3}}{2} \end{bmatrix} \tag{5.26}$$

So, as described in [223], the instantaneous active and reactive powers are defined as:

$$\begin{bmatrix} p(t) \\ q(t) \end{bmatrix} = \begin{bmatrix} v_\alpha(t) & v_\beta(t) \\ -v_\beta(t) & v_\alpha(t) \end{bmatrix} \times \begin{bmatrix} i_\alpha(t) \\ i_\beta(t) \end{bmatrix} \tag{5.27}$$

where

$p(t)$ is the instantaneous active power in W;

$q(t)$ is the instantaneous reactive power in VAr.

In systems with sinusoidal balanced voltages and currents, the average value of $q(t)$ is equal to the conventional reactive power and the instantaneous active power, $p(t)$, is always equal to the conventional active power [223]. Thus, from equation (5.27) it is possible to obtain the currents reference signals to control the PWM-CSI depicted in figure 5.10 as follows

$$\begin{bmatrix} i_a^*(t) \\ i_b^*(t) \\ i_c^*(t) \end{bmatrix} = C^{-1} \times \begin{bmatrix} i_\alpha(t) \\ i_\beta(t) \end{bmatrix} \tag{5.28}$$

where

$$\begin{bmatrix} i_\alpha(t) \\ i_\beta(t) \end{bmatrix} = \begin{bmatrix} v_\alpha(t) & v_\beta(t) \\ -v_\beta(t) & v_\alpha(t) \end{bmatrix}^{-1} \times \begin{bmatrix} P_m \\ Q_{ref} \end{bmatrix} \tag{5.29}$$

and

$$C^{-1} = \sqrt{\frac{3}{2}} \times \begin{bmatrix} 1 & 0 \\ -\frac{1}{2} & \frac{\sqrt{3}}{2} \\ -\frac{1}{2} & -\frac{\sqrt{3}}{2} \end{bmatrix} \tag{5.30}$$

The references of currents, i_a^*, i_b^* and i_c^* are calculated instantaneously without any time delay by using the boundary bus instantaneous voltages and both active and reactive power values.

The procedure described above was implemented in a *Simulink* S-function coded in *MatLab* m-file, following the scheme presented in figure 5.12.

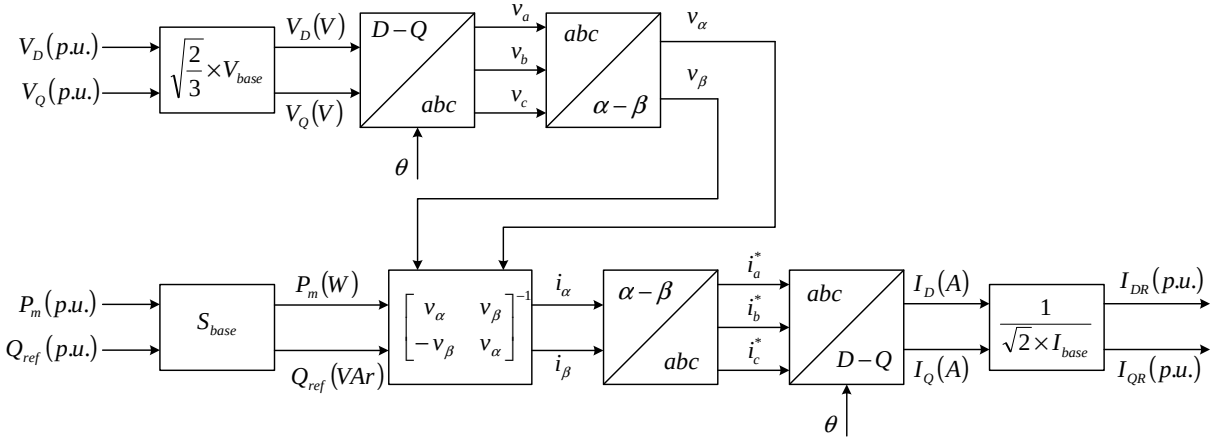

Figure 5.12: Schematic representation of instantaneous power theory implementation

5.4.2 The identification method

In order to estimate the parameters of the physically parameterized model structure, a suitable identification method is required. As discussed in chapter 4, EPSO, as a global optimization tool, together with MSE or MEE criteria constitute promising approaches.

Therefore, the algorithm presented in subsection 4.4.4.2 of chapter 4 is used. Under this context the parameter vector θ given by (5.23) provides particle phenotype descriptions corresponding to the particle positions into the parameter space. The particle performances are expressed through the MEE given by equations (4.47), (4.48) and (4.49) described in subsection 4.4.4.2 of chapter 4.

Since the identification method aims to find the values of parameters that minimize the error entropy and therefore the MSE, the MEE criterion plays the role of loss or cost function under system identification terminology as well as the particle fitness in an evolutionary sense. Thus, a suitable evaluation function was implemented for particles MEE calculation. In contrast with TDNN, the determination of the parameter vector given by (5.23) in carried out on-line. This means that the loss function of each particle is evaluated on the dynamic simulation platform. For this purpose the MG slow dynamics model structure is embedded in the validation package forming a potential MMG equivalent model. Therefore, some interaction between the EPSO

algorithm and the dynamic simulation platform, concerning the validation package, is required, as can be observed from the flow-chart depicted in figure 5.13.

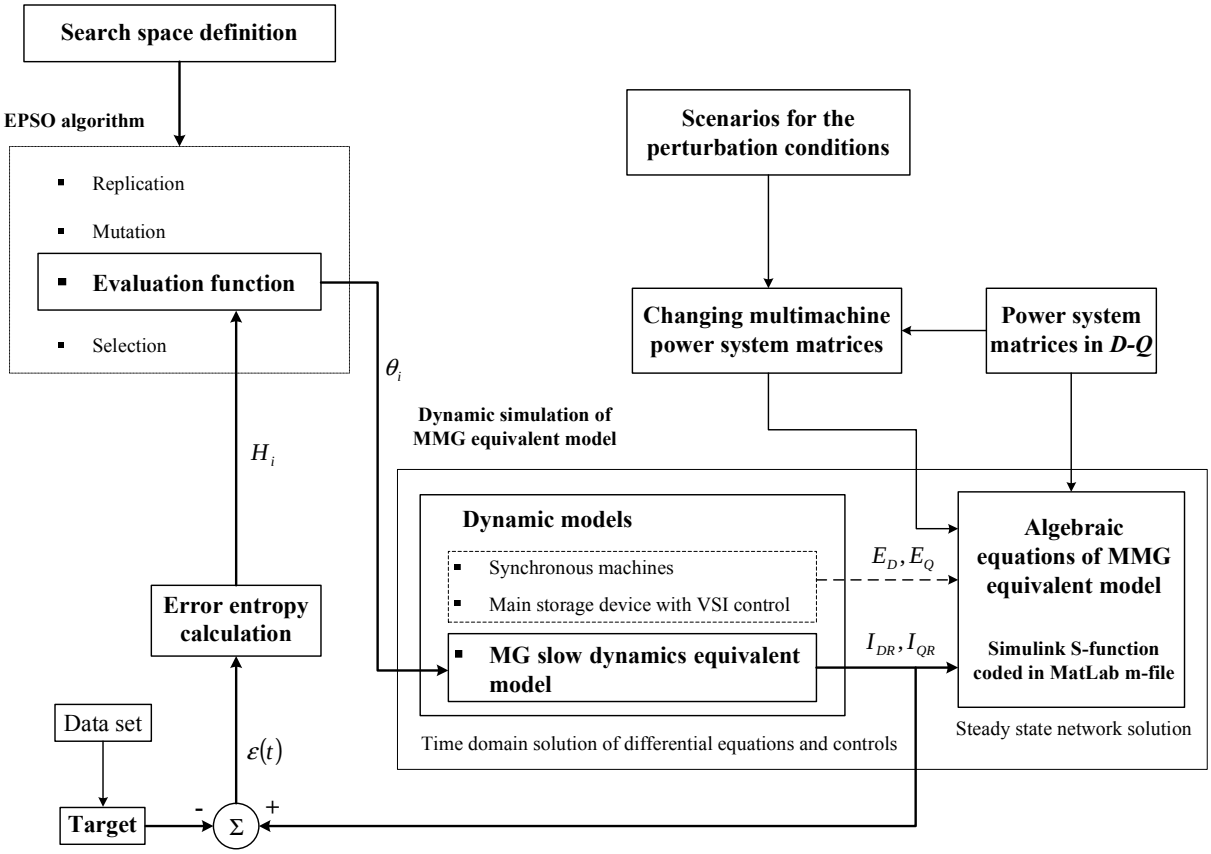

Figure 5.13: Flow-chart of physical parameters estimation

After defining the search space through both the minimum and maximum values of each parameter into the parameter vector, it is expected that the EPSO algorithm will perform the search to the global optimum or, at least, to a good local optimum under the MEE sense. For this purpose, after mutation has been performed by the EPSO algorithm, the following sequence of steps have to be carried out for each particle in the swarm.

- The evaluation function sends the particle object parameters to the MG slow dynamics equivalent model;
- A pre-specified set of disturbances occurring at defined time instants are simulated during a certain time period;
- The MMG equivalent model response is compared with the target response, which was generated from the MMG detailed model, yielding an error sequence;

- The entropy of the error sequence is then calculated and sent back to the evaluation function;
- Based on the error entropy information, EPSO algorithm performs selection in order to build the swarm corresponding to the next generation.

The above procedure is repeated while the EPSO algorithm termination condition is not verified. A similar procedure is carried out if MSE is adopted as the loss function.

5.4.3 Model validation

Taking into account the particular fact that the parameter vector is estimated on-line, on the environment in which it will be used, model validation is in some sense embedded into the parameter estimation stage, since models with poor performances have been eliminated by the selection operator during the parameter estimation procedure. The set of particle object parameters thus identified allows the best performance of the MG slow dynamics equivalent model evaluated on the validation software package.

Thus, as a final validation test, the model performance is evaluated considering disturbances not used during parameter estimation.

5.4.4 Summary and main conclusions

In this chapter two suitable approaches for deriving MG dynamic equivalents were developed. One exploits black-box modelling based on a TDNN while the other exploits physical modelling, being the physically parameterized model structure selected taking into account the available physical knowledge.

The application of these two developed methodologies to MicroGrids yielded two kinds of MG dynamic equivalents:

- The TDNN based MG dynamic equivalent;
- The physical MG dynamic equivalent.

In order to generate high quality data sets as well as to evaluate the performance of both types of MG dynamic equivalents, two dynamic simulation packages were also developed: The MMG detailed model and the MMG equivalent model, respectively. The integration of TDNN based MG dynamic equivalents into the MMG equivalent model for validation purposes was

also addressed. Concerning the physical MG dynamic equivalents, the MMG equivalent model is also used during the parameter estimation procedure.

Chapter 6
MicroGrid Dynamic Equivalents Study Cases

6.1 Introduction

In this chapter the two methodologies developed in chapter 5 are applied to derive dynamic equivalents for MG, being their performances also evaluated through the comparison of the results obtained from both MMG detailed and equivalent models. For these purposes two MMG are considered corresponding to two different test systems denoted as TS-01 and TS-02. The developed dynamic equivalents will reproduce the MG dynamic behaviour during MMG islanding and load following in islanded mode.

Thus, in section 6.2, the black-box modelling approach based on TDNN is applied to TS-01, yielding the TDNN based MG dynamic equivalents. The MG slow dynamics equivalent model is embedded into the dynamic simulation package corresponding to the MMG equivalent model of TS-01, being its performance evaluated. The results obtained are presented and discussed as well as some remarks concerning this methodology.

In section 6.3 the physical modelling approaches are applied to derive dynamic equivalents for the MG of TS-02, yielding the physical MG dynamic equivalents. Their performances are evaluated considering the MMG of TS-02 and, in addition, compared with the performance of the TDNN based MG dynamic equivalent considering the MMG of TS-01. Afterwards, the performance of the physical MG dynamic equivalents are also evaluated using *Eurostag*®. The results obtained from dynamic simulations are also presented and discussed.

Finally, the summary and main conclusions are presented in section 6.4.

6.2 MG dynamic equivalents based on TDNN

The TDNN based approach presented in section 5.3 is used in this section to derive a dynamic equivalent for the MG of the test system presented in figure 6.1. The MMG system presented in figure 6.1 (a) comprises two round rotor synchronous machines of $500\,kVA$

connected to the MV network together with MV loads and a LV feeder connected to a MV/LV distribution transformer – the MicroGrid. The MG contains an $80\,kW$ SSMT, the main storage device (flywheel) and three PV panels with a total capacity of $45\,kW$. The amount of load connected to the LV network is around $150 + j60\,kVA$ and the MV load is $400 + j60\,kVA$. A more detailed description of the electrical and mechanical parameters of the several components of this test system is presented in appendix A.

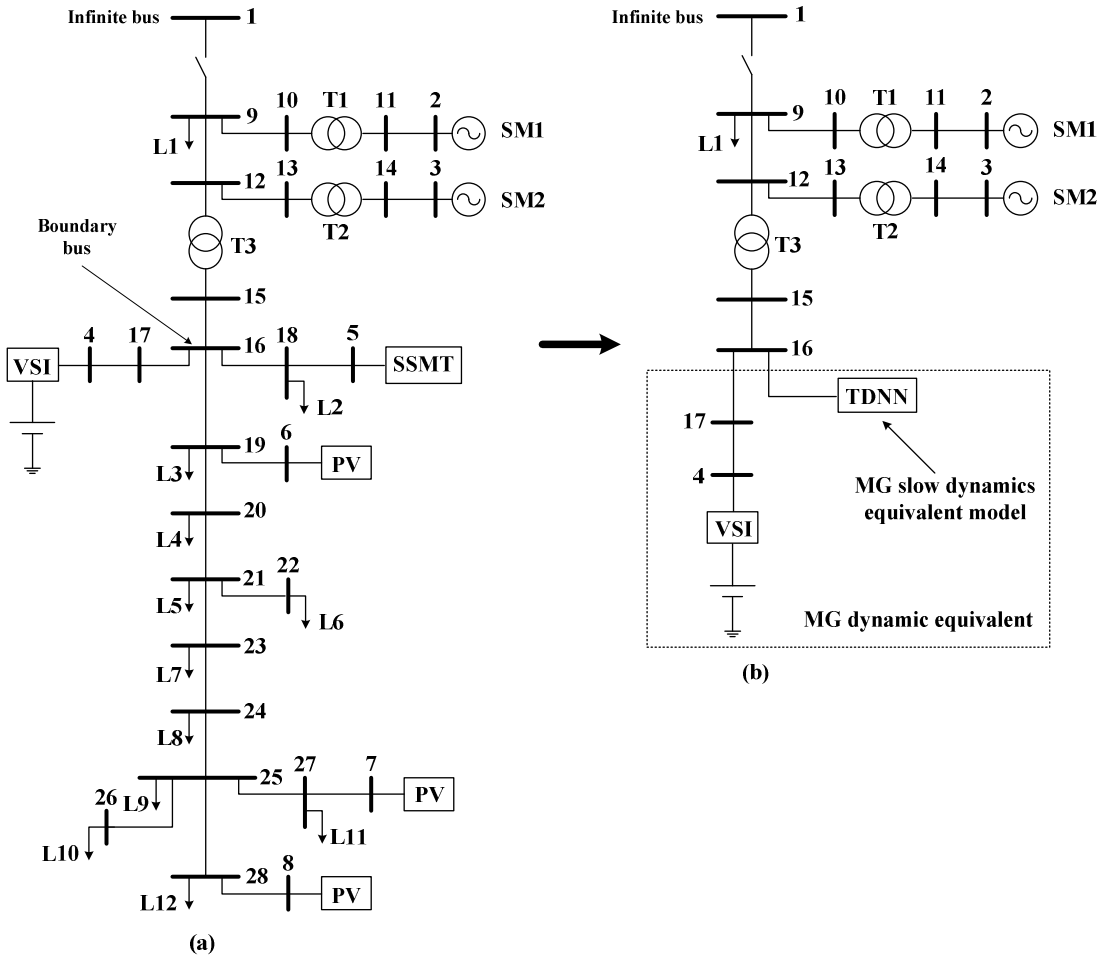

Figure 6.1: Single-line diagram of TS-01: (a) MMG detailed model; (b) MMG equivalent model.

The MG without the main storage device is replaced by a TDNN, which provides the NFIR model structure. This structure operating in parallel with the MG main storage device connected to the LV network through its VSI control forms the MG dynamic equivalent. The retained subsystem corresponds to the rest of the network, as can it be observed from figure 6.1 (b).

6.2.1 MG dynamic equivalents using TDNN

The idea behind the adopted approach is to replace all components belonging to the MG, except the main storage device feeder by a TDNN, which is connected to the retained subsystem through the boundary bus.

For training purposes, several amounts of load connection and disconnection are simulated at different locations in the MV network, when it is operated in islanded mode, using the package corresponding to the MMG detailed model. The simulation of each sudden load change is carried out for $40\,s$, which is enough to restore the steady state conditions after these disturbances. Thus, the load is connected at $t = 2\,s$ and disconnected at $t = 20\,s$. The dynamic simulation is carried out using the variable step size solver *ode15s* with a relative tolerance 1×10^{-6}.

A $10\,ms$ sample time was selected through a trial and error approach in order to avoid too large training and validation data sets and to guarantee simultaneously informative enough data sets, allowing a good performance of the TDNN based model. Thus each amount of load connection and disconnection results in 4000 patterns. The $D-Q$ components of boundary bus voltage, the $D-Q$ components of the injected current from the MG slow dynamics subsystem (MG without the main storage device feeder) as well as system frequency are stored during the simulation and subsequently used to prepare suitable patterns for TDNN training and validation purposes, as described in subsection 5.3.1 of chapter 5.

The TDNN has three inputs: $D-Q$ components of normalized voltage deviations at boundary bus and the normalized system frequency deviations. However, the MLP neural network receives the outputs from the external dynamic filter bank, which in this case realizes the regression vector corresponding to the 5 past measurements of the TDNN inputs. Therefore the MLP neural network has 15 inputs. On the other hand, two outputs representing the normalized deviations of the $D-Q$ injected current components at the actual time step are obtained from the MLP neural network. In what concerns the MLP neural network internal architecture, one and two hidden layers were considered with different number of hidden neurons, based on trial and error approaches and using the knowledge obtained from the first attempts. Therefore, a considerable number of MLP neural networks has to be trained and

evaluated in order to derive a MG slow dynamics equivalent model with good performance in the sense of the final model validation criterion, as it can be observed from figure 6.2.

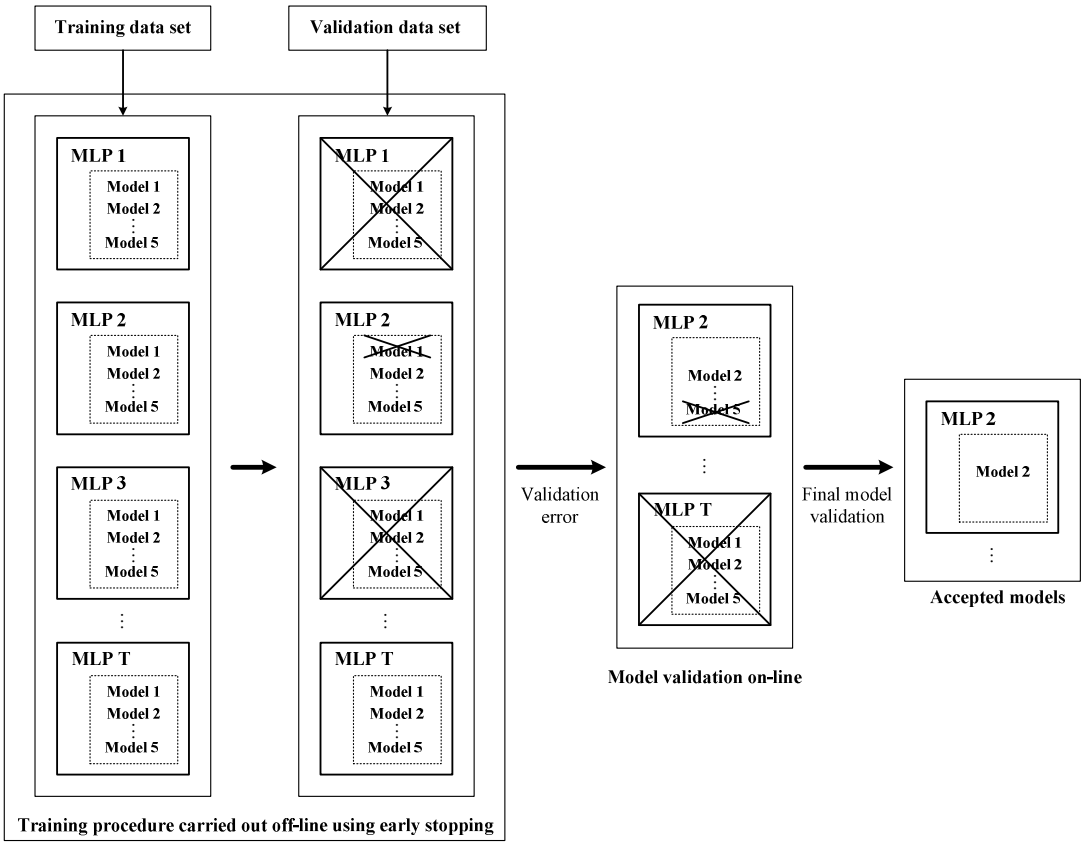

Figure 6.2: TDNN based MG slow dynamics model estimation and validation

Patterns corresponding to MMG islanding and 6 different load connection and disconnection sequences, upon MMG islanding, are used to train the MLP neural networks while patterns corresponding to 4 different load connection and disconnection sequences are kept for validation purposes. The training procedure was accomplished offline, as already mentioned previously in subsection 5.3.3. The obtained MLP neural networks are saved in order to be integrated in the validation dynamic simulation package, following the procedure described in subsection 5.3.4. For this purpose the command *gensim(net,st)* is used to create a *Simulink* system containing a block that simulates the neural network *net* with a sampling time *st*, which, in this case, is 10 *ms* .

The best accuracy in the sense of the final model validation criterion was obtained from a two hidden layer feedforward neural network with 31 and 11 neurons in the first and second

hidden layers, respectively, with a tan-sigmoid activation function. The output layer has two neurons with linear activation functions. The training procedure was automatically stopped when the error in the validation data set started increasing in order to avoid overfitting. This happened when around 400 epochs were elapsed, being the MSE value near 1×10^{-6} (for the normalized deviations of $D-Q$ components of the injected current).

6.2.2 Simulation results and discussion

As stated before, in order to evaluate the performance of the MG dynamic equivalent based on TDNN obtained as described in the previous section, the MG slow dynamics equivalent model is embedded in the dynamic simulation platform, replacing the detailed model of this subsystem and forming thus the MMG equivalent model.

The accuracy and validity of the TDNN based MG dynamic equivalent is evaluated by comparing the time domain responses obtained from dynamic simulations of disturbances tacking place in the MV network using both simulation packages corresponding to the MMG equivalent and detailed models.

It was assumed that the MMG is initially interconnected with the upstream power system and operated under the steady state conditions presented in table 6.1.

Table 6.1: TS-01 operating conditions before MMG islanding

		Generation	**Consumption**
MV network	SM1	$250\ kW$	
	SM2	$100\ kW$	
	Total	$350\ kW$	$400+j60\ kVA$
MicroGrid	Storage device	$10\ kVAr$	
	SSMT	$53{,}3+j2\ kVA$	
	PVs	$45\ kW$	
	Total	$98{,}3+j12\ kVA$	$148{,}9+j58{,}8\ kVA$

Based on these operating conditions before MMG islanding, a general overview of the several microgeneration systems dynamic behaviour is given firstly. For this purpose, the following sequence of actions was carried out in the MMG detailed model:

- MMG islanding at $t = 5\,s$;
- Connection of an amount of load, $100 + j25\,kVA$, to bus 9 of TS-01, as represented in the single line diagram of figure 6.1 (a), at $t = 20\,s$;
- Disconnection of the amount of load previously connected at $t = 40\,s$.

Afterwards, for model validation purposes, this sequence of disturbances is simulated using both the MMG detailed and equivalent models and the obtained time domain responses are compared. It should be noted that this amount of load was not used to extract training patterns. The TDNN based dynamic equivalent performance was also evaluated under different operating conditions before MMG islanding taking into account new load and generation conditions in the MV network as well as in the MG. Thus, the following operating scenarios were considered.

- **Scenario 0:** Initial steady state conditions presented in table 6.1;
- **Scenario 1:** New generating conditions is MV network;
- **Scenario 2:** New load conditions in MV network;
- **Scenario 3:** New generating conditions in MicroGrid;
- **Scenario 4:** New load conditions in MicroGrid.

The TDNN based MG slow dynamics equivalent model is integrated into the simulation package corresponding to the MMG equivalent model following the procedure described in subsection 5.3.4. Thus, the initial values of the TDNN based MG slow dynamics equivalent model inputs and outputs as well as their maximum variations have to be determined in order to derive suitable mapping and demapping functions, f_1 and f_2, given by equations (5.21) and (5.22), respectively.

The initial and maximum values obtained based on the initial steady state conditions presented in table 6.1 were updated for scenarios 1 to 4, as presented in table 6.2.

Table 6.2: TDNN based MG slow dynamics equivalent model inputs and outputs initial values and maximum deviations

	Initial values (p.u.)					**Maximum deviations**				
Scenario	$V_D^{(0)}$	$V_Q^{(0)}$	$I_{DR}^{(0)}$	$I_{QR}^{(0)}$	$\omega^{(0)}$	$\Delta V_{D,\max}$	$\Delta V_{Q,\max}$	$\Delta I_{DR,\max}$	$\Delta I_{QR,\max}$	$\Delta\omega_{\max}$
0	1,0088	$-9{,}56\times10^{-3}$	-0,1230	0,1198	1	0,0322	0,1436	0,074	0,006	0,0247
1	1,0092	$-9{,}2\times10^{-3}$	-0,1240	0,1198	1	0,0273	0,09853	0,0605	$4{,}7\times10^{-3}$	0,0247
2	1,0078	-0,0106	-0,1240	0,1201	1	0,048	0,2073	0,0908	0,0103	0,0323
3	1,0075	-0,0161	-0,1889	0,1215	1	0,0373	0,1657	0,0889	12×10^{-3}	0,0254
4	1,0136	$-1{,}68\times10^{-3}$	-0,0397	0,0857	1	0,0252	0,1274	0,0575	0.004	0,0250

The results obtained from the numerical simulations are presented and discussed in subsection 6.2.2.1 to 6.2.2.6. Some remarks of TDNN based MG dynamic equivalents are described in subsection 6.2.2.7.

6.2.2.1 Dynamic behaviour of microgeneration systems

In order to provide a general overview about the dynamic behaviour of the microgeneration systems, the above sequence of disturbances was simulated using the MMG detailed model. The microgeneration systems active and reactive power responses are presented in figure 6.3. In turn, figure 6.4 shows the system frequency and the MG main storage device terminal bus voltage.

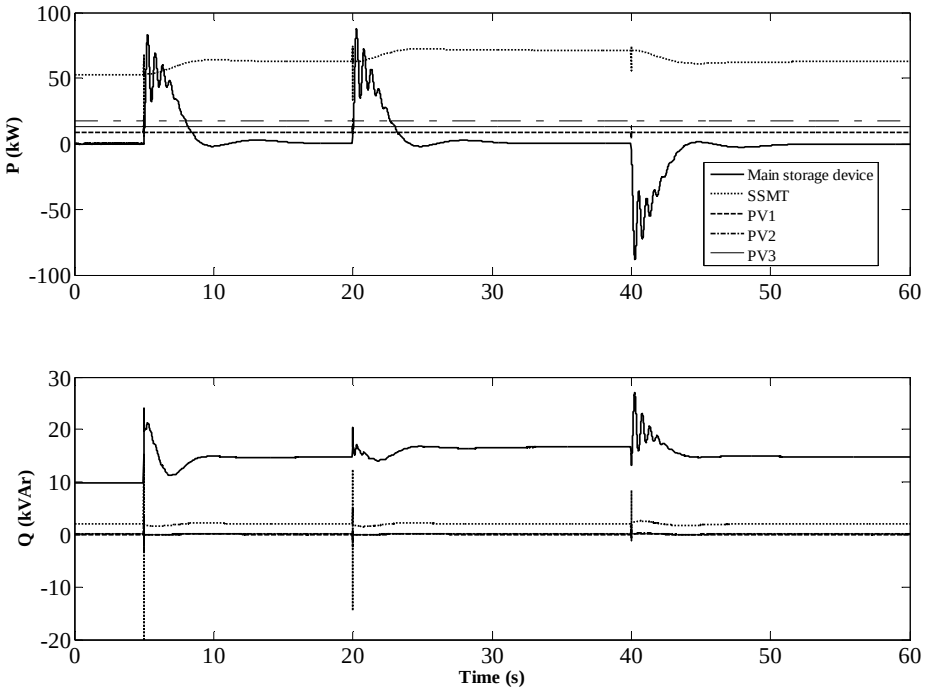

Figure 6.3: Active and reactive power outputs of microgeneration systems of TS-01

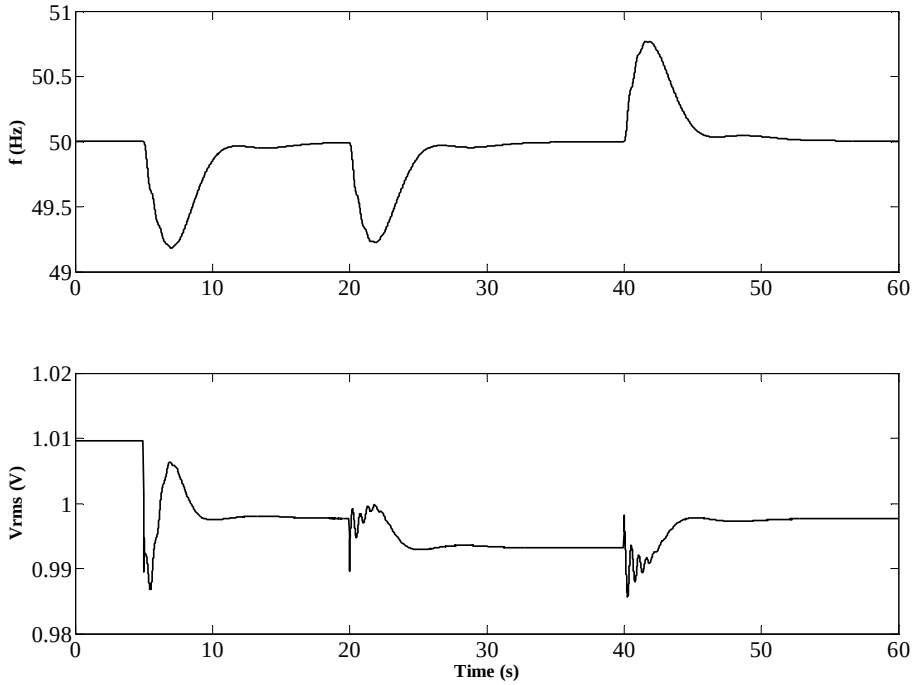

Figure 6.4: System frequency and MG main storage device terminal bus voltage of TS-01

When the MMG is operated in normal interconnected mode, all the microgeneration systems are supplying active and reactive powers according to the steady state operating conditions described in table 6.1. It should be noted that the PQ inverter controls of the PV systems are operated with a unity power factor, injecting in the LV network the maximum active power produced taking into account only the temperature and irradiance conditions, which are considered to be constant during the simulation time. Concerning the SSMT, it was considered as supplying a constant reactive power based on a given set-point defined centrally by the MGCC and sent to the MC embedded in its PQ inverter control.

Following a MMG disconnection from the upstream system, the MG is kept in operation connected with the MV network. The synchronous machines connected to the MV level provide both voltage and frequency references, as already mentioned previously, and are also the main responsible to balance demand and supply. Both active and reactive power outputs of PV systems are kept constants. Although the SSMT reactive power output experiments small variations during transient situations, it can be considered approximately constant over the simulation time and equal to the pre-specified set-point.

However, following the sequence of disturbance in the MV level, due to the load unbalance, transient system frequency changes and bus voltage variations arise. Therefore, the MG main storage device active and reactive power outputs experiment variations proportionally to the system frequency and bus voltage deviations from their nominal values, respectively, according to the frequency/active power and voltage/reactive power droops implemented in the VSI control interface. Thus, the active power is either injected or absorbed only during transients, whenever the system frequency deviations differ from zero, while the reactive power output is increased or decreased according to bus voltage deviations, as can be observed from figures 6.3 and 6.4.

Concerning to the SSMT, the local secondary load frequency control tries to restore the system frequency to the nominal value through the definition of a new active power set point for the primary energy source, based on the frequency deviation error. Therefore, the MG contributes together with the synchronous machines to meet power demand upon MMG islanding. The MG main storage device acts as a primary load frequency control while the SSMT provides secondary load frequency control. These features are key issues to assure the MG operation in islanded mode, as already mentioned previously in subsection 2.4 of chapter 2.

It can also be observed from figure 6.3 the two time scales that characterize the dynamic responses of the several microgeneration systems concerning the active and reactive power outputs. It should be noted that the MG system separation between the MG slow dynamics subsystem and the main storage device feeder was based on this physical knowledge and constitutes the basis for the developed MG dynamic equivalent methodologies, as stated before in chapter 4.

6.2.2.2 Scenario 0: Initial steady state conditions

After simulating the above sequence of disturbances, the TDNN based MG slow dynamics equivalent model outputs are compared with these ones obtained from the MG replaced subsystem. Figure 6.5 shows these comparisons.

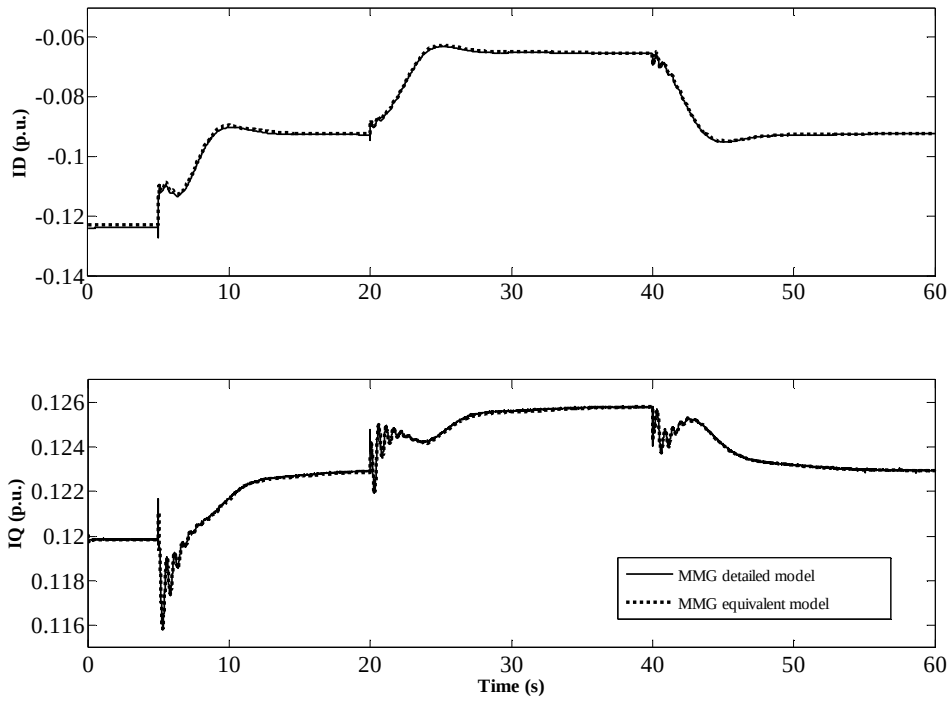

Figure 6.5: TS-01 TDNN based MG slow dynamics equivalent model injected current in scenario 0

The coincidence between the responses of the MG slow dynamics detailed and equivalent models indicates that the TDNN not only learned with success the nonlinear behaviour of the

replaced subsystem, but also presents a good generalization capability. This can also be observed from figure 6.6, where the performance of the TDNN based MG dynamic equivalent is compared with the one of the MG detailed model. The active and reactive power outputs of both models are very similar, demonstrating the effectiveness of this MG dynamic equivalent in reproducing the MG dynamic behaviour following MMG islanding and during load following transients when embedded in the dynamic simulation platform.

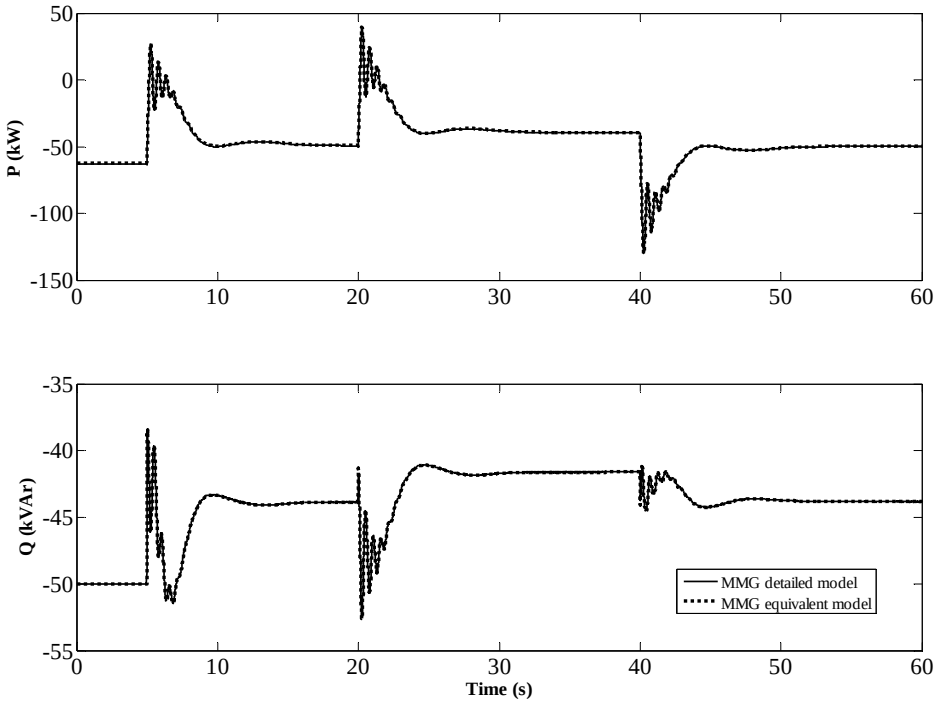

Figure 6.6: TS-01 MG dynamic equivalent power outputs in scenario 0

Before MMG islanding the MG was importing active and reactive power in order to face the LV consumption, as it is indicated by the negative signs in figure 6.6. This importing scenario is also kept after MMG islanding. The SSMT increases its active power production following MMG islanding as well as when the load is connected, reducing the injected active power when the load is disconnected. These variations are guided by appropriate set-points based on the system frequency deviation, as already mentioned previously. The main storage device supplies active power only during transients and varies its reactive power output proportionally to the bus voltage deviations. These active and reactive power variations can also be observed from figure 6.6. The TDNN based MG dynamic equivalent performance is also evaluated on

the retained subsystem. Thus, in figure 6.7, a comparison between boundary bus voltage and system frequency obtained from the MMG detailed and equivalent models is presented.

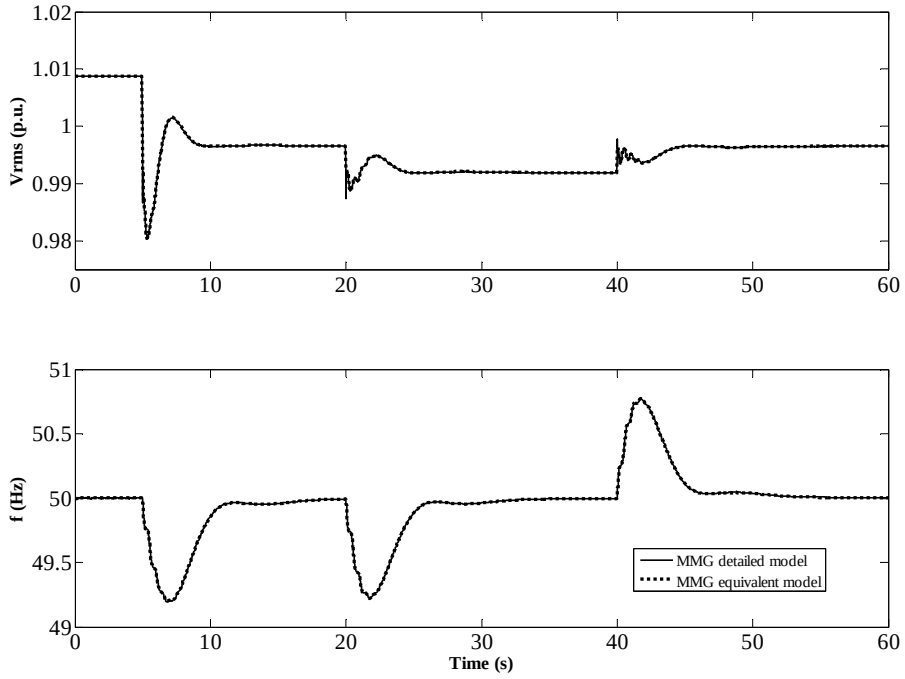

Figure 6.7: TS-01 Boundary bus voltage and system frequency in scenario 0

The quality of the results observed from figure 6.7 suggests that the TDNN based MG dynamic equivalent reproduces with high accuracy the MG dynamic behaviour with respect to the MV network, following MMG islanding as well as during both load following transients and steady state conditions when the MMG is operated in islanded mode. This can also be observed from figures 6.8 and 6.9, in which the active and reactive powers supplied by synchronous machines SM1 and SM2, respectively, are presented.

In order to balance generation and demand following the MMG islanding and during load following situations the synchronous machines SM1 and SM2 adjusted their active and reactive power productions, as it can be observed from figures 6.8 and 6.9, respectively.

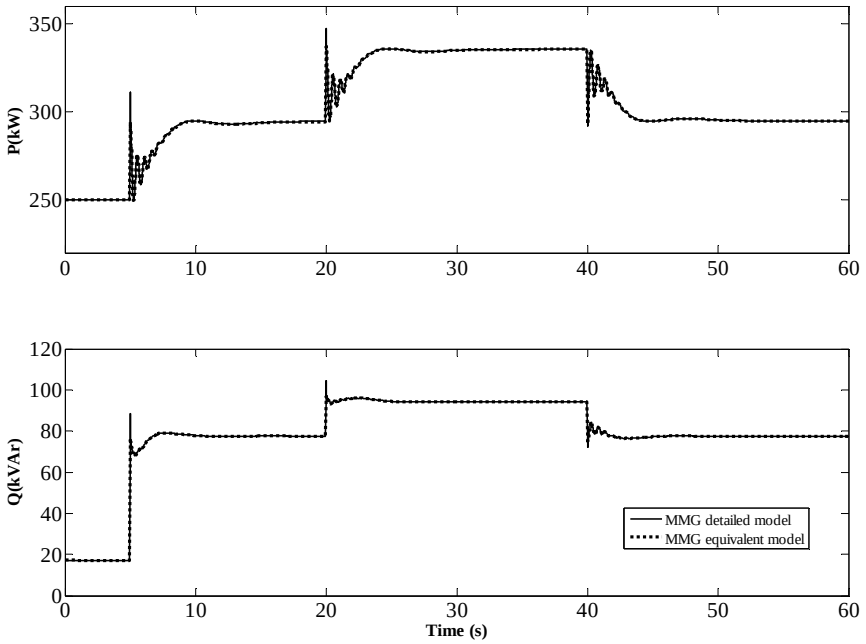

Figure 6.8: TS-01 SM1 active and reactive powers in scenario 0

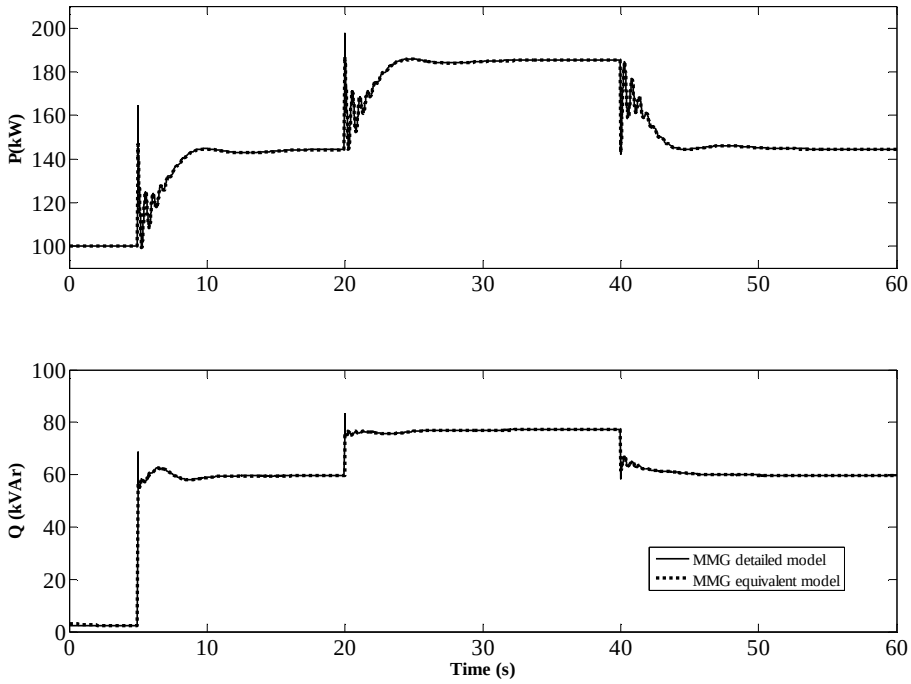

Figure 6.9: TS-01 SM2 active and reactive powers in scenario 0

Several comparisons were carried out under new disturbances resulting from the connection and disconnection of different amounts of loads, when the MMG is operated in islanded mode. The MMG equivalent model responses are in a very good agreement with these ones of the MMG detailed model. This ensures a good performance of TDNN based MG dynamic equivalent in reproducing the MG dynamic behaviour under load following transient conditions upon MMG islanding.

6.2.2.3 Scenario 1: New generating conditions in MV network

In order to evaluate the MG dynamic equivalent capability to cover new operating conditions, its behaviour is studied for new power flow conditions before MMG islanding, by increasing the active power produced by SM2 from 100 to 150 kW . The generated power and demand in the MG are kept constant, so that the total power transferred to the LV network is not significantly changed.

Figure 6.10 compares the powers supplied by the MG detailed model and by the TDNN based MG dynamic equivalent.

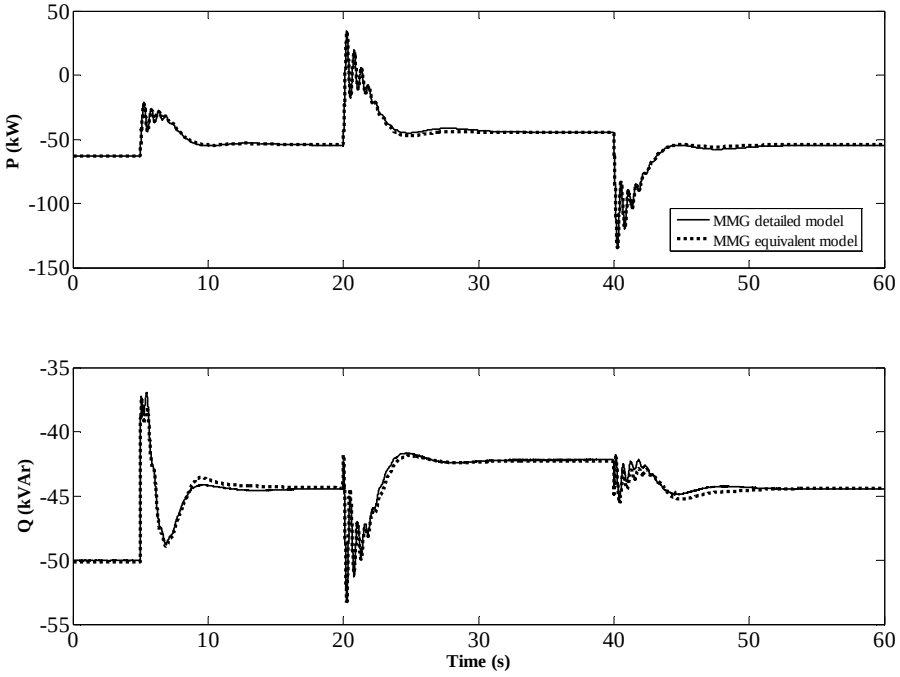

Figure 6.10: TS-01 TDNN based MG dynamic equivalent power outputs in scenario 1

Before MMG islanding, the MG is importing active and reactive power like in scenario 0. However, as the MMG active power generation was increased, the active power unbalance between demand and supply following MMG islanding was reduced and therefore the system frequency deviation from its nominal value is smaller than the one verified in scenario 0, as it can be observed from figure 6.10. As a result, the MG main storage device active power injection during this transient situation is smaller.

Figure 6.10 shows a small loss of accuracy between the power response of the MG dynamic equivalent and the MG detailed model, being the maximum errors $3kW$ for active power and $0{,}6kVAr$ for reactive power. This is not surprising since the MLP neural network was not trained under this initial steady state conditions. However, the results obtained show that the performance of the MG dynamic equivalent performs in a good agreement with the MG detailed model. The use of normalized deviations extends the validity of the dynamic equivalent to cover new initial MV generating conditions before MMG islanding without significant loss of accuracy, as can it also be observed from figures 6.11, 6.12 and 6.13.

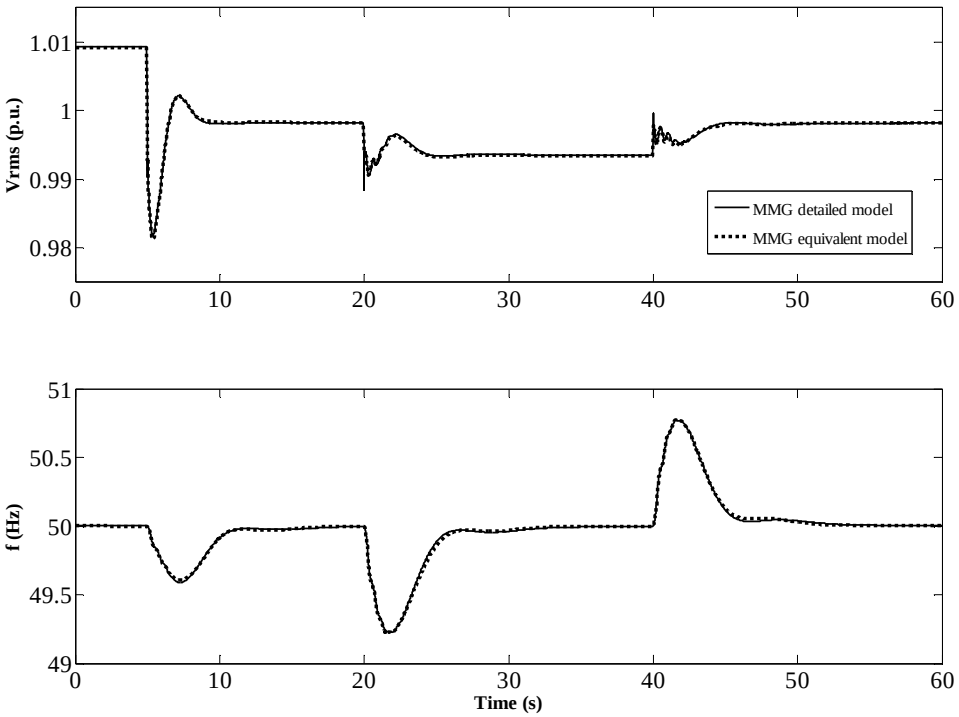

Figure 6.11: TS-01 boundary bus voltage and system frequency in scenario 1

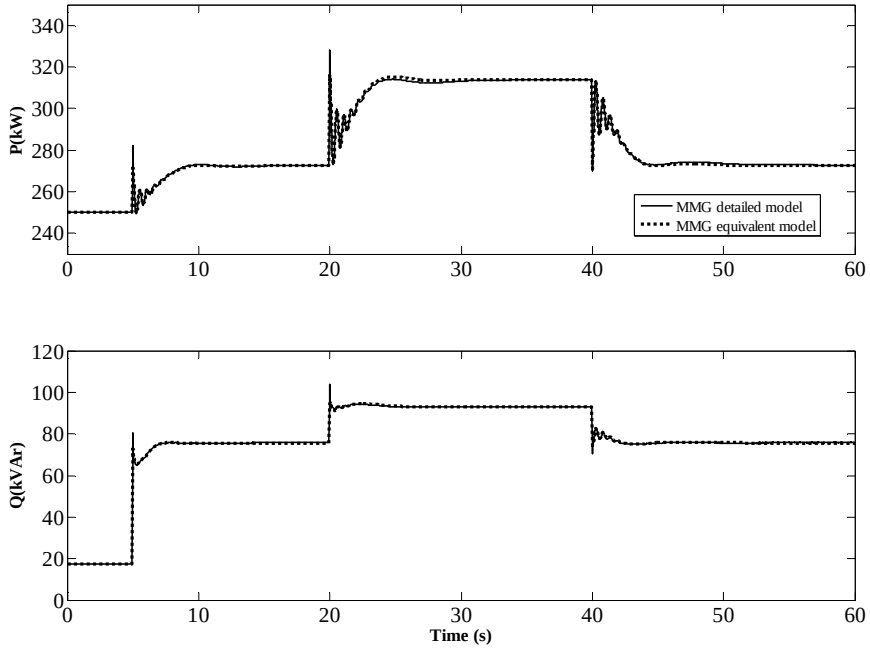

Figure 6.12: TS-01 SM1 active and reactive powers in scenario 1

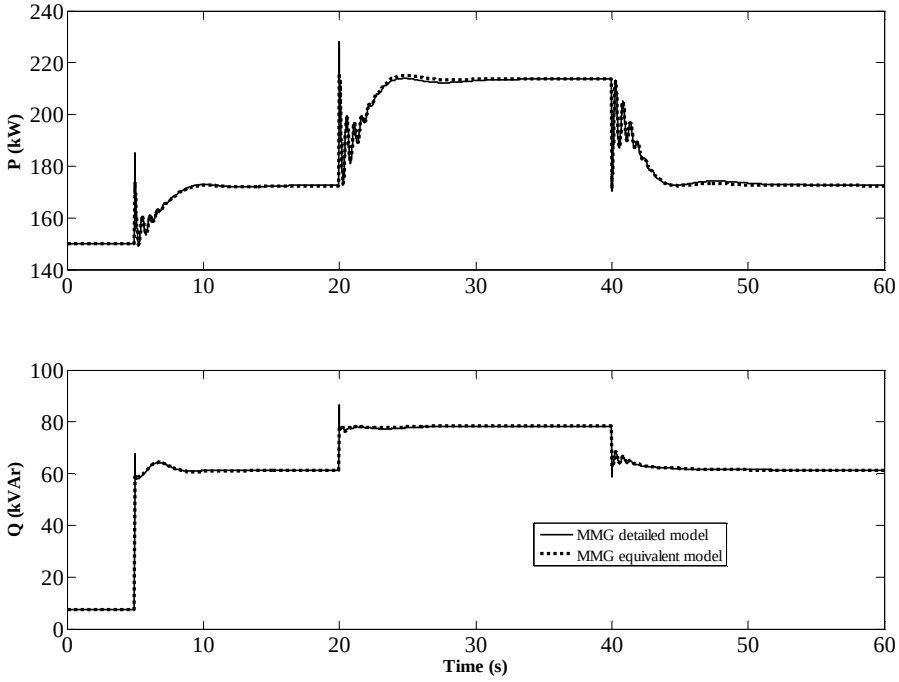

Figure 6.13: TS-01 SM2 active and reactive powers in scenario 1

It should be noted that the small loss of accuracy verified in the MG dynamic equivalent power responses does not affect significantly the accuracy of the results on the MV network, as it can be observed from figures 6.12 and 6.13, where power errors lower than $1{,}2 + j0{,}4\,kVA$ are verified for both synchronous machines.

Like in scenario 0, several simulations of connection and disconnection of different amounts of load were performed. In all of them the TDNN based MG dynamic equivalent presents a good matching with the MG detailed model during load following transients upon MMG islanding even under new operating conditions resulting from changes in the MV network steady state generation.

6.2.2.4 Scenario 2: New load conditions in MV network

The TDNN based MG dynamic equivalent performance was also evaluated under new MV network steady state load conditions. For this purpose an additional load, $L = 100 + j10\,kVA$, connected to bus 12 of TS-01 was considered. Since the MG load and generation conditions were not changed, the power flow from the MV network to the MG when the MMG is operated in interconnected mode was not significantly modified, as it can be observed from figure 6.14.

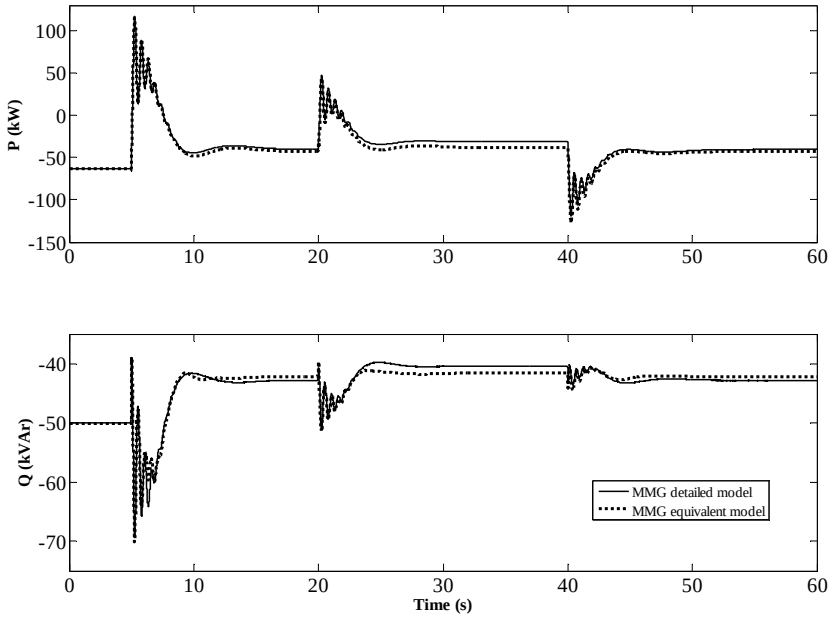

Figure 6.14: TS-01 TDNN based MG dynamic equivalent power outputs in scenario 2

Figure 6.14 shows the active and reactive power outputs of both the TDNN based MG dynamic equivalent and the MG detailed model. Although a certain loss of accuracy can be observed, the dynamic behaviour of the TDNN based dynamic equivalent is identical to the MG detailed model over the whole simulation time.

Like in scenario 1, the loss of accuracy verified in the TDNN based MG dynamic equivalent power outputs is not surprising, since both the sequence of disturbances and the steady state operating conditions are not in the training data base. In this case the experimented errors are lower than $7kW$ for active power and $0{,}6kVAr$ for reactive power. However, its effect at the MV level is reduced and the results present an acceptable level of accuracy, as can be observed from figures 6.15, 6.16 and 6.17.

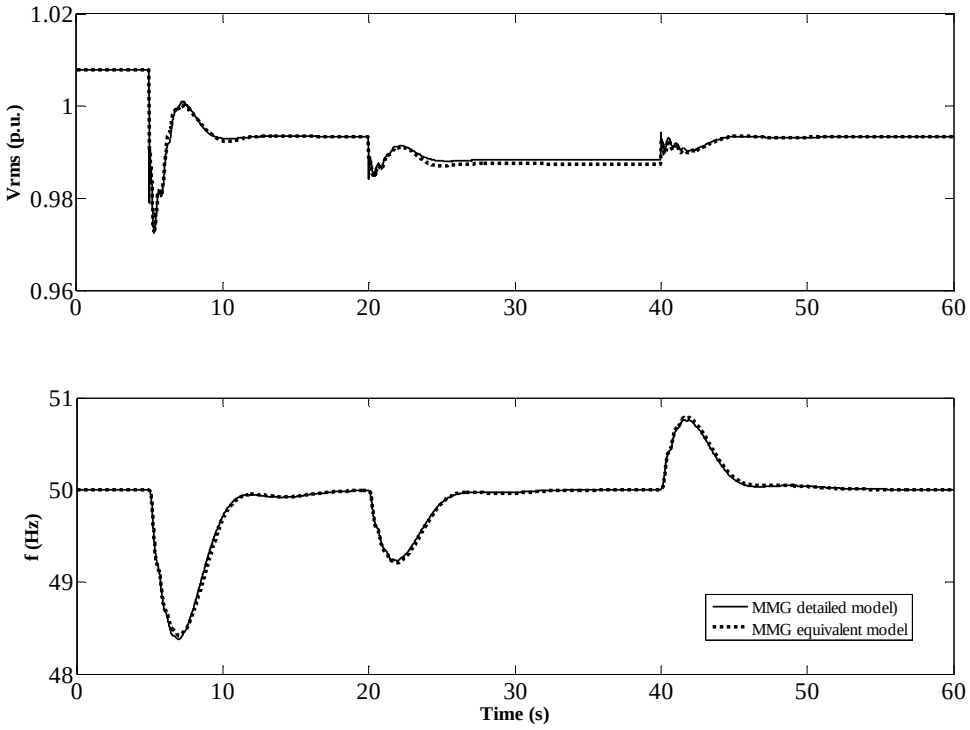

Figure 6.15: TS-01 boundary bus voltage and system frequency in scenario 2

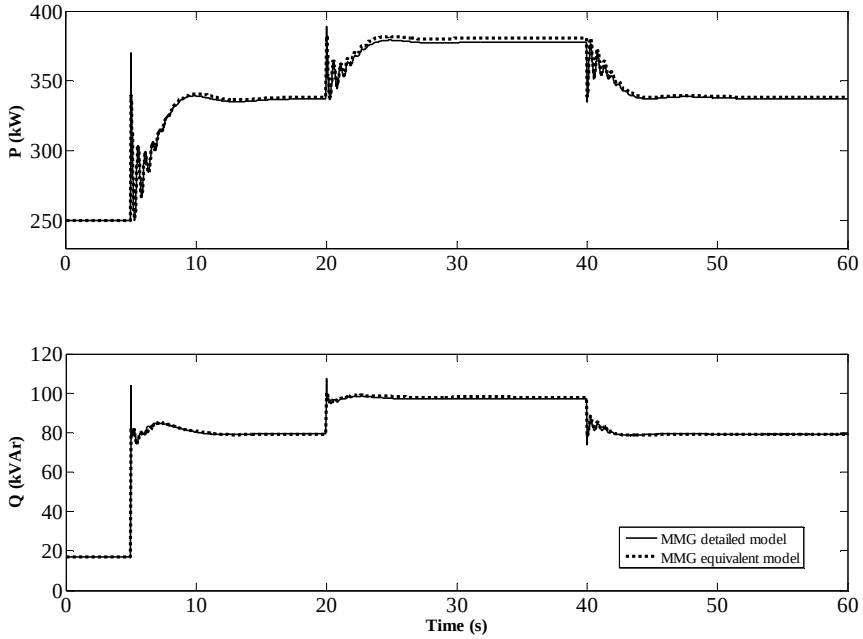

Figure 6.16: TS-01 SM1 active and reactive powers in scenario 2

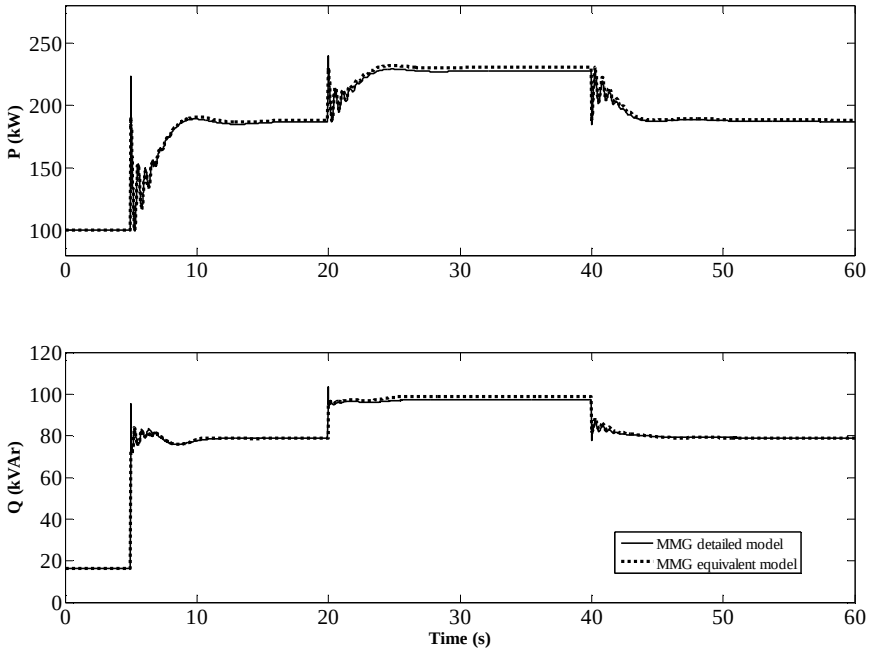

Figure 6.17: TS-01 SM2 active and reactive powers in scenario 2

Before the disconnection from the main grid, the MMG active load demand in covered only in part by the local production of both synchronous machines, SSMT and PV systems, requiring a large power import from the upstream power system, which supplies the reactive power requirements as well. Upon MMG islanding the system frequency drops to a lower value and the MG main storage device as well as the synchronous machines increase their outputs to compensate the loss of MMG import. Although with a large time delay, the SSMT active power generation also increases, as it can be observed from figure 6.14, when the active power output of the MG main storage device is around zero.

The effects of the loss of accuracy experimented by the MG dynamic equivalent based on TDNN can also be observed from figures 6.16 and 6.17. However, the maximum errors associated with the synchronous machines power responses obtained from the MMG equivalent model are lower than $3 + j1\,kVA$ for both SM1 and SM2. Therefore, the previous four figures suggest that the TDNN based MG dynamic equivalent successfully captures the MG dynamic behaviour considering the changed load steady state operating conditions in the MV network.

6.2.2.5 Scenario 3: New generating conditions in MicroGrid

Most of the conventional dynamic equivalents fail to simulate the dynamic behaviour of power systems if any change occurs inside the external subsystem, requiring the development of a new dynamic equivalent [123, 124]. In this case, the performance of the TDNN based MG dynamic equivalent is also evaluated under new power flow conditions inside the MG. For this purpose the SSMT active power generation is considerably reduced from $53{,}3\,kW$ to $20\,kW$.

Under these new operating conditions the above sequence of disturbances was simulated again. The TDNN based MG dynamic equivalent active and reactive power outputs are presented in figure 6.18, where a good agreement can be observed. Since the MG active power generation was reduced, a larger amount of active power is being imported from the MV network before MMG islanding.

The small loss of accuracy verified (the maximum deviations are less than $1{,}5\,kW$ for active power and less than $0{,}5\,kW$ for reactive power) is acceptable, since its effect on the boundary bus and studied subsystem is quite reduced, as can be observed from figures 6.19, 6.20 and 6.21.

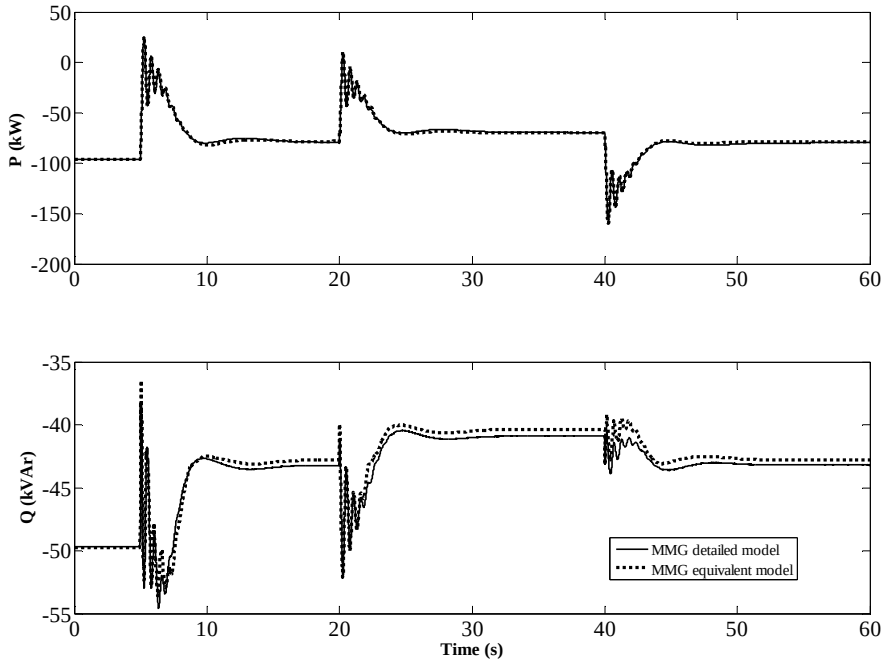

Figure 6.18: TS-01 TDNN based MG dynamic equivalent active and reactive power outputs in scenario 3

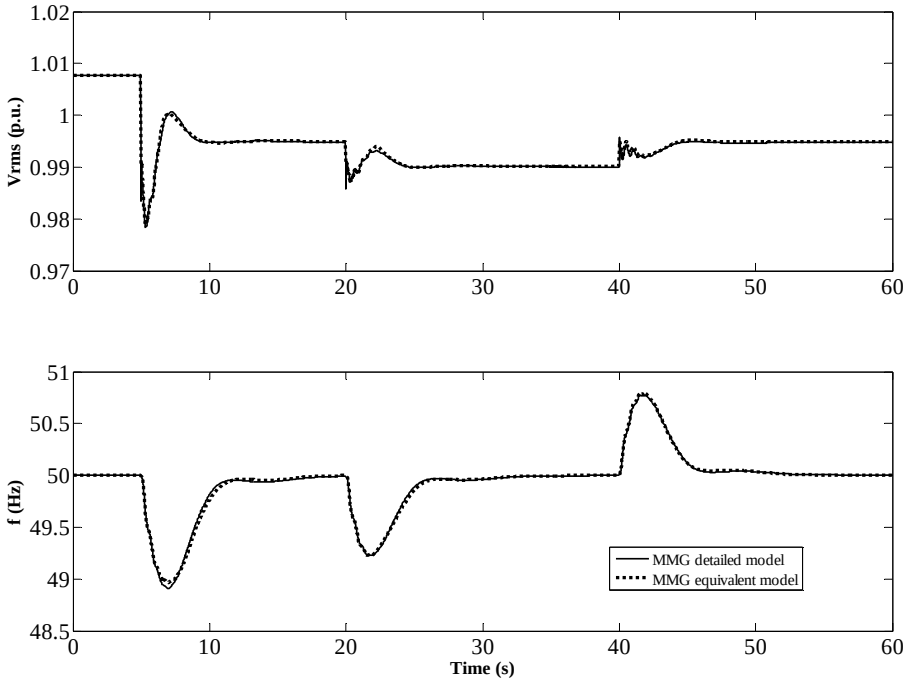

Figure 6.19: TS-01 boundary bus voltage and system frequency in scenario 3

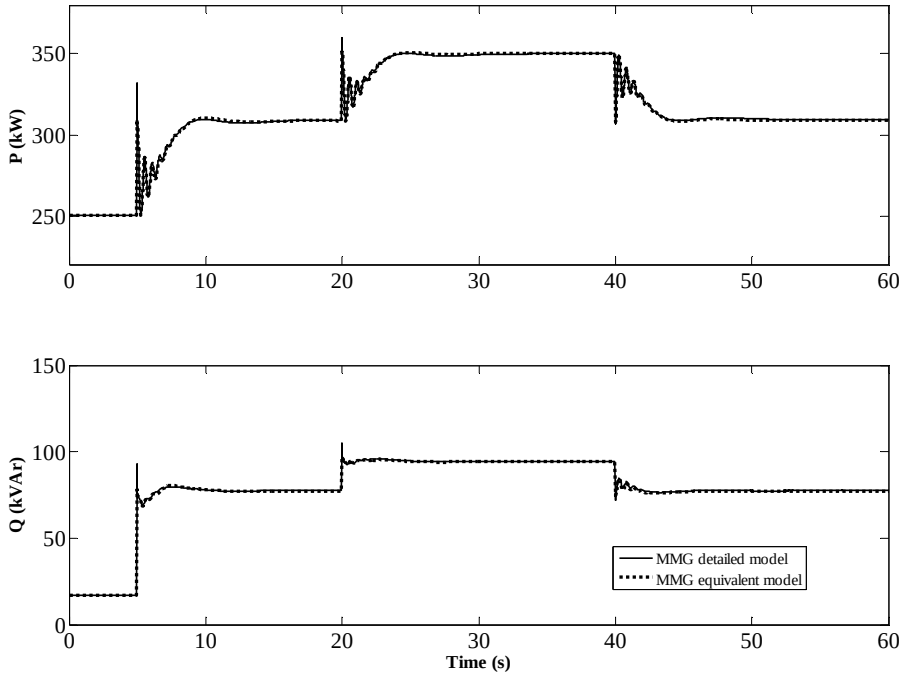

Figure 6.20: TS-01 SM1 active and reactive power outputs in scenario 3

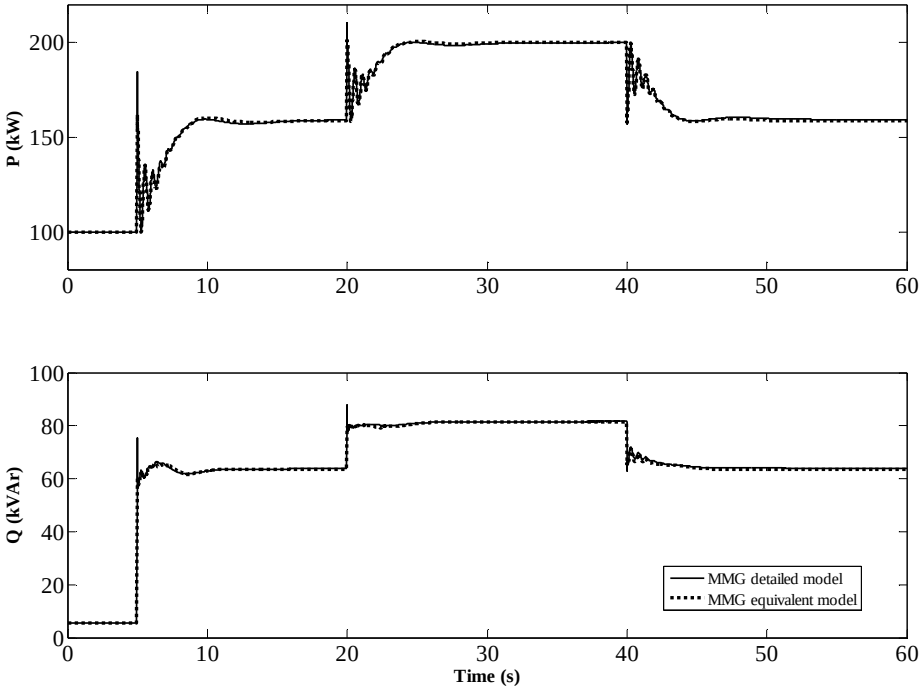

Figure 6.21: TS-01 SM2 active and reactive power outputs in scenario 3

In fact, figures 6.19, 6.20 and 6.21 show that the TDNN based MG dynamic equivalent reproduces with high accuracy the MG dynamic behaviour with respect to the studied subsystem following the study sequence of disturbances.

Several amounts of load connection and disconnection were simulated under this steady state operating scenario and similar performances were observed, even when different SSMT active power production levels were considered. Therefore, the TDNN based MG dynamic equivalent effectiveness can also be extended to different generating conditions inside the MG.

6.2.2.6 Scenario 4: New load conditions in MicroGrid

In this case, the performance of the TDNN based MG dynamic equivalent is also evaluated under new power flow load conditions inside the MG. For this purpose the load $L11 = 38{,}6 + j15{,}3\,kVA$ was disconnected from bus 27 of TS-01. Under these steady state operating conditions the above sequence of actions is simulated again and the comparison between the MG dynamic equivalent and the MG detailed model power responses is presented in figure 6.22.

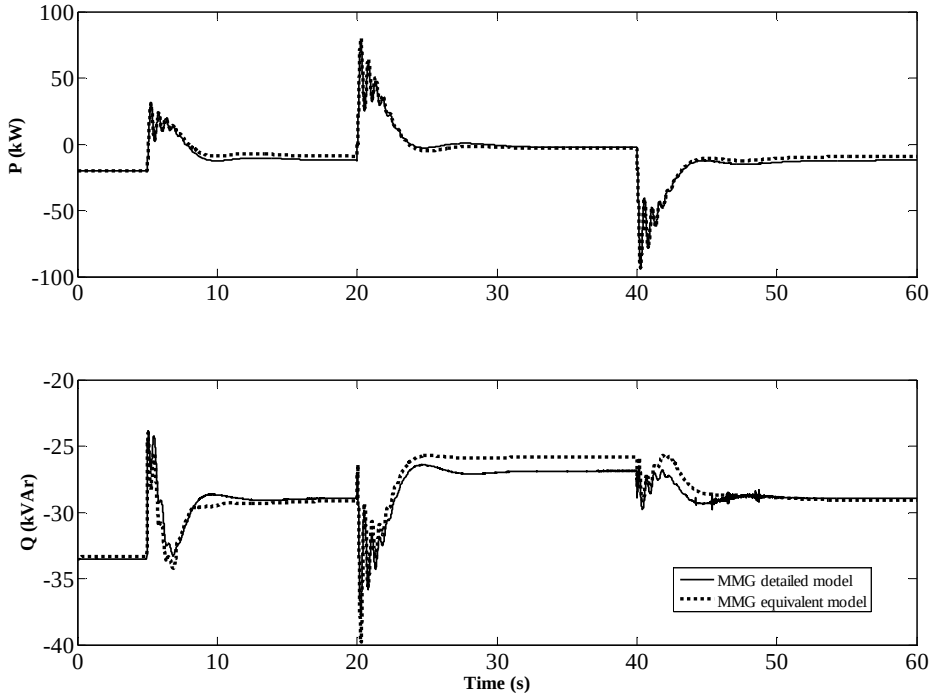

Figure 6.22: TS-01 TDNN based MG dynamic equivalent power outputs in scenario 4

As the active and reactive power consumptions into the MG were reduced, the local power unbalance was also reduced and therefore a less amount of both active and reactive power is being imported from the network when the MMG is operated in interconnected mode, as it can be observed from figure 6.22. Since the MMG power unbalance was also reduced, the system frequency deviation from its nominal value following MMG islanding is smaller than this one verified in scenario 0, as presented in figure 6.23. Therefore a smaller active power injection from the MG main storage device was experimented, as it can be observed from figure 6.22.

Figure 6.22 displays a small loss of accuracy, being the errors experimented lower than $3+j1kVA$. However, the effect of this small loss of accuracy in the study system is diminished as it can be observed from figures 6.23, 6.24 and 6.25.

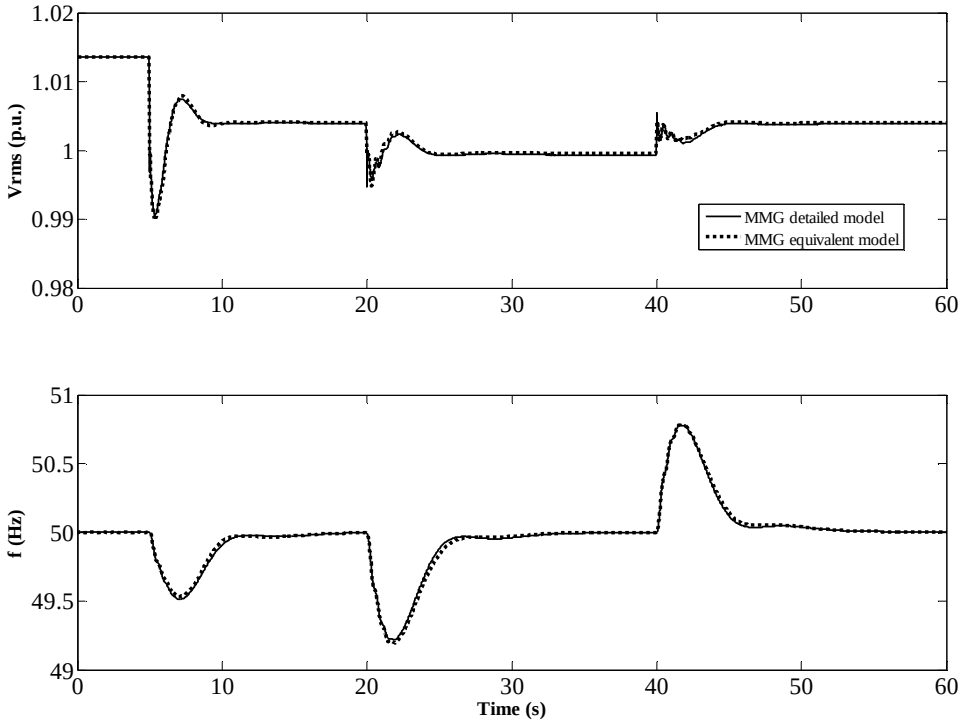

Figure 6.23: TS-01 TDNN boundary bus voltage and system frequency in scenario 4

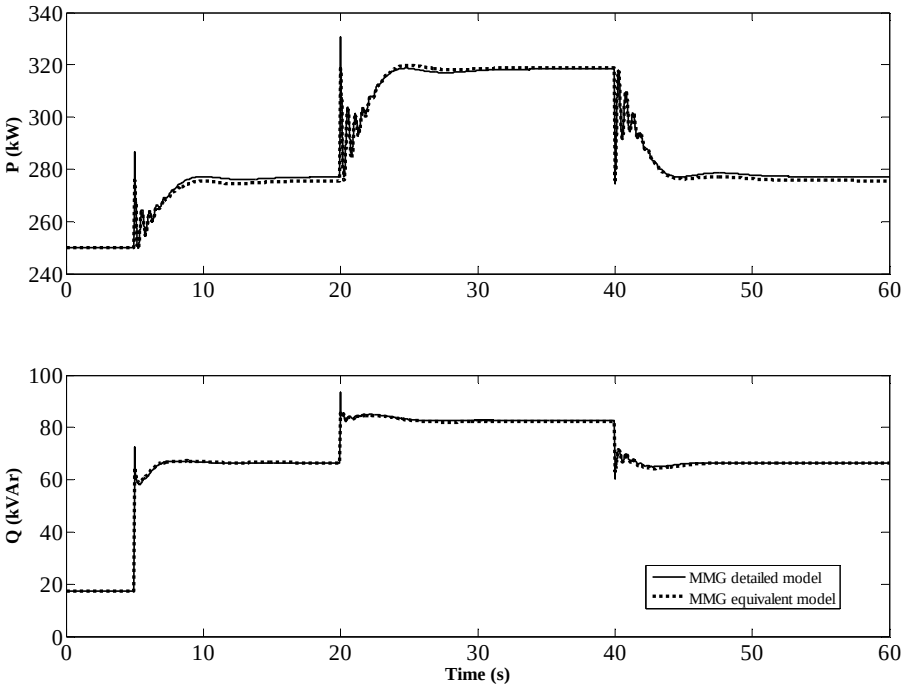

Figure 6.24: TS-01 SM1 active and reactive powers in scenario 4

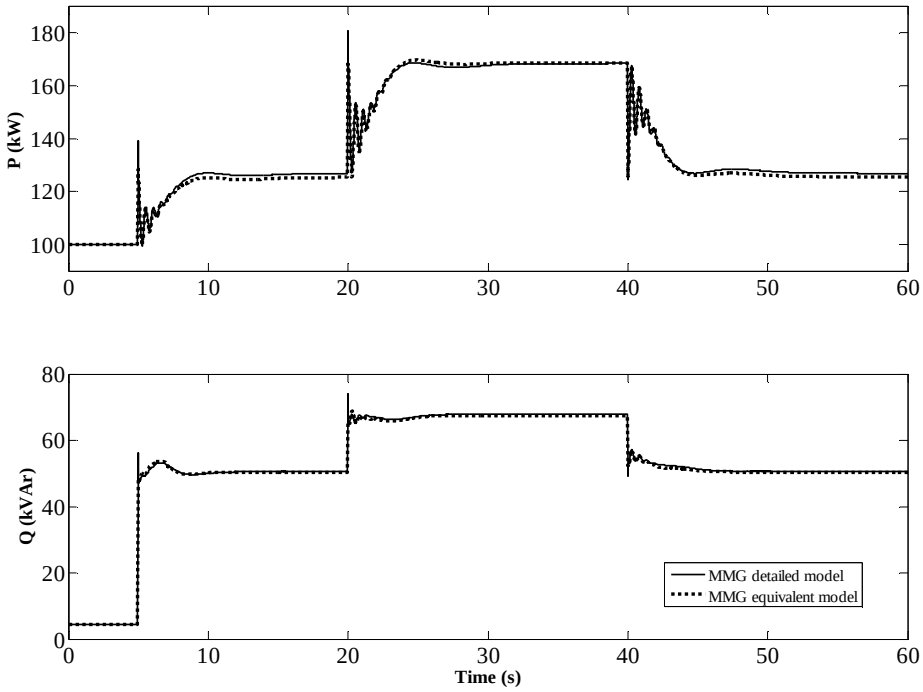

Figure 6.25: TS-01 SM2 active and reactive powers in scenario 4

The maximum errors observed from figures 6.24 and 6.25 are around $1{,}5 + j0{,}6\,kVA$ for both synchronous machines. Thus, the MG dynamic equivalent based on TDNN reproduces the MG dynamic behaviour with high accuracy following the simulated sequence of disturbances.

Several simulations of different amounts of load connection and disconnection were carried out under different MG steady state load conditions before MMG islanding and the MMG equivalent model responses are kept in a good agreement with these ones obtained using the MMG detailed model. Therefore, the TDNN based MG dynamic equivalent can also be used to replace the MG, even when its steady state load condition are changed.

6.2.2.7 Some remarks of TDNN based MG dynamic equivalents

The TDNN based MG dynamic equivalent thus obtained was implemented on the dynamic simulation package corresponding to the MMG equivalent model and its capability to reproduce the MG dynamic behaviour was investigated. The effectiveness of the TDNN based MG dynamic equivalent was demonstrated using the MG of TS-01. The results obtained allow to conclude that the TDNN based MG dynamic equivalent provided a very good matching with the results obtained using the MG detailed model over the whole simulation time, requiring simulation results or measurements only at the boundary bus.

Several initial steady state load and generation conditions in both the MV network and inside the MG, before MMG islanding, were considered and a good performance was observed without modifications in the structure or parameters of the MLP neural network. The use of normalized deviations from the initial steady state values of both TDNN inputs and outputs extends the neural network generalization capability to simulate sequences of disturbances under steady state operating conditions not used to extract training patterns. Moreover the total simulation time of the studied sequence of disturbances is around 90 times faster with the MMG equivalent model than with the MMG detailed model.

Under this context the TDNN seems to be an excellent tool to derive dynamic equivalents for MicroGrids. However, although the features presented before have been ambitious regarding the application of classical methodologies to conventional power systems, the following weaknesses have to be pointed out concerning MG dynamic equivalents.

- High computational effort. To derive a TDNN based dynamic equivalent involves the following main stages: **1)** Generation of very large data sets; **2)** Pre-processing data; **3)**

Training many MLP neural networks with different internal architectures in order to select the best ones in the sense of the MSE criterion verified for the validation data set; **4)** Integration of a number of MLP neural networks into the dynamic simulation package corresponding to the MMG equivalent model for final validation purposes.

All these stages are very time consuming tasks.

- High loss of accuracy when the TDNN is used to replace a new MG. To obtain a TDNN based MG dynamic equivalent with an acceptable performance requires a new MLP neural network, which has to be trained with a data set generated using the new MG.

In order to overcome these drawbacks an alternative methodology exploiting the available physical knowledge has been developed, as described in the following section.

6.3 MG dynamic equivalents based on the physical model approach

The physical modeling approach described in section 5.4 is used in this section to derive a dynamic equivalent for the MG of the test system presented in figure 6.26 (a), denoted as TS-02.

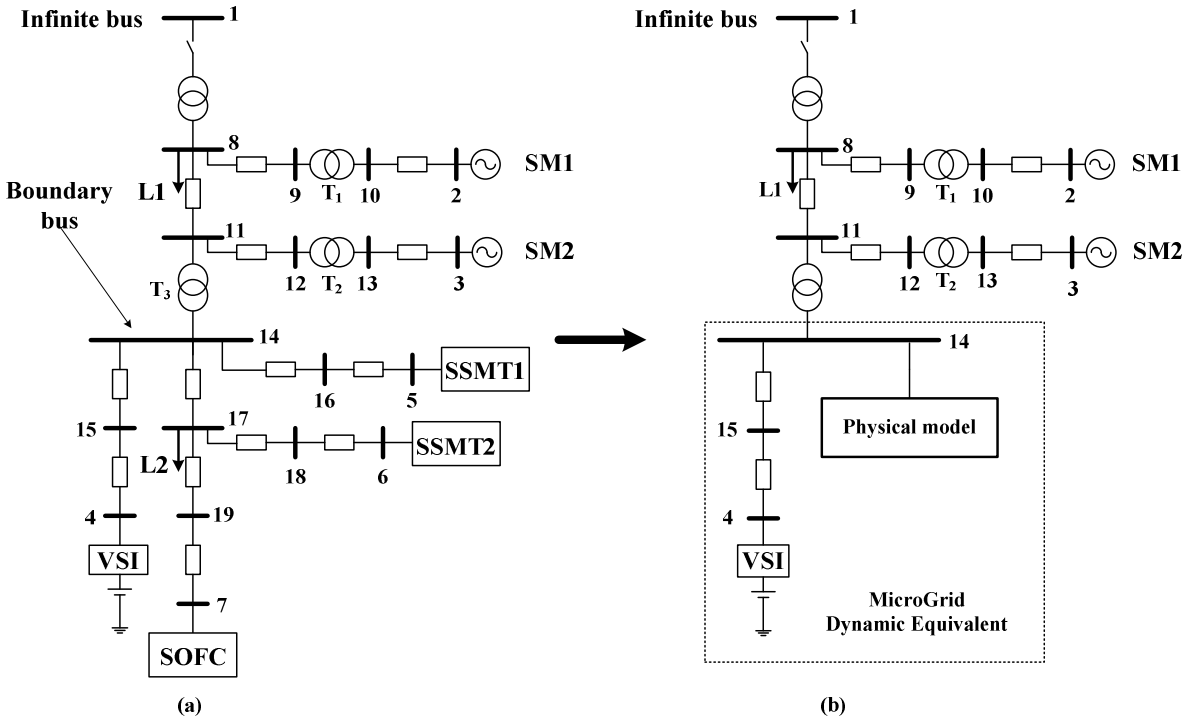

Figure 6.26: Single-line diagram of TS-02: (a) MMG detailed model; (b) MMG equivalent model.

The MMG system presented in figure 6.26 (a) comprises two round rotor synchronous machines of $500\,kVA$ connected to the MV network together with MV loads and to a MV/LV distribution transformer – the MicroGrid. This MG comprises two 30 kW SSMT, a 30 kW SOFC and the main storage device (flywheel). The amount of load connected to the LV network is $50 + j10\,kVA$ and the load connected to the MV level is $500 + j100\,kVA$. A more detailed description of the electrical and mechanical parameters of the several components of this test system is presented in appendix A.

The physical model to be obtained replaces the MG slow dynamics subsystem, as depicted in figure 6.26 (b). Like in the TDNN based approach, the MG dynamic equivalent comprises this model operating in parallel with the MG main storage device feeder.

6.3.1 Development of physical MG dynamic equivalents

In this approach, like in the first one, the MG slow dynamics equivalent model to be derived represents a current source directly connected to the boundary bus. The injected current is predicted from the model structure described in subsection 5.4.1 of chapter 5 through a suitable set of values for the parameter vector given by (5.23). As already mentioned previously, in subsection 5.4.2 of chapter 5, the parameter estimation procedure of the physical model structure described in subsection 5.4.1 is performed online. For this purpose, the physical model structure is integrated into the dynamic simulation package corresponding to the MMG equivalent model and its parameter values are adjusted using the algorithm schematically represented through the flow chart depicted in figure 5.13 of chapter 5.

In order to build an informative enough data set, only the following sequence of disturbances occurring at the MV level of test system TS-02, presented through its single line diagram in figure 6.26, is simulated using, obviously, the MMG detailed model simulation package:

- MMG islanding at $t = 2\,s$;
- Connection of the amount of load $100 + j25\,kVA$ at bus 8 of TS-02 at $t = 20\,s$;
- Disconnection of the amount of load previously connected at $t = 40\,s$.

The simulation of this sequence of disturbances is carried out over $60\,s$, since those timings are sufficient to restore the steady state conditions following MMG islanding and

sudden load connection and disconnection as well. A variable step size solver *ode15s* available in *Simulink* is used with a relative tolerance of 1×10^{-6}.

It was assumed that the reactive power generated by SSMT1, SSMT2 and SOFC corresponds to the reactive power set-points, defined centrally by the MGCC and received by their MC, which are kept constant during the simulation time. Thus, the value of Q_{ref} in figure 5.10 of chapter 5 matches the initial reactive power flow from the MG slow dynamics subsystem, which is determined through the initial load flow calculations. For a given active power produced by the physical model structure depicted in figure 5.9 of chapter 5, the $D-Q$ components of the injected current are determined based on the boundary bus voltage, as it can be observed from figure 5.12 of chapter 5.

Then, for a known and fixed value of Q_{ref}, to estimate the model parameters that fit the MG slow dynamics subsystem injected current is equivalent to estimate the model parameters that fit its active power output. Therefore the target output is done by the MG slow dynamics subsystem active power output and, therefore, the corresponding equivalent model simplifies to a MISO model.

The data set thus obtained is stored in a *file.mat*, without pre-processing, in order to be used directly in the MMG equivalent model as the target output for parameter estimation purposes, as it can be observed from figure 5.13 of chapter 5.

In order to find suitable parameters for the physical MG slow dynamics equivalent model, the EPSO algorithm with 20 particles, replication factor $r=1$ (each parent gives birth to one descendant) and Gaussian mutation with learning rate $\tau=0{,}5$ was used. For the MEE criterion a Gaussian Parzen window with fixed size, $\sigma=0.0001$, was adopted. The stopping criterion involves 10 consecutive generations without finding a better global fitness.

After finding the parameter vector, which provides the best performance in the sense of the MEE, the average value of the error PDF has to be added to the active power output, P_m, of the physical model structure depicted in figure 5.9 of chapter 5 and the physical MG slow dynamics equivalent model performance is evaluated by comparing the time domain responses obtained from the MMG equivalent model with those ones obtained from the MMG detailed model, as presented in the following subsections.

6.3.2 TS-02 simulation results and discussion

For parameter estimation purposes it was assumed that the MMG is initially interconnected with the upstream power system and operated under the steady state conditions presented in table 6.3.

Table 6.3: TS-02 operating conditions before MMG islanding

		Generation	Consumption
MV network	SM1	$250\ kW$	
	SM2	$200\ kW$	
	Total	$450\ kW$	$500 + j100\ kVA$
MicroGrid	Storage device	$5\ kVAr$	
	SSMT1	$20 + j2\ kVA$	
	SSMT2	$15 + j2\ kVA$	
	SOFC	$10 + j2\ kVA$	
	Total	$45 + j6\ kVA$	$50 + j10\ kVA$

In order to evaluate the performance of the physical MG dynamic equivalent a new sequence of disturbances occurring at the MV level was simulated under the steady state operating conditions presented in table 6.3, as well as under different operating conditions. Thus, the following scenarios were considered:

- **Scenario 0:** Initial MMG operating conditions presented in table 6.3;
- **Scenario 1:** New generation and load conditions in MV network;
- **Scenario 2:** New generation conditions in MG;
- **Scenario 3:** New MG composition and new MG load conditions.

Under each one of the above scenarios corresponding to different steady state operating conditions before MMG islanding, the following sequence of disturbances was simulated:

- MMG islanding at $t = 2\ s$;

- Connection of an amount of load, $60 + j15\,kVA$, not used during parameter estimation to bus 8 of TS-02, represented through its single-line diagram in figure 6.26 (a), at $t = 20\,s$;
- Disconnection of the amount of load previously connected at $t = 40\,s$.

Firstly, a general overview of the active and reactive power produced by the several MS is presented. Afterwards the results obtained from the dynamic simulations concerning the physical MG dynamic equivalent and the MG detailed model are compared and discussed.

6.3.2.1 Dynamic behaviour of microgeneration systems of TS-02

Figure 6.27 plots the active and reactive power outputs of all the microgeneration systems of TS-02 following the above mentioned sequence of disturbances. In addition it displays the fast and slow dynamics that characterize the microgeneration system responses.

Before MMG islanding the MS active and reactive production levels are according to the steady state conditions presented in table 6.3. The MMG is importing a certain amount of power from the upstream system in order to balance the local power demand and supply.

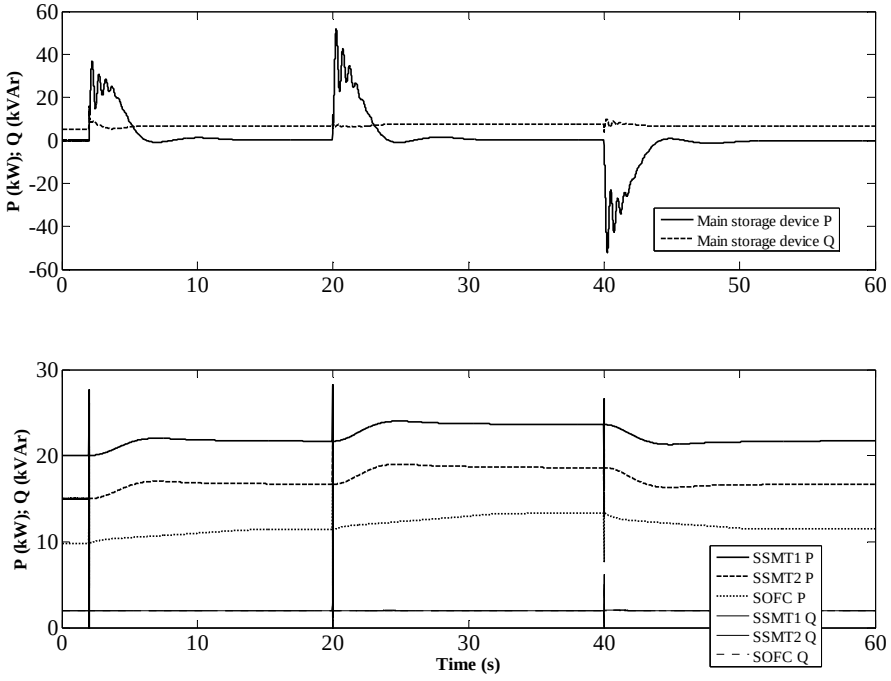

Figure 6.27: TS-02 active and reactive powers generated by microgeneration systems

Following MMG islanding, the MG main storage device acts as a primary load frequency control, through its VSI control, in an attempt to balance active power demand and supply due to the loss of MMG imported power. Similar responses can be observed during transient situations following sudden load connection and disconnection. After the system frequency is restored to its nominal value, the main storage device active power output is kept around zero, as it can be observed from figure 6.27. The microturbines and SOFC vary their active power outputs according to the secondary load frequency control scheme implemented in their PQ inverter controls. However, the SOFC presents a very slow response regarding its active power output. The increasing/decreasing of SOFC active power output to the set-points derived from system frequency error involves timings around tens of seconds.

Concerning the reactive power outputs, the controllable microsources with PQ inverter controls are supplying a constant reactive power according to its pre-specified reference defined centrally by the MGCC. The reactive power produced by the MG main storage device upon MMG islanding is proportional to the terminal bus voltage variations arising from MMG islanding and load following situations, as depicted in figure 6.27.

6.3.2.2 Scenario 0: Initial steady state operating conditions

Figure 6.28 shows a comparison between the active and reactive power outputs of the physical MG slow dynamics equivalent model. As it can be observed, a notable degree of accuracy of the predicted active power output is obtained following a non-trained amount of load connection and disconnection. Concerning the reactive power output, since Q_{ref} was kept constant over the whole simulation time, a small error is displayed upon MMG islanding. However this error does not affect considerably the accuracy of results with impact at the MV network, as it can be observed from figure 6.28, since the physical MG dynamic equivalent power outputs experiment errors around $0{,}04 + j0{,}06\,kVA$.

Before MMG islanding the MG is importing a small amount of active power to balance its own demand and supply, as the negative sign corresponding to the active power output in figure 6.29 indicates. In contrast, the reactive power produced into the MG is not fully absorbed from both the MG own load and losses, being the exceeding exported to the MV network.

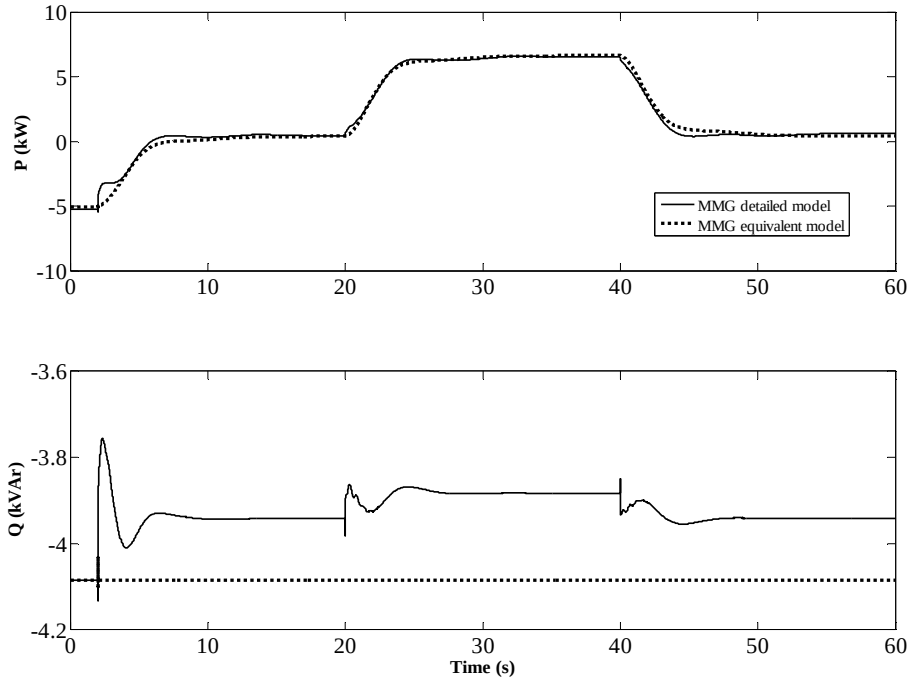

Figure 6.28: TS-02 physical MG slow dynamics equivalent model power outputs in scenario 0

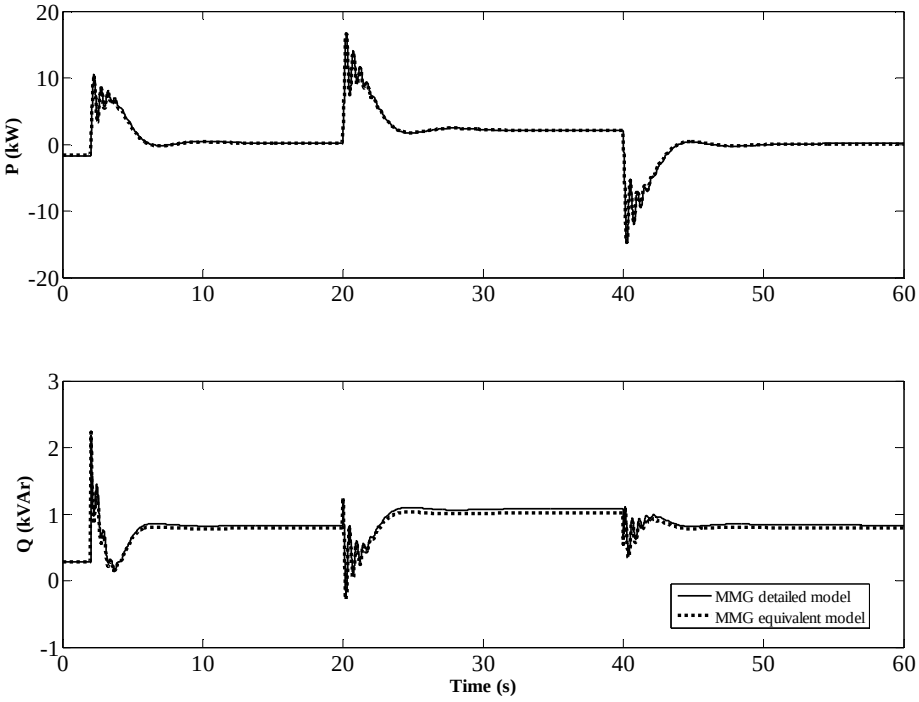

Figure 6.29: TS-02 physical MG dynamic equivalent active and reactive power outputs in scenario 0

Following MMG islanding transients the whole power system is balanced in a new steady state operating point in which the MG active and reactive power productions are increased as a result of the controllable microsources secondary load frequency control and the voltage/reactive power droop of the main storage device VSI control. In this situation the active power generated equals the MG demand and losses, so that the MG active power output is around zero. After load connection the MG exports a small amount of active power and increases the reactive power output. These active and reactive power variations are accomplished by boundary bus voltage variations and frequency deviations from its nominal value, as illustrated in figure 6.30. It should be noted that the physical MG dynamic equivalent reproduces with a high degree of accuracy the boundary bus voltage and system frequency behaviour.

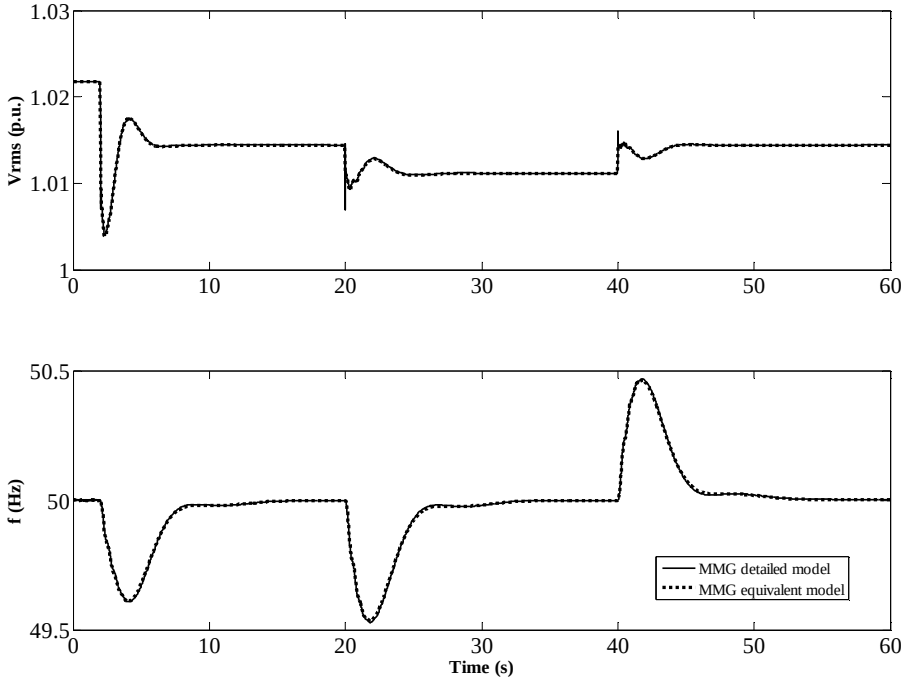

Figure 6.30: TS-02 boundary bus voltage and system frequency in scenario 0

A good response matching can also be observed from figures 6.31 and 6.32, regarding the synchronous machines output active and reactive powers. In fact, considering constant the reactive power output of the MG slow dynamics equivalent model over the whole simulation time does not degrade the quality of results.

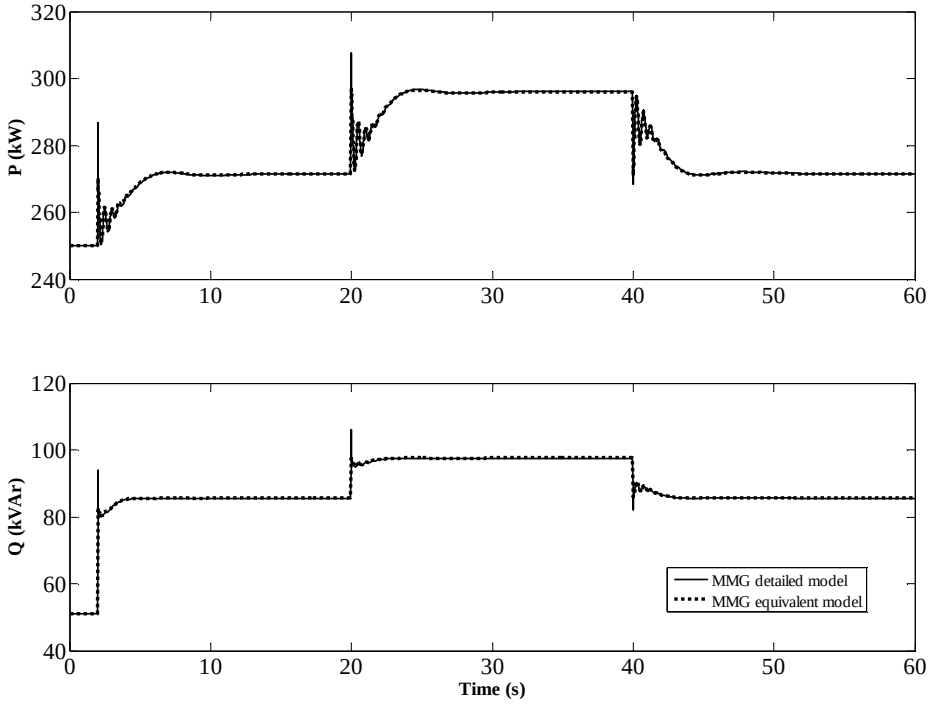

Figure 6.31: TS-02 SM1 active and reactive powers in scenario 0

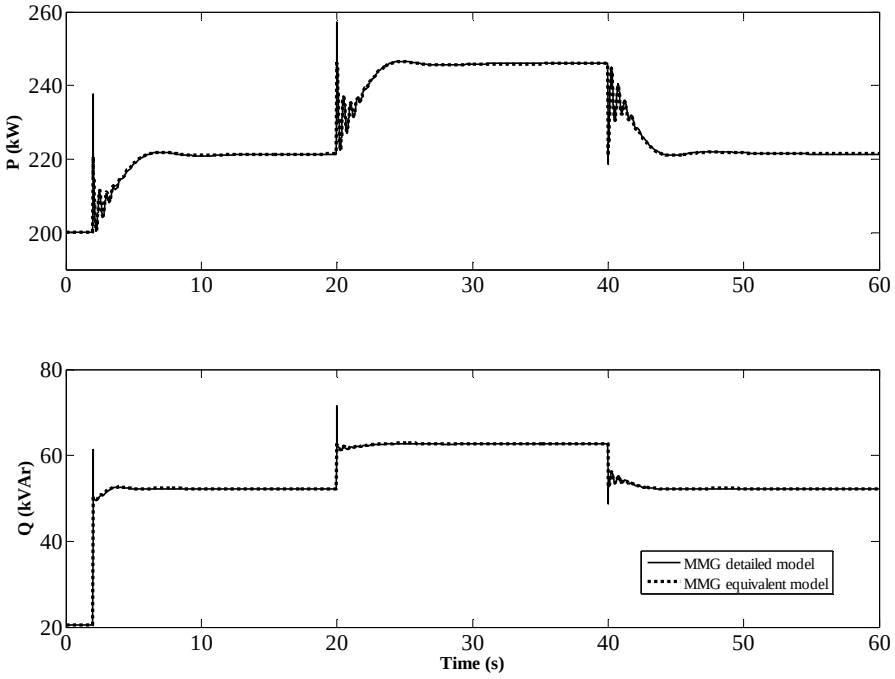

Figure 6.32: TS-02 SM2 active and reactive powers in scenario 0

Similar performances can also be observed for different amounts of load connection and disconnection, demonstrating the MG dynamic equivalent effectiveness under different load following conditions. Thus, it can be concluded that the physical MG dynamic equivalent thus obtained presents a good performance, concerning the MG dynamic behaviour with respect to the study subsystem under transient and steady state conditions.

6.3.2.3 Scenario 1: New generation and load conditions at MV network

The physical MG dynamic equivalent performance was also evaluated under different steady state operating conditions before MMG islanding. Then the active power produced by SM2 was increased from $200\,kW$ to $300\,kW$ and a new load, $L = 200 + j40\,kVA$, was connected to bus 5 of the TS-02. Under these new steady state operating conditions before MMG islanding, the above sequence of actions was simulated again and the results obtained are presented. Figure 6.33 plots the physical MG dynamic equivalent power outputs.

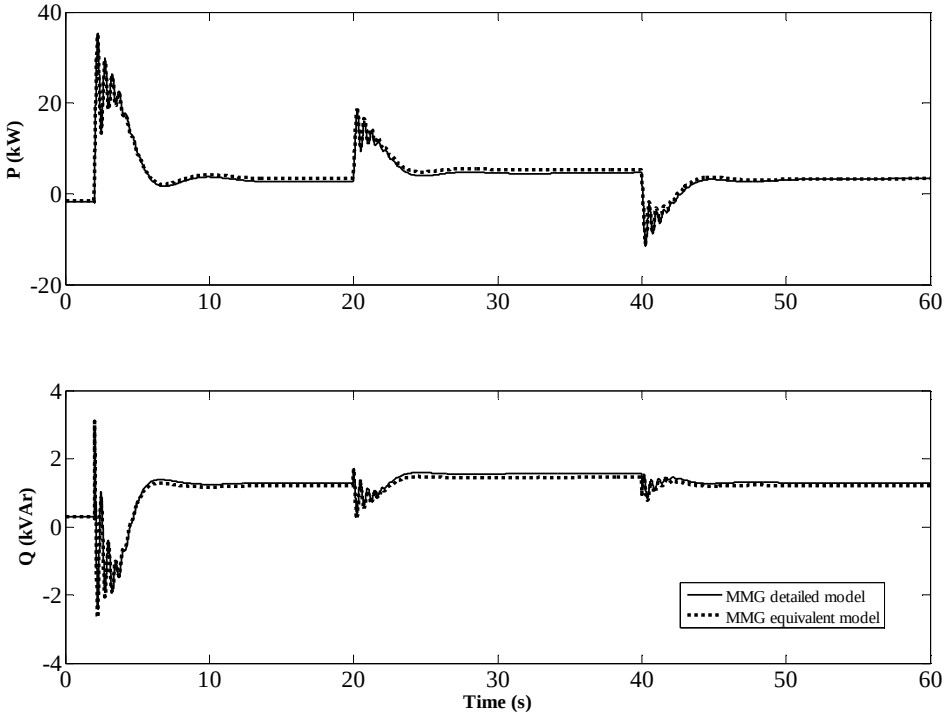

Figure 6.33: TS-02 physical MG dynamic equivalent power outputs in scenario 1

Taking into account the previous scenario, a small loss of accuracy regarding the active power response can be observed from figure 6.33. The maximum error is experimented after transients and is lower than $1\,kW$. Concerning the reactive power output, basically the same performance was achieved. However, the effect of the physical MG dynamic equivalent response deviations from the responses of the MG detailed model with respect to the study subsystem is very small, as can be observed from figures 6.34, 6.35 and 6.36.

The small loss of accuracy observed from figures 6.35 and 6.36 concerning the synchronous machines active power corresponds to a maximum error lower than $1{,}5\,kW$. Therefore figures from 6.34 to 6.36 suggested that the physical MG dynamic equivalent reproduces very well the dynamic behaviour of the MG with respect to the MV network.

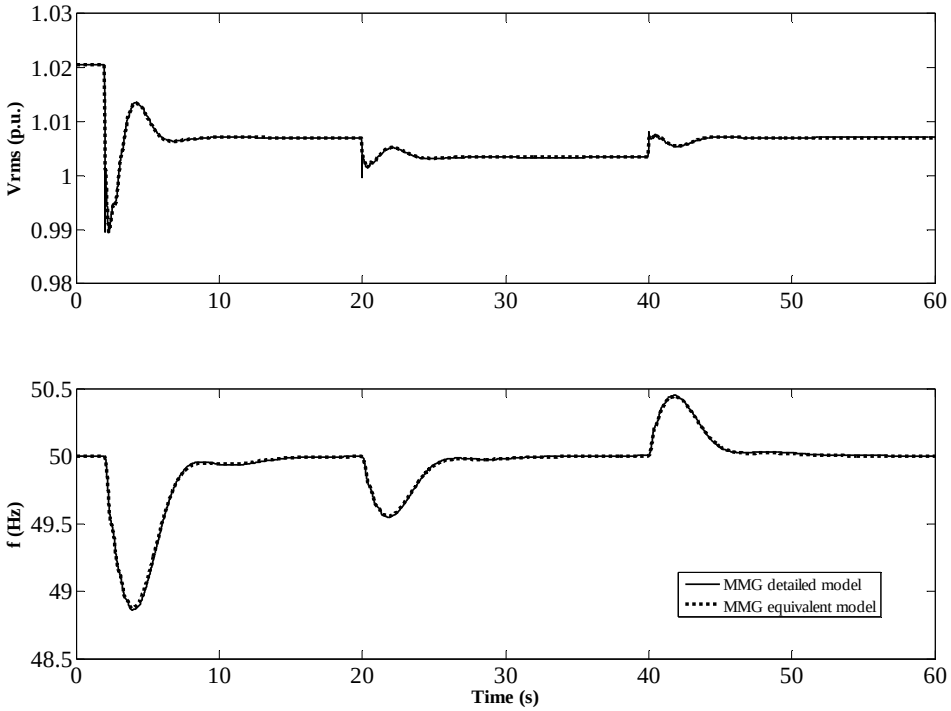

Figure 6.34: TS-02 boundary bus voltage and system frequency in scenario 1

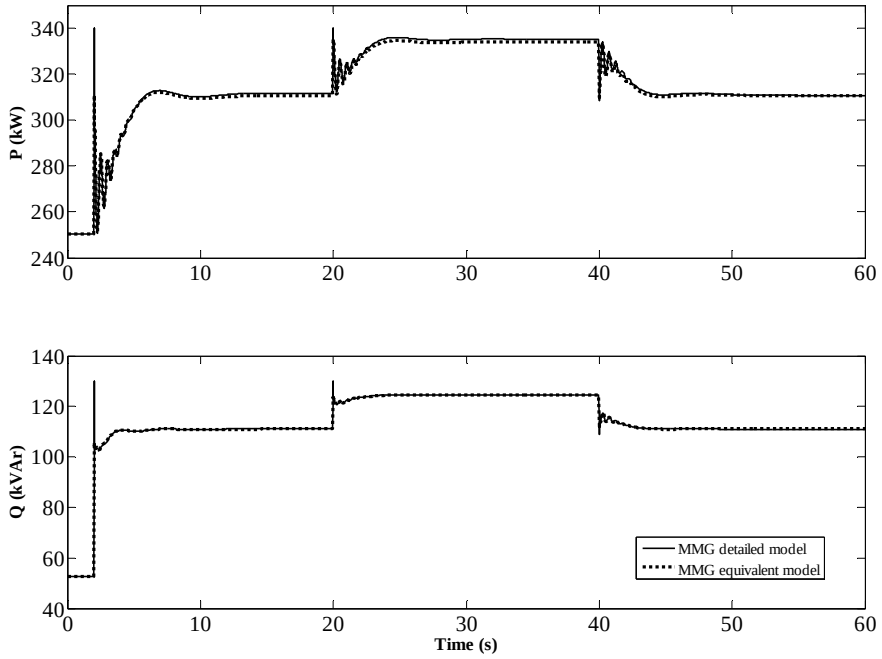

Figure 6.35: TS-02 SM1 active and reactive powers in scenario 1

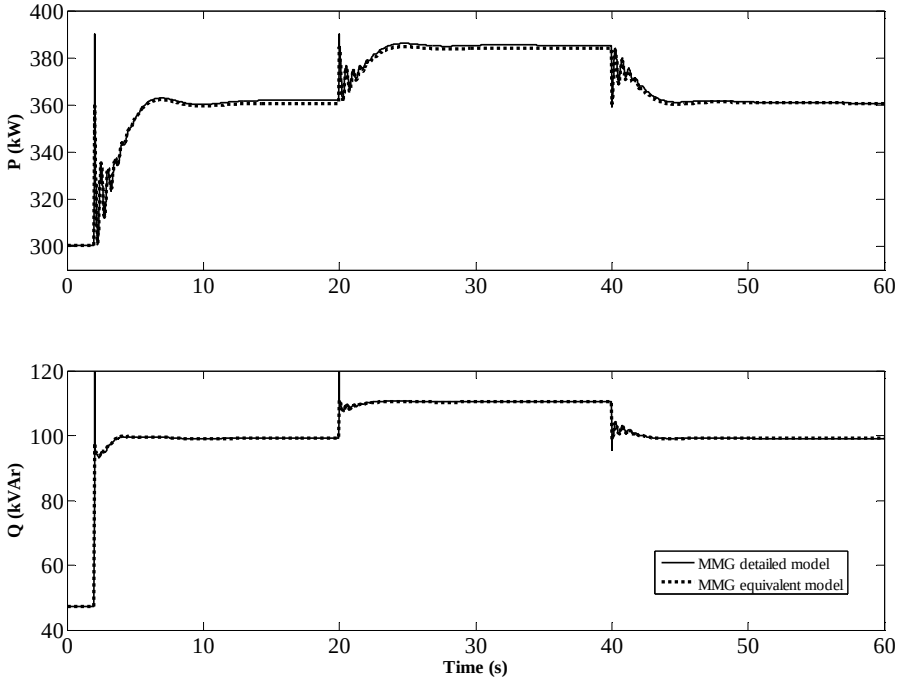

Figure 6.36: TS-02 SM2 active and reactive powers in scenario 1

Similar performances can also be observed following different amounts of load connections and disconnections under these steady state operating conditions, demonstrating the physical MG dynamic equivalent ability to represent the MG relevant dynamics with respect to the MV network when the MV steady state operating conditions are changed, considering in simultaneous new load and generation.

6.3.2.4 Scenario 2: New generation conditions inside the MG

Now the performance of the MG dynamic equivalent is assessed under new power flow conditions inside the MG, resulting from a different generation scenario before MMG islanding. For this purpose the active powers of SSMT1, SSMT2 and SOFC were increased for $20\,kW$ and the above sequence of actions was simulated again.

Under these new initial steady state operating conditions the MG is exporting both active and reactive power before MMG islanding, as it can be observed from the positive sign in figure 6.37.

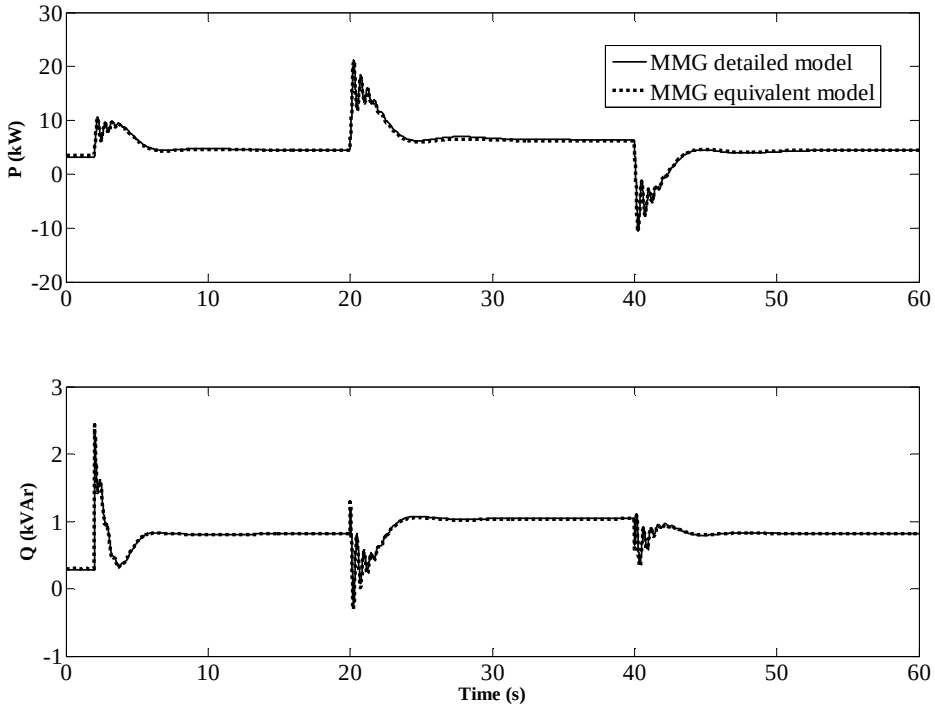

Figure 6.37: TS-02 physical MG dynamic equivalent active and reactive power in scenario 2

As the active power generation was increased and the load was kept constant, the MMG own generation and demand are nearly balanced being the MMG importing a small amount of active power. Therefore a small system frequency deviation from its nominal value was experimented following MMG islanding leading with a small power injection from the MG main storage device. After system frequency restoration the VSI active power output is kept near zero. Sudden load connection and disconnection leads with larger frequency deviations and therefore with larger amounts of active power injected or absorbed by the VSI of MG main storage device, as it can be observed from figures 6.37 and 6.38.

Concerning to the reactive power, as the controllable microgeneration systems outputs are kept constant the MG main storage device is responsible for the reactive power variations based on its voltage/reactive power output.

Figure 6.37 shows a good matching between the MG dynamic equivalent response and this one obtained from the MG detailed model, under these new MG generation conditions, being the errors experimented lower than $0{,}4 + j0{,}06\,kVA$. Thus, the MG dynamic behaviour reproduced by the physical MG dynamic equivalent is in good agreement with this one of the MG detailed model, as it can also be observed from figures 6.38, 6.39 and 6.40.

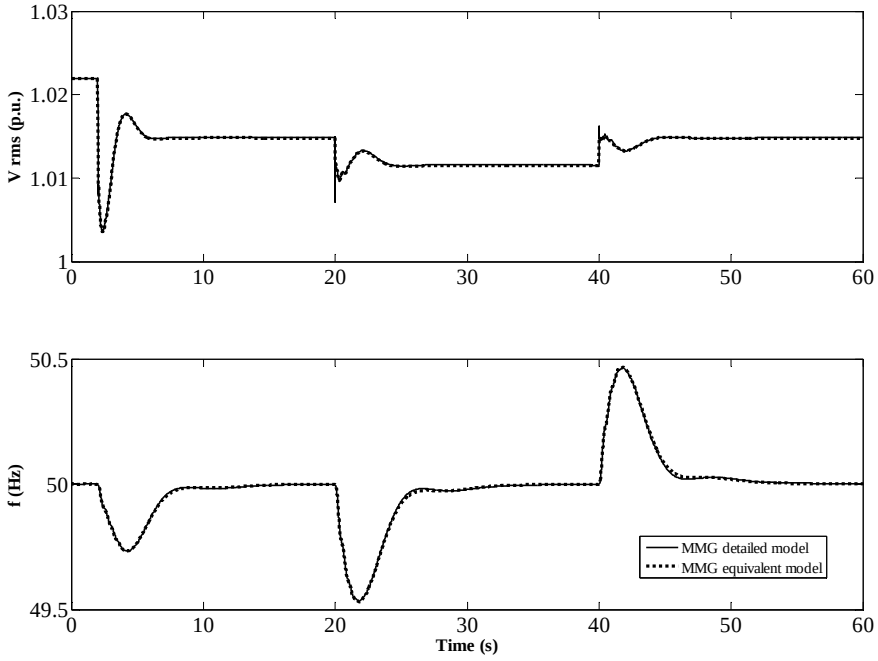

Figure 6.38: TS-02 boundary bus voltage and system frequency in scenario 2

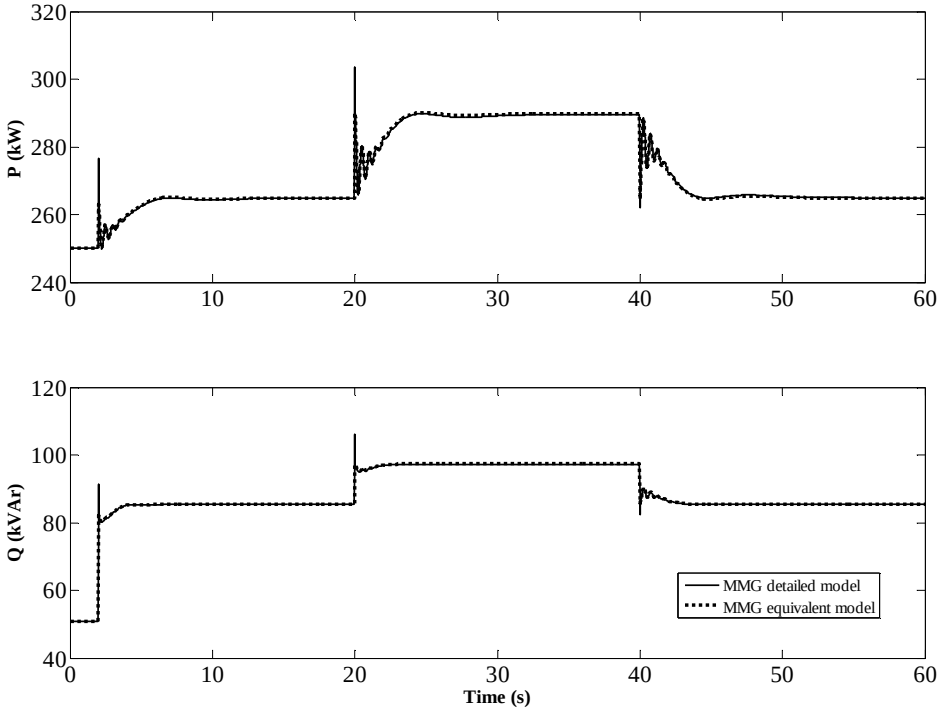

Figure 6.39: TS-02 SM1 active and reactive powers in scenario 2

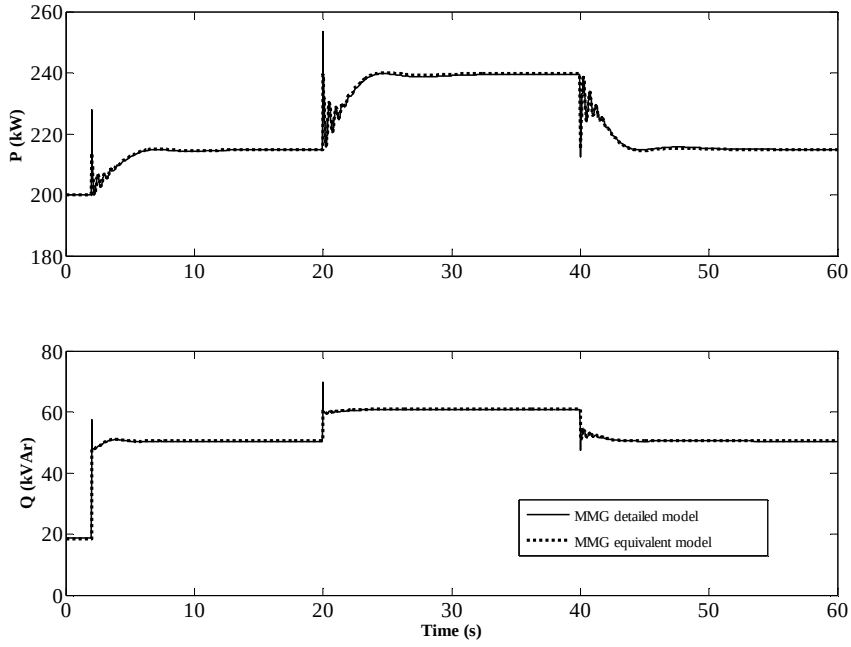

Figure 6.40: TS-02 SM2 active and reactive powers in scenario 2

Similar performances can also be observed when different amounts of load are connected and disconnected in different locations of MV network. This stresses the good performance of the MG dynamic equivalent under new initial steady state generating conditions into the MG. This is an important feature, since any equivalent model should be flexible enough to consider potential variations in the power supplied for microgeneration systems.

6.3.2.5 Scenario 3: New MG load conditions and new MG composition

The robustness of the physical MG dynamic equivalent was also evaluated considering one MG with a different composition. For this purpose the SSMT2 of TS-02 was replaced by one fuel cell. Before MMG islanding the active power production of SSMT1 as well as of each one of the SOFC is $20\,kW$, like in scenario 2. Concerning the reactive power production, each one of these controllable MS is kept on injecting a constant reactive power of $2\,kVAr$, according to the reactive power set point defined centrally by the MGCC. The load conditions inside the MG were also changed by adding a new load, $L = 15 + j3\,kVA$, to bus 16 of TS-02.

The study sequence of disturbances was simulated again being the results obtained presented in figures 6.41 to 6.45.

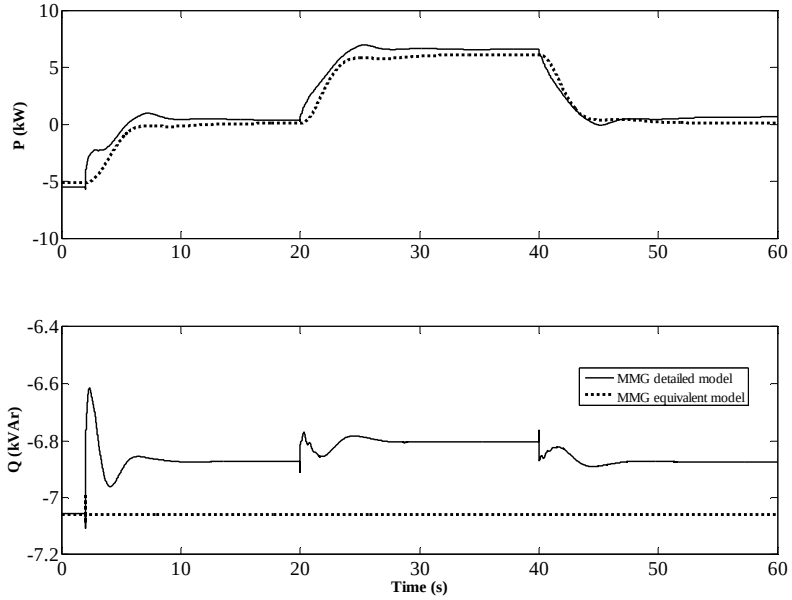

Figure 6.41: TS-02 physical MG dynamic equivalent active and reactive power outputs in scenario 3

Figure 6.41 plots the active and reactive power outputs of the physical MG slow dynamics equivalent model. Concerning the active power output, a certain loss of accuracy is experimented by the physical MG slow dynamics equivalent model, namely during transients. This is due to the fact that the active power output of MG slow dynamics subsystem is dominated by the SOFC active power output.

However, a good agreement between the physical MG dynamic equivalent and the MG detailed model responses can be observed from figure 6.42, being the errors experimented by the MG dynamic equivalent lower than $0{,}5 + j0{,}08\,kVA$.

As it can be observed from figures 6.43, 6.44 and 6.45, the physical MG dynamic equivalent provides quite identical results than these ones obtained using the MG detailed model. The maximum errors experimented from the synchronous machines active and reactive powers are lower than $1 + j0{,}02\,kVA$.

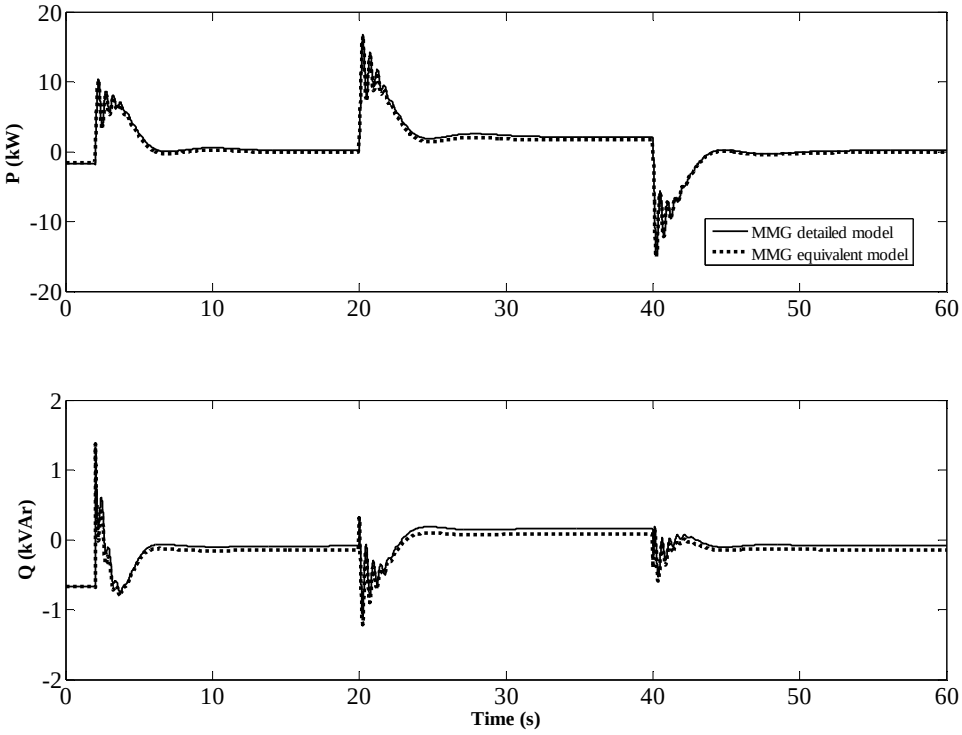

Figure 6.42: TS-02 physical MG dynamic equivalent active and reactive power outputs in scenario 3

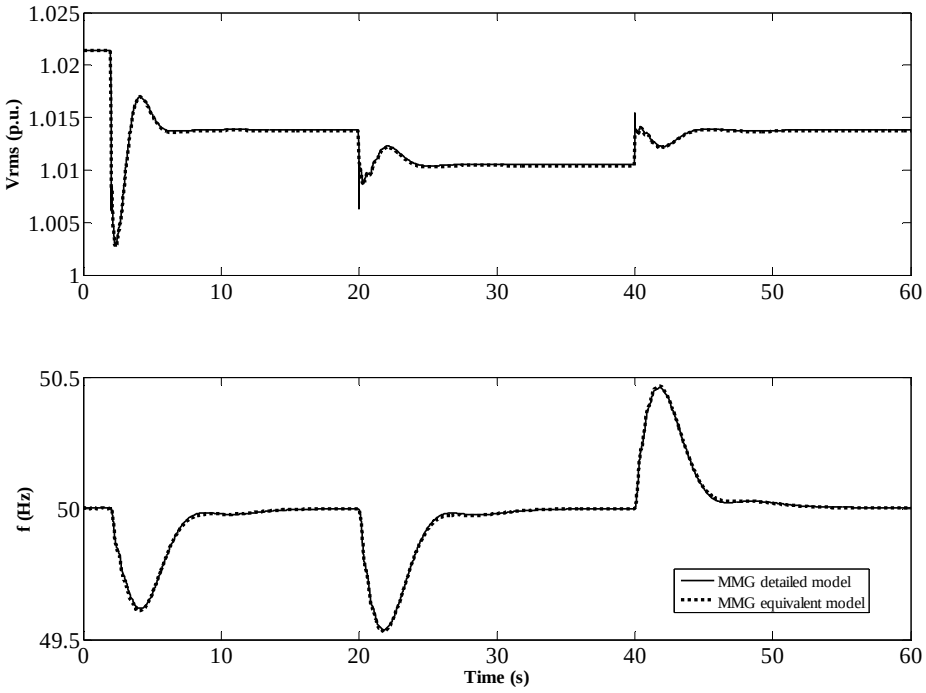

Figure 6.43: TS-02 boundary bus voltage and system frequency in scenario 3

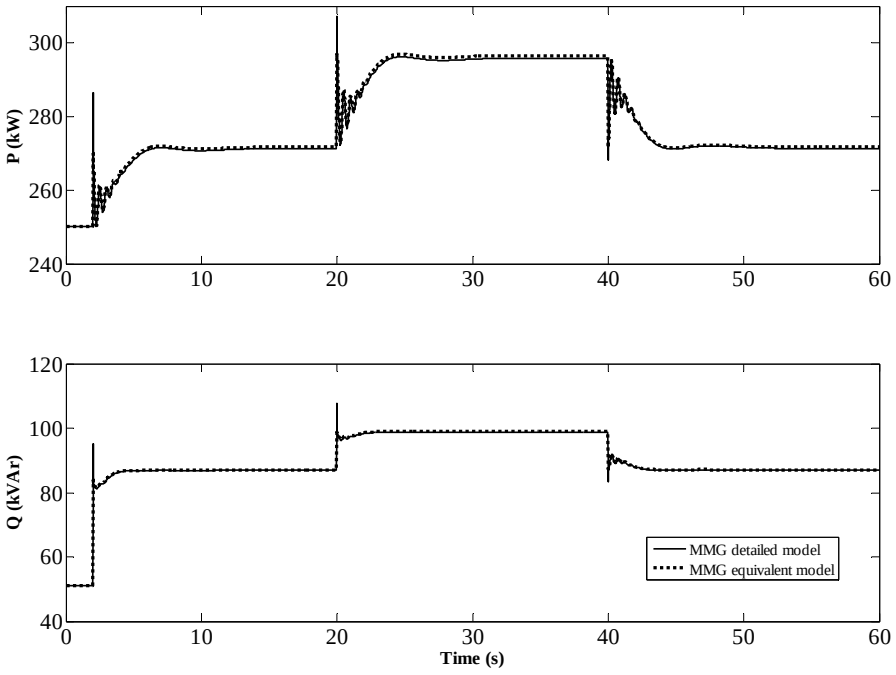

Figure 6.44: TS-02 SM1 active and reactive power outputs in scenario 3

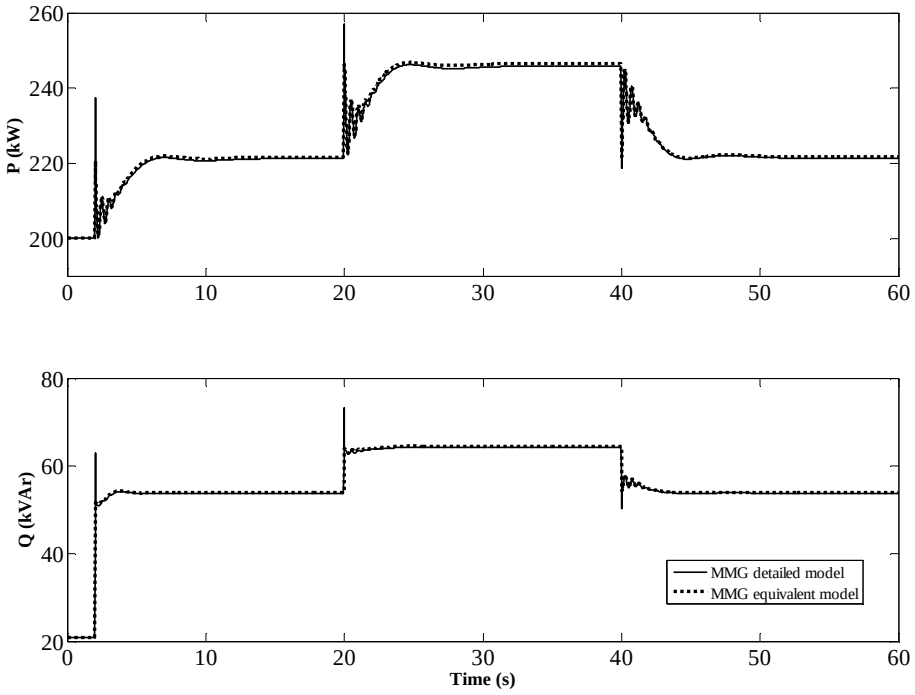

Figure 6.45: TS-02 SM2 active and reactive power outputs in scenario 3

Several sequences of disturbances were also simulated under these initial steady state operating conditions (scenario 3), considering different amounts of load connection and disconnection. Similar levels of accuracy can be observed, so that it can be concluded that the physical MG dynamic equivalent thus developed is appropriate to represent the MG dynamic behaviour of TS-02 with respect to the MV network following MMG islanding and during load following conditions when the MMG is operated in islanded mode.

Although the MG composition was changed, a good performance was achieved without modifications in the model structure or parameters. However, in the case of the MG active power response be predominantly dominated by fuel cells, if an unacceptable loss of accuracy of the MG dynamic equivalent performance arises, the model parameters have to be estimated again or the possibility of the MG slow dynamics equivalent model be represented by more than one physical model structure should be considered.

6.3.2.6 Some remarks of physical MG dynamic equivalent

In this subsection the performance of the physical MG dynamic equivalent derived as described in section 5.4 of chapter 5 was evaluated considering MMG islanding and load following is islanded mode. For this purpose several initial steady state conditions were considered and for each one of them an amount of load not used during training is connected and disconnected.

The comparison of the results obtained using both MMG detailed and equivalent models demonstrate the success of the physical MG dynamic equivalent in reproducing the MG dynamic behaviour with respect to the MV network, even when the MG detailed model composition was changed. Moreover, the simulation time is quite reduced. The MMG equivalent model runs around 130 times faster than the MMG detailed model under the same time domain simulation conditions.

On the other hand, the computational effort and therefore the elapsed time to derive the physical MG slow dynamics equivalent model are largely reduced, regarding the procedure carried out to derive the TDNN based MG slow dynamics equivalent model. In addition, the required used interaction is also largely reduced not only during the data generation procedure, but also during the model validation stage. It should be stressed that the physical model is easier to integrate into the dynamic simulation tools and no parameter updates are required when the initial steady state conditions are changed.

Finally, EPSO allowed the introduction of the MEE criterion as the objective function, constituting an identification method successfully used to derive the physical MG dynamic equivalent.

6.3.3 Comparing physical models obtained using MEE and MSE criteria

In this subsection the performance of the physical MG dynamic equivalent obtained previously is compared with this one of another physical MG dynamic equivalent obtained through the same procedure described in section 5.4 of chapter 5, but using the MSE as the fitness or loss function instead of MEE. When the termination criterion was verified (10 successive generations without finding a better global fitness) the training procedure was

stopped. The number of generations evaluated, the total elapsed time in both cases and the value of the errors entropy is presented in table 6.4.

Table 6.4: Number of generations and timings required to obtain the MSE and MEE physical models

	Number of generations	**Elapsed time (s)**	**Entropy**
MSE physical model	30	11270	-5.8513
MEE physical model	15	6400	-6.3152

It is interesting to notice that for MEE model the parameter vector values were found during the first 5 generations with smaller error entropy, while the MSE model required the evaluation of 20 generations. As a result, a considerable reduction of both computational effort and time consuming was verified, without loss of accuracy, when the MEE criterion was used as the loss function.

The performance of both MSE and MEE physical models was evaluated considering the same sequence of disturbances simulated in the previous subsection, but under new steady state operating conditions inside the MG, corresponding to a new scenario of TS-02, denoted as scenario 4.

6.3.3.1 Scenario 4: New MG generation and load conditions

In this scenario the active the active power productions of SSMT1, SSMT2 and SOFC were increased for $20\,kW$ and a new load, $L = 10 + j3\,kVA$, was connected to bus 16 of TS-02. The comparison between the results obtained from both physical models, and from the MG detailed model is presented in the following figures.

Figure 6.46 shows the active power outputs of both MG slow dynamics equivalent models. Both MEE and MSE models display similar performances over the whole simulation time. Concerning the MG slow dynamics subsystem active power output, an acceptable agreement can be observed and therefore, a similar degree of accuracy. This can also be observed from figures 6.47 and 6.48.

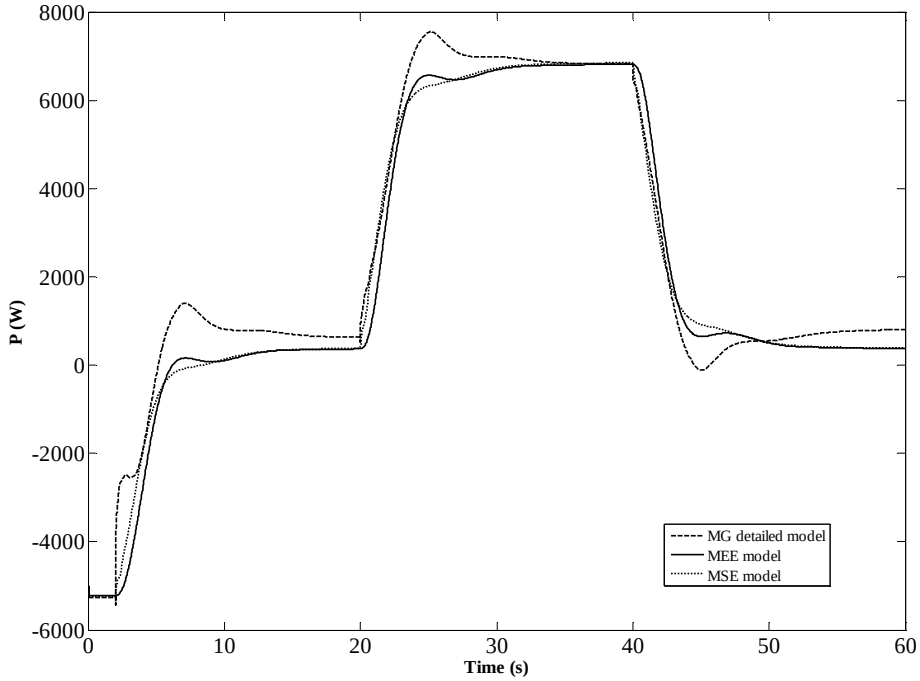

Figure 6.46: TS-02 physical MG slow dynamics equivalent models active power output in scenario 4

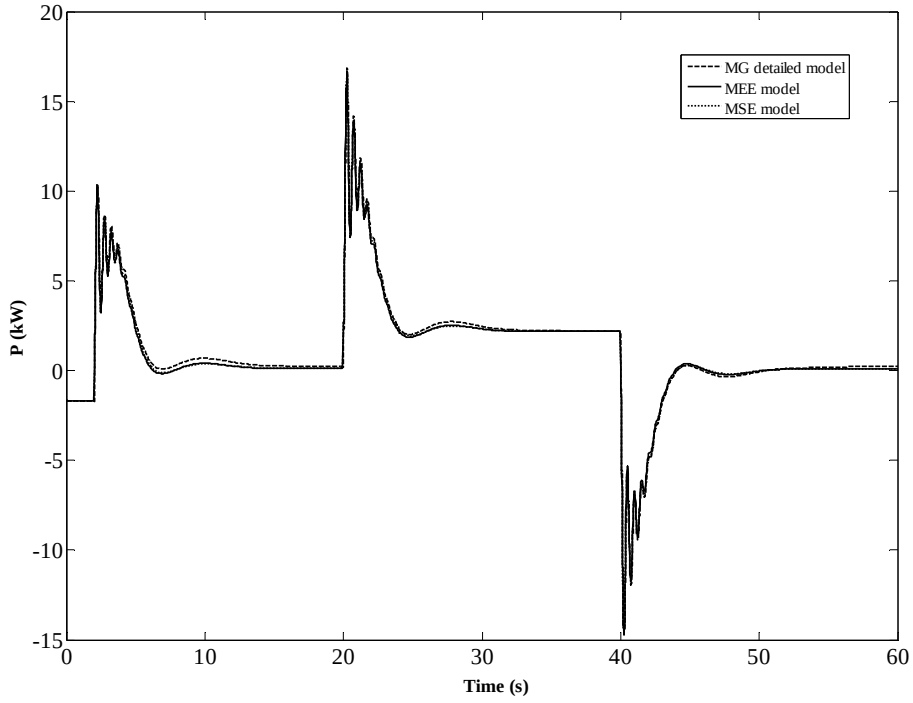

Figure 6.47: TS-02 physical MG dynamic equivalent active power output in scenario 4

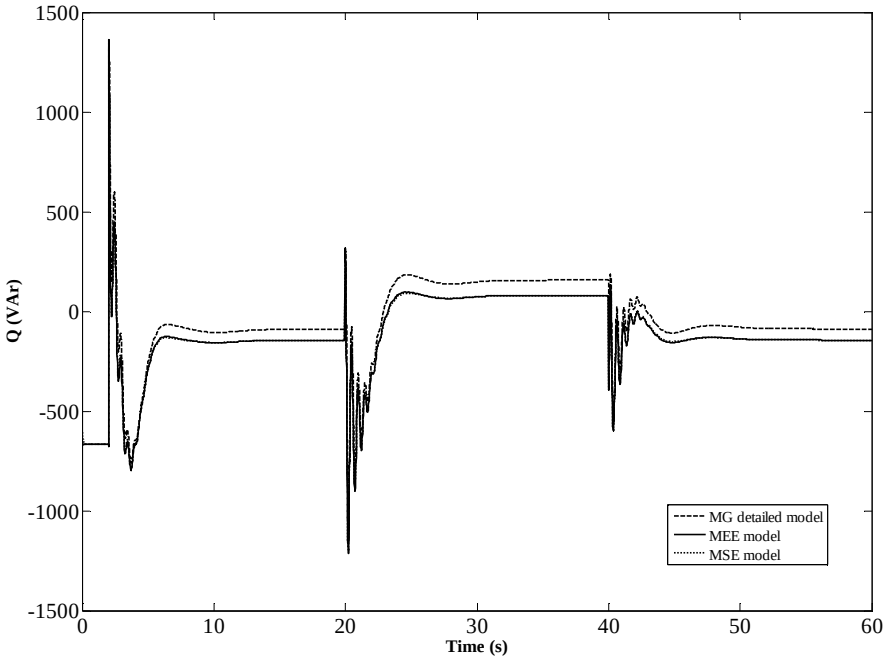

Figure 6.48: TS-02 physical MG dynamic equivalent reactive power output in scenario 4

In fact, as it can be observed from figures 6.47 and 6.48, the power outputs of both physical MG dynamic equivalents present a very good matching between them, either in steady state or during the transient periods. Comparing their responses with the power outputs obtained from the MG detailed model allows to conclude that both equivalent models represent with high accuracy the MG dynamic behaviour with respect to the MV network following MMG islanding as well as under load following conditions upon MMG islanding.

Therefore, the reduction of both computational effort and time that arises when MEE criterion was used as the loss function is an important advantage concerning the development of MG dynamic equivalents based on the physical modeling approaches. Thus, the use of EPSO as the optimizer together with the MEE loss function constitutes a very useful identification method.

6.3.4 TS-01 simulation results and discussion

The robustness of the physical MG dynamic equivalent trained with MEE was also evaluated in a different MMG. For this purpose, the MG slow dynamics subsystem of TS-01

was replaced by this physical MG slow dynamics equivalent model. It was also assumed that the MMG is initially operated in interconnected mode under the steady state operating conditions corresponding to the scenario 4 of TS-01 described in subsection 6.2.2.6. The same sequence of disturbances used to evaluate the TDNN based MD dynamic equivalent performance in TS-01 was simulated using both the MMG detailed model and the MMG equivalent model simulation packages and the obtained results are plotted in the figures presented in the following.

Figure 6.49 shows the active and reactive power outputs of the physical MG dynamic equivalent. It can be observed that the physical MG dynamic equivalent active and reactive power outputs are in a good agreement with these ones of the MG detailed model of TS-01 following the simulated sequence of disturbances. The power outputs experiment errors lower than $2{,}5 + j1\,kVA$, which are, in turn, inferior to these ones experimented by the TDNN based MG dynamic equivalent, concerning namely the active power output.

The impact of the physical MG dynamic equivalent at the study subsystem can be observed from figure 6.50, in which the boundary bus voltage and system frequency are represented.

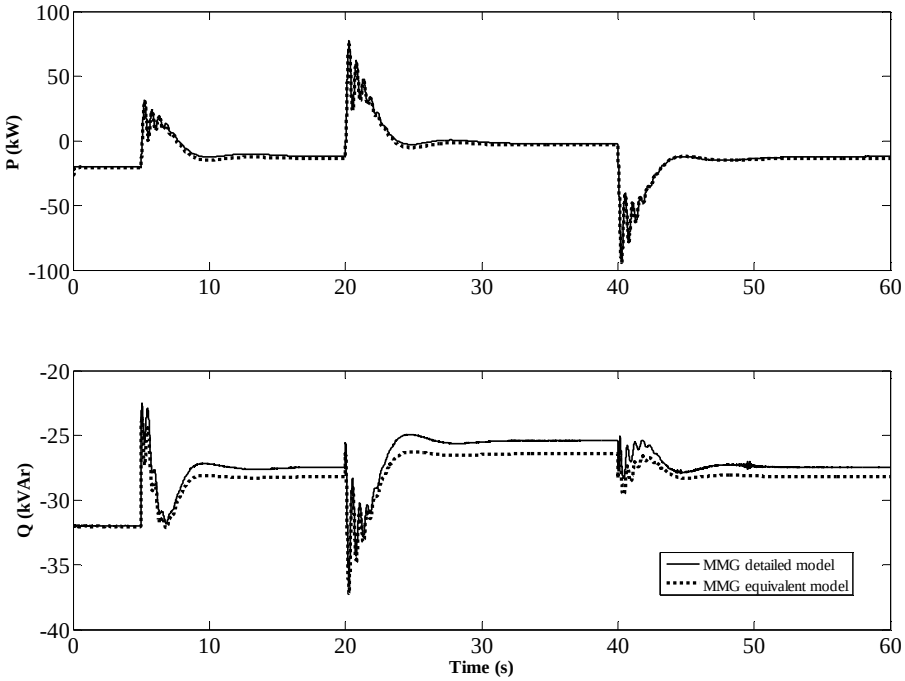

Figure 6.49: TS-01 physical MG dynamic equivalent active and reactive powers in scenario 3

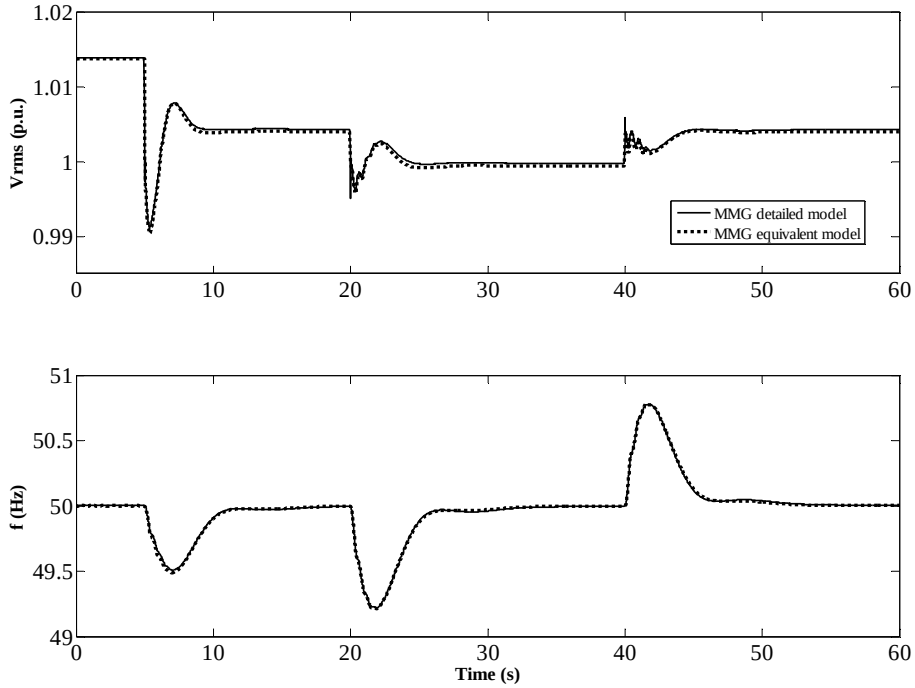

Figure 6.50: TS-01 boundary bus voltage and system frequency in scenario 3

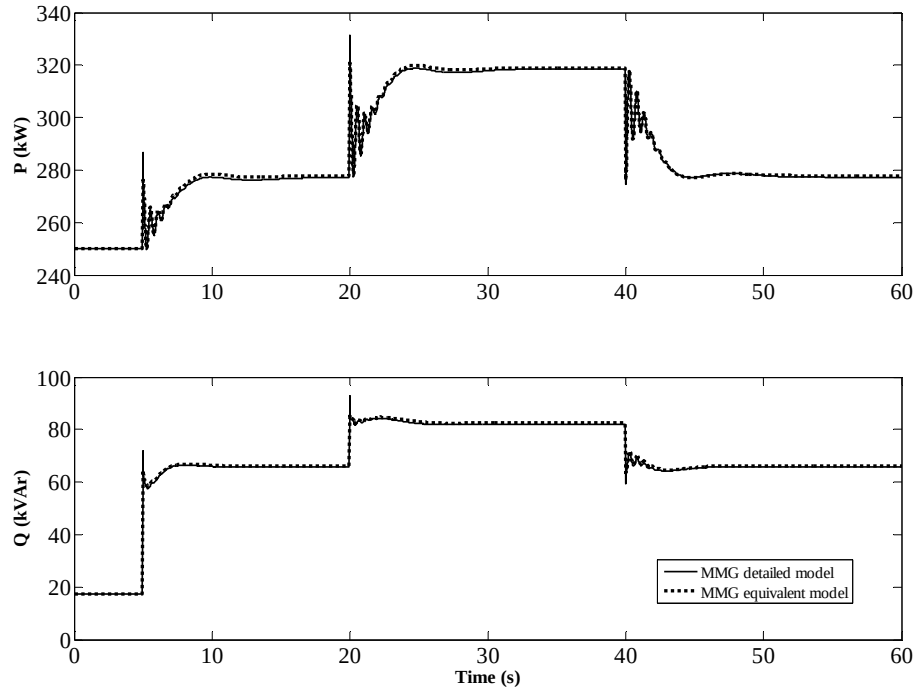

Figure 6.51: TS-01 SM1 active and reactive powers in scenario 3

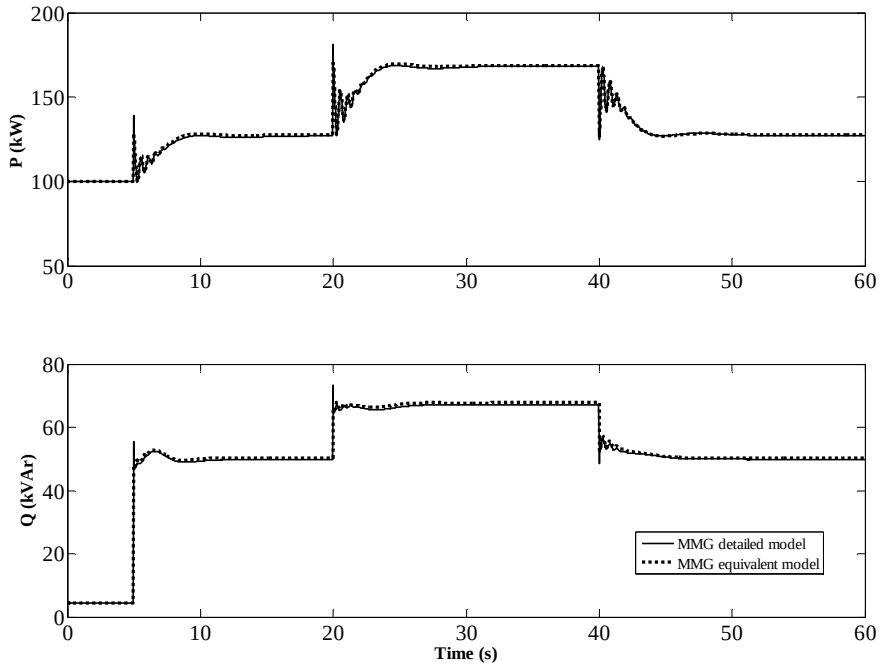

Figure 6.52: TS-01 SM2 active and reactive powers of scenario 3

As it can be observed from figures 6.50, 6.51 and 6.52 the physical MG dynamic equivalent response is in a good agreement with this one obtained using the MMG detailed model. Moreover the total simulation time of the considered sequence of disturbances is around 120 times faster with the MMG equivalent model than with the MMG detailed model.

Considering the TDNN based MG dynamic equivalent, a better performance was achieved using the physical MG dynamic equivalent under the same validation conditions, since the accuracy of results was improved and, at the same time, the time domain simulation speeds up. Concerning the last aspect, this is due to the fact that the TDNN based MG dynamic equivalent was derived based on a given sample time ($10\,ms$), which limits the maximum step size, although the time domain simulation be carried out with a variable step size while the MMG equivalent model based on the physical MG dynamic equivalent runs without step size constrains.

A similar prediction quality can also be obtained when other sudden load connection and disconnections are simulated, demonstrating that the physical MG dynamic equivalent can replace the MG detailed model, without structure modification or parameters adjusting, preserving its dynamic behaviour with respect to the MV network with a notable accuracy.

6.3.5 TS-02 simulation results using *Eurostag* ®

The performance of the physical MG dynamic equivalent was also evaluated when it is embedded in a different dynamic simulation tool, commonly used to simulate the dynamic behaviour of large conventional power systems. For this purpose, the MMG detailed and equivalent models of TS-02 was implemented in the simulation platform developed under the framework of the More-MicroGrids Project using *Eurostag* ® [226].

The microgeneration systems of TS-02 were implemented in *Eurostag* ® environment as power injectors, based on their dynamic models described in chapter 2. A quite simple model was implemented concerning the VSI control of the MG main storage device. It is also modelled as a power injector and is programmed to emulate the behaviour of a synchronous machine, injecting active power when system frequency drops proportionally to grid frequency deviations. The voltage/reactive power droop was not considered. Rather a voltage regulation system was implemented, so that the VSI reacts to voltage variations like a synchronous machine of constant excitation [226].

For synchronous machines SM1 and SM2 an $6\,th$ order model available from *Eurostag* ® library was used. Concerning the MG slow dynamics equivalent model, it was directly connected to the boundary bus without instantaneous power theory implementation, injecting the active power predicted by the physical model and a constant reactive power value, Q_{ref}.

It was assumed that initially the MMG is interconnected with the upstream power system under changed generation conditions inside the MG, regarding these ones described in table 6.3. The active power output of SSMT1 and SSMT2 were decreased to $15\,kW$ and the SOFC active power was increased to $15\,kW$. Under these initial steady state conditions, corresponding to a new scenario of TS-02, the scenario 5, the following sequence of disturbances was simulated:

- MMG islanding at $t = 2\,s$;
- Connection of an amount of load, $80 + j20\,kVA$ to bus 8 of TS-02, not used during parameter estimation, at $t = 20\,s$;
- Disconnection of the amount of load previously connected at $t = 40\,s$.

The results obtained using both the MMG detailed and equivalent models are presented and compared in order to evaluate the performance of the physical MG dynamic equivalent.

Figure 6.53 and 6.54 plot the active and reactive power outputs, respectively, of both MG detailed model and physical MG dynamic equivalent. As it can be observed from these figures, the physical MG dynamic equivalent active and reactive power outputs present an acceptable agreement with these ones provided by the MG detailed model over the whole simulation time.

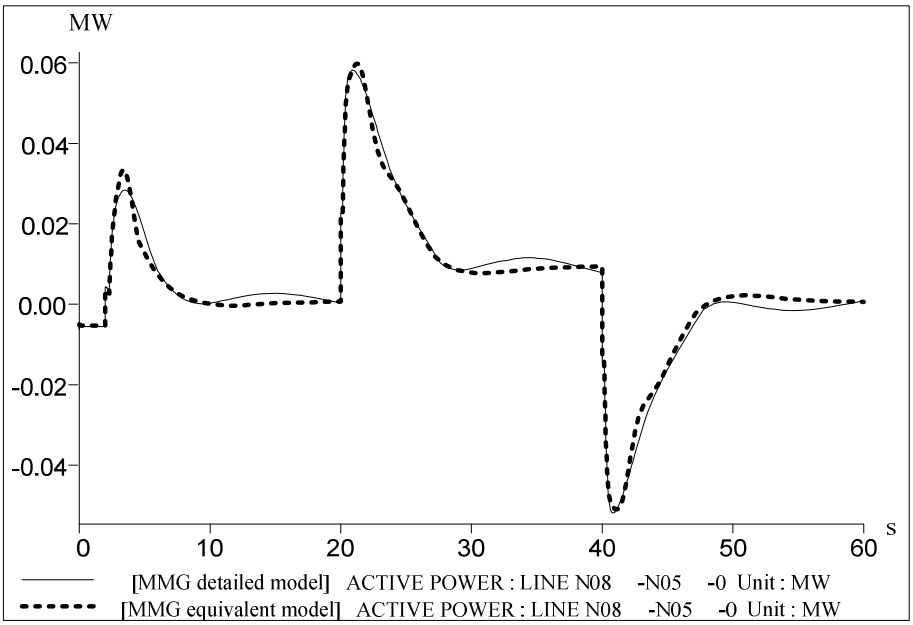

Figure 6.53: TS-02 physical MG dynamic equivalent active power output in scenario 5

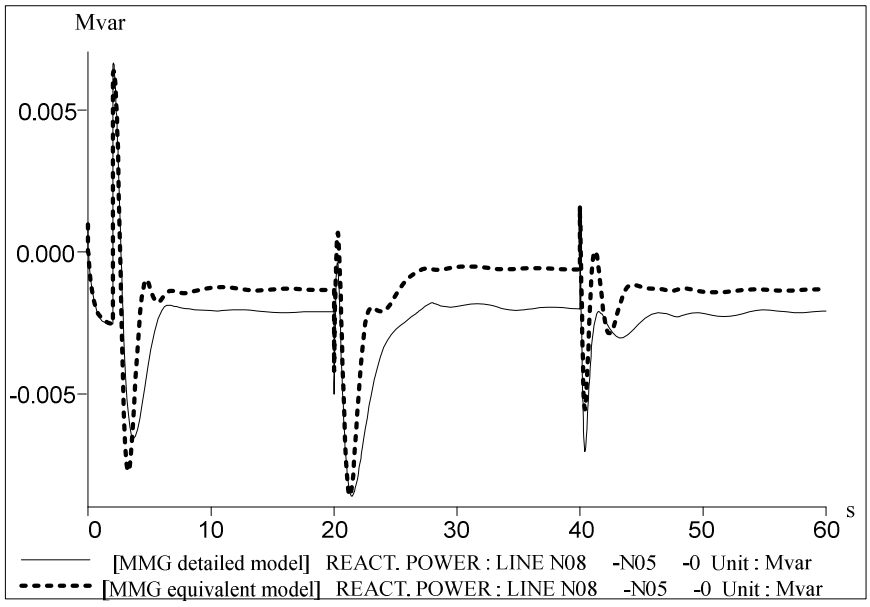

Figure 6.54: TS-02 physical MG dynamic equivalent reactive power output in scenario 5

An acceptable performance can also be observed from boundary bus voltages and system frequency presented in figures 6.55 and 6.56, respectively.

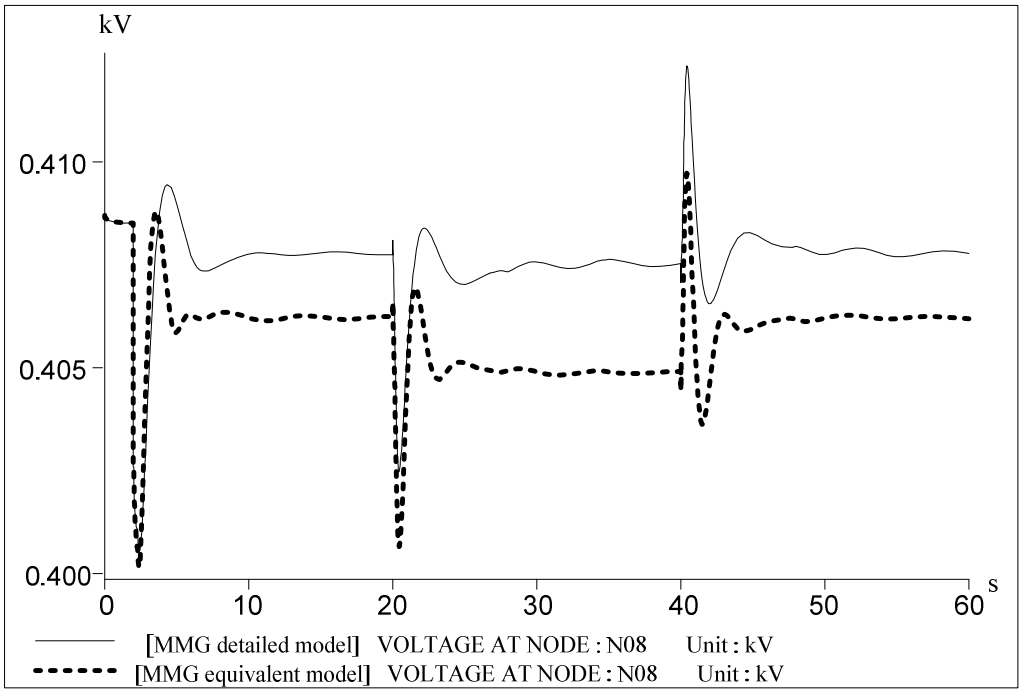

Figure 6.55: TS-02 boundary bus voltage in scenario 5

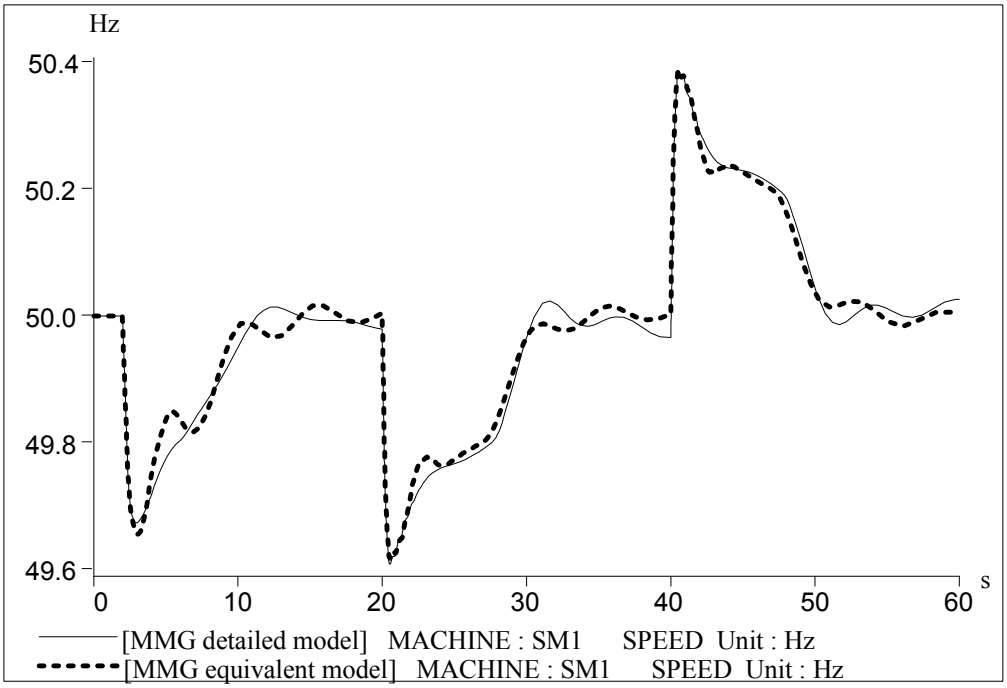

Figure 6.56: TS-02 system frequency in scenario 5

Concerning the active and reactive power of synchronous machines SM1 and SM2, a good matching can also be observed from figures 6.57, 6.58, 6.59 and 6.60.

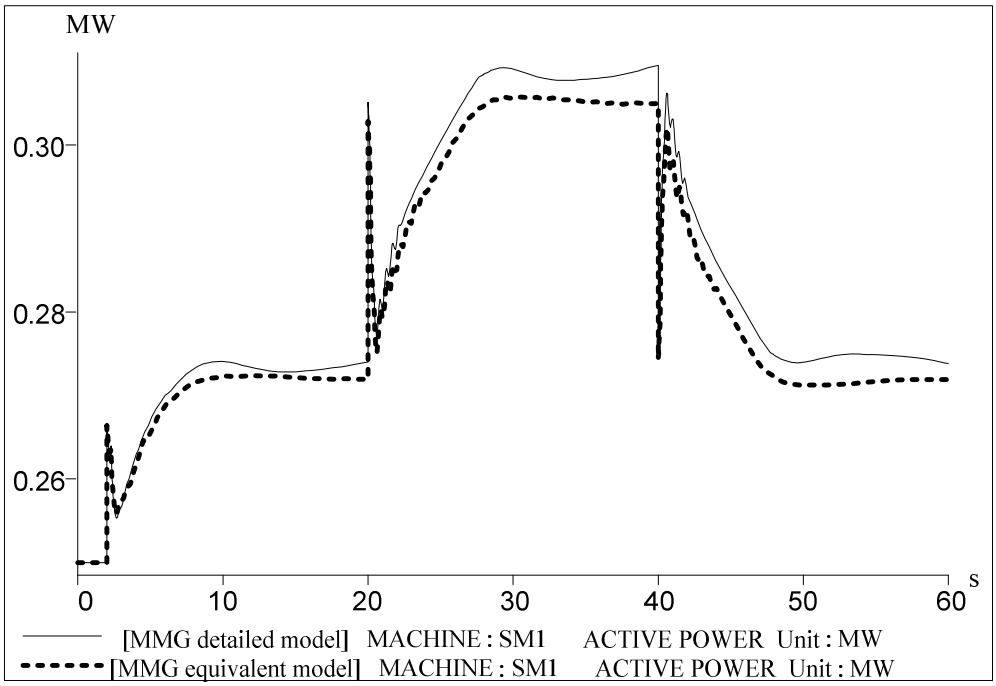

Figure 6.57: TS-02 MS1 active power in scenario 5

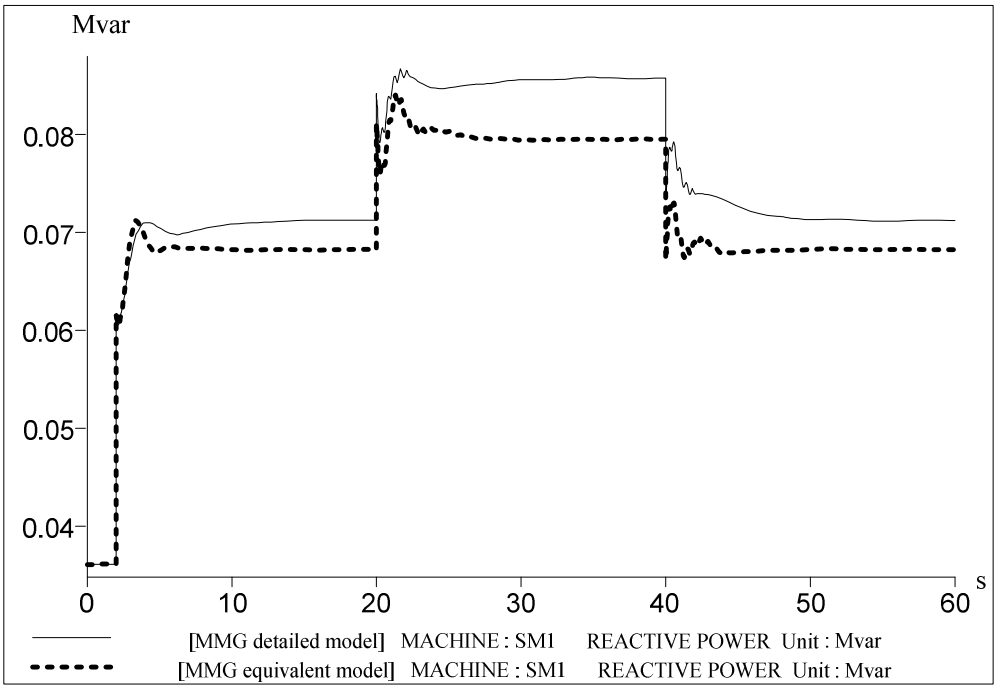

Figure 6.58: TS-02 MS1 reactive power in scenario 5

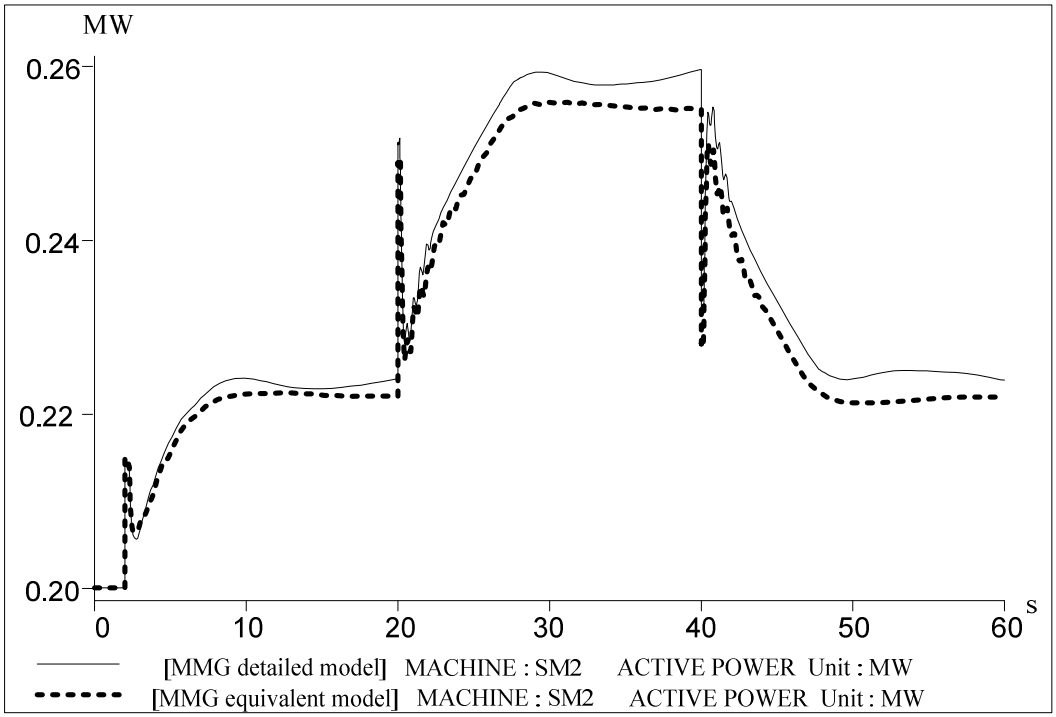

Figure 6.59: TS-02 MS2 active power in scenario 5

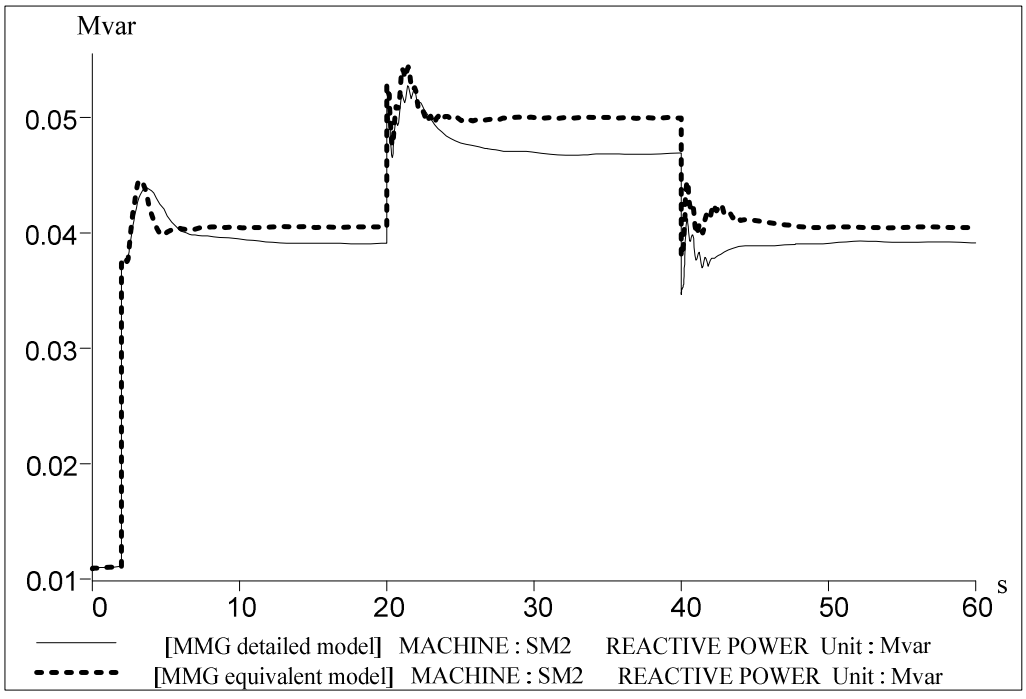

Figure 6.60: TS-02 MS2 reactive power in scenario 5

The results obtained stress the effectiveness of the physical MG dynamic equivalent when a different dynamic simulation tool, such as *Eurostag* ®, was used. A good performance was achieved following MMG islanding as well as during load following conditions upon MMG islanding without modifications on both structure and parameters. The physical MG dynamic equivalent preserves the important features of the MG system when it is represented through its detailed model.

6.4 Summary and main conclusions

Both TDNN based and physical MG dynamic equivalents were integrated into the dynamic simulation platform in order to evaluate their performances following MMG islanding and under load following conditions upon MMG islanding considering two studied cases. The results obtained allow to present the following main conclusions.

The TDNN based MG dynamic equivalent reproduces with high accuracy the MG dynamic behaviour under several operating conditions, even differing far from those ones used to extract training patterns. In addition, a notable speed up was achieved. However, a considerable computational effort is required to derive the TDNN based MG dynamic equivalent which is a very time consuming task requiring a frequently user interaction. Moreover, although the additional mapping and demapping functions required to embed the TDNN into the dynamic simulation platform extended its generalization capability, the initial values of both TDNN inputs and outputs as well as their maximum deviations from the initial values have to be updated whenever the initial steady state conditions are changed.

Although the high computational effort, the TDNN based MG dynamic equivalent domain of validity is restricted to the test system used to generate the data set. To replace a different MG requires another training procedure.

These weaknesses were overcame through the physical MG dynamic equivalent development. On the one hand, the computational effort required to derive the MG dynamic equivalent is quite reduced and, on the other hand, its domain of validity is largely extended. At the same time, the time domain simulations can be speed up without loss of accuracy, concerning the results obtained using both MMG detailed and equivalent models.

In fact, the use of the available physical knowledge allowed to select an appropriate model structure with physical representation, which can be easily integrated in dynamic simulation

tools commonly used to study power system dynamics. These features together with an effective identification method, exploiting both EPSO and MEE, contributed largely for the computational effort reduction assuring, simultaneously, a good model performance. This identification method constitutes a powerful tool to derive dynamic equivalents for MG.

Chapter 7
Conclusions and Future Developments

7.1 Conclusions and main contributions

Large scale integration of small modular RES and DG units in LV distribution systems exploiting the MG concept allows the transition from the vertically operated power systems to a future horizontally operated ones extended to the LV distribution systems. When dealing with such distribution networks, it will not be possible to neglect the dynamics introduced by MG connected to the MV distribution system, especially when several MG are operated under a MMG philosophy, being the MMG operated autonomously. On the other hand, the use of detailed models that are able to accurately simulate the MG dynamic behaviour becomes not practical due to the considerable computational effort required to solve the resulting system with a large number of nonlinear ordinary differential equations.

Thus, the major focus of this research work was to develop dynamic equivalents for MG able to reproduce their dynamic behaviours with respect to the MV distribution system, following MMG islanding and during load following transients upon MMG islanding. Since conventional dynamic equivalencing techniques have no practical applicability concerning MG dynamic equivalents, system identification techniques were exploited for this purpose. Then the main stages of classical methods, such as modal analysis and coherency based methods, are replaced by common system identification procedures, which aim to find a reduced order model built upon the corresponding MG detailed model, creating thus, the conditions for the development of dynamic equivalents able to describe the MG dynamic behaviour with respect to the upstream MV distribution system.

Based on the studies presented and discussed over this thesis, the main conclusions and contributions are presented in the following subsections.

7.1.1 Suitable approaches

The MG is an inverter dominated LV distribution system integrating microgeneration systems with different technologies controlled in a coordinate manner as a single entity. When connected to the upstream MV distribution network, even upon MMG islanding, the MG is operated according a SMO control strategy. Therefore, the MG is able for participating in primary frequency control as well as in secondary load frequency control of the MMG being operated autonomously.

Thus, concerning the transient analysis to be performed, two different time scales and phenomena are distinguished among the controllable MS, allowing the MG system to be spitted between two subsystems:

The MG main storage device;

The MG slow dynamics subsystem.

In fact, the MG main storage device connected to the LV network through a VSI control interface displays a fast dynamic response allowing the MG to participate in primary frequency control, while the remaining MG subsystem displays slow dynamic responses, according to the time constants of SSMT and SOFC connected to the LV network through PQ inverter controls. These controllable MS allow the MG to participate in secondary load frequency control. In turn, non controllable MS, such as PV and small wind generators, are considered to generate a constant active power over the simulation time.

As the MG slow dynamics subsystem is the responsible for the large simulation times, the MG dynamic equivalent involves the equivalent model of the MG slow dynamics subsystem, represented as a current source, and the detailed model of the MG main storage device, both connected to the boundary bus.

Under a system identification framework, concerning the MG slow dynamics subsystem, two suitable model structures (mathematical representations) were selected and subsequently appropriate identification methods were adopted and developed, leading to the following two proposed approaches:

- **Black-box modelling**: The model structure is based on TDNN, which comprise MLP neural networks to combine the NFIR regressors into one-step-ahead predictions. The ANN adjustable parameters are estimated using the Levenberg-Marquardt algorithm

and the classical MSE criterion, being the best bias/variance trade-off achieved by means of early stopping.

- **Physical modelling:** A physically parameterized model structure was adopted to represent the MG slow dynamics subsystem dynamic behaviour. EPSO is exploited, as the global optimization tool, together with both MSE and MEE criteria, as fitness functions, to estimate the parameters of the physical model.

These approaches were successfully applied to derive dynamic equivalents for MG, yielding two kinds of MG dynamic equivalents: The TDNN based MG dynamic equivalents and the physical MG dynamic equivalents.

7.1.2 The numerical set up

In order to derive dynamic equivalents for MG a numerical set-up was developed. It contains two dynamic simulation packages:

- The MMG detailed model, which comprises a fully representation of the MG connected to the MV network. The dynamic models of microgeneration systems as well as their inverter interfaces and controls were linked with the algebraic equations describing the LV network and loads, as a multi-machine power system model. This dynamic simulation package allows the simulation of the MG relevant dynamic behaviour with respect to the MV network, under transient and steady state conditions, generating high quality data sets.
- The MMG equivalent model is obtained by replacing the detailed model of the MG slow dynamics subsystem by its corresponding equivalent model. This dynamic simulation package is used not only for validation of the derived MG slow dynamic equivalent models, but also for estimating the parameters of the physically parameterized model structure purposes.

The inverter interfaces modelling based on their control functions only was an important assumption concerning the simulation of MG dynamic behaviour with respect to the MV network and subsequent data set generation.

The experience acquired previously with the detailed system modelling suggested the MG system separation between slow and fast dynamics. In addition, it provided the physical intuition that guided selection of the proposed physically parameterized model structure,

concerning the physical MG dynamic equivalent, as well as the development of its interface exploiting power instantaneous theory.

7.1.3 The TDNN based MG dynamic equivalents

The TDNN based MG dynamic equivalent preserves the MG dynamic behaviour with respect to the upstream MV network, being the MG represented through its detailed model, with a considerable computational time saving. It is valid for several initial steady state operating conditions, even far from the ones used to extract training patterns, considering different load and generation conditions either in the MV network or inside the MG.

This TDNN based MG dynamic equivalent success was achieved through a wide range data set and the normalization of both TDNN inputs and outputs magnitudes with respect to an initial steady state operating point. For a practical view point, the fact that only data collected at the boundary bus was required to derive the TDNN based MG dynamic equivalents can be considered as an advantage.

However, the TDNN based MG dynamic equivalent domain of validity is restricted to the MG that was used to generate the data set. Thus, in order to replace another MG in dynamic simulations a new system identification procedure has to be carried out using another data set. In addition, the cost of building TDNN based MG dynamic equivalents is very high concerning both the computational effort and the time consumed. These main drawbacks may render the proposed black box modelling approach applicability to MG unfeasible.

7.1.4 The physical MG dynamic equivalents

The physical MG dynamic equivalents successfully replace the MG detailed model in dynamic simulations considering new initial steady state generation and load conditions either in the MV network or inside the MG, allowing a considerable time saving. Very similar performances were achieved regarding both dynamic equivalent models derived using MSE and MEE.

In contrast with TDNN based MG dynamic equivalents, the required computational effort as well as the time consumed to derive the physical MG dynamic equivalents are quite reduced. This is especially stressed when the MEE is used as the loss function. In fact, EPSO combined

with MEE is an effective identification method to derive dynamic equivalents for MG. In addition, the physical MG dynamic equivalents perform better than the TDNN based MG dynamic equivalents improving the solution speed.

Moreover, the physical MG dynamic equivalent domain of validity extends to MG not used to generate the reduced data set. Thus, the weaknesses pointed out concerning the performance of TDNN based MG dynamic equivalents were overcame by the physical MG dynamic equivalent. The cost of building a physical MG dynamic equivalent is, of course, much smaller than the cost of performing the dynamic behaviour analysis, considering the detailed models of many MG.

The physical MG slow dynamics equivalent model has an important advantage, which arises from the fact that the known physical relationships are built in and no parameters have to be wasted. The physical interpretation of model parameters suggests that this physical model can be exploited in order to derive dynamic equivalents for MG in an expedite way.

Furthermore, the physical MG dynamic equivalent is compatible with other components in electrical networks allowing its successful and easy integration in dynamic simulation tools used to simulate the dynamic behaviour of large power systems, such as *Eurostag* ®.

7.1.5 Expected impact

The approaches and MG dynamic equivalents presented in this thesis, concerning especially the physical MG dynamic equivalents, will contribute to develop new tools and simulation approaches required to perform dynamic behaviour studies of MMG, providing contributions to:

- Overcome the lack of knowledge regarding large scale integration of microgeneration in LV distribution systems exploiting the MG concept and, simultaneously, ensuring future power supply reliability and quality;
- Quantify the benefits of MG;
- Allow the identification of technical and regulatory changes that will be required as a result of a large deployment of MG;
- Dissemination and development of microgeneration technologies.

7.2 Future developments

The derived MG dynamic equivalents can be used to replace MG in dynamic simulations when several disturbances at the MV level occur, like MMG islanding and load following in islanded mode. However, some simplifications were considered over the development of this thesis. Thus, future developments include:

- To exploit the physical meaning of parameters concerning the physical model in order to derive dynamic equivalents for MG in an expedite way;
- To derive dynamic equivalents including more appropriate models of loads, like motors;
- To include the intermittent effects of renewable energy systems, such as micro wind systems and PV, in MG dynamic equivalents;
- The derivation of dynamic equivalents capable of reproducing the MG dynamic behaviour during short-circuits;
- The development of models able to simulate the dynamic behaviour of single-phase microgeneration systems and MG operating under unbalanced conditions;
- The derivation of MG dynamic equivalents with capacity to reproduce the MG dynamic behaviour under unbalanced conditions.

Bibliographic References

[1] N. Jenkins, R. Allan, P. Crossley, D. Kirschen, G. Strbac, *Embedded Generation*. London, United Kingdom: IEE Power and Energy Series 31, 2000.

[2] *An Energy Policy for Europe*: Communication from the Commission to the European Council and the European Parliament, ec.europa.eu/energy/energy_policy/doc/01_energy_policy_for_europe_en.pdf 2007.

[3] M. Sánchez-Jiménez, "Smart Electricity Networks: European drivers and projects for the integration of RES and DG into the electricity grids of the future," presented at 3rd European Conference PV-Hybrid and Mini-Grid, Aix en Provence, France, 2006.

[4] "European research project MicroGrids " in *http://microgrids.power.ece.ntua.gr*.

[5] "European Research project More MicroGrids," in *http://microgrids.power.ece.ntua.gr*.

[6] J. A. Peças Lopes, C. L. Moreira, A. G. Madureira, "Defining Control Strategies for MicroGrids Islanded Operation," in *IEEE Transactions on Power Systems*, vol. 21, 2006, pp. 916-924.

[7] J. A. Peças Lopes, C. L. Moreira, A. G. Madureira, "Defining Control Strategies for Analysing MicroGrids islanded operation," presented at IEEE St. Petersburg PowerTech St. Petersburg, Russia, 2005.

[8] D. Georgakis, S. Papathanassiou, N. Hatziargyriou, A. Engler, C. Hardt, "Operation of a prototype microgrid system based on micro-sources equipped with fast-acting power electronics interfaces," presented at IEEE 35th PESC, Aachen, Germany, 2004.

[9] C. L. Moreira, F. O. Resende, J. A. Peças Lopes, "Using Low Voltage MicroGrids for Service Restoration " in *IEEE Transactions on Power Systems*, vol. 22, 2006, pp. 395-403.

[10] J. A. Peças Lopes, C. L. Moreira, F. O. Resende, "MicroGrids Black Start and Islanded Operation," presented at 15 th Power Systems Computation Conference, Liège, Belgium, 2005.

[11] S. Barsali, M. Ceraolo, P. Pellacchi, "Control techniques of dispersed generators to improve the continuity of electricity supply " in *Proc. PES Winter Meeting*, vol. 2, 2002, pp. 789-794.

[12] R. Caldon, F. Rossetto, R. Turri "Analysis of dynamic performance of dispersed generation connected through inverters to distribution networks," presented at 17th Int. Conf. Electricity Distribution Barcelona, Spain, 2003.

[13] M. Y. El-Sharkh, A. Rahman, M. S. Alam, A. A. Sakla, P. C. Byrne, T. Thomas, "Analysis of active and reactive power control of a standalone PEM fuel cell power plant," in *IEEE Transactions on Power Systems*, vol. 19, 2004, pp. 2022-2028.

[14] F. Katiraei, M. R. Irvani, P. W. Lehn "Micro-grid autonomous operation during and subsequent to islanding process," in *IEEE Transactions on Power Delivery*, vol. 20, 2005, pp. 248-257.

[15] R. Lasseter, P. Piagi, "Providing Premium Power through Distributed Resources " presented at 33rd Hawaii International Conference System Science 2000.

[16] F. O. Resende, C. L. Moreira, J. A. Peças Lopes, "Identification of Dynamic Equivalents for MicroGrids with High Penetration of Solar Energy using ANNs,"

presented at 3rd. European Conference of PV-Hybrid and Mini-Grid, Aix en Provence, France, 2006.

[17] F. O. Resende, J. A. Peças Lopes, "Development of Dynamic Equivalents for MicroGrids using System Identification Theory," presented at IEEE Lausanne PowerTech'07, Lausanne, Switzerland, 2007.

[18] J. A. Peças Lopes, C. L. Moreira, F. O. Resende, "Control strategies for microgrids black start and islanded operation," in *International Journal of Distributed Energy Resources*, vol. 1, 2005, pp. 242-261.

[19] J. A. Peças Lopes, C. L. Moreira, A. G. Madureira, F. O. Resende, X. Wu, N. Jayawarna, Y. Zhang, N. Jenkins, F. Kanellos, N. Hatziargyriou, "Control strategies for microgrids emergency operation," in *International Journal of Distributed Energy Resources*, vol. 2, 2006, pp. 211-232.

[20] J. A. Peças Lopes, T. J. Saraiva, N. Hatziargyriou, N. Jenkins, "Management of microgrids," in *http://microgrids.power.ece.ntua.gr/documents/Microgrids_management_jieec2003.pdf*, 2003.

[21] J. A. Peças Lopes, C. L. Moreira, A. G. Madureira, F. O. Resende, P. G. Abia, X. Wu, N. Jayawarna, Y. Zhang, N. Jenkins, F. Kanellos, N. Hatziargyriou, C. Duvauchelle, "Emergency strategies and algorithms," MicroGrids Project, Deliverable DD1, http://microgrids.power.ece.ntua.gr/micro/micro2000/index.php?page=deliverables 2004.

[22] H. Hatziargyriou, F. Kanellos, G. Kariniotakis, X., Le Pivert, N, Jenkins, N. Jayawarna, J. Peças Lopes, N. Gil, C. Moreira, J. Oyarzabal, Z. Larrabe, "Modelling of micro-sources for security studies," presented at CIGRE Session France, 2004.

[23] G. Kariniotakis, R. Almeida, S. Busquet, C. Camez, K. Elmasidis, N. Gil, N. Hatziargyriou, N. Jayawarna, N. Jenkins, F. Kanellos, J. Labbe, Z. Larrabe, X. Le Pivert, R. Metkemeyer, J. Oyarzabal, J. A. Peças Lopes, J. Sousa Pinto, "Digital models for Microsources," MicroGrids Project, Deliverable DA1, http://microgrids.power.ece.ntua.gr/micro/micro2000/index.php?page=deliverables 2003.

[24] Y. Zhu, K. Tomsovic, "Development of models for analysing the load-following performance of microturbines and fuel cells," in *Electric Power Systems Research* vol. 62, 2002, pp. 1-11.

[25] P. A. Pilavachi, "Mini- and micro-gas turbines for combined heat and power," in *Applied Thermal Engineering*, vol. 22, 2002, pp. 2003-2014.

[26] R. Anahara, S. Yokokawa, M. Sacurai, "Present status and future prospects for fuel cell power systems," presented at IEEE, Proceedings (ISSN oo18-9219), vol. 81,1993, pp. 399-408.

[27] A. Dicks, A. Siddle, "Assessment of commercial prospects of molten carbonate fuel cells," in *Journal of Power Sources*, vol. 86, 2000, pp. 316-323.

[28] F. Gonzalez-Longatt, A. Hernandez, F. Guillen, C. Fortoul, "Load following function of fuel cell plant in distributed environment," http://www.giaelec.org/Articulos/A2005_02.pdf, 2005.

[29] D. J. Hall, R. G. Colclaser, "Transient modelling and simulation of tubular solid oxide fuel cells," in *IEEE Transactions on Energy Conversion*, vol. 14, 1999, pp. 749-753.

[30] F. Jurado, "Modelling SOFC plants on the distribution system using identification algorithms," in *Journal of Power Sources*, vol. 129, 2004, pp. 205-215.

[31] F. Jurado, Manuel Valverde, Antonio Cano, "Effect of a SOFC plant on distribution system stability," in *Jpurnal of Power Sources*, vol. 129, 2004, pp. 170-179.

[32] R. Lasseter, "Dynamic models for microturbines and fuel cells," presented at IEEE Power Engineering Society Summer Meeting, 2001.

[33] M. D. Lukas, K. Y. Lee, H. Ghezel-Ayagh, "Development of a stack simulation model for control study on direct reforming molten carbonate fuel cell power plant," in *IEEE Transactions on Energy Conversion*, vol. 14, 1999, pp. 1651-1657.

[34] M. D. Lukas, K. Y. Lee, H. Ghezel-Ayagh, "An explicit dynamic model for direct reforming carbonate fuel cell stack," in *IEEE Transactions on Energy Conversion*, vol. 16, 2001, pp. 289-295.

[35] J. Padullés, G. W. Ault, J. R. McDonald, "An integrated SOFC plant dynamic model for power systems simulation," *Journal Power Sources*, vol. 86, pp. 495-500, 2000.

[36] J. Padullés, G. W. Ault, J. R. McDonald, "An approach to the dynamic modelling of fuel cell characteristics for distributed generation operation," presented at IEEE Power Engineering Society Winter Meeting, 2000.

[37] K. Sedghisigarchi, A. Feliachi, "Dynamic and transient analysis of power distribution systems with fuel cells - Part1: Fuel-cell dynamic model," in *IEEE Transactions on energy conversion*, vol. 19, 2004, pp. 423-428.

[38] K. Sedghisigarchi, A. Feliachi, "Dynamic and transient analysis of power distribution systems with fuel cells - Part II: Control and stability enhancement " in *IEEE Transactions on Power Conversion*, vol. 19, 2004, pp. 429-434.

[39] I. Zamora, J. I. San Martín, J. Mazón, S. Díaz, J. J. San Martín, J. M. Arrieta, V. Aperribay, "Performance analysis of fuel cells by modelling."presented atInternational Conference on Renewable Energies and Power Quality, Zaragoza, Spain, 2005.

[40] A. Al-Hinai, A. Feliachi, "Dynamic model of a microturbine used as a distributed generator," presented at IEEE 34th Southeastern Symposium on System Theory, Huntsville, Alabama, 2002.

[41] J. H. Watts, "Microturbines: a new class of gas turbine engines," *Gas Turbine News in Brief*, vol. 39, pp. 5-11, 1999.

[42] O. Fethi, L. A. Dessaint, K. Al-Haddad, "Modelling and simulation of the electric part of a grid connected micro turbine," presented at IEEE Power Engineering Society General Meeting, Denver, Colorado, USA, 2004.

[43] L. H. Willis, W. G. Scott, *Distributed power generation. Planning and evaluation.* New York, 2000.

[44] G. Joos, B. T. Ooi, D. McGillis, F.D. Galiana, R. Marceau, "The potential of distributed generation to provide ancillary services," presented at IEEE Power Enginnering Society Summer Meeting, 2000.

[45] H. Nikkhajoei, M. R.Iravani, "Modelling and analysis of a microturbine generation system," presented at IEEE Power Engineering Society Summer Meeting, 2002.

[46] L. N. Hannet, A. Khan, "Combustion turbine dynamic model validation from tests," in *IEEE Transactions on Power Systems*, vol. 8, 1993.

[47] L. N. Hannet, G. Jee, B. Fardanesh, "A governor/turbine model for a twin-shaft combustion turbine," in *IEEE Transactions on Power Systems*, vol. 10, 1995, pp. 133-140.

[48] M. Nagpal, A. Moshref, G. K. Morison, P. Kundur, "Experience with testing and modelling of gas turbines," presented at IEEE/PES 2001 Winter Meeting, Columbus, Ohio, USA, 2001.

[49] B. K. Bose, *Power Electronics and AC drives*. New Jersey, 1986.
[50] *Fuel Cell Handbook*, 5th ed: EG & G Services Parsons, Inc. Science Applications International Corporation, 2000.
[51] M. R. V. S. Ellis M. W., D. J. Nelson, "Fuel cell systems: Efficient, flexible energy conversion for trhe 21st century," presented at IEEE, 2001.
[52] A. M. Azmy, I. Erlich "Dynamic simulation of fuel cells and microturbines integrated in a multi-machine network," presented at IEEE Bologna PowerTech Bologna, Italy, 2003.
[53] L. J. Blomen, M. N. Mugerwa, *Fuel cell systems*. New York: Wiley, 1993.
[54] "Installing photovoltaic systems. A question and answer guide for solar electric systems," in *http://www.fsec.uef.edu/en/research/photovoltaics/vieo/resources/documents/PVPrimer.pdf*, 1999.
[55] D. L. King, *Photovoltaic module and array performance characterization methods for all system operating conditions*: NREL/SNL Program Review, AIP Press, 1996.
[56] J. C. H. Phang, D. S. H. Chan, J. R. Phillips, "Accurate analytical method for the extraction of solar cell model parameters," in *Electronics Letters*, vol. 20, 1984, pp. 406-408.
[57] B. P. Alencar, F. L. M. Antunes, R. P. S. Leão, A. S. Bukvic-Schafer, "LabVIEW-based simulation tool for photovoltaic systems," presented at 3rd European Conference PV-Hybrid and Mini-Grid,Aix en Provence, France, 2006.
[58] P. Kundur, *Power system stability and control*: McGraw-Hill, 1994.
[59] R. Hebner, J. Beno, A. Walls, "Flywheel batteries come around again," in *IEEE Spectrum* vol. 39, 2002.
[60] R. Lasseter, Abbas Akhil, Chris Marnay, John Stephens, Jeff Dagle, Ross Guttromson, A. Sakis Meliopoulous, Robert Yinger, Joe Eto "White Paper on Integration of Distributed Energy Resources - The CERTS MicroGrid Concept," in *http://certs.lbl.gov/pdf/LBNL_50829.pdf*, 2002.
[61] M. C. Chandorkar, D. M. Divan, R. Adapa, "Control of parallel connected inverters in standalone AC supply systems " in *IEEE Transactions on Industry Applications*, vol. 29, 1993, pp. 136-143.
[62] A. Engler, "Applicability of droops in low voltage grids," in *International Journal of Distributed Energy Resources*, vol. 1, 2005.
[63] X. Lei, D. Povh, O.Ruhle, "Industrial Approaches for Dynamic Equivalents of Large Power Systems," 2002, pp. 1036-1042.
[64] E. Pires de Sousa, A. Leite da Silva, "An efficient methodology for coherency-based dynamic equivalents," in *IEE Proceedings-Generation, Transmission and Distribution*, vol. 139, 1992, pp. 371-382.
[65] S.-K. Joo, Chen-Ching Liu, Lawrence E. Jones, Jong-Woong Choe, "Coherency and Aggregation Techniques Incorporating Rotor and Voltage Dynamics," in *IEEE Transactions on Power Systems*, vol. 19, 2004, pp. 1068-1075.
[66] W. W. Price, A.W.Hargrave, B.J. Hurysz, J.H. Chow, P.M. Hirsch, "Large-scale system testing of a power system dynamic equivalencing program " in *IEEE Transactions on Power Systems*, vol. 13, 1998, pp. 768-773.
[67] W. T. Brown, W.J. Cloues, "Combination load-flow and stability equivalents for power system representation on the ac network analysers," in *AIEE Transactions*, vol. 74, Part III, 1955, pp. 782-786.

[68] H. E. Brown, R.B. Shipley, D. Coleman, R.E. Neid, Jr., "A study of stability equivalents," in *IEEE Transactions on Power Apparatus and Systems*, vol. PAS-88, 1969, pp. 200-207.

[69] J. B. Ward, "Equivalent circuits for power-flow studies," in *AIEE Transactions*, vol. 68, Part I, 1949, pp. 373-382.

[70] S. Nishida, S. Takeda, "Derivation of equivalents for dynamic security assessment," in *Electric Power and Energy Systems*, vol. 6, 1984, pp. 15-23.

[71] J. M. Undrill, J. A. Casazza, E.M. Gulachemski, L. K. Krichmayer, "Electromechanical equivalents for use in power system stability studies," in *IEEE Transactions on Power Apparatus and Systems*, vol. PAS-90, 1971, pp. 2060-2071.

[72] J. M. Undrill, A.E. Turner, "Construction of Power System Electromechanical Equivalents by Modal Analysis," in *IEEE Transactions on Power Apparatus and Systems* vol. 90, 1971, pp. 2049-2059.

[73] A. Chang, M. M. Adibi "Power system dynamic equivalents," in *IEEE Transactions on Power Apparatus and Systems*, vol. 89, 1970, pp. 173-175.

[74] A. J. Germong, R. Podmore, "Dynamic aggregation of generating unit models," in *IEEE Transactions on Power Apparatus and Systems*, vol. PAS-97, 1978, pp. 1060-1069.

[75] R. Podmore, "Identification of coherent generators for dynamic equivalents," in *IEEE Transactions on Power Apparatus and Systems*, vol. PAS-97, 1978, pp. 1344-1354.

[76] J. S. Lawler, R.A. Schlueter, "Computational algorithms for constructing modal-coherent dynamic equivalents," in *IEEE Transactions on Power Apparatus and Systems*, vol. PAS-101, 1982, pp. 1070-1080.

[77] L. Wang, M. Klein, S. Yirga, P. Kundur "Dynamic reduction of large power systems for stability studies," in *IEEE Transactions on Power Systems*, vol. 12, 1997, pp. 889-895.

[78] Y. Mansour, E. Vaahedi, A.Y. Chang, B.R. Corns, B.W. Garret, K. Demaree, T. Athay, K. Cheung, "B.C. Hydro's On-line Transient Stability Assessment (TSA) Model Development, Analysis and Post-processing," in *IEEE Transactions on Power Systems*, vol. 10, 1995, pp. 241-253.

[79] R. J. Newell, M.D. Risan, L. Allen, K.S. Rao, D.L. Stuehm, "Utility Experience with Coherency-based Dynamic Equivalents of Very Large Systems," in *IEEE Transactions on Power Apparatus and Systems*, vol. PAS-104, 1985, pp. 3056-3063.

[80] G. Troullinous, J. Dorsey, H. Wong, J. Myers, "Reducing the Order of Very Large Power System Models," in *IEEE Transactions on Power Systems*, vol. 3, 1988, pp. 127-133.

[81] S. D. Olivera, J. D. Queiroz, "Modal dynamic equivalents for electric power systems. I-Theory," in *IEEE Transactions on Power Systems*, vol. 3, 1988, pp. 1723-1730.

[82] S. D. Olivera, A. Massaud, "Modal dynamic equivalents for electric power systems. II-Stability simulation tests," in *IEEE Transactions on Power Systems*, vol. 3, 1988, pp. 1731-1737.

[83] W. W. Price, B.A. Roth, "Large-Scale Implementation of Modal Dynamic Equivalents," in *IEEE Transactions on Power Apparatus and Systems*, vol. 100, 1981, pp. 3811-3817.

[84] J. P. Yang, G.H. Cheng, Z. Xu, "Dynamic Reduction of Large Power Systems in PSS/E," presented at 2005 IEEE/PES Transmission and Distribution Conference & Exhibition, Asia and Pacific Dalian, China, 2005.

[85] F. F. Wu, N. Narasimhamurthi, "Coherency identification for power system dynamic equivalents," in *IEEE Transactions on Circuits and Systems*, vol. 30, 1983, pp. 140-147.

[86] S. Lee, F. Schweppe, "Distance measures and coherency recognition for transient stability equivalents " in *IEEE Transactions on Power Apparatus and Systems*, vol. PAS-92, 1973, pp. 1550-1557.

[87] M.-H. Wang, Hong-Chan Chang, "Novel Clustering Method for Coherency Identification Using an Artificial Neural Network," in *IEEE Transactions on Power Systems*, vol. 9, 1994, pp. 2056-2062.

[88] J. R. Winkelman, J. H. Chow, B. C. Bowler, B. Avramovic, P. V. Kokotovic, "An analysis of interarea dynamics of multi-machine systems," in *IEEE Transactions on Power Apparatus and Systems*, vol. PAS-100, 1981, pp. 754-763.

[89] J. H. Chow, "New algorithms for slow coherency aggregation of large power systems," in *Proc. Institute of Mathematics and its applications*, 1993, pp. 95-115.

[90] J. Machowski, A. Cichy, F. Gubina, P. Omahen, "External Subsystem Equivalent Model for Steady-State and Dynamic Security Assessment," in *IEEE Transactions on Power Systems*, vol. 3, 1988, pp. 1456-1463.

[91] P. M. van Oirsouw, "A Dynamic Equivalent using Modal Coherency and Frequency Response," in *IEEE Transactions on Power Systems*, vol. 5, 1990, pp. 289-285.

[92] S. B. Yusof, G.J. Rogers, R.T.H. Alden, "Slow coherency based network partitioning including load buses," in *IEEE Transactions on Power Systems*, vol. 8, 1993, pp. 1375-1381.

[93] J. H. Chow, R. J. Galarza, P. Accari, W.W. Price "Inertial and Slow Coherency Aggregation Algorithms for Power System Dynamic Model Reduction," in *IEEE Transactions on Power Systems*, vol. 10, 1995, pp. 680-685.

[94] N. Gacic, A.I. Zecevic, D.D. Siljak, "Coherency recognition using epsilon decomposition," in *IEEE Transactions on Power Systems*, vol. 13, 1998, pp. 314-319.

[95] S. Geeves, "A modal-coherency technique for deriving dynamic equivalents," in *IEEE Transactions on Power Systems*, vol. 3, 1988, pp. 44-51.

[96] C. Grande-Moran, M. D. Brown, "Coherency-based low order models for shaft systems of turbine-generator sets," in *IEEE Transactions on Power Systems*, vol. 12, 1997, pp. 217-224.

[97] M. H. Haque, A. H. Rahim "An efficient method of identifying coherent generators using Taylor series expansion," in *IEEE Transactions on Power Systems*, vol. 3, 1988, pp. 1112-1118.

[98] M. H. Haque, A. H. Rahim, "Identification of coherent generators using energy function," in *IEE Proceedings-Generation Transmission and Distribution*, vol. 137, 1990, pp. 255-260.

[99] M. H. Haque, "Identification of coherent generators for power systems dynamic equivalents using unstable equilibrium point," in *IEE Proceedings-Generation, Transmission and Distribution*, vol. 138, 1991, pp. 546-552.

[100] T. Hiyama, "Identification of coherent generators using frequency response," in *IEE Proceedings-Generation, Transmission and Distribution*, vol. 128, 1981, pp. 262-268.

[101] H. Kim, G. Jang, K. Song, "Dynamic reduction of the large-scale power systems using relation factor," in *IEEE Transactions on Power Systems*, vol. 19, 2004, pp. 1696-1699.

[102] K. L. Lo, Z. Z. Qi, D. Xiao, "Identification of coherent generators by spectrum analysis," in *IEE Proceedings-Generation, Transmission and distribution*, vol. 142, 1995, pp. 367-371.

[103] T. N. Nababhushana, K.T. Veeramanju, Shivanna "Coherency identification using growing self organizing feature maps," presented at International Conference of Energy Management and Power Delivery, Singapore, 1998.

[104] A. Nuhanovic, M. Glavic, N. Prljaca, "Validation of a clustering algorithm for voltage stability analysis of Bosnian electric power system " in *IEE Proceedings-Generation, Transmission and Distribution*, vol. 145, 1998, pp. 21-26.

[105] Y. Ohsawa, M., Hayashi, "Coherency recognition for transient stability equivalents using Lyapunov function," presented at 6th PSCC - Power Systems Computation Conference, Darmstadt, 1978.

[106] M. A. Pai, R.P. Adgaonkar, "Electromechanical distance measure for decomposition of power systems," in *Electrical Power Energy Systems*, vol. 6, 1984, pp. 249-254.

[107] I. J. Perez-Arriaga, G.C. Verghese, F.C. Schweppe "Selective modal analysis with applications to electric power system. I: Heuristic introduction," in *IEEE Transactions on Power Apparatus and Systems*, vol. PAS-101, 1982, pp. 3117-3125.

[108] G. N. Ramaswamy, L. Rouco, O. Fillatre, G.C. Verghese, P. Panciatici, B.C. Lesieutre, D. Peltier, "Synchronic modal equivalencing (SME) for structure-preserving dynamic equivalents," in *IEEE Transactions on Power Systems*, vol. 11, 1996, pp. 19-29.

[109] H. Rudnick, R. I. Patino, A. Brameller, "Power system dynamic equivalents: coherency recognition via the rate of change of kinetic energy," in *IEE Proceedings C. Generation Transmission and Distribution* vol. 128, 1981, pp. 325-333.

[110] Z. Shuqiang, C. Xianring, P. Yunjiang, H. Renmu, "A reduced order method for swing mode eigenvalue calculating based on fuzzy coherency recognition," presented at International Conference on Power System Technology, Beijing, China, 1988.

[111] B. D. Spalding, H. Yee, D. B. Goudle, "Coherency recognition for transient stability studies using singular points," in *IEEE Transactions on Power Apparatus and Systems*, vol. PAS-96, 1977, pp. 1368-1375.

[112] G. Troullinous, J. Dorsey, "Coherency and model reduction: State space point of view," in *IEEE Transactions on Power Systems*, vol. 4, 1989, pp. 988-995.

[113] P.-H. Huang, Shu-Chen Wang, Feng-Shun Chien, "Hierarchical clustering for coherency recognition in power systems " presented at International Conference on Power System Technology, Beijing, China, 1988.

[114] O.-C. Yucra Lino, Michael Fette, "Electromechanical identity recognition as alternative to the coherency identification," presented at International Universities Power Engineering Conference, Bristol, United Kingdom, 2004.

[115] R. Nath, S.S. Lamba, K.S. Prakasa Rao, "Coherency based system decomposition in study and external areas using weak coupling," in *IEEE Transactions on Power Apparatus and Systems*, vol. PAS-104, 1985, pp. 1443-1449.

[116] R. J. Galarza, J.H. Chow, W.W. Price, A.W. Hargrave, Peter M. Hirsch, "Aggregation of exciter models for constructing power system dynamic equivalents," in *IEEE Transactions on Power Systems*, vol. 13, 1998.

[117] X. Lei, E. Lerch, D. Povh, O.Ruhle, "A Large Integrated Power System Software Package - NETOMAC," presented at International Conference of Power Systems Technology, Beijin, China, 1998.

[118] X. Lei, D. Povh, E., Lerch, B. Kulicke, "Optimization - a new tool in simulation program system," in *IEEE Transactions on Power Systems*, vol. 12, 1997, pp. 598-604.

[119] A. M. Stankovic, Andrija T. Saric, M. Molosevic, "Identification of Nonparameteric Dynamic Power System Equivalents with Artificial Neural Networks," in *IEEE Transactions on Power Systems*, vol. 18, 2003, pp. 1478-1486.

[120] A. M. Stankovic, Andrija T. Saric, "Transient Power System Analysis with Measurement-Based Gray Box and Hybrid Dynamic Equivalents," in *IEEE Transactions on Power Systems*, vol. 19, 2004, pp. 455-462.

[121] E. De Tuglie, L. Guida, F. Torelli, D. Lucarella, M. Pozzi, G. Vimercati "Identification of Dynamic Voltage-Current Power System Equivalents through Artificial Neural Networks," presented at Bulk Power System Dynamics and Control - VI, Cortina d'Ampezzo, Italy, 2004.

[122] O.-C. Yucra Lino, "Robust Recurrent Neural Network-based Dynamic Equivalencing in Power System," in *IEEE Transactions on Power Systems*, 2004.

[123] A. M. Azmy, István Erlich, "Identification of Dynamic Equivalents for Distribution Power Networks using Recurrent ANNs," in *IEEE Transactions on Power Systems*, 2004.

[124] A. M. Azmy, István Erlich, P. Sowa, "Artificial neural network-based dynamic equivalents for distribution systems containing active sources," in *IEE Proc.-Generation, Transmission and Distribution* vol. 151, 2004, pp. 681-688.

[125] F. C. Véliz, Sergio Gomes, Sergio Luis Varricchio, Sandoval Carneiro Junior, "Dynamic Equivalents for Large ac Networks using Modal Analysis for s-Domain Models," presented at IEEE Power Engineering Society General Meeting, 2005.

[126] D. Chaniotis, M.A. Pai "Model Reduction in Power Systems Using Krylov Subspace Methods," in *IEEE Transactions on Power Systems*, vol. 20, 2005, pp. 888-894.

[127] S. Demmig, Habil Hans Pundt, István Erlich, "Identification of external system equivalents for power system stability studies using the software package MATLAB," presented at 12th Power System Computation Conference, Desdren, Germany, 1996.

[128] L. A. Aguirre, "Quantitative measure of modal dominance for continuous system," presented at IEEE 32nd Conference Decision Control, San Antonio, TX, 1993.

[129] D. Bonvin, D.A. Mellichamp, "A unified derivation and critical review of modal approaches to model reduction," *International Journal of Control*, vol. 35, pp. 829-848, 1982.

[130] J. B. Moore, "Principal component analysis in linear systems: Controlability, observability, and model reduction " in *IEEE Transactions on Automatic Control*, vol. AC-26, 1981, pp. 17-32.

[131] K. Glover, "All optimal Hankel-norms approximations of linear multivariable systems and their L∞ error bounds," *International Journal of Control*, vol. 39, pp. 1115-1193, 1984.

[132] R. M. G. Castro, J.M.Ferreira de Jesus, "A Wind Park Reduced-Order Model using Singular Perturbations Theory " in *IEEE Transactions on Energy Conversion*, vol. 11, 1996, pp. 735-741.

[133] P. V. Kokotovic, R.E. O'Malley, P. Sannuti, "Singular Perturbations and Order Reduction in Control Theory - An Overview," in *Automatica*, vol. 12, 1976, pp. 123-132.

[134] P. V. Kokotovic, John J. Allemong, James R. Winkelman, Joe H. Chow, "Singular Perturbation and Iterative Separation of Time Scales," in *Automatica*, vol. 16, 1980, pp. 23-33.

[135] R. M. G. de Castro, *Equivalentes dinâmicos de parques eólicos*. Lisboa: Tese de Doutoramento, Universidade Técnica de Lisboa, Instituto Superior Técnico, 1994.

[136] A. Ishchenco, A. Jokic, J.M.A. Myrzik, W.L. Kling, "Dynamic Reduction of Distribution Networks with Dispersed Generation," presented at International Conference on Future Power Systems, Amesterdam, The Netherlands, 2005.

[137] K. Fujimoto, Jacquelien M. A. Scherpen, "Nonlinear balanced realization based on singular value analysis of Hankel operators," presented at 42nd IEEE Conference on Decision and Control, Maui, Hawaii USA, 2003.

[138] J. Machowski, Janusz W. Bialek, James R. Bumby, *Power System Dynamics and Stability*. Banfins Lane, Chichester: John Wiley & Sons Ltd, 1997.

[139] J. H. Chow, J. Cullum, R. A. Willoughby, "A sparsity-based technique for identifying slow-coherent areas in large power systems," in *IEEE Transactions on Power Apparatus and Systems*, vol. PAS-103, 1984, pp. 463-473.

[140] J. H. Chow, "A toolbox for power system dynamics and control engineering education and research," in *IEEE Transactions on Power Systems*, vol. 7, 1992, pp. 1559-1564.

[141] L. Wang, A. Semlyen, "Application of sparse eigenvalue techniques to the small signal stability analysis of large power systems," in *IEEE Transactions on Power Systems*, vol. 5, 1990, pp. 635-642.

[142] M. L. Ourari, L.A. Dessaint, V. Q. Do, "Generating units aggregation for dynamic equivalent of large power systems," presented at Power Engineering Society General Meeting 2004, Denver, USA, 2004.

[143] A. A. Mohd, B.C. Kok, M. W. Mustafa, K. L. Lo, A. E. Ariffin, "Time domain dynamic aggregation of generating unit based on structure preserving approach," presented at PECon 2003, Power Engineering Conference 2003.

[144] M. L. Ourari, L.A. Dessaint, V. Q. Do, "Dynamic equivalent modelling of large power systems using structure preservation technique," in *IEEE Transactions on Power Systems* vol. 21, 2006, pp. 1284-1295.

[145] J. M. Ramírez Arredondo, "Obtaining dynamic equivalents through minimization of a line fows function," in *Electric Power and Energy Systems*, vol. 21, 1999, pp. 365-373.

[146] A. H. M. A. Rahim, A. J. Al-Ramadhan, "Dynamic equivalent of external power system and its parameter estimation through artificial neural networks," in *Electric Power and Energy Systems*, vol. 24, 2002, pp. 113-120.

[147] V. Knyazkin, Claudio A. Cañizares, Lennard H. Söder, "On the parameter estimation and modelling of aggregate power system loads," in *IEEE Transactions on Power Systems*, vol. 19, 2004, pp. 1023-1031.

[148] A. M. Stankovic, Andrija T. Saric "An integrative approach to transient power system analysis with standard and ANN-based dynamic models," presented at 2003 IEEE Bologna PowerTech Conference, Bologna, Italy, 2003.

[149] H. Ren-mu, A. J. Germond, "Comparison of dynamic load modelling using neural network and traditional method," presented at 2nd International Forum on Applications of Neural Networks to Power Systems, Yokohama, 1993.

[150] J. Y. Wen, L. Jiang, Q. H. Wu, S. J. Cheng, "Power system load modelling by learning based on system measurements," in *IEEE Transactions on Power Systems*, vol. 18, 2003, pp. 346-371.

[151] M. Miah, "Simple dynamic equivalent for fast online transient stability assessment," in *IEE Proceedings of Generation, Transmission and Distribution*, vol. 145, 1998, pp. 49-55.
[152] M. G. Burth, C. Verghese, M. Vélez-Reyes, "Subset selection for improved parameter estimation in online identification of a synchronous generator," in *IEEE Transactions on Power Systems*, vol. 14, 1999, pp. 218-225.
[153] I. A. Hiskens, "Nonlinear dynamic model evaluation from disturbance measurements," in *IEEE Transactions on Power Systems*, vol. 16, 2001, pp. 702-710.
[154] W. W. Price, D.N. Ewart, E.M. Gulachenski, R.F. Silva, "Dynamic equivalents from on-line measurements," in *IEEE Transactions on Power Apparatua and Systems*, vol. PAS-94, 1975, pp. 1349-1357.
[155] P. Ju, X. Y. Zhou, "Dynamic equivalents of distribution systems for voltage stability studies," in *IEE Proceedings of Generation, Transmission and Distribution*, vol. 148, 2001, pp. 49-53.
[156] J. Y. Kim, D.J. Won, S.I. Moon, "Development of dynamic equivalent model for large power systems," presented at IEEE Power Engineering Society Summer Meeting Vancouver, Canada, 2001.
[157] J. M. A. E. T. Undrill, "Construction of Power System Electromechanical Equivalents by Modal Analysis," in *IEEE Transactions on Power Apparatus and Systems* vol. 90, 1971, pp. 2049-2059.
[158] L. Ljung, Jorkel Glad, *Modelling of Dynamic Systems*: Prentice Hall Information and System Sciences Series, 1994.
[159] L. Ljung, *System Identification. Theory for the user* Second ed: Prentice Hall, 1999.
[160] L. Ljung, J. Sjoberg, "A System Identification Perspective on Neural Nets ", pp. 423-435, 1992.
[161] O. Nelles, *Nonlinear System Identification. From Classical Approaches to Neural Networks and Fuzzy Models*: Springer, 2001.
[162] T. Soderstrom, P. Stoica *System Identification*. New York: Prentice Hall, 1989.
[163] L. Ljung, "Nonlinear black box models in system identification," presented at IFAC Symposium on Advanced Control of Chemical Processes, ADCHEM'97, Banff, Canada, 1997.
[164] M. Norgaard, O. Ravn, N. K. Poulsen and L. K. Hansen, *Neural Networks for Modelling and Control of Dynamic Systems: A Practitioner's Handbook*. United Kingdom: Springer, 2003.
[165] M. Norgaard, Ole Ravn, Niels Kjolstad Poulsen, "NNSYSID and NNCTRL Tools for system identification and control with neural networks," *Computing & Control Engineering Journal* 2001.
[166] L. Ljung, *MATLAB System Identification Toolbox, Version 4.0*. Natick, MA: The Matworks Inc., 1998.
[167] R. Haber, H. Unbehauen, "Structure Identification of Nonlinear Dynamic Systems - A Survey of Input/Output Approaches," in *Automatica*, vol. 26, 1990, pp. 651-677.
[168] A. Juditsky, H. Hjalmarsson, A. Benveniste, B. Deyon, L. Ljung, J. Sjoberg and Q. Zhang, "Nonlinear Black Box Models in System Identification: Mathematical Foundations," in *Automatica*, vol. 31, 1995, pp. 1725-1750.
[169] J. Sjoberg, Q. Zhang, L. Ljung, A. Benveniste, B. Delyon, P. Y. Glorennec, H. Hjalmarsson and A. Judisky, "Nonlinear Black-box Modelling in System Identification: A Unified Overview," in *Automatica*, vol. 31, 1995, pp. 1691-1724.

[170] T. Poggio, F. Girosi, "Neural Networks for Approximation and Learning," in *proceedings of the IEEE*, vol. 78, 1990, pp. 1481-1497.
[171] K. S. Narendra, K. Parthasarathy, "Identification and control of dynamical systems using neural networks," in *IEEE Transactions on Neural Networks*, vol. 1, 1990, pp. 4-27.
[172] J. C. Principe, Neil R. Euliano and W.CurtLefebvre, *Neural and Adaptive Systems: Fundamentals Through Simulations*. USA: John Wiley & Sons, INC., 2000.
[173] J. V. Beck, K. J. Arnold, *Parameter Estimation in Engineering and Science* New York: John Wiley and Sons, 1977.
[174] Q. Z. Sjoberg J., L. Ljung, A. Benveniste, B. Delyon, P. Y. Glorennec, H. Hjalmarsson and A. Judisky, "Nonlinear Black-box Modelling in System Identification: A Unified Overview," in *Automatica*, vol. 31, 1995, pp. 1691-1724.
[175] S. Geman, E. Bienenstock, R. Doursat, "Neural networks and the bias/variance dillema," in *Neural Computation*, vol. 4, 1992, pp. 1-58.
[176] T. Heskes, "Bias/variance decomposition for likelihood-based estimators," in *Neural Computation* vol. 10, 1998, pp. 1425-1433.
[177] H. Akaike, "A new look at the statistical model identification," in *IEEE Transactions on Automatic Control*, vol. 19, 1974, pp. 716-723.
[178] J. G. Lennart Ljung, *Modelling of Dynamic Systems*: Prentice Hall Information and System Sciences Series, 1994.
[179] R. E. Bellman, *Adaptive Control Processes*. New Jersey: Princeton University Press, 1961.
[180] S. Haykin, *Neural Networks: a Compreensive Foundation*. New York: Macmillan, 1994.
[181] S. R. Chu, R. Shoureshi, M. Tenorio, "Neural networks for system identification," in *IEEE Control Systems Magazine*, vol. 10, 1990, pp. 36-43.
[182] S. Chen, S. A. Billings, C. F. N. Cowan, P. M. Grant, "Nonlinear systems identification using radial basis functions " *International Journal of Systems Science*, vol. 21, pp. 2513-2539, 1990.
[183] S. A. Billings, H. B. Jamaluddin, S. Chen, "Properties of neural networks with applications to modelling nonlinear dynamical systems," *International Journal of Control*, vol. 55, pp. 193-224, 1991.
[184] A. R. Barrom, "Universal approximation bounds for superpositions of a sigmoid function," in *IEEE Transactions on Information Theory*, vol. 39, 1993, pp. 930-945.
[185] A. U. Levin, K. S. Narendra, "Identification using feedforward networks," in *Neural Computation*, vol. 7, 1995, pp. 349-357.
[186] D. E. Rumellart, J. L. McClelland, *Parallel Distributed Processing: Extrapolations in the Microstructure of Cognition: Foundations* vol. 1. Cambridge: MIT Press, 1986.
[187] K. Hornik, M. Stinchombe, H. White, "Multilayer feedforward networks are universal approximators," in *Neural Computation*, vol. 2, 1989, pp. 359-366.
[188] D. Erdogmus, José C. Principe, "Comparison of entropy and mean square error criteria in adaptive system training using higher order statistics," presented at Independent Components Analysis (ICA), Helsinki, Finland, 2000.
[189] D. Erdogmus, José C. Principe, "An Error-Entropy Minimization Algorithm for Supervised Training of Nonlinear Adaptive Systems," in *IEEE Transactions on Signal Processing*, vol. 50, 2002, pp. 1780-1786.

[190] D. Erdogmus, José C. Principe, "Generalized Information Potential Criterion for Adaptive System Training," in *IEEE Transactions on Neural Networks*, vol. 13, 2002, pp. 1035-1044.
[191] C. E. Shannon, "A mathematical theory of communications," *Bell Systems Technical Journal*, vol. 27, pp. 379-423, 1948.
[192] A. Renyi, *Some Fundamental Questions of Information Theory. Selected Papers of Alfred Renyi* vol. 2. Budapest: Akademia Kiado, 1976.
[193] J. Principe, J. Fisher, "Entropy manipulation of arbitrary nonlinear mappings," presented at Proc. IEEE Workshop Neural Nets for Signal Proc., Amelia Island, 1997.
[194] R. A. Morejon, J. C. Principe, "Advanced Search Algorithms for Information Theoretical Learning with Kernel -Based Estimators," in *IEEE Transactions on Neural Networks*, vol. 15, 2004.
[195] J. E. Dennis, R. B. Schnabel, *Numerical Methods for Unconstrained Optimization and Nonlinear Equations*. Englewood Cliffs, NJ: Prentice-Hall, 1983.
[196] E. D. Karnin, "A simple procedure for prunning back-propagation trained neural networks," in *IEEE Transactions on Neural Networks*, vol. 1, 1990, pp. 239-242.
[197] R. Reed, "Pruning algorithms: A survey," in *IEEE Transactions on Neural Networks*, vol. 4, 1993, pp. 740-747.
[198] X. Yao, "Global Optimization by Evolutionary Algorithms," 1997.
[199] J. Kennedy, Eberhart, R. C. , "Particle Swarm Optimization " presented at IEEE International Conference on Neural Networks, Perth, Australia, 1995.
[200] J. Kennedy, "The Particle Swarm: Social Adaptation of Knowledge," presented at International Conference on Evolutionary Computation, Indiana, USA, 1997.
[201] H. P. Schwefel, *Evolution and Optimum Seeking*. New York: Ed. Wiley, 1995.
[202] Y. Fukuyama, Yoshida, H., "A particle swarm optimization for reactive power and voltage control in electric power systems " presented at IEEE Evolutionary Computation, 2001.
[203] S. N. Omkar, Dheevatsa Mudigere, "Non-Linear Dynamical System Identification Using Particle Swarm Optimization " presented at International Conference on Advances in Control and Optimization of Dynamical Systems (ACODS2007), Bangalore, Índia, 2007.
[204] M. Clerc, J. Kennedy, "The particle swarm - Explosion, stability and convergence in a multidimensional complex space," in *IEEE Transactions on Evolutionary Computation*, vol. 6, 2002.
[205] R. Mendes, P. Cortez, M. Rocha, J. Neves, "Particle swarms for feed-forward neural network training," presented at International Joint Conference Neural Networks, 2002.
[206] C. Zhang, H. Shao, Y. Li, "Particle swarm optimization for evolving artificial networks," presented at IEEE International Conference on Systems Management and Cibernautics, 2000.
[207] V. Miranda, N. Fonseca, "EPSO - Best of two worlds meta-heuristic applied to power system problems," presented at WCCI'2002 - CEC - World Congress of Computational Intelligence - Conference of Evolutionary Computing, Honolulu, Hawaii, USA, 2002.
[208] M. Clerc, "The Swarm and the Queen: Towards a Deterministic and Adaptive Particle Swarm Optimization," presented at Congress of the Evolutionary Computation, Washington, USA, 1999.

[209] M. Lovberg, et al, "Hybrid Particle Swarm Optimiser with Breeding and Sub-populations," presented at GECCO2001 - Genetic and Evolutionary Computation Conference, San Francisco CA, USA, 2001.

[210] A. Mendonça, J. A. Peças Lopes, "Robust Tuning of PSS in Power Systems with Different Operating Conditions," presented at IEEE Bologna PowerTech'2003, Bologna, Italy, 2003.

[211] V. Miranda, N. Fonseca, "Reactive Power Dispatch with EPSO - Evolutionary Particle Swarm Optimization," presented at PMAPS'2002 - International Conference on Probablistic Methods Applied to Power Systems, Naples, Italy, 2002.

[212] V. Miranda, N. W. Oo, "Evolutionary Algorithms and Evolutionary Particle Swarms (EPSO) in Modeling Evolving Energy Retails," presented at PSCC-15th Power Systemd Computation Conference, Liège, Belgium, 2005.

[213] H. Mori, Y. Komatsu "A Hybrid Method of Optimal Data Mining and Artificial Neural Network for Voltage Stability Assessment," presented at IEEE St. Petersburg PowerTech, St. Petersburg, Russia, 2005.

[214] V. Miranda, C. Cerqueira, C. Monteiro, "Training a FIS with EPSO under an Entropy Criterion for Wind Power Prediction." presented at 9th. International Conference of Probabilistic Methods Applied to Power Systems, Stockholm, Sweden, 2006

[215] J. Kennedy, R. Mendes, "Population Structure and Particle Swarm Performance," presented at WCCI/CEC - World Conference on Computational Intelligence, Conference on Evolutionary Computation, Hnolulu (Hawaii), USA, 2002.

[216] M.-S. Chen, Tsai-Hsiang Chen, Hsiao-Dong Chiang, A. A. Fouad, J. A. Jativa, Wei-Jen Lee, Werner Leonhard, Young-Hwan Moon, M. A. Pai, Arun G. Phadke, P. W. Sauer, R. R. Shoults, J. S. Thorp, V. Vittal, *Control and dynamic systems. Advances in theory and applications*, vol. 43: Academic Press, Inc, 1993.

[217] G. N. Kariniotakis, G. S. Stavrakakis, "General simulation algorithm for the accurate assessment of isolated diesel-wind turbines systems interaction. Part II: Implementation of the algorithm and case-studies with induction generators," in *IEEE Transactions on Energy Conversion*, vol. 10, 1995, pp. 584-590.

[218] G. S. Stavrakakis, G. N. Kariniotakis, "A general simulation algorithm for the accurate assessment of isolated diesel-wind turbine systems interaction. Part I: A general multimachine power system model " in *IEEE Transactions on Energy Conversion*, vol. 10, 1995, pp. 577-583.

[219] N. L. Soultanis, Stavros A. Papathanasiou, Nikos D. Hatziargyriou, "A stability algorithm for the dynamic analysis of inverter dominated unbalanced LV microgrids," in *IEEE Transactions on Power Systems*, vol. 22, 2007, pp. 294-304.

[220] J. Arrillaga, C. P. Arnold, *Computer modelling of electrical power systems*: John Wiley & Sons Ltd, 1983.

[221] P. C. Krause, *Analysis of Electric Machinery*. New York: McGraw-Hill, 1987.

[222] H. Demuth, M. Beale, *Neural Network Toolbox: User's Guide, Version 3.0*. Natick, MA: The MathWorks, Inc 1998.

[223] H. Akagi, Y. Kanazawa, A. Nabae, "Instantaneous reactive power compensators comprising switching devices without energy storage components," in *IEEE Transactions on Industry Applications* vol. IA-20, 1984, pp. 625-630.

[224] P. G. Barbosa, I. Misaka, E. H. Watanabe, "Advanced var compensators using PWM - voltage source inverters," presented at 2º Congresso Brasileiro de Electrónica de Potência - COBEP/93, Urbelândia-MG, 1993.

[225] P. G. Barbosa, L. G. B. Rolim, E. H. Watanabe, R. Hanitsch, "Control strategy for grid-connected DC-AC converters with load power factor correction," in *IEE Proc. Generation, Transmission and Distribution*, vol. 145, 1998.

[226] N. J. Gil, J. A. Peças Lopes, "Hierarchical frequency control scheme for islanded multi-microgrids operation," presented at Power Tech 2007, Lausanne, Switzerland, 2007.

Appendix A
Round Rotor Synchronous Machine Modelling and Test Systems Parameters

A.1 Introduction

In this appendix the mathematical model of the round rotor synchronous machine is presented as well as the parameters of the several microgeneration systems and electrical networks corresponding to test systems TS-01 and TS-02 used over this thesis.

A.2 Round rotor synchronous machine

The equations of synchronous generator are obtained from the modified Park's equations of [216] after some simplifications.

- Stator transients are neglected since they are much faster compared to the rotor ones;
- The mechanical damping is usually small and it is also neglected, $D \approx 0$;
- It was assumed that the rotor speed is near the synchronous speed, $\omega = \omega_s$, in transient and subtransient states.

Thus, the round rotor synchronous machines presented in TS-01 and TS-02 are modelled using the 6th order model described in [216] through the following fundamental equations.

Algebraic equations of stator in per unit

$$V_d = E_{gd} + X_q^{"} I_q - R_s I_d \tag{A.1}$$

$$V_q = E_{gq} - X_d^{"} I_d - R_s I_q \tag{A.2}$$

where

$$E_{gd} = k_q \frac{X_q^{'} - X_q^{''}}{X_q^{'} - X_l} E_d^{''} + \frac{X_q^{''} - X_l}{X_q^{'} - X_l} E_d^{'} \tag{A.3}$$

$$E_{gq} = k_d \frac{X_d^{'} - X_d^{''}}{X_d^{'} - X_l} E_q^{''} + \frac{X_q^{''} - X_l}{X_q^{'} - X_l} E_q^{'} \tag{A.4}$$

$$k_d = 1 + \frac{\left(X_d^{'} - X_l\right)\left(X_d^{''} - X_l\right)}{\left(X_d^{'} - X_d^{''}\right)\left(X_d - X_l\right)} \tag{A.5}$$

$$k_q = 1 + \frac{\left(X_q^{'} - X_l\right)\left(X_q^{''} - X_l\right)}{\left(X_q^{'} - X_q^{''}\right)\left(X_q - X_l\right)} \tag{A.6}$$

Differential equations of rotor transients and subtransients in per unit/s

$$\frac{dE_d^{'}}{dt} = \frac{1}{T_{q0}^{'}}\left[-\frac{\left(X_q - X_q^{'}\right)\left(X_q^{'} - X_q^{''}\right)}{\left(X_q^{'} - X_l\right)^2} k_q E_d^{''} + \left\{ 1 + \frac{\left(X_q - X_q^{'}\right)\left(X_q^{'} - X_q^{''}\right)}{\left(X_q^{'} - X_l\right)^2} \right\} E_d^{'} \right] - \frac{\left(X_q - X_q^{'}\right)\left(X_q^{'} - X_q^{''}\right)}{X_q^{'} - X_l} I_q \tag{A.7}$$

$$\frac{dE_q^{'}}{dt} = \frac{1}{T_{d0}^{'}}\left[E_{fd} + \frac{\left(X_d - X_d^{'}\right)\left(X_d^{'} - X_d^{''}\right)}{\left(X_d^{'} - X_l\right)^2} k_d E_q^{''} - \left\{ 1 + \frac{\left(X_d - X_d^{'}\right)\left(X_d^{'} - X_d^{''}\right)}{\left(X_d^{'} - X_l\right)^2} \right\} E_q^{'} \right] - \frac{\left(X_d - X_d^{'}\right)\left(X_d^{'} - X_d^{''}\right)}{X_d^{'} - X_l} I_d \tag{A.8}$$

$$\frac{dE_d^{''}}{dt} = -\frac{1}{T_{q0}^{''} k_q}\left[k_q E_d^{''} - E_d^{'} + \left(X_q^{'} - X_l\right) I_q \right] \tag{A.9}$$

$$\frac{dE_q^{''}}{dt} = -\frac{1}{T_{d0}^{''} k_d}\left[k_q E_q^{''} - E_q^{'} + \left(X_d^{'} - X_l\right) I_d \right] \tag{A.10}$$

Swing equation in per unit/s

$$\frac{d\omega}{dt} = \frac{1}{2H}\left(T_m - T_e\right) \tag{A.11}$$

Electrical rotor angle in radians

$$\frac{d\delta}{dt} = \omega - 1 \tag{A.12}$$

Electromagnetic torque equation in per unit

$$T_e = E_q^{''} I_q + E_d^{''} I_d + \left(X_d^{''} - X_q^{''}\right) I_d I_q \tag{A.13}$$

Since $X_d^{''} = X_q^{''}$ for round rotor synchronous machines, the equation (A.13) simplifies to

$$T_e = E_q^{''} I_q + E_d^{''} I_d \tag{A.14}$$

where:

V_d and V_q are the generator terminal voltages in direct d and quadrature q axis, respectively;

E_{gd} and E_{gq} are the generator internal voltages in direct d and quadrature q axis, respectively;

I_d and I_q are the generator terminal currents in direct d and quadrature q axis, respectively;

$E_d^{'}$ and $E_q^{'}$ are the transient voltages in direct d and quadrature q axis, respectively;

$E_d^{''}$ and $E_q^{''}$ are the subtransient voltages in direct d and quadrature q axis, respectively;

E_{fd} is the synchronous generator field voltage;

$T_{d0}^{'}$ and $T_{q0}^{'}$ are the open circuit transient time constants of direct d and quadrature q axis, respectively, in seconds;

$T_{d0}^{''}$ and $T_{q0}^{''}$ are the open circuit subtransient time constants of direct d and quadrature q axis, respectively, in seconds;

T_m and T_e are the mechanical and electrical torques, respectively;

R_s is the stator resistance;

X_d and X_q are the stator reactances in direct d and quadrature q axis, respectively;

$X_d^{'}$ and $X_q^{'}$ are the stator transient reactances in direct d and quadrature q axis, respectively;

$X_d^{''}$ and $X_q^{''}$ are the stator subtransient reactances in direct d and quadrature q axis, respectively ($X_d^{''} = X_q^{''}$ for a round rotor synchronous machine);

X_l is the leakage reactance in the direct d axis of the stator coil;

ω is the rotor angular velocity;

A.2.1 Automatic voltage regulator

The purpose of the AVR is to provide the proper field voltage, E_{fd}, to the synchronous machine in order to maintain the desired voltage. The most commonly used AVR general models are those defined by the IEEE, especially the type 1 model [58], as depicted in figure A.1,

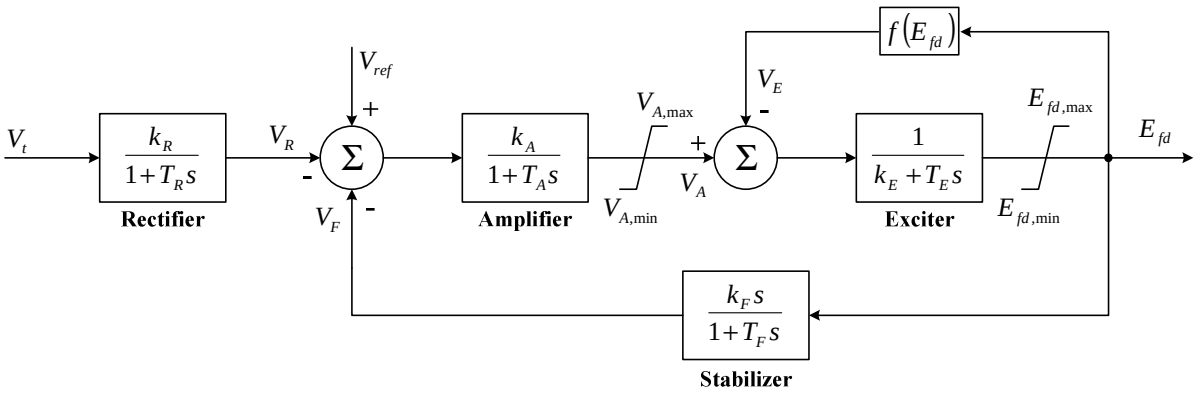

Figure A.1: Automatic voltage regulator, IEEE type 1 model

where:

V_R, V_A, V_F and V_E are the voltage values from the control subsystems, rectifier, amplifier, stabilization and exciter, respectively;

k_R, k_A, k_F and k_E are the gains of each one of the control subsystems;

T_R, T_A, T_F and T_E are time constants of each one of the control subsystems;

V_{ref} is the reference voltage value;

E_{fd} is the voltage field

The saturation effect was neglected and thus the saturation function in figure A.1, $f(E_{fd})$, was not considered.

A.2.2 Governor-turbine system

A governor is a mechanical or electromechanical device used to automatically control the speed of a prime mover in order to keep the system frequency near to its nominal value. In this thesis a diesel engine was adopted as the prime mover. The speed regulator comprises both the primary and secondary control functions.

Thus, the static increase in diesel engine power output is directly proportional to the static frequency. The value of R is considered always positive and since the frequency and power variations are in per unit, R is also in per unit. After the primary control function, which brings the system to an equilibrium state with a permanent frequency error, the secondary control (frequency error signal integrator) is needed to establish the nominal rotational speed by eliminating the static frequency error [217]. The model for speed-governing system is a first order model with a time constant τ_2, representing the governor delay and the prime mover is represented by a simplified first order model [58], as depicted in figure A.2,

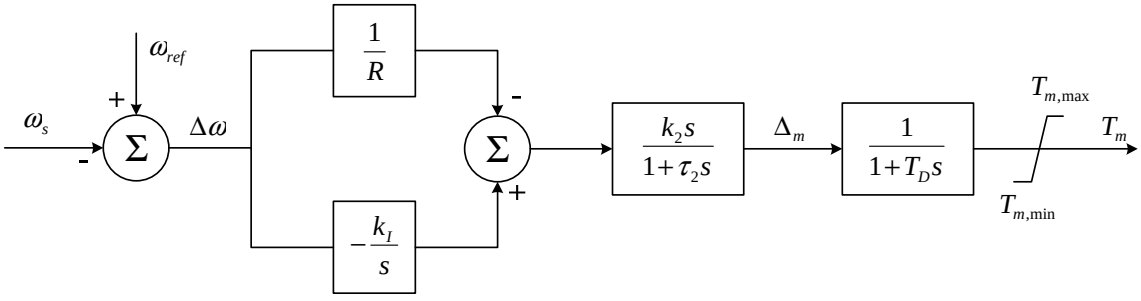

Figure A.2: Governor-turbine system model

where:

$\Delta\omega$ is the frequency deviation;

R is the diesel engine permanent speed droop (statism);

K_I is the governor summing loop amplification factor (integral gain);

k_2 is the fuel actuator gain constant;

τ_2 is the governor time delay;

Δm is the fuel variation;

T_D is the diesel engine time delay;

T_m is the mechanical torque

A.3 Test systems parameters

In this subsection, the parameters used in the several test systems and models are presented, taking into account the dynamic models adopted to describe the dynamic behaviour of microgeneration systems described in chapter 2, the round rotor synchronous machine model and the models of the remain electrical network components (loads, branches and transformer) described in chapter 5 for TS-01 and TS-02.

A.3.1 Test system TS-01

The TS-01 electrical network represented through the single line diagram in figure 6. 14 comprises two round rotor synchronous generators, the MG main storage device, one SSMT and three PV systems. Their parameters are presented in tables A1 to A6. Tables A.7 and A.8 present the parameters of branches and transformers, respectively.

Parameters of generators at MV level

System base quantities: $S_b = 500\,kVA$; Voltage base: $V_b = 690\,V$;

Table A.1: Parameters of TS-01 round rotor synchronous machine units SM1 and SM2

Round rotor synchronous generator *				
$S_n(kVA)$	$V_n(V)$	$R_s(p.u.)$	$X_d(p.u.)$	$X_q(p.u.)$
500	690	0,0014	1,25	1,22
$X_d^{'}(p.u.)$	$X_q^{'}(p.u.)$	$X_d^{''}(p.u.)$	$X_q^{''}(p.u.)$	$H(p.u.)$
0,232	0,715	0,120	0,120	1
$X_l(p.u.)$	$T_{d0}^{'}(s)$	$T_{q0}^{'}(s)$	$T_{d0}^{''}(s)$	$T_{q0}^{''}(s)$
0,134	4,75	1,5	0,059	0,210
Prime mover: $T_D = 1\,s$				
Speed governor				
$R(p.u.)$	$k_1(p.u.)$	$k_2(p.u.)$	$\tau_2(s)$	
0,25	1,5	1	0,1	
Automatic voltage regulator				
k_R	$T_R(s)$	k_A	$T_A(s)$	
1	0,01	15	0,05	
k_E	$T_E(s)$	k_F	$T_F(s)$	
1	0,5	0,02	0,8	

*The per unit parameter quantities are referred to the machine base $(S_b = 500\,kVA; V_b = 690\,V)$

Parameters of microgenerators of TS-01

System base quantities: $S_b = 500\,kVA$; Voltage base: $V_b = 400\,V$;

Table A.2: Parameters of TS-01 VSI control of MG main storage device

Parameter	Reference	Value	Unit
P_n	Nominal power	30	*kW*
V_n	Nominal voltage	400	*V*
T_{dP}	Active power delay	1,2	*s*
T_{dQ}	Reactive power delay	0,25	*s*
K_P	Frequency versus active power droop	$-1{,}2566\times10^{-4}$	*rad/W*
K_Q	Voltage versus reactive power droop	$-1{,}6\times10^{-6}$	*V/VAr*
K_{ff}	Phase feed-forward gain	$-3{,}333\times10^{-6}$	-
T_{inv}	Inverter time constant	0,0001	*s*
$\underline{Z}_f$	Filter impedance	$0{,}005 + j0{,}2314$	*Ω*

Table A.3: Parameters of TS-01 PV systems

Parameter	Reference	Value	Unit
V_n	Nominal voltage	400	V
G_a	Ambient irradiance	870	W/m^2
T_a	Ambient temperature	20	ºC
$P_{Max,0}$	Module maximum power at STC	25	W
μP_{Max}	Maximum power variation with module temperature	-0.005	-
$NOCT$	Normal cell operation temperature	47	ºC
N_1	Number of modules of PV1 system	400	-
N_2	Number of modules of PV2 system	800	-
N_3	Number of modules of PV3 system	600	-

Table A.4: Parameters of TS-01 PQ inverter of PV systems: PV1, PV2 and PV3

Parameter	Reference	Value	Unit
P_n	Nominal power	30	kW
V_n	Nominal voltage	400	V
$\underline{Z}_f$	Filter impedance	0,01+j0,1571	Ω
C	DC link capacitor	0,008	F
$V_{dc,ref}$	Voltage reference of DC link	800	V
k_{P1}	Proportional gain of PI-1	-5	-
k_{I1}	Integral gain of PI-1	-3	-
k_{P2}	Proportional gain of PI-2	0	-
k_{I2}	Integral gain of PI-2	100	-

Table A.5: Parameters of SSMT system of TS-01

Parameter	Reference	Value	Unit
P_n	Nominal power	80	*kW*
V_n	Nominal voltage	400	*V*
Active power control			
K_p	Proportional gain	4	-
K_i	Integral gain	0,2	-
Single shaft microturbine engine			
T_1	Fuel system lag time constant 1	15	*s*
T_2	Fuel system lag time constant 2	0,2	*s*
T_3	Load limit time constant	3	*s*
$L_{\max}$	Load limit	1,5	*s*
$V_{\max}$	Maximum value position	1,2	-
$V_{\min}$	Minimum value position	-0,1	-
K_T	Temperature control loop gain	1	-
Permanent magnet synchronous machine			
L_d	d-axis inductance	$6{,}875\times10^{-4}$	*H*
L_q	q-axis inductance	$6{,}875\times10^{-4}$	*H*
R_s	Resistance of the stator windings	0,25	*Ω*
Φ_m	Flux induced in the stator windings	0,0534	*Wb*
p	Number of poles pairs	1	-
J	Combined rotor and load inertia	0,003	$Kg.m^2$
F	Combined rotor and load viscous friction	0,0000005	
Machine side converter control			
k_{P1}	Proportional gain of PI-1	30	-
k_{I1}	Integral gain of PI-1	10	-
k_{P2}	Proportional gain of PI-2	100	-
k_{I2}	Integral gain of PI-2	150	-
k_{P3}	Proportional gain of PI-3	50	-
k_{I3}	Integral gain of PI-3	20	-
Secondary load frequency control			
k_P	Proportional gain	12,5	-
k_I	Integral gain	2	-

Table A.6: Parameters of TS-01 PQ inverter of SSMT

Parameter	Reference	Value	Unit
P_n	Nominal power	30	kW
V_n	Nominal voltage	400	V
$\underline{Z}_f$	Filter impedance	0,005+j0,0785	Ω
C	DC link capacitor	0,008	F
$V_{dc,ref}$	Voltage reference of DC link	800	V
k_{P1}	Proportional gain of PI-1	-5	-
k_{I1}	Integral gain of PI-1	-3	-
k_{P2}	Proportional gain of PI-2	0	-
k_{I2}	Integral gain of PI-2	100	-

Parameters of branches and transformers of TS-01

Table A.7: Parameters of branches of TS-01

Line	Bus i	Bus j	R (Ω)	X (Ω)
1	1	9	0,1757	0,219618
2	9	10	0,8	1
3	9	12	2	1,85
4	12	13	0,8	1
5	15	16	0,004	0,01
6	16	17	0,016	0,008
7	16	18	0,008	0,011
8	16	19	0,0534	0,0156
9	19	20	0,0085	0,0025
10	20	21	0,0114	0,0033
11	21	22	0,10164	0,011
12	21	23	0,0153	0,0045
13	23	24	0,0094	0,0027
14	24	25	0,0256	0,0075
15	25	26	0,0094	0,0027
16	25	27	0,0626	0,0126
17	25	28	0,02535	0,0051

Table A.8: Parameters of transformers of TS-01

Transformer	Bus i	Bus j	$V_i / V_j\ (kV)$	$S_n\ (kVA)$	$x(\%)$
T1	10	11	15/0,69	800	5
T2	13	14	15/0,69	800	5
T3	12	15	15/0,4	400	5

A.3.2 Test system TS-02

The TS-02 electrical network presented through its single line diagram as depicted in figure 6. 39 comprises two round rotor synchronous generators, the MG main storage device, two single shaft microturbines, SSMT1 and SSMT2, and one SOFC. The synchronous machines in this test system are those used in TS-02. The parameters of microgeneration systems are presented in tables from A9 to A12 while the parameters of branches and transformers are presented in tables A.13 and A.14, respectively.

Parameters of microgenerator systems of TS-02

System base quantities: $S_b = 500\,kVA$; Voltage base: $V_b = 400\,V$;

Table A.9: Parameters of TS-02 VSI control of MG main storage device

Parameter	Reference	Value	Unit
P_n	Nominal power	30	*kW*
V_n	Nominal voltage	400	*V*
T_{dP}	Active power delay	1,2	*s*
T_{dQ}	Reactive power delay	0,25	*s*
K_P	Frequency versus active power droop	$-1{,}2566\times10^{-4}$	*rad/W*
K_Q	Voltage versus reactive power droop	$-3{,}3\times10^{-6}$	*V/VAr*
K_{ff}	Phase feed-forward gain	$-3{,}333\times10^{-6}$	-
T_{inv}	Inverter time constant	0,0001	*s*
$\underline{Z}_f$	Filter impedance	$0{,}005 + j0{,}2$	Ω

Table A.10: Parameters of SSMT1 and SSMT2 of TS-02

Parameter	Reference	Value	Unit
P_n	Nominal power	30	kW
V_n	Nominal voltage	400	V
Active power control			
K_p	Proportional gain	4	-
K_i	Integral gain	0,2	-
Single shaft microturbine engine			
T_1	Fuel system lag time constant 1	15	s
T_2	Fuel system lag time constant 2	0,2	s
T_3	Load limit time constant	3	s
$L_{\max}$	Load limit	1,5	s
$V_{\max}$	Maximum value position	1,2	-
$V_{\min}$	Minimum value position	-0,1	-
K_T	Temperature control loop gain	1	-
Permanent magnet synchronous machine			
L_d	d-axis inductance	$6{,}875\times10^{-4}$	H
L_q	q-axis inductance	$6{,}875\times10^{-4}$	H
R_s	Resistance of the stator windings	0,25	Ω
Φ_m	Flux induced in the stator windings	0,0534	Wb
p	Number of poles pairs	1	-
J	Combined rotor and load inertia	0,003	$Kg.m^2$
F	Combined rotor and load viscous friction	0,0000005	
Machine side converter control			
k_{P1}	Proportional gain of PI-1	30	-
k_{I1}	Integral gain of PI-1	10	-
k_{P2}	Proportional gain of PI-2	100	-
k_{I2}	Integral gain of PI-2	150	-
k_{P3}	Proportional gain of PI-3	50	-
k_{I3}	Integral gain of PI-3	20	-
Secondary load frequency control			
k_P	Proportional gain	12,5	-
k_I	Integral gain	2	-

Table A.11: Parameters of SOFC of TS-02

Parameter	Reference	Value	Unit
P_n	Nominal power	30	kW
V_n	Nominal voltage	400	V
V_C	Cell desired voltage	338,8	V
T	Absolute temperature	1273	^oK
F	Faraday's constant	96487	C/mol
R	Universal gas constant	8,314	$J/(mol\cdot^o K)$
E_0	Ideal standard potential	1,18	V
N_0	Number of cells in series in the stack	384	-
$U_{\max}$	Maximum fuel utilization	0,90	-
$U_{\min}$	Minimum fuel utilization	0,80	-
U_{opt}	Optimal fuel utilization	0,85	-
K_{H_2}	Valve molar constant for hydrogen	$8{,}43\times10^{-4}$	$kmol/(s\cdot atm)$
K_{H_2O}	Valve molar constant for water	$2{,}81\times10^{-4}$	$kmol/(s\cdot atm)$
K_{O_2}	Valve molar constant for oxygen	$2{,}52\times10^{-3}$	$kmol/(s\cdot atm)$
τ_{H_2}	Response time for hydrogen flow	26,1	s
τ_{H_2O}	Response time for water flow	78,3	s
τ_{O_2}	Response time for oxygen flow	2,91	s
r	Ohmic loss	0,126	Ω
T_e	Electric response time	0,8	s
T_f	Fuel processor response time	5	s
r_{H-O}	Ratio of hydrogen to oxygen	1,145	-
Secondary load frequency control			
k_P	Proportional gain	12,5	-
k_I	Integral gain	2	-

Table A.12: Parameters of SSMT1, SSMT2 and SOFC PQ inverter of TS-02

Parameter	Reference	Value	Unit
P_n	Nominal power	30	kW
V_n	Nominal voltage	400	V
$\underline{Z}_f$	Filter impedance	0,005+j0,0785	Ω
C	DC link capacitor	0,008	F
$V_{dc,ref}$	Voltage reference of DC link	800	V
k_{P1}	Proportional gain of PI-1	-5	-
k_{I1}	Integral gain of PI-1	-3	-
k_{P2}	Proportional gain of PI-2	500	-
k_{I2}	Integral gain of PI-2	800	-

Parameters of branches and transformers of TS-02

Table A.13: Parameters of branches of TS-02

Line	Bus i	Bus j	R (Ω)	X (Ω)
1	1	2	0,1757	0,219618
2	2	3	0,8	1
3	2	5	2	1,85
4	5	6	0,8	1
5	8	9	0,016	0,008
6	9	10	0,005	0,2
7	8	11	0,004	0,01
8	8	12	0,004	0,01
9	12	13	0,004	0,01
10	12	14	0,004	0,01

Table A.14: Parameters of transformers of TS-02

Transformer	Bus i	Bus j	$V_i/V_j\ (kV)$	$S_n\ (kVA)$	$x(\%)$
T1	9	10	15/0,69	800	5
T2	12	13	15/0,69	800	5
T3	11	14	15/0,4	400	5